DIFFRACTION OF WAVES THROUGH A GAP BETWEEN TWO INCLINED BREAKWATERS

by

Constantinos Memos, Dipl. Civil Eng., NTU, Athens,
Dipl. Math., U. Patras, Greece.

November, 1976

A thesis submitted for the degree of Doctor of Philosophy of the University of London and for the Diploma of Imperial College

Civil Engineering Department,
Imperial College,
London S.W.7.

ABSTRACT

The theory for the diffraction of water waves has previously been limited to two simple cases; the diffraction around a semi-infinite breakwater and the diffraction through an opening in a rigid plane. A useful harbour configuration is two breakwaters forming an arbitrary angle between themselves. A solution for this case has been derived with the objective of finding the wave heights in the lee of two breakwaters simulating a harbour.

Numerical results using the new method agree with the known classical solution of the special case where the two breakwaters lie in the same plane. Experimental verification has also shown good agreement.

The tables and figures presented here give the wave heights in the region of interest as related to the angle between the two arms, the breadth of the opening, and the angle of incidence. The waves are assumed to be of small amplitude.

The information obtained from the new solution can be useful to the design engineer whenever he is undertaking coastal studies involving diffraction of water waves.

ACKNOWLEDGEMENTS

Among the many members of the staff at Imperial College who helped me in one way or another I express my gratitude in particular, to my supervisor Mr B. MacMahon, Dr F.G. Leppington, Dr K.E. Pitman, Mr P.M. Johnston, Professor J.R.D. Francis, Professor J.T. Stuart.

My thanks are due also to the State Scholarships Foundation, Greece, for providing financial support during a major part of my studies.

TABLE OF CONTENTS

LIST OF TABLES

NOTATION

Numbers in brackets - [ ] - refer to papers or books listed at the end of the book. Numbers in rounded brackets - ( ) - refer to equations in the text.

The most frequently occurring symbols with their meaning are:-

d	gap width
F, F_i, F_s	wave function of the total, incident, scattered field in two space dimensions
F_o	incident plane wave in two space dimensions
G	Green's function
H_ν	Hankel function of the first kind $(= J_\nu + iY_\nu)$
H	wave height
h	water depth
$I_\nu(x)$	modified Bessel function of the first kind $\{=i^{-\nu}J_\nu(ix)\}$
J_ν	Bessel function of the first kind
$K_\nu(x)$	modified Bessel function of the second kind $\left[= \frac{\pi}{2}\{i^{\nu+1}H_\nu(ix)\}\right]$
k	wavenumber
K	diffraction coefficient
(r,ω)	polar co-ordinates of point of observation
(r_o,ω_o)	polar co-ordinates of line source
$r_>, r_<$	greater, smaller distance from a given set
(x,y,z)	axes of orthogonal co-ordinate system

Y_ν	Bessel function of the second kind
δ	dimensionless gap width $(= d/\lambda)$
ε_n	equals 1, n = 0; equals 2, n ≥ 1
η	surface elevation
θ	angle between breakwaters
θ_o	angle of incidence $(= 2\pi + \theta - \zeta)$
λ	wavelength
π	3.14159... radians
ρ	dimensionless polar co-ordinate $(= r/\lambda)$
σ	circular frequency of waves
ϕ	velocity potential
Φ	wave function in three space dimensions
(1),(2)	'weather', 'protected' breakwater arm
Δ	Laplace differential operator $\left(= \frac{\partial^2}{\partial x^2} + \frac{\partial^2}{\partial y^2} + \frac{\partial^2}{\partial z^2}\right)$
∇	divergence
Im,Re	imaginary, real part of complex nubmer
log	natural logarithm
U,∩	union, intersection

C H A P T E R A

GENERAL INTRODUCTION AND OUTLINE

A1 INTRODUCTION AND NOMENCLATURE

Almost any field of science or engineering involves some questions of wave motion, one of the broadest scientific subjects. Here we limit ourselves to a domain that particularly concerns the harbour engineer; nevertheless a great deal of our theory can be easily transposed to other branches of science, a common practice where waves are concerned.

The difficulty that arises from the above limitation is that the mathematical material must act as a servant to the practical aspect of the problem and each theoretical development has to lead us towards that end, the bridge between the two standpoints being very delicate. In spite of this role that the mathematics has to play here, effort has been made that as much rigour as possible is retained for the sake of completeness.

From a phenomenological point of view we deal exclusively with diffraction, that is the propagation of waves into a sheltered region - the 'shadow' according to geometrical optics terminology. A 'flow of energy' is taking place along the wave crests rather than normal to them. When the engineer considers the problem of designing a harbour, this phenomenon, as well as refraction, plays a major part in his hydrodynamical considerations. Indeed, having ascertained the maximum wave height at every point of the sea surface in the harbour he has at his disposal a criterion for the general lay-out of mooring places and other harbour installations. Conversely, knowing the solution of the diffraction problem he can arrange the exterior structures of the harbour (breakwaters, etc.) to obtain a

wave height distribution close to his requirements, which are dictated by operational factors. The same applies also to other coastal engineering works which involve wave diffraction processes.

Most water waves diffraction problems fall in one of the two general classes: (a) the passage of waves around the tip of a rigid semi-infinite barrier; and (b) the passage of waves through a gap in a similar but infinite breakwater. The complete theory of the first problem has been developed many years ago by Penney and Price and is given in the following chapter. The second has been solved so far only for the special case where the two branches of the breakwater are 'in line', i.e. lie on the same vertical plane. The aim of this study is to provide a solution for the general case where the two arms form between them an arbitrary angle θ. The most significant values from an application viewpoint are $\frac{1}{2}\pi < \theta < \pi$ in which region the numerical computations were performed. Nevertheless the theory holds over the entire range of θ from 0 to 2π. The main parameters of the problem are shown in fig. 1, where the x and y axes of the Cartesian co-ordinate system lie on the undisturbed water surface.

Our objective is to determine the diffraction patterns behind such a configuration of breakwaters as in fig. 1, which is met in almost any harbour. No restriction to the magnitude of the opening has been put.

Another point that our formulation reveals is that the most significant values of the angle of approach θ_o of the plane wave are $\pi \leq \theta_o \leq \pi + \theta$ because for these values the agitation in the harbour becomes great. The formulation of the solution holds for every angle θ_o (as for every θ too), but results have been found for θ_o in

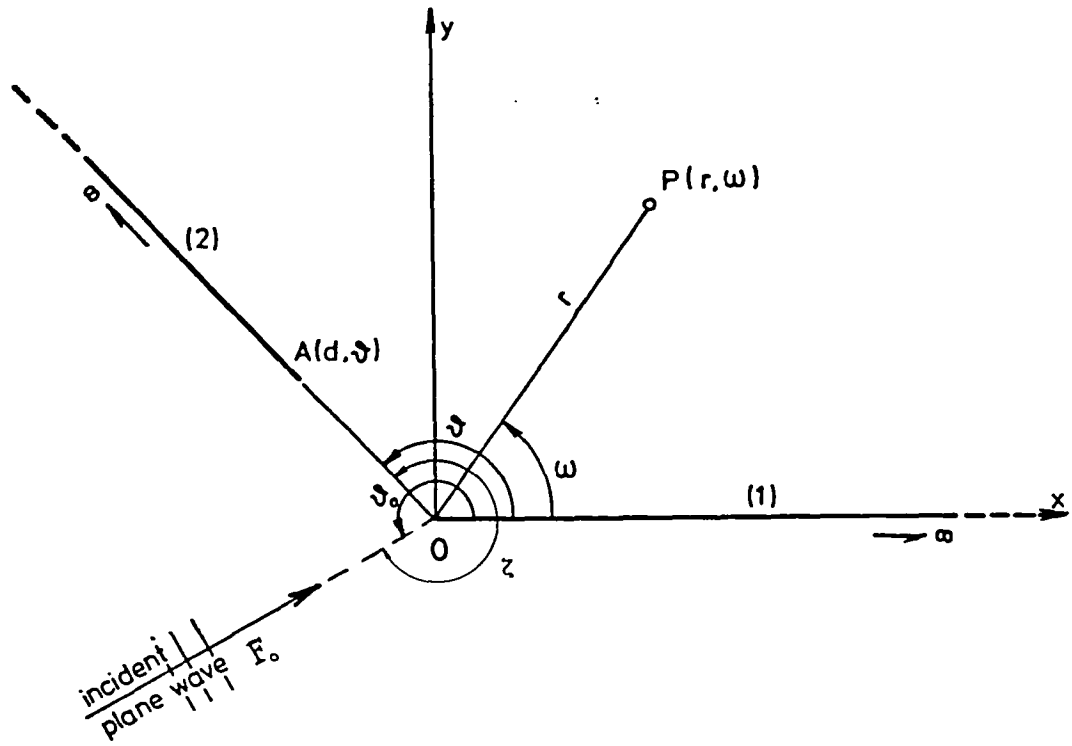

Fig. 1. Nomenclature of the problem

the above range. Of course our interest is focused on the region behind the breakwater for obvious reasons.

Our tool is the first-order linear theory with the usual assumptions, which has been proved a good approximation for our purposes. Indeed the current practice in maritime engineering is based on this theory when dealing with diffraction problems. These assumptions are:

(1) Outside the sources of wave radiation the fluid is homogeneous and isotropic, i.e. uniform in space and time, and non-absorbing, i.e. wavenumber $k = 2\pi/\lambda > 0$, λ wavelength. A deviation is made for convenience when examining the Wiener-Hopf

technique where k is a complex number with $0 < \mathrm{Im}(k) \ll 1$, and also in the solution of the wedge problem.

(2) The height of the waves 2a is small compared with their length and the water depth h; therefore it can be established that the wave-profile is nearly sinusoidal. This means that Ursell's parameter $2a\lambda^2/h^3$ is less than 15, say.

(3) The water depth is uniform or slowly varying.

(4) The breakwaters are of vanishing thickness and completely reflecting.

(5) The motion throughout the fluid is irrotational.

(6) The water is an ideal, incompressible fluid.

(7) The pressure at the water surface is constant.

Applying the conventional first-order theory we derive the water motion from a velocity potential $\phi(r,\omega,z;t)$, the z axis pointing upwards, t the time, satisfying the equation

$$\Delta \phi = 0 \qquad (1)$$

where Δ is the Laplace differential operator $(= \frac{\partial^2}{\partial x^2} + \frac{\partial^2}{\partial y^2} + \frac{\partial^2}{\partial z^2}$ in Cartesian co-ordinates x,y,z).

The depth of the water being h we have at the bottom the condition

$$\frac{\partial \phi}{\partial z} = 0, \qquad z = -h \qquad (2)$$

while at the faces of the barriers it is $\frac{\partial \phi}{\partial n} = 0$, where n is the outward normal to the surface of the object at any point. When the wave height is not too great, as our assumption states, the pressure p is given approximately by $p = \rho_o\left(\frac{\partial \phi}{\partial t} - gz\right)$, $z \lesssim 0$, where ρ_o represents the water density and g the gravitational acceleration. In order that p be constant at the surface $z = \eta$ we require to the

first order

$$\eta = \frac{1}{g}\frac{\partial \phi}{\partial t} \tag{3}$$

Also since the normal component of the fluid velocity at the surface must equal the normal component of the velocity of the surface itself, we have approximately

$$\frac{\partial \eta}{\partial t} = -\frac{\partial \phi}{\partial z}, \qquad z = 0 \tag{4}$$

whence, from eqs (3), (4)

$$\frac{\partial^2 \phi}{\partial t^2} + g\frac{\partial \phi}{\partial z} = 0, \qquad z = 0 \tag{5}$$

The property that any particle once on the free surface remains on it, which is expressed by eq. (4), is a basic assumption in continuum mechanics.

A solution of eq. (1) simple harmonic in time is

$$\phi(x,y,z;t) = \mathrm{Re}[\Phi(x,y,z)\exp\{-i\sigma t\}] \tag{6}$$

where Re denotes the real part and σ the circular frequency of the waves = $\frac{2\pi}{\lambda}$ × the phase velocity of plane waves propagating in free space. It is convenient to factorise the function Φ

$$\Phi(x,y,z) = G(z)\,F(x,y) \tag{7}$$

where G(z) behaves like coshk(z + h).

Boundary conditions (2) and (5) are satisfied as one can easily verify. Now, eq. (1) in virtue of eqs (6) and (7) is replaced by

$$\left(\frac{\partial^2}{\partial x^2} + \frac{\partial^2}{\partial y^2} + k^2\right)F(x,y) = 0 \tag{8}$$

known as the Helmholtz equation. This equation provides the link between the study of waves in many branches of science and engineering e.g. optics, electromagnetism, acoustics etc., being the starting point for any investigation of the diffraction problem in two horizontal dimensions. The complex function F is called the wave function and eq. (8) the Helmholtz equation or the reduced wave equations throughout this study.

The incident plane wave F_o in fig. 1 can be described as $\exp\{-ik(x \cos\theta_o + y \sin\theta_o)\}$ leaving any constants to be incorporated in G(z). Then if we denote by K the diffraction coefficient, that is the ratio of the maximum wave height at any point $(x,y) \equiv (r,\omega)$ to the maximum height of the incoming waves far away from the breakwater, we have easily

$$K = |F| \tag{9}$$

The main aim in the diffraction problem is the determination of K. Knowledge of the phase difference between the incident waves at the point (x,y) if they had not been disturbed by the breakwater and the actual waves at the same point is sometimes useful but not always necessary, except when dealing with wave forces on structures.

But is the above orderly scheme of physical laws and equations of any use, when apparently it contrasts with the disorder that reigns on the surface of the ocean? Or is it a mere mathematical structure for its own sake?

Observing the chaotic appearance of the sea we must not forget the underlying order governed by a probability law. The great development of wave statistics and generalised Fourier analysis offers us a powerful tool with which we can analyse the randomness of the sea into simple components to each of which our diffraction procedure could be applied. So, the more complicated situations

dictated by the nature of the sea could be analysed into simple components which would be subject to our analytical treatment; the individual results could afterwards be summed to produce the final answer.

A2 OUTLINE OF MATERIAL

The theory leading to the solution of our problem presented in section A1 is given in chapter C. The approach is followed step by step until the final result is reached; all this material is contained in section C3. Another approach is developed independently in section C5, based on the method of the matched asymptotic expansions; this method could eventually provide a kind of checking of the principal approach and on the other hand it could stand by itself as a means of solving such a problem to a lower level of accuracy. Further refinement of it to increase the accuracy is possible but for the engineer rather cumbersome. Checking of the main theory was thought desirable, for to my knowledge no other solution of the problem exists so far apart from a special case.

This special case is covered in chapter B by four different methods to provide another test of our theory. These methods are well established having been examined and cross-examined over the years and represent classical solutions for the case where the angle θ equals π radians.

The computing part of the solution found in section C3 is presented in section C4, while section C2 is devoted to an essential prerequisite for the development of our theory, namely the application to water waves of the theory of diffraction by a wedge. An outline of the methods normally used for solving diffraction problems is presented in section C1, where the method of matched asymptotic expansions is not mentioned because it has been developed mainly on problems other than diffraction; nevertheless a brief account of it

is given in section C5 where it is also applied.

A third and final checking is provided by experiment. A description of the procedure, together with considerations on the laboratory equipment involved (wave maker, filters, etc.), are to be found in chapter D.

The last chapter comprises the presentation of the results, comparisons with theory and experiment, and critical discussion of the work together with a brief account of some allied topics.

C H A P T E R B

BACKGROUND

B1 GENERAL

The objective of this chapter is to provide a means of checking the results of the main theory which is developed in chapter C, in the case where the two branches of the breakwater are in the same vertical plane; the incident field is a plane wave and approaches the screen at any angle. Although the above case is an extreme one for our problem, it is of great importance because no other established theory or practice to check the results of the present study in a wide range exists so far. Furthermore by referring briefly to the solutions of a similar case a link and continuity are established within the framework of the diffraction problem as viewed by the hydraulic engineer.

The problem of diffraction of water waves through a gap with vertical edges in a plane screen (breakwater) has been thoroughly investigated. The rigorous solution has been published in a paper by Carr and Stelzriede [1], based on the theoretical work of Morse and Rubenstein [2] for the diffraction of waves by ribbons and by slits. As it is explained in subsection B3.2 this exact solution has the disadvantage of not being of practical use for gaps wider than about two wavelengths; therefore we must apply ourselves to other theories, approximate ones, in order to cover as wide a range of cases as possible.

Three approximate solutions are covered briefly in subsection B3.1; those attributed to: Penney and Price [3] (subdivision B3.1.1), Lacombe [4] (subdivision B3.1.2) and Lamb [5] Art. 305, 2^{o} (subdivision B3.1.3). The first one is convenient and accurate enough for

engineering purposes if the gap width is greater than two or three wavelengths but it has been presented for only normal incidence of the incoming plane waves. Oblique incidence is covered in the second approximate solution which is based on Huyghens' principle; the third one is of small interest for direct engineering calculations because it is not accurate for gaps wider than one wavelength and it gives wave amplitude as a function of the distance from the opening and of the gap width (both expressed in wavelengths) but not of the angle of the incident wave nor of the specific position of the point of observation. However it extends the range of gap widths applicable to the approximate solutions to the smallest values and consequently the range of checking with the results of this study. An indirect reference to that solution is made in section C6.

While section B3 deals with the above-mentioned problem, section B2 refers to the comparatively simpler problem of diffraction by a semi-infinite breakwater the solution of which forms the basis of Penney and Price's method for the gap. The main reference [3] is based on Sommerfeld's solution [6] for the diffraction of light waves at the edge of a semi-infinite screen.

The picture of the diffraction problem has its principle features arranged at three main levels: semi-infinite breakwater, breakwater gap and two inclined breakwaters, the theoretical investigation of this latter being dealt with in chapter C.

A complete survey of the literature on diffraction of waves by planes is out of the scope of this chapter which is simply to provide a reference frame by retaining the results obtained by the methods cited.

B2 THE SEMI-INFINITE BREAKWATER

The problem whose solution is presented in this section has been the subject of numerous investigations in several branches of physics. Sommerfeld [6] obtained the first rigorous solution for the case of diffraction of light by a semi-infinite perfectly reflecting plane. He arrived at an integral representation along a contour, that bears now his name, by a method involving Riemann surfaces and a transformation technique of surface spherical harmonics. It is on this work that the extension and adaption to the water waves due to Penney and Price [3] is based.

Having in mind the assumptions laid down in chapter A and applying the conventional first-order theory, we derive the water motion from a velocity potential $\phi(r,\omega;t)$, with the variables as defined in the introduction (section A1) and which satisfies Laplace's equation (1).

Solutions of eq. (1) periodic in time and satisfying condition (2) are of the form

$$\phi = \mathrm{Re}[A \cosh k(z+h)\, F(r,\omega) \exp\{-i\sigma t\}]$$

where Re denotes the real part, A is a constant related to the wave amplitude and $F(r,\omega)$ represents a complex function, the wave function, satisfying the Helmholtz equation (8), or in polar co-ordinates centred on the breakwater tip (fig. 1)

$$\frac{\partial^2 F}{\partial r^2} + \frac{1}{r}\frac{\partial F}{\partial r} + \frac{1}{r^2}\frac{\partial^2 F}{\partial \omega^2} + k^2 F = 0 \qquad (10)$$

The boundary conditions at the breakwater are

$$\frac{\partial \phi}{\partial y} = 0 \qquad \text{at } y = 0,\ x \geq 0$$

or in terms of the wave function

$$\frac{\partial F}{\partial y} = 0 \qquad \text{at } y = 0,\ x \geq 0 \tag{11}$$

Consider now a line source located at a point (r_o, θ_o) and radiating waves of wave function $\frac{i}{4} H_o(kr)$, $H_o = J_o + iY_o$ being the Hankel function of the first kind and zeroth order, (see fig. 2).

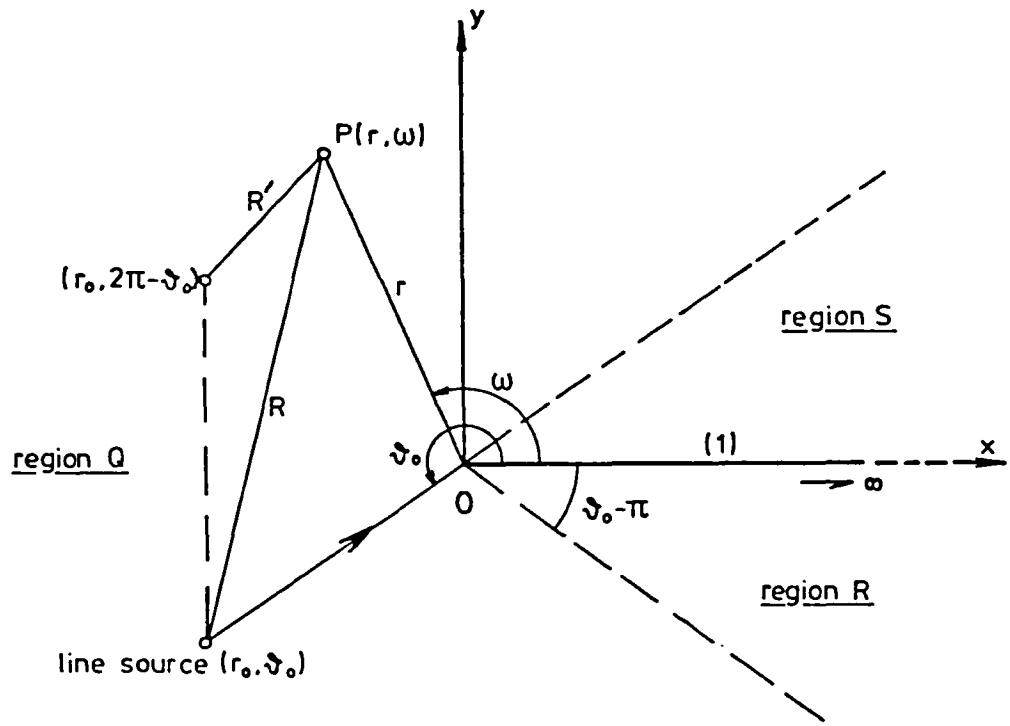

Fig. 2. Waves from a line source incident on a semi-infinite breakwater

It is convenient to divide the whole plane into three distinct

regions following Penney and Price's method for an incident plane wave [3]:

(1) Region S, where $0 < \omega < \theta_o - \pi$

(2) Region Q, where $\theta_o - \pi < \omega < 3\pi - \theta_o$

(3) Region R, where $3\pi - \theta_o < \omega < 2\pi$

The problem of finding the velocity potential at any point (r,ω) of the plane x-y has been solved. The solution given by Bowman and Senior [7] following the notation of fig. 2 is

$$F(r,\omega) = \frac{1}{2\pi}\left[e^{ikR} \int_{-m}^{\infty} \frac{\exp\{i\mu^2\}}{(\mu^2 + 2kR)^{\frac{1}{2}}}\, d\mu + \right.$$

$$\left. + e^{ikR'} \int_{-m}^{\infty} \frac{\exp\{i\mu^2\}}{(\mu^2 + 2kR')^{\frac{1}{2}}}\, d\mu \right] \qquad (12)$$

where

$$m = 2\sqrt{\frac{kr_o r}{R_1+R}} \cos\frac{\omega-\theta_o}{2} = \begin{cases} +\sqrt{k(R_1-R)}, & \cos\dfrac{\omega-\theta_o}{2} > 0 \quad \text{(regions Q,R)} \\ -\sqrt{k(R_1-R)}, & \cos\dfrac{\omega-\theta_o}{2} < 0 \quad \text{(S)} \end{cases}$$

$$m' = 2\sqrt{\frac{kr_o r}{R_1+R}} \cos\frac{\omega+\theta_o}{2} = \begin{cases} +\sqrt{k(R_1-R')}, \cos\dfrac{\omega+\theta_o}{2} > 0 \quad \text{(R)} \\ -\sqrt{k(R_1-R')}, \cos\dfrac{\omega+\theta_o}{2} < 0 \quad \text{(Q,S)}, \end{cases}$$

and $R_1 = r + r_o$

This result is to be used later on in subsection C3.2.

Now, by letting $r_o \to \infty$ and making use of the identy

$$\sqrt{\frac{2}{\pi}} \int_w^\infty \exp\{i\mu^2\}d\mu = \frac{1+i}{2} - \int_{-\infty}^{(2/\pi)^{\frac{1}{2}}w} \exp\{\tfrac{1}{2}i\pi t^2\}dt,$$

we find the corresponding solution for an incident plane wave of the form $\exp\{-ikr\cos(\omega-\theta_o)\}$, $\pi < \theta_o < 2\pi$, which is the well-known Sommerfeld solution to a similar problem in optics:

$$\sqrt{2}\, F(r,\omega) = (\text{inc}) \int_{-\infty}^{u_1} \exp\{\tfrac{1}{2}i\pi t^2\}dt + (\text{ref}) \int_{-\infty}^{u_1} \exp\{\tfrac{1}{2}\pi i t^2\}dt \qquad (13)$$

where we have put

$$(\text{inc}) = \exp\{-ikr\cos(\omega-\theta_o) - \tfrac{1}{4}i\pi\}$$

$$(\text{ref}) = \exp\{-ikr\cos(\omega+\theta_o) - \tfrac{1}{4}i\pi\}$$

and $$u_1 = 2\left(\frac{kr}{\pi}\right)^{\frac{1}{2}} \cos\frac{\omega-\theta_o}{2}\,,\quad u_2 = 2\left(\frac{kr}{\pi}\right)^{\frac{1}{2}} \cos\frac{\omega+\theta_o}{2}$$

The first term in eq. (13) arises from the directly diffracted incident wave and the second accomodates the effect of the diffraction of the reflected part. For the simplified solution where the second term is omitted see e.g. Putnam and Arthur [8]. For partial reflection a proportion of the second component should be used but the phase relative to the first component must be taken into account (see Silvester and Lim [9]).

The composite solution to the gap problem, which is based on the results of this section, has been developed only for normal incidence. Therefore we put in eq. (13) $\theta_o = \frac{3}{2}\pi$ and obtain the

following expression when the incidence is normal to the breakwater

$$\sqrt{2}\, F(x,y) = \exp\{+iky - \tfrac{1}{4}i\pi\} \int_{-\infty}^{w_1} \exp\{\tfrac{1}{2}i\pi u^2\}du \cdot +$$

$$+ \exp\{-iky - \tfrac{1}{4}i\pi\} \int_{-\infty}^{w_2} \exp\{\tfrac{1}{2}i\pi u^2\}du \qquad (14)$$

where $w_1^2 = \frac{4}{\lambda}(r-y)$, $\qquad w_2^2 = \frac{4}{\lambda}(r+y)$

The signs of w_1, w_2 depend on the position of the point of observation $P(x,y) \equiv P(r,\omega)$ and can be derived from the corresponding values of u_1, u_2 in eq. (13). It is found that when the point lies in region S,Q,R the signs of w_1, w_2 are (-,-), (+,-), (+,+) respectively. The quantities in eq. (14) can be easily evaluated using tables of the Fresnel integrals or graphically by Cornu's spiral (see e.g. Lacombe [4], p. 347).

B3 THE BREAKWATER GAP

B3.1 Approximate Solutions

Three approximate solutions to the gap problem are studied below. At least two of them are widely used in engineering practice. In particular the assumptions in these are investigated in order to ascertain which regions are inadequately covered by the methods at present available.

B3.1.1 Penney and Price's method [3]. This assumes that the phenomenon of diffraction through the gap can be divided into two independent processes: the diffraction of the waves by (a) the left-hand and (b) the right-hand breakwater each acting independently of the other. In this way the solution for the diffracted wave in the gap problem is the sum of these waves in the two single breakwater problems. Obviously the boundary conditions along the breakwaters are not satisfied because the method does not take into account the interaction effect between the two structures. The error induced decreases with increasing gap width and is acceptable when the simplified solution is employed for widths greater than about three wavelengths.

The case of normal incidence is covered by this method, as mentioned before, and therefore reference to the corresponding equation (14) must be made (see section B2). It can be written

$$F(x,y) = \exp\{+iky\}\, f(w_1) + \exp\{-iky\}\, f(w_2) \qquad (15)$$

where $f(w) = \frac{1}{2}(1+i) \int_{-\infty}^{w} \exp\{-\frac{1}{2}i\pi u^2\}du$

The relation

$$f(w) + f(-w) = 1 \qquad (16)$$

which can be readily verified, makes possible a decomposition of the field (15) according to the position of the point (x,y). Thus we have in each of the three regions (fig. 3)

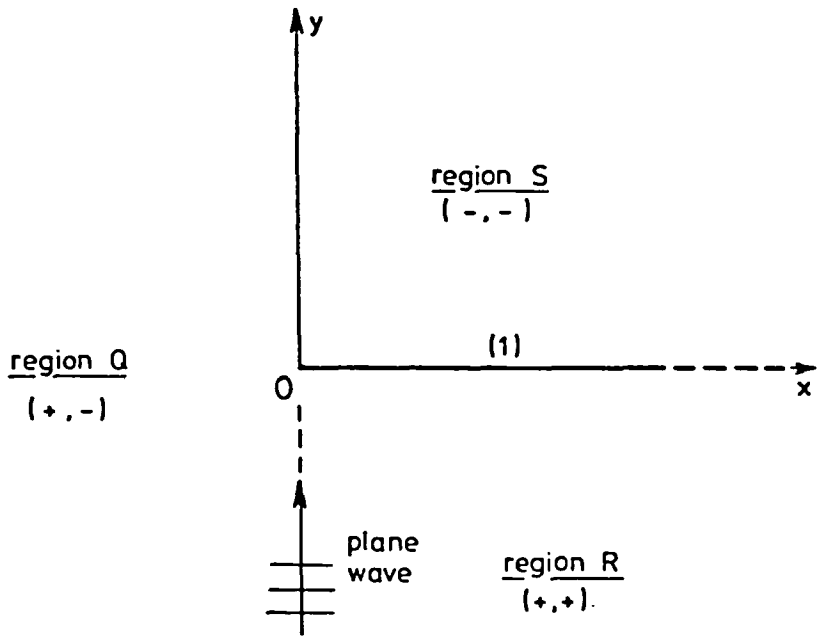

Fig. 3. Signs of w_1, w_2 in the case of normally incident waves on a semi-infinite breakwater

Region Q $\quad w_1 = 2\left(\frac{r-y}{\lambda}\right)^{\frac{1}{2}}, \qquad w_2 = -2\left(\frac{r+y}{\lambda}\right)^{\frac{1}{2}}$

and so $\quad w_1(y) = -w_2(-y)$

Eq. (15) gives

$$F(x,y) = \exp\{+iky\}[1 - f(-w_1)] + \exp\{-iky\}f(w_2) =$$

$$= \exp\{+iky\} - f_1(r,y) + f_1(r,y) \tag{17}$$

where $f_1(r,y) = \exp\{+iky\}\, f\{-2\left(\frac{r-y}{\lambda}\right)^{\frac{1}{2}}\}$ (18)

Region R $\quad w_1 = 2\left(\frac{r-y}{\lambda}\right)^{\frac{1}{2}}, \qquad w_2 = 2\left(\frac{r+y}{\lambda}\right)^{\frac{1}{2}}$

and so $\quad w_1(y) = w_2(-y)$

Eq. (15) gives

$$F(x,y) = \exp\{+iky\}[1 - f(-w_1)] + \exp\{-iky\}[1 - f(-w_2)]$$

$$= \exp\{+iky\} + \exp\{-iky\} - f_1(r,y) - f_1(r,-y) \tag{19}$$

Region S $\quad w_1 = -2\left(\frac{r-y}{\lambda}\right)^{\frac{1}{2}}, \qquad w_2 = -2\left(\frac{r+y}{\lambda}\right)^{\frac{1}{2}}$

and so $\quad w_1(y) = w_2(-y)$

Eq. (15) gives

$$F(x,y) = \exp\{+iky\}\, f(w_1) + \exp\{-iky\}\, f(w_2)$$

$$= f_1(r,y) + f_1(r,-y) \tag{20}$$

Or if we put $g_1(r,y) = f_1(r,-y)$

we have

$$\text{Region Q} : F_1 = \exp\{+iky\} - f_1 + g_1$$

$$\text{R} : F_1 = \exp\{+iky\} + \exp\{-iky\} - f_1 - g_1 \tag{21}$$

$$\text{S} : F_1 = f_1 + g_1$$

where the subscript of the wave function denotes the right breakwater (1) (see fig. 4).

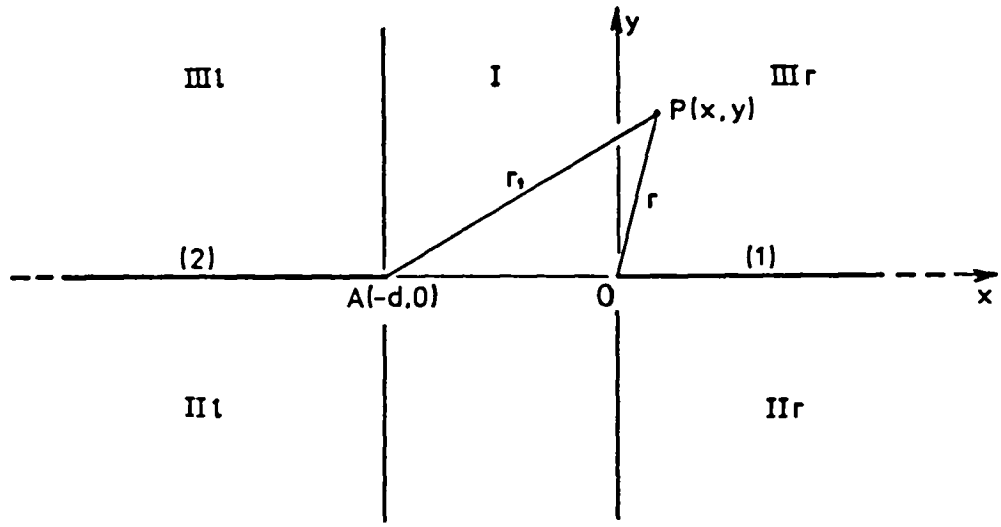

Fig. 4. Breakwater gap: decomposition into two semi-infinite breakwaters

Now having in mind only the left-hand breakwater (2) with corresponding regions q,r,s, we can indicate the composition of the field in the regions as in fig. 4 as follows:

Region I = Q + q

IIℓ = Q + r, IIr = q + R

IIIℓ = Q + s, IIIr = q + S

As with the barrier (1), we find for the barrier (2):

Region q : $F_2(x,y) = \exp\{+iky\} - f_2 + g_2$

r : $F_2(x,y) = \exp\{+iky\} + \exp\{-iky\} - f_2 - g_2$ (22)

s : $F_2(x,y) = f_2 + g_2$

where $f_2 = f_2(r_1,y) = \exp\{+iky\}\, f\left[-2\left[\frac{r_1-y}{\lambda}\right]\right]^{\frac{1}{2}}$ (23)

$g_2 = g_2(r_1,y) = f_2(r_1,-y)$

$r_1 = (r^2 + d^2 + 2xd)^{\frac{1}{2}}$, d breadth of opening (fig. 4)

In both sets of relations (21) and (22) the incident, reflected, diffracted of incident and diffracted of reflected fields clearly emerge as exp{-iky}, exp{+iky}, f and g respectively.

By 'addition' of the fields of the two individual problems we obtain

$$\begin{aligned}
&\text{Region I} \quad : F = F_1 + F_2 = \exp\{+iky\} - f_1 + g_1 - g_2 + g_2 \\
&\text{II}\ell \quad : F = \exp\{+iky\} + \exp\{-iky\} - f_1 + g_1 - f_2 - g_2 \\
&\text{IIr} \quad : F = \exp\{+iky\} + \exp\{-iky\} - f_1 - g_1 - f_2 + g_2 \qquad (24) \\
&\text{III}\ell \quad : F = -f_1 + g_1 + f_2 + g_2 \\
&\text{IIIr} \quad : F = f_1 + g_1 - f_2 + g_2
\end{aligned}$$

For small values of $w < 0$, $f(w)$ can be written

$$f(w) = \tfrac{1}{2}(1+i)\left[-\frac{1}{\pi w}\exp\{-\tfrac{1}{2}\pi i(1+w^2)\} + O(w^{-3})\right]$$

$$\simeq -\frac{1}{\pi w\sqrt{2}}\exp\{-\tfrac{1}{4}\pi i(1+2w^2)\} \qquad (25)$$

which is correct to within 2% of $|f(w)|$ when $w < -2$. We find for the unsatisfied boundary condition along the unoccupied part of the x axis ($x < -d$)

$$\frac{\partial F_1}{\partial y} = \frac{\partial}{\partial y}(-f_1 + g_1) = -\frac{4\pi i}{\lambda}\, f\{-2\left(\frac{r}{\lambda}\right)^{\frac{1}{2}}\} - \left(\frac{2}{\lambda r}\right)^{\frac{1}{2}}\exp\{-\tfrac{1}{4}\pi i + \frac{2\pi i r}{\lambda}\}$$

or substituting the approximate expression for $f(w)$:

$$\frac{\partial F_1}{\partial y} \simeq 0$$

to the same degree of approximation provided $-2\left(\frac{r}{\lambda}\right)^{\frac{1}{2}} < -2$ which means that the gap width must be greater than λ for such an approximation to be achieved.

Considering again the expression (25) which holds good for $w < -2$, we find

$$g_1(r,y) \simeq \frac{1}{2\pi}\left(\frac{\lambda}{2(r+y)}\right)^{\frac{1}{2}} \exp\{-\tfrac{1}{4}i\pi - \frac{2i\pi r}{\lambda}\}$$

whence we deduce that on the leeside of the breakwater ($y > 0$) the functions g_1, g_2 will be small except for points within one or two wavelengths from either tip of the opening. We ignore therefore the influence of the reflected wave on the total field in the lee of the breakwaters and get the widely used 'simplified' solution (see e.g. Blue and Johnson [10])

$$\begin{aligned} &\text{Region I} \quad : F = \exp\{+iky\} - f_1 - f_2 \\ &\text{III}\ell \quad : F = -f_1 + f_2 \\ &\text{IIIr} \quad : F = f_1 - f_2 \end{aligned} \tag{26}$$

A further simplification of the first of eqs (26) is obtained when the gap is relatively narrow, of the order of two wavelengths, and y is large compared with $|x|$:

$$\begin{aligned} &\text{we have} \quad r - y \simeq \frac{1}{2}\frac{x^2}{y} \\ &\text{and similarly } r_1 - y \simeq \frac{1}{2}\frac{(x+d)^2}{y} \end{aligned} \tag{27}$$

Now from eq. (18) we derive

$$f_1 = \tfrac{1}{2}\exp\{+iky\}(1+i)\left[\int_{-\infty}^{0}\exp\{-\tfrac{1}{2}\pi iu^2\}du + \int_{0}^{w}\exp\{-\tfrac{1}{2}\pi iu^2\}du\right]$$

$$= \tfrac{1}{2}\exp\{+iky\}(1+i)\left[\tfrac{1}{2}(1-i) + \int_{0}^{w}\exp\{-\tfrac{1}{2}\pi iu^2\}du\right] \tag{28}$$

where $w = -2\left(\frac{r-y}{\lambda}\right)^{\frac{1}{2}}$,

using the property of Fresnel integrals

$$\int_0^\infty \sin(\tfrac{1}{2}\pi u^2)du = \int_0^\infty \cos(\tfrac{1}{2}\pi u^2)du = \frac{1}{2}$$

A similar expression holds for f_2 with $w = -2\left[\frac{r_1 - y}{\lambda}\right]^{\frac{1}{2}}$. For small values of w we can expand the integrand in eq. (28) as a power series

$$1 - \tfrac{1}{2}\pi i u^2 - \ldots$$

giving

$$f_1 = \tfrac{1}{2}\exp\{+iky\}[1 + w + \frac{1}{6}\pi w^3 - \ldots + i(w - \frac{1}{6}\pi w^3 - \ldots)] \tag{29}$$

and so from eqs (26),(27) and (29) we have

$$F = \exp\{+iky\}d(\lambda y)^{-\frac{1}{2}}[\exp\{\tfrac{1}{4}i\pi\} + \frac{\pi}{3\lambda y}(3x^2 + \tfrac{1}{4}d^2 + 3xd)\exp[-\tfrac{1}{4}\pi i\}] \tag{30}$$

Recapitulating the results of this method we distinguish three solutions with decreasing accuracy or in other words with diminishing domain of applicability in equations (24),(26),(30). The following assumptions apply to each of them:

eqs (24) d > 1 or 2 wavelengths

eqs (26) d > 1 or 2 wavelengths

r+y, r_1+y > 2λ say

eq. (30) d > 1 or 2 wavelengths

r+y, r_1+y > 2λ say

y large compared with |x| so that r = y+2nd-order term,

r_1 = y + 2nd-order term.

The above conditions must be meant when we simply say the Penney and Price's method can be used for d greater than two or so wavelengths. We shall meet these solutions again when making comparisons in sub-

section E2.1.

B3.1.2 Lacombe's method [4]. Professor Lacombe has developed a method based on a generalisation of Huyghens' principle under certain assumptions. For a more detailed account of this principle see subdivision C3.3.1.

With the same notation as before we seek a velocity potential $\phi(x,y,z;t)$ or $\phi(r,\omega,z;t)$ in the form of

$$\phi = \mathrm{Re}[A \cosh k(z+h)\, F(x,y)\exp\{-i\sigma t\}] \qquad (31)$$

The motion being irrotational, the problem reduces to finding the wave function F at every point of the water surface under consideration; F satisfies the Helmholtz equation (8). Applying Green's theorem to the volume V confined between the two vertical cylindrical surfaces Σ, S (fig. 5) we obtain

$$\iiint_V (\phi\Delta\psi - \psi\Delta\phi)dv = \iint_{\Sigma US} \left(\phi \frac{\partial\psi}{\partial n} - \psi \frac{\partial\phi}{\partial n}\right)ds \qquad (32)$$

where $\frac{\partial}{\partial n}$ denotes differentiation along the outward normal to the boundaries of V and ψ a function satisfying Laplace's equation.

A simple and suitable expression for ψ is

$$\psi(x,y,z;t) = \frac{\cosh k(z+h)}{\cosh kh}\, iH_o(x,y)e^{-i\sigma t} \qquad (33)$$

where H_o represents as before the Hankel function of the first kind and zeroth order. On the other hand ϕ can be written

$$\phi(x,y,z;t) = \mathrm{Re}\left[\frac{g}{\sigma}\frac{\cosh k(z+h)}{\cosh kh} F(x,y)e^{-i\sigma t}\right] \qquad (34)$$

after substitution of the value of

$$A = \frac{g}{\sigma \cosh kh}$$

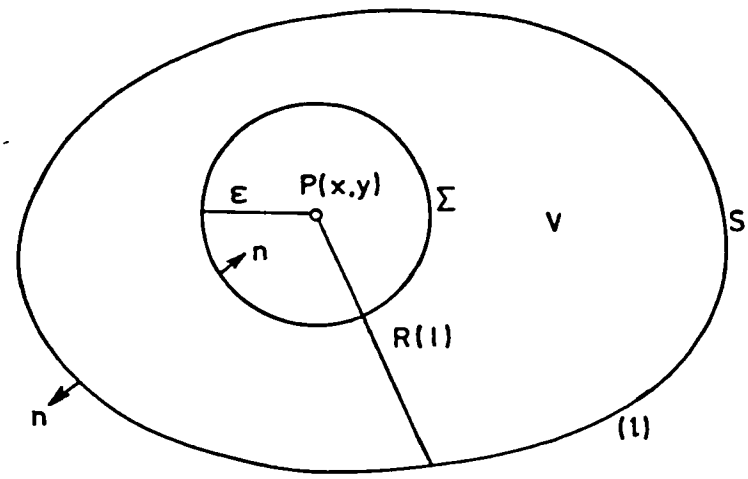

Fig. 5. Generalisation of Huyghens' principle after Lacombe [4]

representing waves of maximum height equal to unity. Putting the above values of ψ,ϕ into eq. (32), suppressing the z and t dependences and letting ε (fig. 5) tend to zero we obtain the fundamental formula

$$\int_{\ell}\left(F\,\frac{\partial H_o}{\partial n} - H_o\,\frac{\partial F}{\partial n}\right)d\ell \;=\; 4iF \qquad (35)$$

We can now apply this relationship to the problem of finding the agitation in the lee of a breakwater with a gap (fig. 6), under the classical Kirchhoff's assumptions discussed later in subdivision C3.3.1:

(1) The function F is zero along the inner face of the breakwaters.

(2) Along the gap, F has the same value as if there were no obstacles.

(3) We can apply Green's theorem despite the discontinuities in F, $\partial F/\partial n$ along the contour.

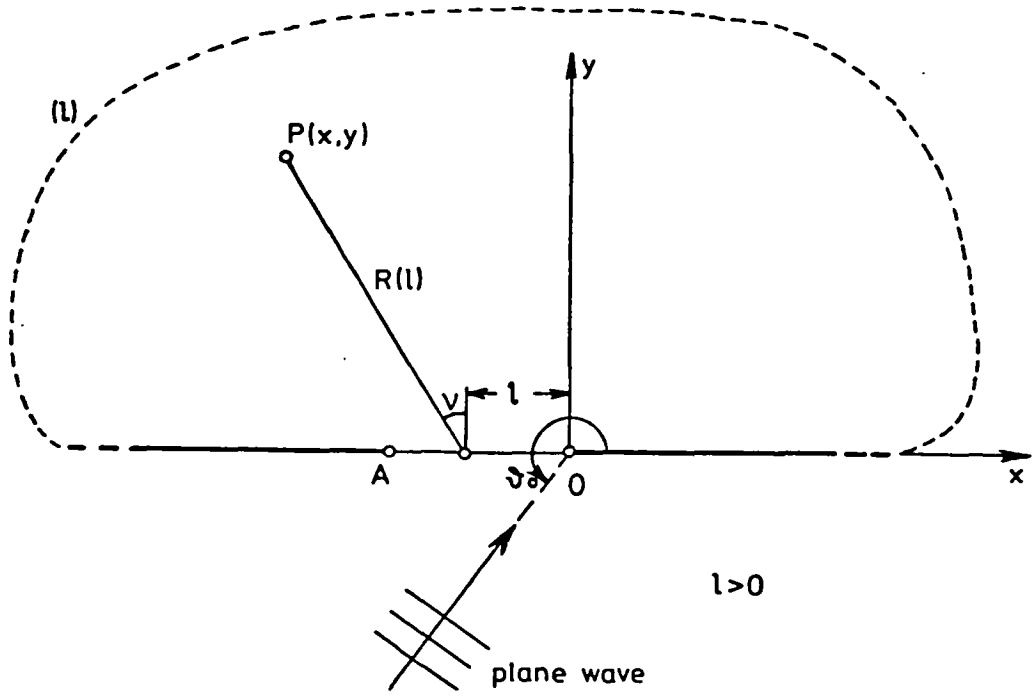

Fig. 6. Application of Green's theorem to the diffraction problem

It can easily be seen that the first of the above three assumptions does not allow for any effect of the relative position of the two branches to the velocity potential; thus any geometry of the problem leads to the same result provided the opening is being kept constant.

Using the asymptotic expression for the Hankel function for large argument we find in the end

$$F(x,y) \simeq \frac{1}{2\sqrt{\lambda}} \int_{OA} \frac{\cos\nu - \sin\theta_o}{\sqrt{R(\ell)}} \exp\{-ik[\ell\cos\theta_o - R(\ell)] - \tfrac{1}{4}i\pi\}d\ell \tag{36}$$

with the symbols as defined in fig. 6.

A fourth restriction has been imposed so far namely that $R(\ell)$ be greater than 2 or 3 wavelengths. The practical evaluation of

eq. (36) is considered in chapter E for the sake of comparison.

B3.1.3 Lamb's Method [5], Art. 305, 2^{o}. When the gap width d is small compared with the wavelength a reasonable approximation can be obtained assuming that the streamlines of the motion of the water through the gap are the same as for a simple uniform streaming of water. This problem has been treated by Lamb as an application of Rayleigh's considerations [11] Arts 341,342. At distances r' large compared with d we have

$$F(x,y) \simeq \frac{\frac{1}{2}\pi}{\log \frac{\pi d}{4\lambda} + \gamma + \frac{1}{2}i\pi} H_o(kr')$$

$$\simeq \left(\frac{\lambda}{4r'}\right)^{\frac{1}{2}} \frac{\exp\{-\frac{1}{4}\pi i + ikr'\}}{\log \frac{\pi d}{4\lambda} + \gamma + \frac{1}{2}\pi i} \qquad (37)$$

where r' is the distance of the point (x,y) from the centre of the gap

$$r' = +[y^2 + (x + \tfrac{1}{2}d)^2]^{\frac{1}{2}}$$

and γ Euler's constant (= 0.5772...).

The expression for the height of the waves may be written

$$|F| = \frac{1}{2[(\log \frac{1}{8} kd + \gamma)^2 + \frac{1}{4}\pi^2]^{\frac{1}{2}}} \left(\frac{\lambda}{r'}\right)^{\frac{1}{2}} \qquad (38)$$

We see from the last equation that it gives the same answer for different angles of approach of the incident wave, as well as for different points of observation (r',ω_i').

It would be useful for further reference to represent graphically eq. (38) in a co-ordinate system with axes d/λ, $K(r'/\lambda)^{\frac{1}{2}}$ where

$K = |F|$ is the diffraction coefficient. The parameter $K(r'/\lambda)^{\frac{1}{2}}$ is suggested by the form of the equation and it is also used later in the following subsection when comparing the theories discussed in this chapter. Relation (38) can be written

$$K\left(\frac{r'}{\lambda}\right)^{\frac{1}{2}} = \frac{0.5}{\left[\left(\log \frac{d}{\lambda} + 0.336\right)^2 + 2.46\right]^{\frac{1}{2}}} \qquad (39)$$

a plot of which is presented in fig. 7

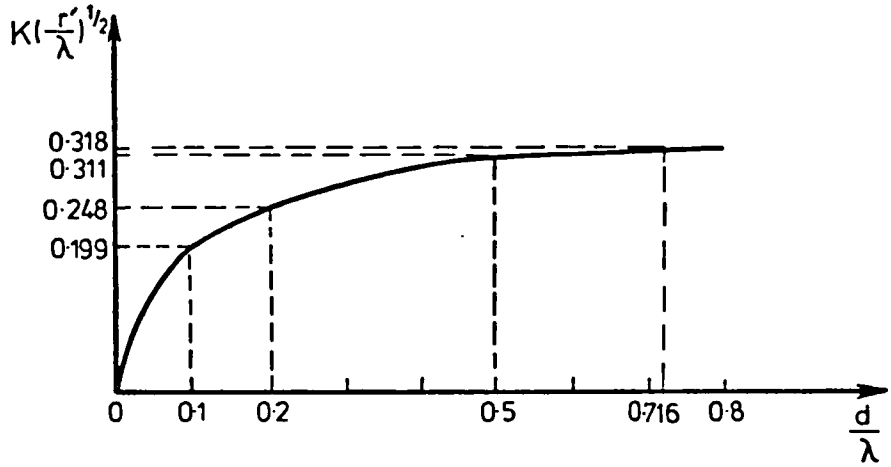

Fig. 7. Graphical representation of equation (38)

The maximum value of the parameter $K(r'/\lambda)^{\frac{1}{2}}$ is $\pi^{-1}(=0.318)$ and it is obtained for $d = 0.716\lambda$.

B3.2 Exact Solution

Carr and Stelzriede [1] have developed a rigorous method for solving the problem of this section extending the work done by Morse and Rubenstein [2] in electromagnetic waves.

The same assumptions as in Penney and Price's method (subdivision B3.1.1) are made. By the use of elliptic-cylinder coordinates (ξ,τ,z) the wave-function $F(\xi,\tau)$ has an assumed solution

$$F(\xi,\tau) = E(\xi)\, H(\tau) \tag{40}$$

where the functions E,H satisfy the differential equations

$$\frac{d^2E}{d\xi^2} + (s\cosh^2\xi - b)E = 0$$

$$\frac{d^2H}{d\tau^2} + (b - s\cosh^2\tau)H = 0 \tag{41}$$

b being a separation constant and $s = \left(\frac{\pi d}{\lambda}\right)^2$.

The solution of eqs (41) is expressed in terms of radial Mathieu functions $Je_m(s,\xi)$, $Ye_m(s,\xi)$ and the series $Se_m(s,\tau) = \sum_{n=o}^{\infty}{}' De_n \cos n\tau$. The subscripts m are index numbers 0,1,2, ... corresponding to increasing characteristic values of the parameter b. The primed summation sign indicates that for even values of m only even values of n are included in the summation, and for odd m only odd values of n are summed. The Mathieu coefficients De_n may be determined by substituting the series representation into the second of eqs (41) expanding the trigonometric functions into series and equating coefficient of like powers of τ to zero.

The final result for the function F is expressed by the equation

$$F(\xi,\tau) = (8\pi)^{\frac{1}{2}} \sum_{m=o}^{\infty}\Big[\frac{i^{m-1}}{N_m} \sin\gamma_m \exp\{i\gamma_m\} Se_m(s,\theta_o-\pi) Se_m(s,\tau) - \\ - [Je_m(s,\xi) + iYe_m(s,\xi)]\Big] \tag{42}$$

N_m is a normalization factor and $\gamma_m = \text{arccotan} \dfrac{Ye_m(s,0)}{Je_m(s,0)}$

The complexity of eq. (42) dictates the use of its asymptotic form at points where the radius of curvature of the wave crest in plan is greater than about three wavelengths. Carr and Stelzriede introduce here the 'intensity factor' defined as $I_{r',\tau} = H^2_{r',\tau}/H^2_i$, where $H_{r',\tau}$ the maximum height of the wave at a point (r',τ) and H_i the corresponding height of the incident wave. They have found that

$$I_{r',\tau} = \frac{4\lambda}{r'} \sum_{m,n} \sin\gamma_m \sin\gamma_n \, Se_m(s,\theta_o-\pi) \, Se_n(s,\theta_o-\pi) \, .$$

$$. \, Se_m(s,\tau) \, Se_n(s,\tau) \, \cos(\gamma_n-\gamma_m) \qquad (43)$$

The above relation is used to present polar plots of the 'intensity factor' $I_{r',\tau}$.

This exact method, a brief account of which has been given, holds for every gap width the only assumption for eq. (43) to be valid being that at the point (r',τ) the radius of curvature of the wave crest be greater than about three wavelengths. However the series in eq. (43) converge slowly for $d > 2$, say, and the method is impracticable. As it stands, it is useful for d less than about two wavelengths and it bridges the gap between Penney and Price's method (subdivision B3.1.1) and Lamb's method (subdivision B3.1.3) viewed in terms of applicable gap width.

To illustrate the above I have plotted three simple diagrams which indicate the variation of the parameter $K(r'/\lambda)^{\frac{1}{2}}$ with d/λ for three angles of incidence. All methods of this chapter have been included so that one can easily get an idea of when each one can be

applied successfully, together with the appropriate assumptions (figs 8, 9,10). 'Penney and Price' method refers to eqs (24), 'Penney and Price (simplified)' to eqs (26) and 'Carr and Stelzriede' to eq. (43).

Observation of these figures reveals that for engineering purposes and on normal incidence Penney and Price's method is adequate for $d > 2\lambda$, while for $d < 2\lambda$ 'Carr and Stelzriede' should be applied. On oblique incidence 'Lacombe' can give satisfactory answers for $240^{o} < \theta_{o} < 300^{o}$, while for $\theta_{o} < 240^{o}$ 'Carr and Stelzriede' covers the range $d < 2\lambda$; for $d > 2\lambda$ the lack of a suitable theory is apparent. This problem — $d > 2\lambda$, $\theta_{o} < 240^{o}$— can be regarded as a special case of the theory developed in chapter C.

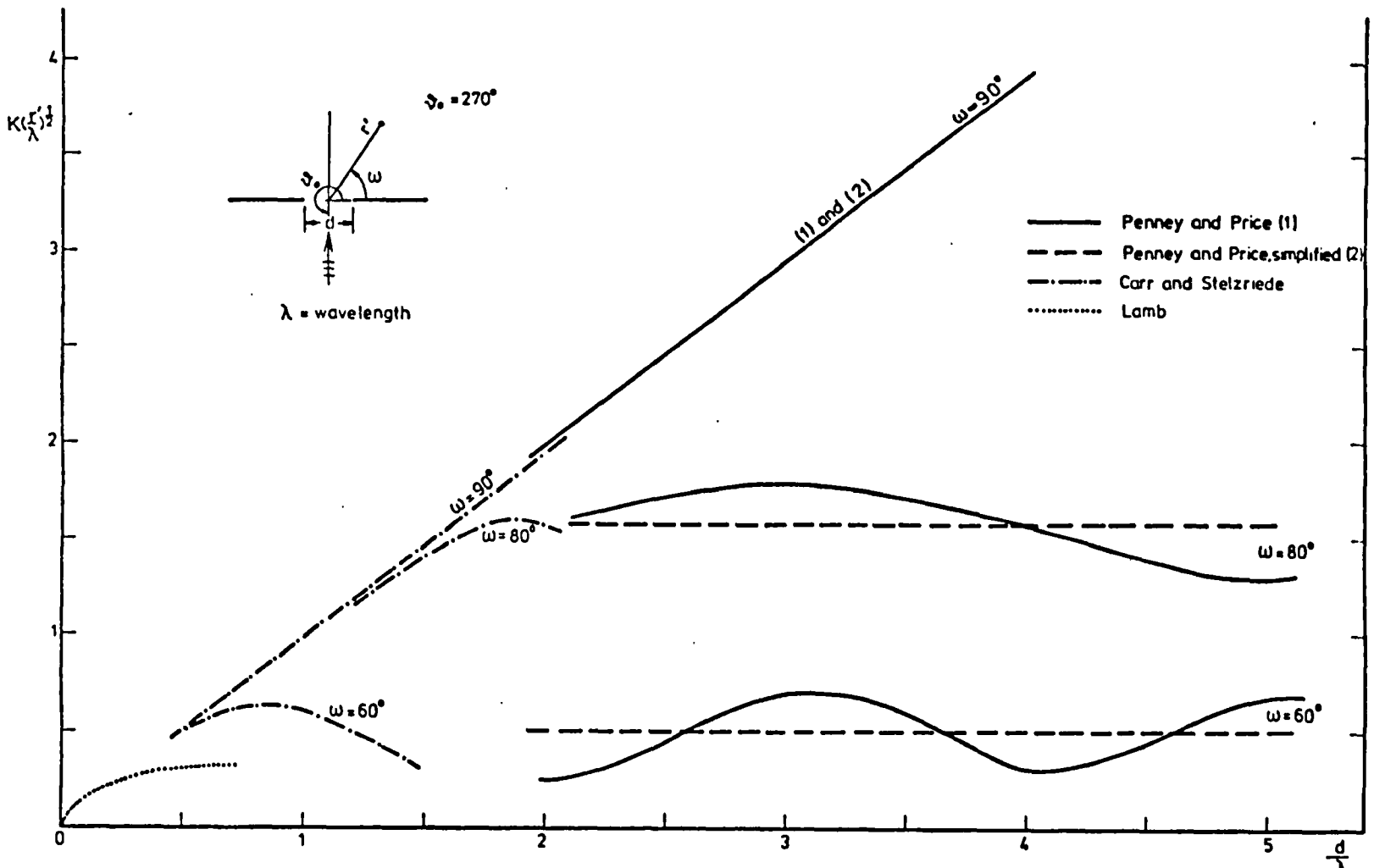

Fig. 8. Comparison of theories with respect to gap width (normal incidence)

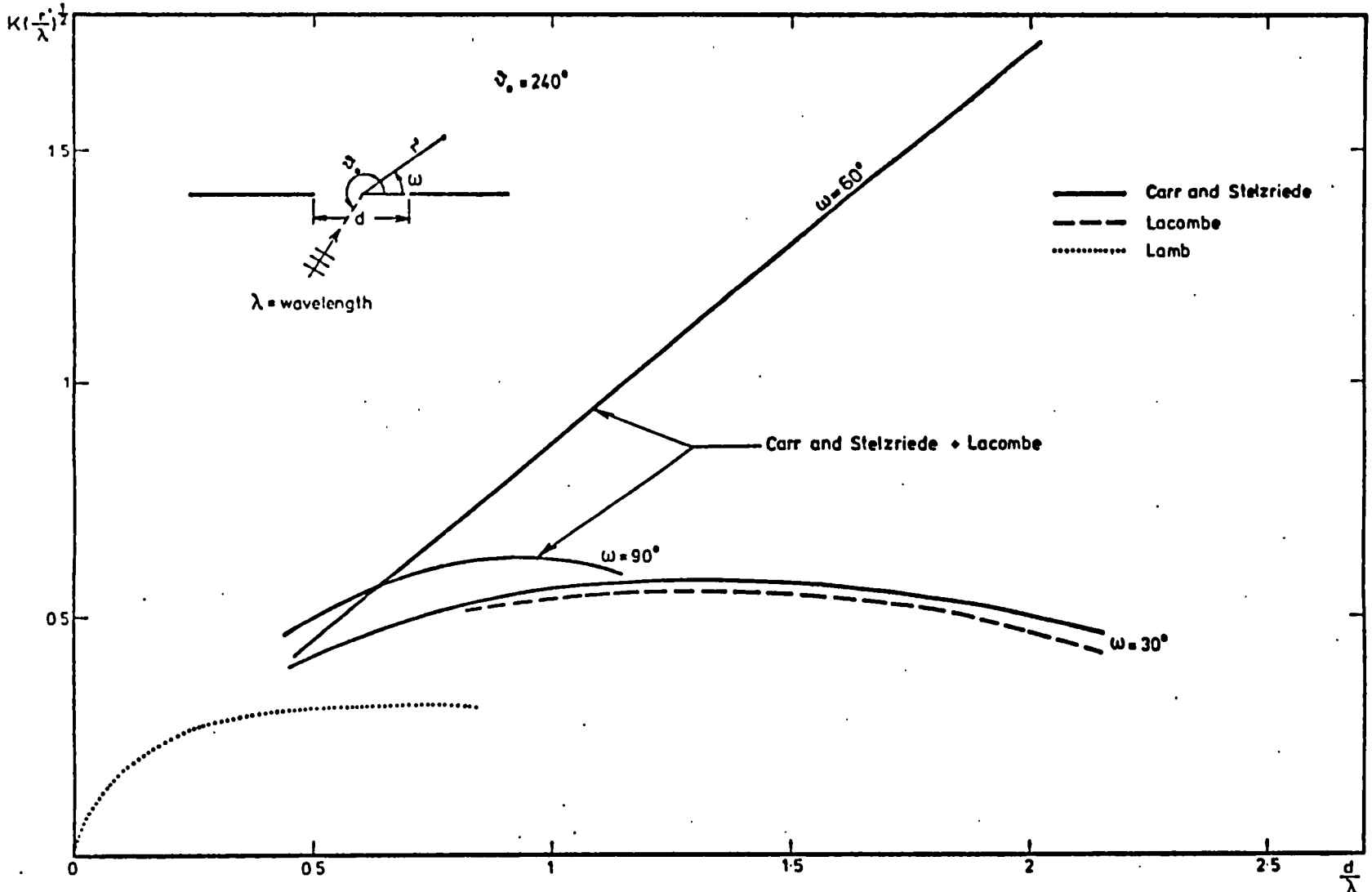

Fig.9. Comparison of theories with respect to gap width (oblique incidence : $\vartheta_0 = 240°$)

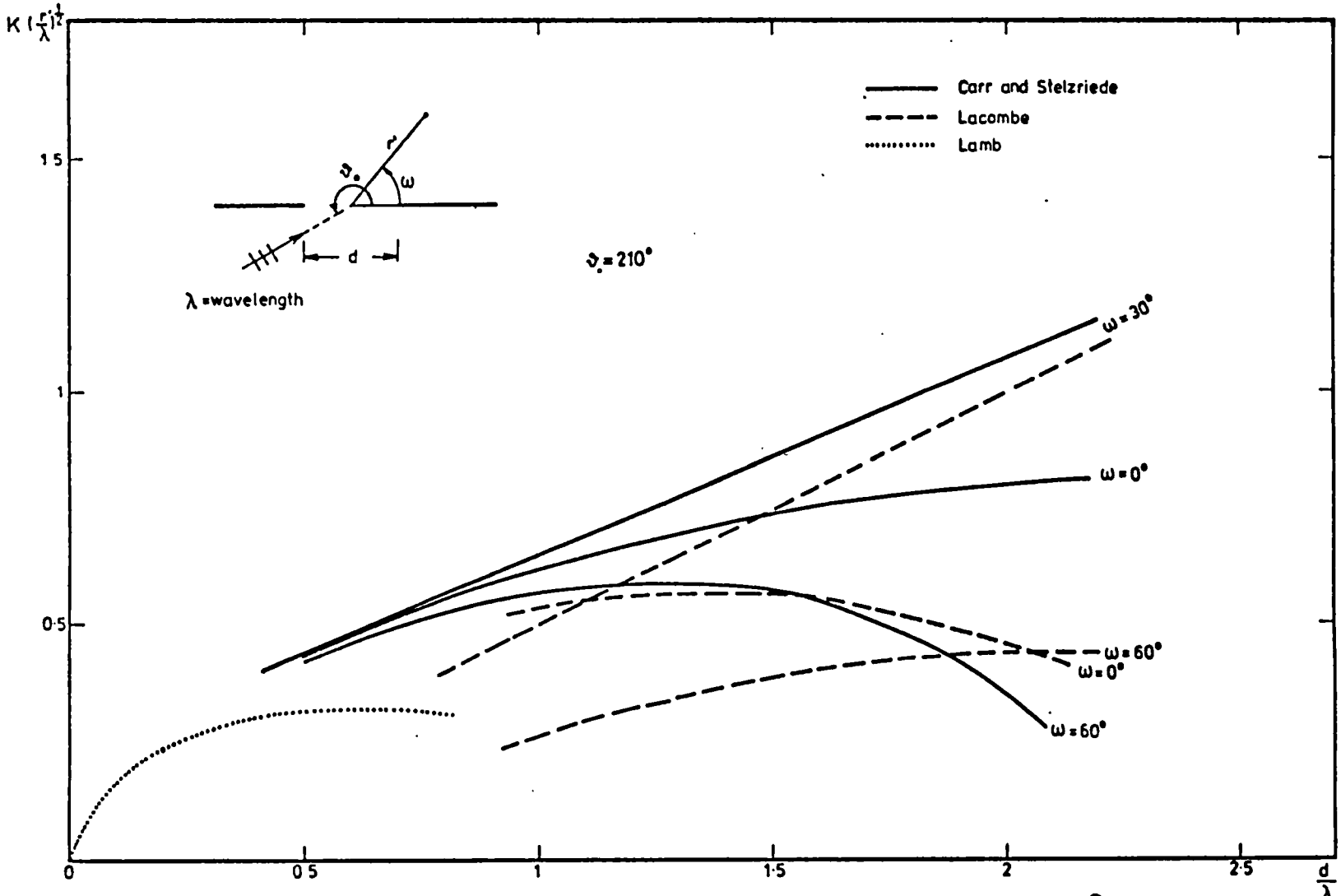

Fig. 10. Comparison of theories with respect to gap width (oblique incidence : $\vartheta_0 = 210°$)

C H A P T E R C

THEORY

C1 OUTLINE OF METHODS IN DIFFRACTION THEORY

C1.1 General Remarks

A glance through the classical diffraction theory for the scalar wave - in contrast with the vectorial wave in electromagnetism for example - will provide the starting point of our investigation that follows in section C3. Plane obstacles only are to be considered and the main methods will be outlined in this section. High frequency approximate methods that are used mainly in optics and electromagnatism having their origin in geometrical optics and the works of Fresnel are not included. A critical review of the classical diffraction theory can be found in Bouwkamp [12].

Diffraction is a subject of several branches of physics, chemistry, meteorology, engineering - the quantum-mechanical scattering processes lying beyond the limits of the classical theory, the ground of our study. Undoubtedly much credit for the new developments through use of Green's functions, integral equations etc. goes to the pioneers of electromagnetism in general and of radio technique specifically. Application to the diffraction of water waves has been carried out in acoustics, optics, electromagnetism especially in two dimensions where the results of a vector problem with a specific polarization can at once be interpreted in terms of scalar theory, by resolving the vectors in rectangular Cartesian components.

Rayleigh's first-order theory has been mentioned already (subdivision B3.1.3); it deals with the extreme case of very long waves. The opposite extreme is covered by the Kirchhoff theory

which with its various modifications is presented in section C3. Lacombe has based his method on Kirchhoff's assumptions (subdivision B3.1.2). Many attempts have been made to bridge the gap between these two extremes. Higher order approximations in Rayleigh's sense have been obtained and various versions of the Kirchhoff theory have been suggested as will be seen in subdivision C3.3.1. On the other hand the integral equation approach to diffraction problems has been widely applied in recent years; it provides the background for the numerical methods (subsection C1.4), proves the Wiener-Hopf technique to be a powerful tool for solving a class of these integral equations (C1.3) and gives birth to the variational formulation of diffraction problems (C1.2).

Consider the diffraction, in the three dimensional space, of an arbitrary incident wave $\Phi_o(x,y,z)$ through an aperture A in an infinite plane screen S of vanishing thickness coinciding with the plane $y = 0$. The field Φ_o is a solution of the reduced wave equation and is incident from the left ($y < 0$).

Our boundary value problem requires the normal derivative of the wave function to vanish on the screen; in this case the total field is given by

$$\Phi(x,y,z) = \begin{cases} \Phi_o(x,y,z) + \Phi_o(x,-y,z) - \Phi_1(x,-y,z), & y \leq 0 \\ \Phi_1(x,y,z), & y \geq 0 \end{cases} \tag{44}$$

where Φ_1, defined for $y \geq 0$ only, has the following properties:

(1) Φ_1 is a solution of the reduced wave equation
$\Delta\Phi_1 + k^2\Phi_1 = 0$ when $y > 0$.

(2) $\partial\Phi_1/\partial y = 0$ on S.

(3) Φ_1 satisfies a suitable radiation condition at infinity.

(4) $\Phi_1 = \Phi_o$ in A.

(5) Φ_1 is everywhere finite.

The above properties characterize Φ_1 completely.

A word must be said here about the radiation condition (property (3)). The requirement is that any secondary waves behave like an expanding outgoing wave at infinity, the analytical expression, due to Sommerfeld, being

$$\lim_{R\to\infty} R \left(\frac{\partial}{\partial R} - ik\right)\Phi_1 = 0 \qquad (45)$$

uniformly with respect to the polar angles for three-dimensional problems, and

$$\lim_{r\to\infty} r^{\frac{1}{2}} \left(\frac{\partial}{\partial r} - ik\right) F(r,\omega) = 0 \qquad (46)$$

uniformly with respect to ω for problems in the two-dimensions;R and r represent distance from a fixed point.
It should be pointed out that condition (45) or (46) is sufficient but not necessary, and can be replaced by weaker requirements.

The above conditions together with the rest four properties determine uniquely the required function in two or three dimensions when the obstacles lie in a bounded domain, as e.g. a vertical circular cylinder. When this is not the case the Sommerfeld conditions may not be appropriate, and we must employ a modified expression of the radiation condition applied on a part of the wave function chosen on physical grounds (as e.g. the case of a semi-infinite breakwater treated by Stoker [13]).

It is difficult, if possible at all, to determine exactly the wave function Φ_1 for an aperture of arbitrary shape. The separation technique, by which the wave equation is separated in appropriate co-ordinates, is applicable only to an elliptical aperture and an infinite slit (subsection B3.2). Numerical evaluation is cumbersome and demands extensive auxiliary tables of Mathieu functions and their generalizations such as spheroidal wave functions.

A much more powerful approach to the solution of our diffraction problems is by means of integral equations. Any solution Φ of the reduced wave equation that is regular inside a closed surface Σ can be expressed in terms of the values on Σ of either Φ or $\partial\Phi/\partial n$ if we know the corresponding Green's functions,which roughly speaking represent for a given problem the effect at any point of a fixed unit source; these are known in the case that Σ consists of an infinite plane and a half-sphere at infinity. Thus for $y \geq 0$ we have the formulas

$$\Phi = -\frac{1}{2\pi}\int \frac{\partial\Phi}{\partial n}\frac{e^{ikR}}{R}\,d\Sigma \tag{47}$$

$$\Phi = \frac{1}{2\pi}\int \Phi\frac{\partial}{\partial n}\left(\frac{e^{ikR}}{R}\right)\,d\Sigma \tag{48}$$

where the integration is over the plane $y = 0$, R denotes the distance between the field point (x,y,z) and the source point (x',y',z') and $\partial/\partial n$ means differentiation with respect to y' and then putting $y' = 0$. Φ of course must satisfy appropriate conditions at infinity.

In spite of the singularities of $\nabla\Phi_1$ at the edge it is legitimate to apply formula (47) to our function Φ_1 ; taking into account property (2) we find

$$\Phi_1 = -\frac{1}{2\pi} \int_A \frac{e^{ikR}}{R} \frac{\partial \Phi_1}{\partial n} \, d\Sigma \qquad (49)$$

Applying the property (4) we get integral equation for the unknown aperture value. If we introduce the kernel $G(x,z;x',z') =$

$$\frac{\exp\{ik[(x-x')^2 + (z-z')^2]^{\frac{1}{2}}\}}{[(x-x')^2 + (z-z')^2]^{\frac{1}{2}}}$$

we find in virtue of (49)

$$-2\pi\Phi_o(x,0,z) = \int_A \frac{\partial}{\partial y'} \Phi_1(x',0,z') G(x,z;x',z') dx'dz' \qquad (50)$$

where $(x,0,z)$ is any point of the aperture.

Other types of integral equation can be obtained if eq. (48) is applied to Φ_1 and use is made of properties (2),(4). The following differential-integral equation is thus found

$$\frac{\partial}{\partial y} \int_S \Phi_1(x',0,z') \frac{\partial}{\partial y'} G(x,z;x',z') dx'dz' \Big|_{y=0}$$

$$= -\frac{\partial}{\partial y} \int_A \Phi_o(x',0,z') \frac{\partial}{\partial y'} G(x,z;x',z) dx'dz' \Big|_{y=0} \qquad (51)$$

This is not suitable for calculations because the domain S is unbounded and eq. (50) is to be preferred (Baker and Copson [14] , p. 183). The formula corresponding to (50) for two-dimensional diffraction problems is readily obtained if it is remembered that (Watson [15] , ch. VI)

$$\int_{-\infty}^{\infty} \frac{e^{ikR}}{R} dz' = i\pi H_o(kr)$$

where $R = +[(x-x')^2 + (y-y')^2 + (z-z')^2]^{\frac{1}{2}}$,

$r = +[(x-x')^2 + (y-y')^2]^{\frac{1}{2}}$

and H_o is the Hankel function of the first kind and zeroth order. When the aperture is a simple slit of width d independent of z eq. (50) gives

$$2iF_o(x,0) = \int_{-d}^{o} H_o(k|x-x'|) \frac{\partial}{\partial y'} F_1(x',0)dx' \qquad (52)$$

in which $-d \leq x \leq 0$, and F_o, F_1 are the corresponding to Φ_o, Φ_1 two-dimensional wave functions.

C1.2 Variational Formulation

The development of variational techniques for analysis of diffraction phenomena is largely due to Schwinger. A formulation of scalar diffraction problems for plane apertures, which permits approximate but accurate numerical evaluation of the diffracted amplitude was given by Levine and Schwinger [16]. It is based on the integral equations already considered in subsection C1.1 but avoiding the need for solving the equations; this is achieved by establishing a symmetry relation of the amplitude with respect to the vectors of the observation point and the direction of propagation of the incident wave, and by proving the stationary character of an expression suitably defining the amplitude a of the waves.

From eq. (50) supposing incident plane wave

$\Phi_o = \exp\{ik(\alpha x + \beta y + \gamma z)\}$ where α, β, γ are the directional cosines, we have

$$\int_A \psi_{\alpha,\gamma}(x',0,z')G(x,z;x',z')dx'dz' = -2\exp\{\pi ik(\alpha x + \gamma z)\} \qquad (53)$$

where $\psi_{\alpha,\gamma}(x',0,z')$ is the value of $\partial\Phi_I/\partial y'$ due to the plane wave Φ_o. The amplitude of the diffracted wave in the direction (l,m,n) is therefore

$$a(l,n;\alpha,\gamma) = -\frac{1}{2\pi}\int_A \psi_{\alpha,\gamma}(x',0,x')\exp\{lx' + nz')\}dx'dz' \quad (54)$$

The amplitude is a symmetrical function of the variables (l,n) and (α,γ) as it is easily verified from eq. (54); thus

$$a(l,n;\alpha,\gamma) = a(\alpha,\gamma;l,n)$$

If we consider the variation δa produced by small variations $\delta\psi_{\alpha,\gamma}$ and $\delta\psi_{l,n}$ about the correct values $\psi_{\alpha,\gamma}$ and $\psi_{l,n}$ given by eq. (53), we find after some algebra that

$$\delta a = 0$$

Hence if

$$a(l,n;\alpha,\gamma) =$$

$$\frac{\int_A \psi_{\alpha,\gamma}(x,z)\exp\{-ik(lx+nz)\}dxdz \int_A \psi_{l,n}(x',z')\exp\{-ik(\alpha x'+\gamma z')\}dx'dz'}{\int_A\int_A \psi_{\alpha,\gamma}(x,z)\psi_{l,n}(x',z')\,G(x,z;x',z')dxdzdx'dx'} \quad (55)$$

then 'a' is stationary in the calculus of variations sense for small variations of $\psi_{\alpha,\gamma}$, $\psi_{l,n}$. We have thus proved the variational principle of Levine and Schwinger that the expression 'a' defined by eq. (55) is the required amplitude of spherical waves at a great distance behind the screen with the aperture A if and only if it is stationary for small variations of $\psi_{\alpha,\gamma}$ and $\psi_{l,n}$.

For the corresponding problem in two dimensions, i.e. a

screen with a gap of breadth d we find the corresponding to eq. (55) relation

$$a(l,\alpha) = \frac{\int_{-d}^{o} \psi_\alpha(x)\exp\{-iklx\}dx \int_{-d}^{o} \psi_1(x')\exp\{-ik\alpha x'\}dx'}{\int_{-d}^{o}\int_{-d}^{o} \psi_\alpha(x)\psi_1(x')H_o(k|x-x'|)dxdx'} \qquad (56)$$

where ψ_α, ψ_1 are the corresponding to $\psi_{\alpha,\gamma}, \psi_{1,n}$ two-dimensional values. The great value of the variational principle is that it enables us to find the amplitude approximately by assuming for ψ physically plausible expressions involving arbitrary constants and then choosing these constants to make 'a' stationary.

For a mathematical survey and criticism of variational methods in general see Dolph [17].

C1.3 Wiener-Hopf Technique

A powerful method of solving a class of diffraction problems has been developed as an extension of the original work by Wiener and Hopf [18]. The method in any of its many versions uses the customary integral transforms (Sneddon [19]) supplemented by function-theoretic techniques such as analytic continuation, Liouville's theorem, factorization of analytic functions (Titchmarsh [20]). It is now recognized that the more general method of singular integral equations of the Cauchy type (Muskhelishvili [21]) contains the Wiener-Hopf technique, which uses the Fourier transform in the complex domain, as a special case. So the whole apparatus of singular integral equations is at our disposal to achieve a solution.

To get an idea of how the technique works, a short account of it will be given as applied to the elementary problem of diffraction of a plane wave by a rigid screen (section B2).

Let the plane wave $F_o(x,y) = \exp\{-ik(x\cos\theta_o + y\sin\theta_o)\}$ impinge on the screen $x > 0$, $y = 0$. If $f(x')$ denotes the value of $\partial F/\partial y$ in the aperture, eq. (52) becomes

$$\int_{-\infty}^{o} f(x')H_o\{k|x-x'|\}dx' = 2i\exp(-ikx\cos\theta_o),\ x \leq 0 \qquad (57)$$

In order to make eq. (57) manageable by complex Fourier transforms we define the following

$$f(x') = 0,\quad x' > 0$$

$$g(x) = \begin{cases} 0 & ,\ x > 0 \\ 2i\exp\{-ikx\cos\theta_o\}, & x \leq 0 \end{cases}$$

$$h(x) = \begin{cases} \int_{-\infty}^{o} f(x')H_o\{k|x-x'|\}dx', & x > 0 \\ 0 & ,\ x \leq 0 \end{cases}$$

The extended integral equation then becomes

$$\int_{-\infty}^{\infty} f(x')H_o\{k|x-x'|\}dx' = g(x) + h(x),\quad -\infty < x < \infty \qquad (58)$$

Now, let $F^*(w)$, $G^*(w)$, $H^*(w)$ and $L^*(w)$ denote the Fourier transforms of $f(x)$, $g(x)$, $h(x)$ and $H_o(k|x|)$ respectively.

We have

$$G^*(w) = \int_{-\infty}^{\infty} g(x)\exp\{-iwx\}dx = \frac{2}{w + k\cos\theta_o}$$

where k is assumed to be complex with $\mathrm{Im}(k) > 0$ and $\mathrm{Im}(w) < -\cos\theta_o \mathrm{Im}(k)$.

Similarly,

$$L^*(w) = \int_{-\infty}^{\infty} H_o(k|x|)\exp\{-iwx\}dx = \frac{2}{(k^2 - w^2)^{\frac{1}{2}}}$$

if $-\mathrm{Im}(k) < \mathrm{Im}(w) < \mathrm{Im}(k)$

and the square root is equal to k if w = 0. Under certain assumptions of boundness and integrability of f(x) we can apply the convolution theorem (Sneddon [19], p. 60) and obtain from eq. (58)

$$F^*(w)L^*(w) = G^*(w) + H^*(w) \tag{59}$$

valid in the domain $-\mathrm{Im}(k) < \mathrm{Im}(w) < \min[0, -\cos\theta_o \mathrm{Im}(k)]$.

This can be converted easily into

$$\frac{F^*(w)}{(k-w)^{\frac{1}{2}}} - \frac{(k-k\cos\theta_o)^{\frac{1}{2}}}{w + k\cos\theta_o} = \frac{1}{2}(k + w)^{\frac{1}{2}}H^*(w) + \frac{(k + w)^{\frac{1}{2}} - (k-k\cos\theta_o)^{\frac{1}{2}}}{w + k\cos\theta_o}$$

It can be shown that either side of this equation is the analytic continuation of the other and both define one and the same entire function P(w) which easily is verified to be a constant = 0.

It thus follows that

$$F^*(w) = \frac{(k - w)^{\frac{1}{2}}(k - k\cos\theta_o)^{\frac{1}{2}}}{w + k\cos\theta_o}$$

and consequently

$$f(x) = \frac{\partial F_1}{\partial y} = \frac{1}{2\pi}\int_{-\infty}^{\infty} \frac{(k-w)^{\frac{1}{2}}(k-k\cos\theta_o)^{\frac{1}{2}}}{w + k\cos\theta_o} \exp\{iwx\}dw \tag{60}$$

where the path of integration passes below the branch point w = k and the pole $w = -k\cos\theta_o$ of the integrand.

By closing the path of integration we obtain the complete solution for $-\infty < x < \infty$; the integral in eq. (60) is expressible in

terms of Fresnel's integral which means that we rediscovered the solution of section B2.

For a complete account of the above example see Copson [22], while a slightly different approach is presented by Karp in his paper [23].

C1.4 Numerical Methods

The integral equations which were presented in subsection C1.1 have been solved exactly for a few simple scattering shapes only. For bodies of complex shape the diffraction problem can be solved numerically by dividing the scattering surface in portions over each of which the amplitude and the phase of the field can be considered as varying in an approximately known way, usually regarded as constant.

The integral equation is then replaced by a set of linear algebraic equations, to be solved numerically by a computer. Computer programmes based on this method have been developed for the study of diffraction from various structures.

The integral equation approach is the most logical one for numerical solutions because boundary and radiation conditions are automatically taken into account. The numerical method is well suited to problems in the low-frequency and resonance regions, where comparatively large facets may be taken on the object. If the dimensions of the obstacle are very large compared with the wavelength, the number of linear algebraic equations becomes very large and difficult to handle. We shall meet again this point in subsection C3.2.

The rapid expansion of the numerical methods in recent years

should be seen in connection with the powerful 'Finite Element Method' (Gallagher et al. [24]) that has been applied in many disciplines already and will certainly be used more in the future.

C2 THE WEDGE PROBLEM

C2.1 Uniqueness and Edge Conditions

A modification to Sommerfeld's radiation condition has already been hinted at in subsection C1.1 with respect to infinite bodies, so that uniqueness is achieved. It must be said that a suitable decomposition of the total field is necessary even in cases when the obstacle is bounded, in order to enable application of the radiation condition to the scattered part of the total field. I suggest that whenever the incident field is a plane wave, the radiation condition at infinity be applied on the appropriate part of the total field, subtracting any reflected wave from a plane obstacle bounded or not, as Stoker does for the infinite obstacles [13]. For a rigorous investigation of the field behaviour when the boundary conditions are given on semi-infinite domains see Jones [25].

We shall go a little further here considering obstacles with discontinuous changes of the direction of the surface normal and presenting the additional restrictions that have to be imposed so that uniqueness is ensured. The presence of an edge introduces several distinctive features; for example the radius of curvature is zero at an edge so that it does not diffract waves in the same way as the smooth surface of the obstacle.

The most striking characteristic of an edge is perhaps that a radiation condition at infinity together with the continuity of the function off the obstacle are not sufficient to ensure a unique solution of the reduced wave equation subject to the usual boundary

conditions. This can be clear by imagining for example a source at the edge, which would not violate the above conditions; hence this possibility must be formally excluded by

$$F_s \sim r^{\nu} \qquad \text{as } r \to 0$$

or $$\partial F_s/\partial r \sim r^{\nu-1} \qquad \text{as } r \to 0$$

where r is the local distance from the edge and $\nu = \pi/\theta$, θ being the exterior angle at the corner. The last condition can be written (see e.g. Leppington [26])

$$r \frac{\partial F_s}{\partial r} \to 0 \qquad \text{as } r \to 0$$

In terms of the total field $F = F_i + F_s$, (F_i : incident field), the edge conditions are

$$F \sim 1$$

and $$\frac{\partial F}{\partial r} \sim r^{\nu-1}$$

as in Stoker [13], p. 113 (where his k in (5.5.11) could be $\leq \frac{1}{2}$). For the case of a semi-infinite screen, these give

$$F \sim 1, \quad \frac{\partial F}{\partial r} \sim r^{-\frac{1}{2}}$$

The physical interpretation of these requirements is that the edge shall not radiate any energy,which has been proved by earlier investigators who assumed that the energy in any finite region (including the edge) must be finite. Another physical meaning is that the radial velocity component may be infinite at a corner, but not as strongly as it would be for a source or sink (which behaves like r^{-1}

in two dimensions).

C2.2 Diffraction of Waves by a Corner or Wedge

The diffracted field due to a line source is to be established, whence we can deduce the solution for the incident plane wave. Let the faces of a perfectly reflecting wedge occupy the semi-infinite planes $\omega = 0$ and $\omega = \theta$ the region $0 < \omega < \theta$ being free space (fig. 11). Suppose the incident field is due to a line source at $P_o(r_o,\omega_o)$, the wave function being $\frac{i}{4} H_o(kR)$, where

$R^2 = r^2 + r_o^2 - 2rr_o \cos(\omega_o - \omega)$, (r,ω) denoting always the point of observation. Then we seek a solution of the reduced wave equation

$$\frac{\partial^2 F}{\partial r^2} + \frac{1}{r}\frac{\partial F}{\partial r} + \frac{1}{r^2}\frac{\partial^2 F}{\partial \omega^2} + kF = 0 \qquad (61)$$

such that $\partial F/\partial\omega$ vanishes on the surface of the wedge, F is bounded at $r = 0$ and satisfies a radiation condition at $r \to \infty$.

A common technique of solving this problem is by making use of the Kontorovich-Lebedev transform (see Sneddon [19], ch. 6) and of the edge conditions; thus an integral representation of the scattered field is obtained (Jones [27] , p. 610). We shall not proceed along that line but we will try to find a series representation following a method by Oberhettinger [28].

With the usual notation, a solution of the reduced wave equation representing diverging waves is of the form

$$F = \frac{i}{4} \exp(\pm i\nu\omega) H_\nu(kr) \qquad (62)$$

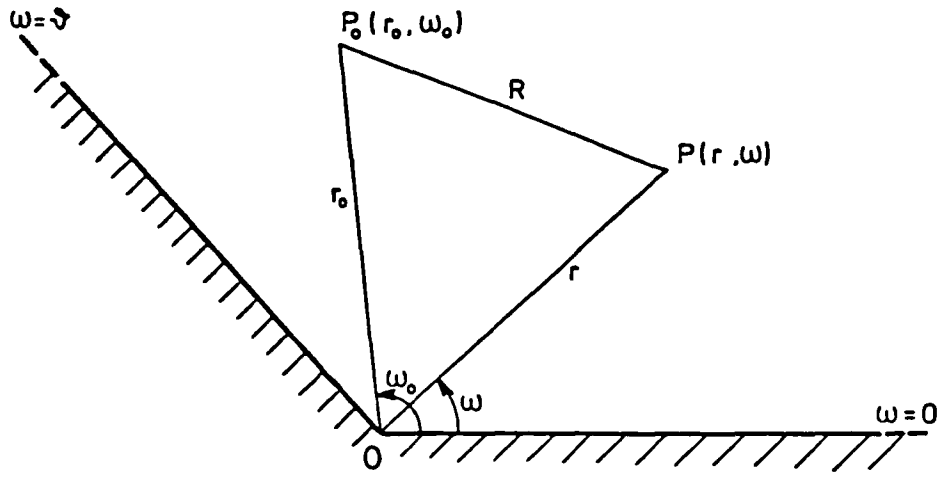

Fig. 11. Diffraction in wedge-shaped region

where ν is an arbitrary parameter. Then making the substitution

$$k = i\gamma$$

we have

$$\Delta F - \gamma^2 F = 0$$

with a particular solution corresponding to eq. (62).

$$F = \frac{i}{4} \exp(\pm i\nu\omega) K_\nu(\gamma r)$$

where K_ν denotes the modified Hankel function of the second kind

$$K_\nu(z) = \tfrac{1}{2}\pi i \exp(\tfrac{1}{2}\pi\nu i) H_\nu(iz)$$

The transition from k to γ amounts to a transition from a wave problem to an exponential decay problem. We solve first the exponential decay problem and we return to the wave problem by substituting γ with its value -ik.

The total field can be represented as the sum of the incident field F_i and the scattered field F_s:

$$F = F_i + F_s \tag{63}$$

The incident field in $P(r,\omega)$ due to the line source $P_o(r_o,\omega_o)$ is given by

$$F_i = \frac{i}{4} H_o(kR) = \frac{1}{2\pi} K_o(\gamma R) = \frac{1}{2\pi} K_o\{\gamma[r^2+r_o^2-2rr_o\cos(\omega-\omega_o)]^{\frac{1}{2}}\} \tag{64}$$

Making use of the relations (see Watson [15])

$$K_\nu(Z)K_\nu(z) = \frac{1}{2}\int_o^\infty \exp\left[-\frac{v}{2} - \frac{Z^2+z^2}{2v}\right]K_\nu\left(\frac{Zz}{v}\right)\frac{dv}{v}$$

$$K_\nu(z) = \int_o^\infty \exp(-z\cosh t)\cosh\nu t\, dt$$

$$= \frac{1}{2}(\tfrac{1}{2}z)^\nu \int_o^\infty \exp\left[-t - \frac{z^2}{4t}\right] t^{-\nu-1} dt$$

which hold under fairly general conditions, we can write eq. (64) in the form

$$F_i = \frac{1}{\pi^2}\int_o^\infty K_{i\nu}(\gamma r)K_{i\nu}(\gamma r_o)\cosh[\nu(\pi - |\omega-\omega_o|)]\,d\nu \tag{65}$$

Let the scattered field be represented in the same form

$$F_s = \frac{1}{\pi^2}\int_o^\infty K_{i\nu}(\gamma r)K_{i\nu}(\gamma r_o)[f_1(\nu)\exp(\nu\omega) + f_2(\nu)\exp(-\nu\omega)]\,d\nu \tag{66}$$

where the introduced unknown functions f_1, f_2 are to be determined by the boundary conditions. On the walls $\omega = 0$ and $\omega = \theta$ of the wedge

we have $\partial F/\partial w = 0$. This leads to

$$f_1 - f_2 = -\sinh[\nu(\pi - \omega_o)]$$
$$f_1\exp(\nu\theta) - f_2\exp(-\nu\theta) = \sinh[\nu(\pi - \theta + \omega_o)] \tag{67}$$

Equations (67) give the values of f_1, f_2 which together with eqs (63), (65) and (66) result to

$$F = \frac{1}{\pi^2}\int_o^\infty K_{i\nu}(\gamma r)K_{i\nu}(\gamma r_o)\,\frac{\sinh(\nu\pi)}{\sinh(\nu\theta)}\,\{\cosh[\nu(\theta - |\omega - \omega_o|)] +$$
$$+ \cosh[\nu(\theta - \omega - \omega_o)]\}d\nu \tag{68}$$

This expression shall now be transformed into an infinite series. For this purpose we recall the relation

$$\frac{\cosh[\nu(\theta - \phi)]}{\sin(\nu\theta)} = \frac{\nu}{\theta}\sum_{m=o}^{\infty}\varepsilon_m\,\frac{\cos\frac{m\pi\phi}{\theta}}{\nu^2+\left(\frac{m\pi}{\theta}\right)^2} \tag{69}$$

where $\varepsilon_m = 1$ for $m = 0$

$\varepsilon_m = 2$ for $m \geq 1$,

valid for $0 \leq \phi \leq 2\theta$. Term by term integration yields

$$\int_o^\infty K_{i\nu}(\gamma r)K_{i\nu}(\gamma r_o)\,\frac{\cosh[\nu(\theta-\phi)]}{\sinh(\nu\theta)}\sinh(\nu\pi)d\nu =$$

$$= \frac{1}{\theta}\sum_{m=o}^{\infty}\varepsilon_m\cos\frac{m\pi\phi}{\theta}\int_o^\infty\frac{\nu\sinh(\nu\pi)}{\nu^2+\left(\frac{m\pi}{\theta}\right)^2}K_{i\nu}(\gamma r)K_{i\nu}(\gamma r_o)d\nu$$

But if I is the modified Bessel function of the first order we have

$$\int_0^\infty \frac{\nu \sinh(\nu\pi)}{\nu^2 + \left(\frac{m\pi}{\theta}\right)^2} K_{i\nu}(\gamma r) K_{i\nu}(\gamma r_o) d\nu = \frac{1}{2}\pi^2 I_{\frac{m\pi}{\theta}}(\gamma r_<) K_{\frac{m\pi}{\theta}}(\gamma r_>)$$

where $r_<$ and $r_>$ denote the lesser and greater of the co-ordinates r and r_o. Therefore the field F can be written as

$$F = \frac{1}{2\theta} \sum_{m=o}^{\infty} \varepsilon_m \{\cos \frac{m\pi}{\theta}(\omega-\omega_o) + \cos \frac{m\pi}{\theta}(\omega+\omega_o)\} I_{\frac{m\pi}{\theta}}(\gamma r_<) K_{\frac{m\pi}{\theta}}(\gamma r_>)$$

Returning now to the wave problem by replacing γ by $-ik$ we arrive at the solution

$$F(r,\omega;r_o,\omega_o) = \frac{\pi i}{2\theta} \sum_{m=o}^{\infty} \varepsilon_m J_\mu(kr_<) H_\mu(kr_>) \cos\mu\omega \cos\mu\omega_o \qquad (70)$$

where $\mu = m\pi/\theta$

This is the wave function at the point (r,ω) in the free space of a corner of angle θ due to waves emitted by a line source at the point (r_o,ω_o); this solution holds in the domain $0 < (r,r_o) < \infty$, $0 \leq (\omega,\omega_o) \leq \theta$.

The other main expression of the same result gives different answers for the different domains of the space, seen from the point of view of geometrical optics as in the solution of the semi-infinite plane found in section B2, and allows a convenient asymptotic expansion. We are not referring to this representation because we are going to use the result in the form of eq. (70).

The behaviour of F near the edge is given by $F \propto$ constant + $+ O[(kr)^{\pi/\varepsilon}]$, as $r \to 0$ where ε is an arbitrarily small positive quantity (Felsen and Marcuvitz [29]). It can be verified that this behaviour

satisfies the edge condition of subsection C2.1.

We now proceed to derive the solution for the case of an incident plane wave. This result and its asymptotic form will help us when working along the lines of the matched asymptotic expansions method in section C5. First we establish a normalization factor for the passing from the line source to the plane wave.

The field at the point (r,ω) due to a line source of unit strength at (r_o,ω_o) in free space is

$$\frac{i}{4} H_o(kR)$$

where $R = +[r^2 + r_o^2 - 2rr_o\cos(\omega-\omega_o)]^{\frac{1}{2}}$

The large-argument approximation for the Hankel function is

$$H_o(kR) \sim \sqrt{\frac{2}{\pi kR}}\, e^{i(kR-\frac{1}{4}\pi)} \qquad \text{for } kR \to \infty$$

Now, as r_o tends to infinity the circular waves of the line source tend to a plane wave. We obtain upon expansion by the binomial theorem

$$R \sim r_o - r\cos(\omega-\omega_o) + O\left(\frac{1}{r_o}\right), \qquad r_o \to \infty$$

For the determination of the amplitude it is sufficient to approximate R by r_o as r_o becomes very large. However, for the determination of the phase we can neglect only those terms which tend to zero as $r_o \to \infty$, i.e. terms of $O\left(\frac{1}{r_o}\right)$. The expression for the field at (r,ω) due to plane wave can be written now

$$\frac{i}{4}\sqrt{\frac{2}{kr_o}}\exp[i(kr_o - kr\cos(\omega-\omega_o) - \tfrac{1}{4}\pi)]$$

and which must be identical with the term $\exp[-ikr\cos(\omega-\omega_o)]$

representing a plane wave of unit amplitude incident along the direction ω_o. Comparing the two expressions we find the normalization factor

$$N = \frac{1}{4}\sqrt{\frac{2}{\pi k r_o}}\exp[i(kr_o + \tfrac{1}{4}\pi)] \tag{71}$$

Thus, to pass from a result derived for a line source of unit strength located at (r_o,ω_o) to the result for a plane wave of unit amplitude incident from the direction ω_o, we first let $r_o \to \infty$ and then set N = 1.

Returning now to the original result of eq. (70) we let $r_o \to \infty$, $\omega_o = \theta_o$ and derive the result for excitation by an incident plane wave $\exp[-ikr\cos(\omega-\theta_o)]$. Since $J_\mu(kr_<)$ decays when $\mu > kr_<$ the contributing range of the series is bounded in μ and negligible error is introduced through use of the asymptotic approximation of the Hankel function

$$H(kr_o) \sim \sqrt{\frac{2}{\pi k r_o}}\exp[i(kr_o - \tfrac{1}{2}\mu\pi - \tfrac{1}{4}\pi)]$$

Imposition of condition (71) yields the following expression for the wave function

$$F(r,\omega;\theta_o) = \frac{2\pi}{\theta}\sum_{m=o}^{\infty}\varepsilon_m J_\mu(kr)\cos\mu\omega\,\cos\mu\theta_o\, e^{-\frac{1}{2}i\mu\pi} \tag{72}$$

with $\mu = m\pi/\theta$

This is the result that we are seeking for the case of plane incidence.

Some approximate expansions of this relation might be useful for further reference (see section C5). If $kr << 1$ a small-argument expansion of the Bessel functions in eq. (72) gives

$$F \sim \frac{2\pi}{\theta} + \frac{4}{\Gamma\left(\frac{\pi}{\theta}\right)} (\tfrac{1}{2}kr)^{\pi/\theta} \exp(-\tfrac{1}{2}i\pi^2/\theta)\cos\frac{\pi\omega}{\theta}\cos\frac{\pi\theta_o}{\theta} + O[(kr)^{2\pi/\theta}] \tag{73}$$

for $\theta > \pi$ and $\Gamma(x)$ the gamma function

$$= \int_o^\infty e^{-t} t^{x-1} dt = \lim_{n\to\infty} \frac{n!n^x}{x(x+1)(x+2)\ \ldots\ (x+n)} \quad \text{for } x \neq 0,-1,-2,\ldots$$

We can also write the relevant expression for $kr >> 1$ (Felsen and Marcuvitz [29], ch. 6) decomposing the total field into two components

$$F = F_{g.o.} + F_d \tag{74}$$

where $F_{g.o.}$ and F_d are the geometrical optics and diffracted fields respectively. The geometrical optics field is

$$F_{g.o.} = \sum_{n_1} \exp(ikr\cos\alpha_{n_1}) + \sum_{n_2} \exp(ikr\cos\theta_{n_2}) \tag{75}$$

where $\alpha_{n_1} = \pi - \omega + \theta_o - 2n_1\theta$

$$\alpha_{n_2} = \pi - \omega - \theta_o - 2n_2\theta$$

and the summations extend over all integers n_1 and n_2 satisfying the inequalities

$$|\omega - \theta_o + 2n_1\theta| < \pi \qquad |\omega + \theta_o + 2n_2\theta| < \pi$$

The diffracted field F_d can be written

$$F_d = V_d(-\pi - \omega + \theta_o) - V_d(\pi - \omega + \theta_o) + V_d(-\pi - \omega - \theta_o) -$$

$$- V_d(\pi - \omega - \theta_o) \tag{76}$$

with

$$V_d(\beta) = \frac{1}{2\theta}\int_0^\infty \exp(ikr\cosh t)\,\frac{\sin\frac{\beta\pi}{\theta}}{\cosh\frac{t\pi}{\theta}-\cos\frac{\beta\pi}{\theta}}\,dt$$

For values of β away from a geometrical optics boundary we can expand F_d in eq. (76) and from the leading term in this expansion we get

$$F_d \sim \frac{\exp[i(kr+\frac{1}{4}\pi)]}{(2\pi kr)^{\frac{1}{2}}}\,\frac{\pi}{\theta}\sin\frac{\pi^2}{\theta}\left[\frac{1}{\cos\frac{\pi^2}{\theta}-\cos\frac{(\omega-\theta_o)\pi}{\theta}}+\frac{1}{\cos\frac{\pi^2}{\theta}+\cos\frac{(\theta-\omega-\theta_o)\pi}{\theta}}\right] \tag{77}$$

This has the appearance of a cylindrical wave emanating from the edge.

On the geometrical optics boundaries the total field has the following asymptotic representations ($\theta > \pi$)

(i) $\omega = \pi - \theta_o$ with $0 < \theta_o < \pi$

$$F \sim \exp\{ikr\cos 2\theta_o\} + \tfrac{1}{2}\exp(ikr) + \frac{\pi}{\theta}\frac{\exp[i(kr+\frac{1}{4}\pi)]}{(2\pi kr)^{\frac{1}{2}}}\times$$

$$\times\left[\frac{\sin\frac{\pi^2}{\theta}}{\cos\frac{\pi^2}{\theta}+\cos\frac{(\pi+\theta-2\theta_o)\pi}{\theta}}-\frac{1}{2}\cot\frac{\pi^2}{v}\right] \tag{78}$$

(ii) $\omega = 2\theta - \theta_o - \pi$ with $\theta-\pi < \theta_o < \theta$

$$F \sim \exp\{ikr\cos 2(\theta_o-\theta)\} + \tfrac{1}{2}\exp(ikr) + \frac{\pi}{\theta}\frac{\exp[i(kr+\frac{1}{4}\pi)]}{(2\pi kr)^{\frac{1}{2}}}\times$$

$$\times\left[\frac{\sin\frac{\pi^2}{\theta}}{\cos\frac{\pi^2}{\theta}+\cos\frac{(\pi-\theta+2\theta_o)\pi}{\theta}}-\frac{1}{2}\cot\frac{\pi^2}{\theta}\right] \tag{79}$$

(iii) $\omega = \pi + \theta_o$ with $0 < \theta_o < \theta - \pi$

$$F \sim \tfrac{1}{2}\exp(ikr) + \frac{\pi}{\theta}\frac{\exp[i(kr+\frac{1}{4}\pi)]}{(2\pi kr)^{\frac{1}{2}}}\left[\frac{\sin\frac{\pi^2}{\theta}}{\cos\frac{\pi^2}{\theta}+\cos\frac{(\pi+2\theta_o-\theta)\pi}{\theta}}-\right.$$

$$\left.-\frac{1}{2}\cot\frac{\pi^2}{\theta}\right] \tag{80}$$

C3 THEORETICAL INVESTIGATION

C3.1 Combination of two Independent Solutions

As we have already seen in subdivision B3.1.1 an approximate solution for a problem with two breakwaters can be derived from the rigorous solution of the problem of one semi-infinite breakwater. Thus Penney and Price have given such a solution for the case of two screens in line with a gap between them and an incident wave normal to the screens [3]. Their method is based on a combination of the known results of the two independent semi-infinite breakwaters. The approximation achieved is reasonable for application purposes when the gap is greater than about one or two wavelengths for normal incidence.

An extension of this method is attempted in this subsection to cover the case of breakwaters not in line which is our final objective. Remembering the general solution of the diffraction of plane waves incident on a semi-infinite rigid breakwater (eq. (13)) we can write the equations corresponding to the regions S,Q,R (fig. 2) so that the appropriate expressions representing the incident and reflected wave are present when necessary. We denote these waves for simplicity by (inc) and (ref) respectively, being

$$(\text{inc}) = \exp[-ikr\cos(\omega-\theta_o)]$$

$$(\text{ref}) = \exp[-ikr\cos(\omega+\theta_o)]$$

and consequently we have

Region S

$$F(r,\omega) = \frac{1-i}{2}\,(\text{inc}) \int_{-\infty}^{u_1} \exp\{\tfrac{1}{2}\pi i u^2\}du + \frac{1-i}{2}\,(\text{ref}) \int_{-\infty}^{u_2} \exp\{\tfrac{1}{2}\pi i u^2\}du$$

Region Q

$$F(r,\omega) = (\text{inc}) - \frac{1-i}{2}(\text{inc}) \int_{-\infty}^{-u_1} \exp\{\tfrac{1}{2}\pi i u^2\}du +$$

$$+ \frac{1-i}{2}(\text{ref}) \int_{-\infty}^{u_2} \exp\{\tfrac{1}{2}\pi i u^2\}du$$

Region R

$$F(r,\omega) = (\text{inc}) + (\text{ref}) - \frac{1-i}{2}(\text{inc}) \int_{-\infty}^{-u_1} \exp\{\tfrac{1}{2}\pi i u^2\}du -$$

$$- \frac{1-i}{2}(\text{ref}) \int_{-\infty}^{-u_2} \exp\{\tfrac{1}{2}i u^2\}du$$

making use of the property of the Fresnel integrals

$$\int_{-\infty}^{u} \exp\{\tfrac{1}{2}\pi i t^2\}dt + \int_{-\infty}^{-u} \exp[\tfrac{1}{2}\pi i t^2]dt = 1 + i$$

When two breakwaters are present we can write a similar set of equations corresponding to the second plate (2), see fig. 12.

Region s

$$F(r,\omega) = \frac{1-i}{2}(\text{inc})' \int_{-\infty}^{u_1'} \exp\{\tfrac{1}{2}\pi i u^2\}du + \frac{1-i}{2}(\text{ref})' \int_{-\infty}^{u_2'} \exp\{\tfrac{1}{2}\pi i u^2\}du$$

Region q

$$F(r,\omega) = (\text{inc})' - \frac{1-i}{2}(\text{inc})' \int_{-\infty}^{-u_1'} \exp\{\tfrac{1}{2}\pi i u^2\}du +$$

$$+ \frac{1-i}{2}(\text{ref})' \int_{-\infty}^{u_2'} \exp\{\tfrac{1}{2}\pi i u^2\}du$$

Region r

$$F(r,\omega) = (\text{inc})' + (\text{ref})' - \frac{1-i}{2}(\text{inc})' \int_{-\infty}^{-u_1'} \exp\{\tfrac{1}{2}\pi i u^2\}du -$$

$$- \frac{1-i}{2}(\text{ref})' \int_{-\infty}^{-u_2'} \exp\{\tfrac{1}{2}\pi i u^2\}du$$

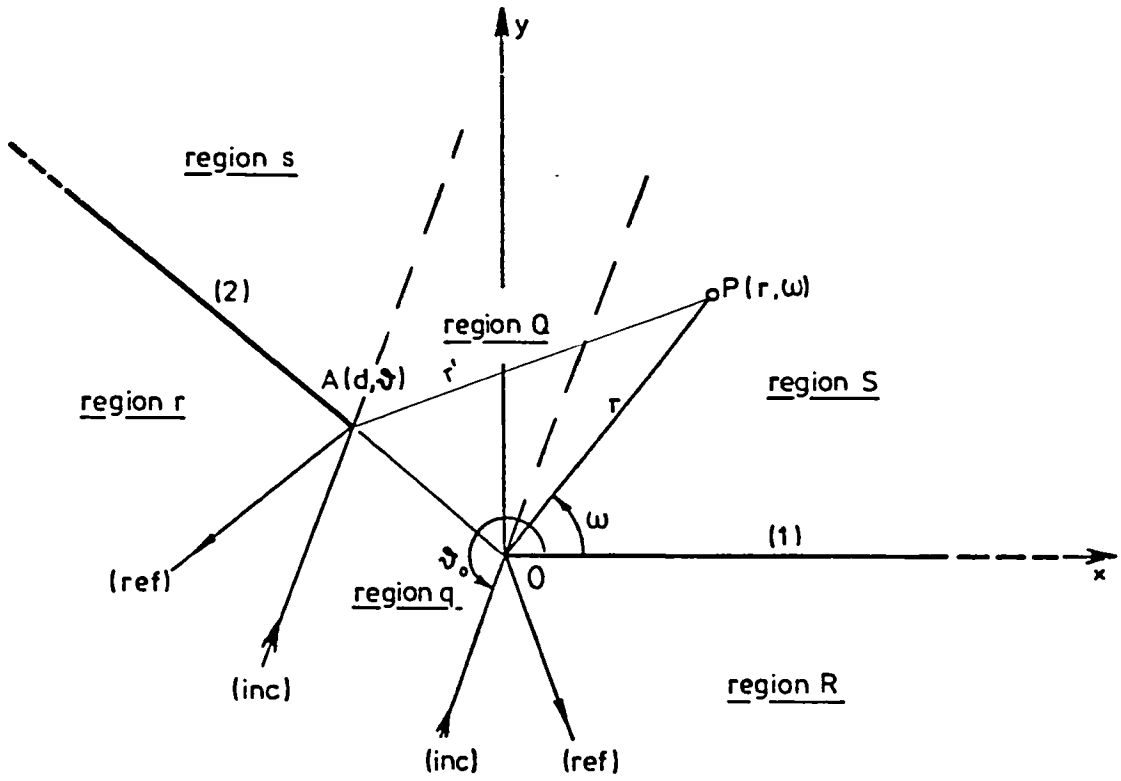

Fig. 12. Two 'independent' breakwaters inclined to each other

where $(inc)' = \exp\{-ikr'\cos(\omega-\theta_o)\}$

$(ref)' = \exp\{-ikr'\cos(\omega+\theta_o-2\theta)\}$

$$u'_1 = 2\left(\frac{kr'}{\pi}\right)^{\frac{1}{2}} \cos\frac{\omega-\theta_o}{2}$$

$$u'_2 = 2\left(\frac{kr'}{\pi}\right)^{\frac{1}{2}} \cos\frac{\omega+\theta_o-2\theta}{2}$$

and

$$r' = +[r^2 + d^2 - 2rd\cos(\theta-\omega)]^{\frac{1}{2}}$$

Following the method of subdivision B3.1.1 we find for the five regions of fig. 12 the compound solution:

Region S

$$F(r,\omega) = (inc)f(u_1) + (ref)f(u_2) - (inc)'f(-u_1') + (ref)'f(u_2')$$

Region R

$$F(r,\omega) = (inc) + (ref) - (inc)f(-u_1) - (ref)f(-u_2) -$$
$$- (inc)'f(-u_1') + (ref)'f(u_2')$$

Region s

$$F(r,\omega) = (inc)'f(u_1') + (ref)'f(u_2') - (inc)f(-u_1) + (ref)f(u_2)$$

Region r

$$F(r,\omega) = (inc)' + (ref)' - (inc)'f(-u_1') - (ref)'f(-u_2') -$$
$$- (inc)f(-u_1) + (ref)f(u_2)$$

Region $q \cap Q$

$$F(r,\omega) = (inc) - (inc)f(-u_1) + (ref)f(u_2) - (inc)'f(-u_1') +$$
$$+ (ref)'f(u_2')$$

where

$$f(x) = \frac{1-i}{2} \int_{-\infty}^{x} \exp\{\tfrac{1}{2}\pi i u^2\} du \qquad (81)$$

The question of the accuracy of this solution arises now. Disregarding for the moment breakwater (2) we shall try to find the deviation from the boundary condition $\frac{1}{r}\frac{\partial F}{\partial \omega} = 0$ along the unoccupied line $r > d$, $\omega = \theta$, of the wave field caused by the presence of breakwater (1). Equation (13) gives easily

$$\frac{\partial F}{\partial \omega} = f(u_1)\frac{\partial}{\partial \omega}(inc) + (inc)\frac{\partial}{\partial \omega}f(u_1) + f(u_2)\frac{\partial}{\partial \omega}(ref) +$$
$$+ (ref)\frac{\partial}{\partial \omega}f(u_2) \qquad (82)$$

But,

$$\frac{\partial}{\partial\omega}(\text{inc}) = (\text{inc})\ ikr\sin(\omega-\theta_o)$$

$$\frac{\partial}{\partial\omega}(\text{ref}) = (\text{ref})\ ikr\sin(\omega+\theta_o)$$

$$(1+i)\frac{\partial}{\partial\omega}f(u_1) = \exp\{\tfrac{1}{2}\pi i u_1^2\}\frac{\partial u_1}{\partial\omega} = -\left(\frac{kr}{\pi}\right)^{\frac{1}{2}}\sin\frac{\omega-\theta_o}{2}\exp\{2ikr\cos^2\frac{\omega-\theta_o}{2}\}$$

$$(1+i)\frac{\partial}{\partial\omega}f(u_2) = \exp\{\tfrac{1}{2}\pi i u_2^2\}\frac{\partial u_2}{\partial\omega} = -\left(\frac{kr}{\pi}\right)^{\frac{1}{2}}\sin\frac{\omega+\theta_o}{2}\exp\{2ikr\cos^2\frac{\omega+\theta_o}{2}\}$$

Equation (82) becomes

$$\frac{1}{r}\frac{\partial F}{\partial\omega} = (\text{inc})ik\sin(\omega-\theta_o)f(u_1) - \frac{1-i}{2}(\text{inc})\left(\frac{k}{\pi r}\right)^{\frac{1}{2}}\sin\frac{\omega-\theta_o}{2}\exp\{2kir\cos^2\frac{\omega-\theta_o}{2}\} +$$

$$+ (\text{ref})ik\sin(\omega+\theta_o)f(u_2) - \frac{1-i}{2}(\text{ref})\left(\frac{k}{\pi r}\right)^{\frac{1}{2}}\sin\frac{\omega+\theta_o}{2}\exp\{2ikr\cos^2\frac{\omega+\theta_o}{2}\} \qquad (83)$$

Keeping the same approximation that has been introduced by Penney and Price [3], which has been proved to be good for engineering purposes, we can substitute the integrals in eq. (83) by the leading terms of their expansion

$$\int_{-\infty}^{x}\exp\{\tfrac{1}{2}\pi i u^2\}du \sim -\frac{i}{\pi x}\exp\{\tfrac{1}{2}\pi i x^2\} + \ldots \qquad (84)$$

We find

$$(1+i)f(u_1) \sim -\frac{i\exp\{2ikr\cos^2\frac{\omega-\theta_o}{2}\}}{2(\pi kr)^{\frac{1}{2}}\cos\frac{\omega-\theta_o}{2}}, \qquad \text{and}$$

$$(1+i)f(u_2) \sim -\frac{i\exp\{2ikr\cos^2\frac{\omega+\theta_o}{2}\}}{2(\pi kr)^{\frac{1}{2}}\cos\frac{\omega+\theta_o}{2}}$$

Putting these values in eq. (83) we have

$$(1+i)\frac{1}{r}\frac{\partial F}{\partial \omega} = \frac{1}{2}(inc)\frac{\sin(\omega-\theta_o)}{\cos\frac{\omega-\theta_o}{2}}\left(\frac{k}{\pi r}\right)^{\frac{1}{2}}\exp\{2ikrcos^2\frac{\omega-\theta_o}{2}\} -$$

$$- (inc)\sin\frac{\omega-\theta_o}{2}\left(\frac{k}{\pi r}\right)^{\frac{1}{2}}\exp\{2ikrcos^2\frac{\omega-\theta_o}{2}\} +$$

$$+\frac{1}{2}(ref)\frac{\sin(\omega+\theta_o)}{\cos\frac{\omega+\theta_o}{2}}\left(\frac{k}{\pi r}\right)^{\frac{1}{2}}\exp\{2ikrcos^2\frac{\omega+\theta_o}{2}\} -$$

$$- (ref)\sin\frac{\omega+\theta_o}{2}\left(\frac{k}{\pi r}\right)^{\frac{1}{2}}\exp\{2ikrcos^2\frac{\omega+\theta_o}{2}\}$$

$$= 0$$

To obtain an adequate level of accuracy —diffraction coefficient to within about 2% as stated at the derivation of eq. (25)— we require for the expansion (84)

$$x < -2$$

which gives the following conditions

$$\cos\frac{\omega-\theta_o}{2} < -\left(\frac{1}{2\delta}\right)^{\frac{1}{2}}$$

$$\cos \frac{\omega+\theta_o}{2} < -\left(\frac{1}{2\delta}\right)^{\frac{1}{2}}$$

where $\delta = d/\lambda$, d being the smallest value of r. It is clear that the first of these two conditions contains the second, and it can be rewritten

$$\delta_{min} > \frac{1}{2\cos^2 \frac{(\theta_o-\omega)}{2}} \tag{85}$$

The above relation is represented graphically in fig.13 where we can see that we have to have large gaps for large angles $\theta_o-\omega$ in order to keep our fixed level of accuracy. I have drawn out of fig. 13 two simplified graphs keeping constant on the one the angle θ_o and on the other the angle ω; these graphs are presented in figs 14 and 15. It is evident now that this method of adding two independent solutions is inadequate for situations other than close to that described by $\omega = 180^o$, $\theta_o = 270^o$ which is the case dealt with in subdivision B3.1.1.

To improve this method we attempt a step which is presented in the rest of this subsection. The idea is to add a quantity to correct the boundary conditions on the breakwater arm where they are not satisfied. This will disturb the conditions at the other arm entailing a further addition and so on until the approximation to the boundary conditions obtained is acceptable. Then by knowing these extra quantities we could derive the whole field.

Let F be the basic solution produced by addition of two independent solutions as found above. In general $\frac{1}{r}\frac{\partial F}{\partial \omega}\Big|_{(2)} \neq 0$

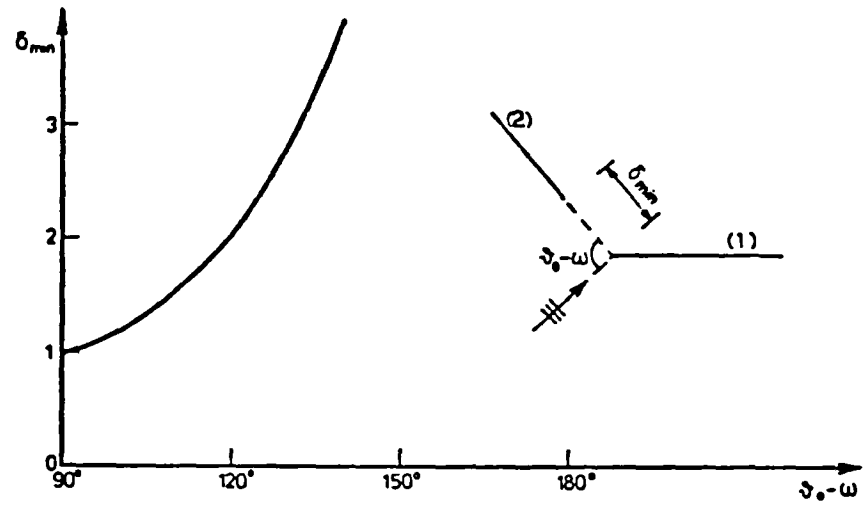

Fig. 13. Relation between $\vartheta_0 - \omega$ and δ_{min} for a given accuracy

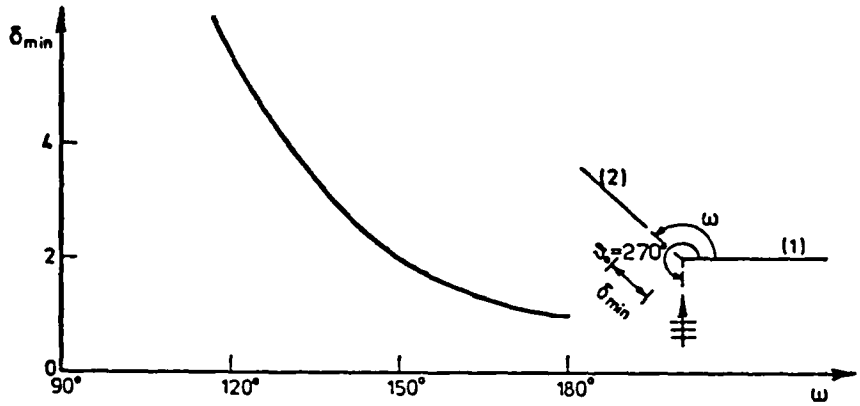

Fig. 14. Relation between ω and δ_{min} for $\vartheta_0 = 270°$

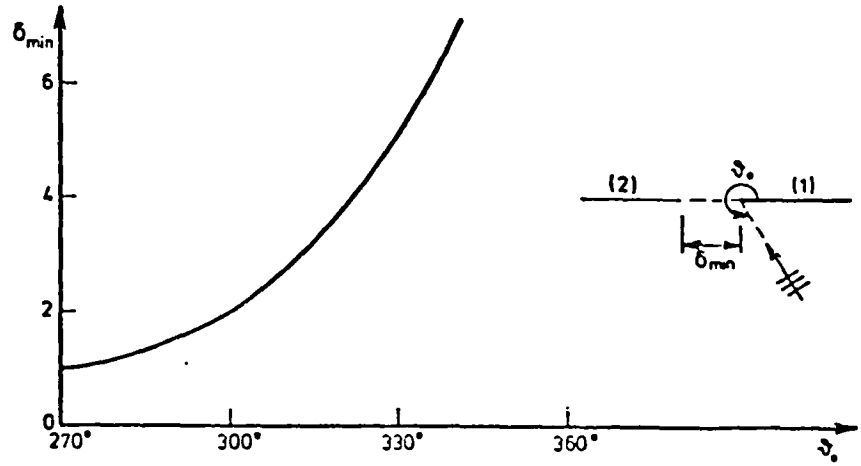

Fig. 15. Relation between ϑ_0 and δ_{min} for $\omega = 180°$

where the subscript (2) denotes evaluation of the differential along the screen (2). We introduce a 'boundary function' $G_1(r,\omega)$ defined along (2) such that

$$\frac{1}{r}\frac{\partial}{\partial\omega}(F + G_1)\Big|_{(2)} = 0$$

and we try to evaluate the effect that G_1 has on the boundary conditions of (1); if this effect be denoted by $G_1^{(1)}$ we have

$$\frac{1}{r}\frac{\partial}{\partial\omega}(F + G_1^{(1)})\Big|_{(1)} \neq 0$$

generally, and we introduce a similar function $G_2(r,\omega)$ defined along (1) with effect $G_2^{(2)}$ on (2) so that

$$\frac{1}{r}\frac{\partial}{\partial\omega}(F + G_1^{(1)} + G_2)\Big|_{(1)} = 0 \quad , \quad \text{but}$$

$$\frac{1}{r}\frac{\partial}{\partial\omega}(F + G_1 + G_2^{(2)})\Big|_{(2)} \neq 0 \quad ,$$

We repeat the same procedure until the truncation errors

$$\frac{1}{r}\frac{\partial}{\partial\omega}(F + G_1 + G_2^{(2)} + \ldots)\Big|_{(2)} - 0 = \varepsilon_1 \qquad \text{and}$$

$$\frac{1}{r}\frac{\partial}{\partial\omega}(F + G_1^{(1)} + G_2 + \ldots)\Big|_{(1)} - 0 = \varepsilon_2$$

are acceptable. Then our solution will be

$$F + g_1 + g_2 + \ldots = F + \sum_i g_i$$

where g_i denotes the field produced by a 'boundary function' G_i.

Although this method is simple in principle, it raises difficult problems when we come to actually finding the effects $G_i^{(n)}$, [(n) = (1) or (2)] on the boundaries of the producing functions G_i, or generally when calculating the fields g_i. The difficulty arises from the fact that G_1, G_2, etc. are no longer plane waves or any other simple form of wave but a wave continuously decaying with increasing r which has to be approximated by an appropriate series of discrete line sources along the appropriate boundary or even by a sum of suitably chosen plane waves. Then the effect of this approximate 'boundary function' can be represented by the addition of known solutions for the diffraction of a line source or of a plane wave by a half-plane. The former is a special case of eq. (70) for $\theta = 2\pi$,

$$F(r,\omega;r_o,\omega_o) = \frac{i}{4}\sum_{m=o}^{\infty}\varepsilon_m J_{\frac{m}{2}}(kr_<)H_{\frac{m}{2}}(kr_>)\cos\frac{m\omega}{2}\cos\frac{m\omega_o}{2}$$

where the latter is express in eq. (13).

The transformation of the 'boundary functions' into line sources or plane waves may be achieved through the following relations (Watson [15]).

$$\int_o^u \exp\{\tfrac{1}{2}\pi t^2\}dt = \sum_{n=o}^{\infty} J_{2n+\frac{1}{2}}(\tfrac{1}{2}\pi t^2) + i\sum_{n=o}^{\infty} J_{2n+\frac{3}{2}}(\tfrac{1}{2}\pi t^2)$$

$$= \frac{\sqrt{2}}{2}\left[\exp\{\tfrac{1}{4}i\pi\} + \exp\{\tfrac{1}{2}i\pi u^2\}[V_{\frac{1}{2}}(\pi u^2,0) - iV_{\frac{1}{2}}(\pi u^2,0)]\right]$$

where

$$V_{\frac{1}{2}}(2z,0) \sim -\left(\frac{4z}{\pi}\right)^{\frac{1}{2}}\left[\frac{1}{(2z)^2} - \frac{1.3.5}{(2z)^4} + \ldots\right]$$

$$V_{\frac{1}{2}}(2z,0) \sim \left(\frac{4z}{\pi}\right)^{\frac{1}{2}}\left[\frac{1}{2z} - \frac{1.3}{(2z)^3} + \frac{1.3.5.7}{(2z)^5} - \ldots\right]$$

and

$$e^x \sim 1 + x + \frac{x^2}{2!} + \frac{x^3}{3!} + \ldots$$

The apparently complicated and extensive calculations involved in the above procedure coupled with the need for repetition of these manipulations as we proceed further to approximate more closely the boundary conditions, suggest that we seek a formulation where the solution $F + \sum_i g_i$ is contained implicitly in the equations. We thus arrive at solving a pair of simultaneous integral equations following a method used by Schwarzschild [30] and presented in the following subsection.

C3.2 Schwarzschild's Diffraction Problem

The difficulty encountered in the preceding subsection is overcome at least partially, if we suppose for the moment that we know the solution we are trying to find and form our equations in terms of the final steady state potential of the scattered wave F_s. The problem that was investigated first along these lines (Schwarzschild [30]) was that of diffraction of waves by two screens on the same plane, a relatively simpler configuration than that which we are considering here due to the fact that the former has a symmetry in its geometry which the latter lacks. However an attempt is made here to apply the same principles in our case following the

presentation by Baker and Copson [14].

Let us consider our two perfectly reflecting breakwaters (1) and (2) obstructing the free propagation of an incident plane wave F_o. We seek a solution F_s of the Helmholtz equation (8) or (10) such that it has no singularities outside (1) and (2), satisfies the radiation condition and the normal derivative $\frac{\partial}{\partial n}(F_o + F_s)$ vanishes on both screens. Then our solution would be $F = F_o + F_s$ everywhere. On an horizontal plane the two plates are considered to be bounded by two closed lines ℓ_1, ℓ_2 as in fig. 16.

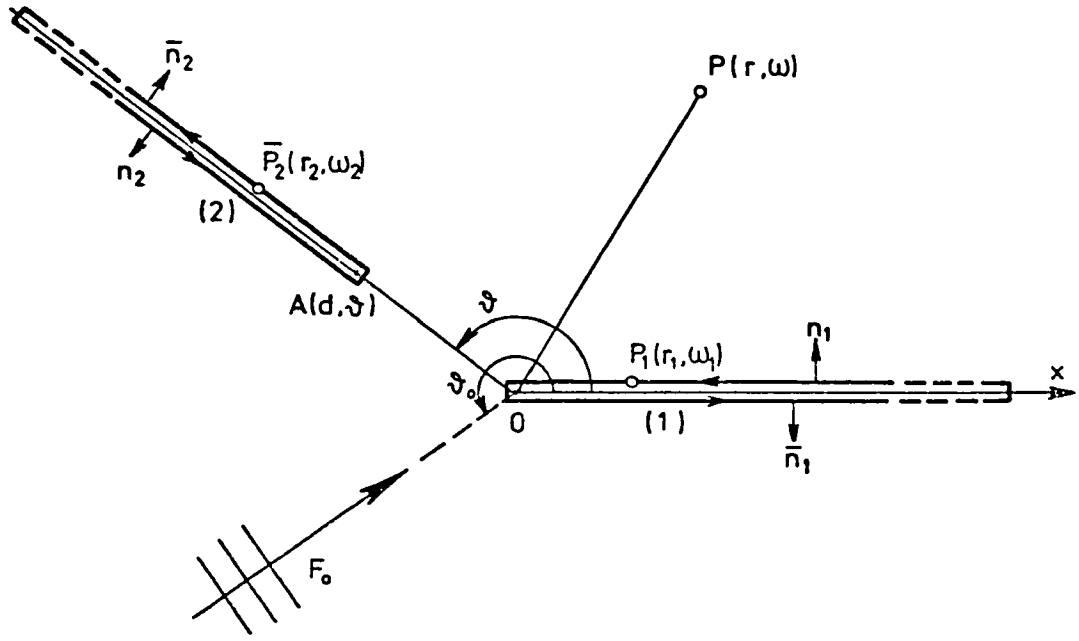

Fig. 16. Nomenclature of Schwarzschild's problem

As will be seen in subdivision C3.3.1 a solution f of the Helmholtz equation is uniquely determined by the values of its normal derivatives on either (1) or (2); a fact that has already been used in eq. (47). We have accordingly

$$f(r,\omega) = -\int_{\ell_1} \frac{\partial}{\partial \nu_1} f(r_1,\omega_1) G_{(1)}(r_1,\omega_1;r,\omega) d\ell_1 \qquad (86)$$

or

$$f(r,\omega) = -\int_{\ell_2} \frac{\partial}{\partial \nu_2} f(r_2,\omega_2) G_{(2)}(r_2,\omega_2;r,\omega) d\ell_2 \qquad (87)$$

where we have put for simplicity $\partial/\partial\nu_1 = \partial/\partial n_1$ or $\partial/\partial\bar{n}_1$, $\partial/\partial\nu_2 = \partial/\partial n_2$ or $\partial/\partial\bar{n}_2$ depending on the position of the point of integration on the contours ℓ_1, ℓ_2,

with n_1, $\bar{n}_1$ and n_2, $\bar{n}_2$ the normal directions to ℓ_1 and ℓ_2 respectively (fig. 16); $P_1(r_1,\omega_1)$, $P_2(r_2,\omega_2)$ points on ℓ_1, ℓ_2 and $G_{(1)}, G_{(2)}$ the Green's functions for the regions outside ℓ_1, ℓ_2 respectively.

Now, we consider the potential F_s to be the sum of two functions F_1 and F_2, not in general independent, satisfying the pair of equations

$$F_1(r,\omega) = +\int_{\ell_2} \frac{\partial}{\partial \nu_2} \{F_2 + F_o\}(r_2,\omega_2) G_{(2)}(r_2,\omega_2;r,\omega) d\ell_2 \qquad (88)$$

$$F_2(r,\omega) = +\int_{\ell_1} \frac{\partial}{\partial \nu_1} \{F_1 + F_o\}(r_1,\omega_1) G_{(1)}(r_1,\omega_1;r,\omega) d\ell_1 \qquad (89)$$

This assumption is legitimate because the function $F_s = F_1 + F_2$ satisfies all the requirements of the problem. Indeed it is a solution of the Helmholtz equation, it satisfies the radiation condition and it has no singularities outside ℓ_1 and ℓ_2; for each of its terms by assumption is a solution of $(\Delta + k^2)F = 0$ and satisfies the radiation condition while the sum of them has no singularities outside ℓ_1 and ℓ_2. Moreover by comparing eqs (87) and (88) we see that

$$-\frac{\partial}{\partial \nu_2} F_1(r_2,\omega_2) = \frac{\partial}{\partial \nu_2} F_2(r_2,\omega_2) + \frac{\partial}{\partial \nu_2} F_o(r_2,\omega_2)$$

so that the normal derivative of $F_o + F_1 + F_2 = F_o + F_s = F$

vanishes on (2); similarly we find by comparing eqs (86) and (89)

$$-\frac{\partial}{\partial \nu_1} F_2(r_1,\omega_1) = \frac{\partial}{\partial \nu_1} F_1(r_1,\omega_1) + \frac{\partial}{\partial \nu_1} F_o(r_1,\omega_1)$$

which means that our requirement $\frac{\partial}{\partial \nu_1} F(r_1,\omega_1) = 0$ is satisfied.

Equations (88) and (89) involve four unknown functions, namely $F_1(P)$, $F_2(P)$, $\frac{\partial}{\partial \nu_1} F_1(P_1)$, $\frac{\partial}{\partial \nu_2} F_2(P_2)$; to overcome this difficulty we let point P on breakwater (1) for eq. (88) and on (2) for eq. (89) and take the corresponding normal derivative:

$$\frac{\partial}{\partial \nu_1} F_1(P_1) = \int_{\ell_2} \frac{\partial}{\partial \nu_2} \{F_2 + F_o\}(P_2) \frac{\partial}{\partial \nu_1} G_{(2)}(P_2,P_1) d\ell_2 \quad (90)$$

$$\frac{\partial}{\partial \nu_2} F_2(P_2) = \int_{\ell_1} \frac{\partial}{\partial \nu_1} \{F_1 + F_o\}(P_1) \frac{\partial}{\partial \nu_2} G_{(1)}(P_1,P_2) d\ell_1 \quad (91)$$

The above equations involve only two unknown functions $\frac{\partial}{\partial \nu_1} F_1(P_1)$, $\frac{\partial}{\partial \nu_2} F_2(P_2)$ and therefore in principle can be solved. Subsequently eqs (88) and (89) can give $F_1(P)$ and $F_2(P)$ and solve the problem of finding function $F_s (= F_1 + F_2)$.

As we said before $G_{(1)}(P_1,P)$ is the total velocity potential at P_1 when waves from a line source at P are incident on breakwater (1), which means that it is the solution of the problem of diffraction by (1). Similarly $G_{(2)}(P_2,P)$ represents the solution of the problem of diffraction of waves emanating from a line source at P by the plate (2). Hence, since this problem has been solved (see section B2), eqs (90), (91) together with eqs (88), (89) constitute an analytical formulation of the problem of diffraction by both breakwaters simultaneously.

We now proceed to solving the pair of simultaneous integral equations (90) and (91). The incident plane wave $F_o(r,\omega)$ is expressed

by $\exp\{-ikr\cos(\omega-\theta_o)\}$, therefore we have

$$\frac{\partial}{\partial n_1} F_o(P_1) = \frac{\partial}{\partial n_1} F_o(P)\Big|_{P=P_1} = \frac{1}{r}\frac{\partial}{\partial \omega} F_o(P)\Big|_{\omega=0}$$

$$= -ik\sin\theta_o \exp\{-ikr\cos\theta_o\} \tag{92}$$

$$\frac{\partial}{\partial \bar{n}_1} F_o(\bar{P}_1) = -\frac{1}{r}\frac{\partial}{\partial \omega} F_o(P)\Big|_{\omega=2\pi} = ik\sin\theta_o \exp\{-ikr\cos\theta_o\}$$

$$= -\frac{\partial}{\partial n_1} F_o(P_1) \tag{93}$$

$$\frac{\partial}{\partial n_2} F_o(P_2) = \frac{1}{r}\frac{\partial}{\partial \omega} F_o(P)\Big|_{\omega=\theta} = ik\sin(\theta-\theta_o)\exp\{-ikr\cos(\theta-\theta_o)\} \tag{94}$$

$$\frac{\partial}{\partial \bar{n}_2} F_o(\bar{P}_2) = -\frac{1}{r}\frac{\partial}{\partial \omega} F_o(P)\Big|_{\omega=2\pi+\theta} = -ik\sin(\theta-\theta_o)\exp\{-ikr\cos(\theta-\theta_o)\}$$

$$= -\frac{\partial}{\partial n_2} F_o(P_2) \tag{95}$$

Equations (90) and (91) can be written following the notation of fig. 16

$$\frac{\partial}{\partial n_1} F_1(P_1) = \int_{\ell_2} \frac{\partial}{\partial \nu_2}\{F_2 + F_o\}(P_2)\,\frac{\partial}{\partial n_1} G_{(2)}(P_2,P_1)\,d\ell_2, \tag{96}$$

and

$$\frac{\partial}{\partial \bar{n}_1} F_1(\bar{P}_1) = \int_{\ell_2} \frac{\partial}{\partial \nu_2}\{F_2 + F_o\}(P_1)\,\frac{\partial}{\partial \bar{n}_1} G_{(2)}(P_2,\bar{P}_1)\,d\ell_2 \tag{97}$$

$$\frac{\partial}{\partial n_2} F_2(P_2) = \int_{\ell_1} \frac{\partial}{\partial \nu_1}\{F_1 + F_o\}(P_1)\,\frac{\partial}{\partial n_2} G_{(1)}(P_1,P_2)\,d\ell_1, \tag{98}$$

and

$$\frac{\partial}{\partial \bar{n}_2} F_2(\bar{P}_2) = \int_{\ell_1} \frac{\partial}{\partial \nu_1} \{F + F_o\}(P_1) \frac{\partial}{\partial \bar{n}_2} G_{(1)}(P_1, \bar{P}_2) d\ell_1 \qquad (99)$$

Or, using eq. (95)

$$\frac{\partial}{\partial n_1} F_1(P_1) = \int_d^\infty \frac{\partial}{\partial \bar{n}_2} \{F_2 + F_o\}(\bar{P}_2) \frac{\partial}{\partial n_1} G_{(2)}(\bar{P}_2, P_1) dr +$$

$$+ \int_d^\infty \frac{\partial}{\partial n_2} \{F_2 + F_o\}(P_2) \frac{\partial}{\partial n_1} G_{(2)}(P_2, P_1) dr$$

$$= \int_d^\infty \frac{\partial}{\partial \bar{n}_2} F_o(\bar{P}_2) \frac{\partial}{\partial n_1} \left[G_{(2)}(\bar{P}_2, P_1) - G_{(2)}(P_2, P_1) \right] dr +$$

$$+ \int_d^\infty \left[\frac{\partial}{\partial \bar{n}_2} F_2(\bar{P}_2) \frac{\partial}{\partial n_1} G_{(2)}(\bar{P}_2, P_1) + \right.$$

$$\left. + \frac{\partial}{\partial n_2} F_2(P_2) \frac{\partial}{\partial n_1} G_{(2)}(P_2, P_1) \right] dr$$

Similarly eq. (97) gives in view of eq. (93)

$$\frac{\partial}{\partial \bar{n}_1} F_1(\bar{P}_1) = \int_d^\infty \frac{\partial}{\partial \bar{n}_2} \{F_2 + F_o\}(\bar{P}_2) \frac{\partial}{\partial \bar{n}_1} G_{(2)}(\bar{P}_2, \bar{P}_1) dr +$$

$$+ \int_d^\infty \frac{\partial}{\partial n_2} \{F_2 + F_o\}(P_2) \frac{\partial}{\partial \bar{n}_1} G_{(2)}(P_2, \bar{P}_1) dr$$

$$= \int_d^\infty \frac{\partial}{\partial \bar{n}_2} F_o(\bar{P}_2) \frac{\partial}{\partial \bar{n}_1} \{G_{(2)}(\bar{P}_2, \bar{P}_1) - G_{(2)}(P_2, \bar{P}_1)\} dr +$$

$$+ \int_d^\infty \left[\frac{\partial}{\partial \bar{n}_2} F_2(\bar{P}_2) \frac{\partial}{\partial \bar{n}_1} G_{(2)}(\bar{P}_2, \bar{P}_1) + \right.$$

$$\left. + \frac{\partial}{\partial n_2} F_2(P_2) \frac{\partial}{\partial \bar{n}_1} G_{(2)}(P_2, \bar{P}_1) \right] dr$$

But

$$\frac{\partial}{\partial \bar{n}_1} G_{(2)}(\bar{P}_2, \bar{P}_1) = - \frac{\partial}{\partial n_1} G_{(2)}(\bar{P}_2, P_1) \text{ and}$$

$$\frac{\partial}{\partial \bar{n}_1} G_{(2)}(P_2, \bar{P}_1) = - \frac{\partial}{\partial n_1} G_{(2)}(P_2, P_1)$$

So we find that

$$\frac{\partial}{\partial \bar{n}_1} F_1(\bar{P}_1) = - \frac{\partial}{\partial n_1} F_1(P_1)$$

Similarly

$$- \frac{\partial}{\partial \bar{n}_2} F_2(\bar{P}_2) = + \frac{\partial}{\partial n_2} F_2(P_2)$$

The set of the four equations (96), (97), (98) and (99) can be replaced now by the following two equations

$$X = \int_d^\infty \{Y + \frac{\partial}{\partial n_2} F_o(P_2)\} \frac{\partial}{\partial n_1} [G_{(2)}(P_2, P_1) - G_{(2)}(\bar{P}_2, P_1)] dr \qquad (100)$$

$$Y = \int_o^\infty \{X + \frac{\partial}{\partial n_1} F_o(P_1)\} \frac{\partial}{\partial n_2} [G_{(1)}(P_1, P_2) - G_{(1)}(\bar{P}_1, P_2)] dr \qquad (101)$$

where $X = \frac{\partial}{\partial n_1} F_1(P_1)$, $Y = \frac{\partial}{\partial n_2} F_2(P_2)$.

The values X,Y having been found from eqs (100) and (101), we can derive F_1, F_2 from eqs (88), (89):

$$F_1(P) = \int_d^\infty \{Y + \frac{\partial}{\partial n_2} F_o(P_2)\}[G_{(2)}(P_2,P) - G_{(2)}(\overline{P}_2,P)]dr \qquad (102)$$

$$F_2(P) = \int_o^\infty \{X + \frac{\partial}{\partial n_1} F_o(P_1)\}[G_{(1)}(P_1,P) - G_{(1)}(\overline{P}_1,P)]dr \qquad (103)$$

As we said before $G_{(2)}(P_2,P)$ represents the total velocity potential at the point P_2 due to a unit line source located at the point P when only the breakwater (2) is present; and similarly for the other Green's functions.

Let us employ first the integral form of the velocity potential; from section B2, eq. (12) we get

$$G_{(1)}(P_1,P) = \frac{1}{\pi} e^{ikR_1} \int_{-\sqrt{k(r_1+r-R_1)}}^\infty \frac{\exp\{i\mu^2\}}{(\mu^2 + 2kR_1)^{\frac{1}{2}}} d\mu \qquad (104)$$

where $R_1 = +(r_1^2 + r^2 - 2r_1 r\cos\omega)^{\frac{1}{2}}$; similarly we have

$$G_{(1)}(\overline{P}_1,P) = \frac{1}{\pi} e^{ikR_1} \int_{+\sqrt{k(r_1+r-R_1)}}^\infty \frac{\exp\{i\mu^2\}}{(\mu^2 + 2kR_1)^{\frac{1}{2}}} d\mu \qquad (105)$$

$$G_{(2)}(P_2,P) = \frac{1}{\pi} e^{ikR_2} \int_{+\sqrt{k(R_A+r_2-d-R_2)}}^\infty \frac{\exp\{i\mu^2\}}{(\mu^2 + 2kR_2)^{\frac{1}{2}}} d\mu \qquad (106)$$

with $R_2 = +[r^2 + r_2^2 - 2rr_2\cos(\theta-\omega)]^{\frac{1}{2}}$ and

$$R_A = +[r^2 + d^2 - 2rd\cos(\theta-\omega)]^{\frac{1}{2}}$$

$$G_{(2)}(\bar{P}_2,P) = \frac{1}{\pi} e^{ikR_2} \int_{-\sqrt{k(R_A+r_2-d-R_2)}}^{\infty} \frac{\exp\{i\mu^2\}}{(\mu^2 + 2kR_2)^{\frac{1}{2}}} d\mu \quad (107)$$

Now,

$$\frac{\partial}{\partial n_1} G_{(2)}(\bar{P}_2,P_1) = \frac{\partial}{\partial n_1} G_{(2)}(\bar{P}_2,P)\Big|_{P=P_1}$$

$$= \frac{1}{\pi r}\frac{\partial}{\partial \omega}\left[e^{ikR_2} \int_{-\sqrt{k(R_A+r_2-d-R_2)}}^{\infty} \frac{\exp\{i\mu^2\}}{(\mu^2 + 2kR_2)^{\frac{1}{2}}} d\mu \right]\Bigg|_{\substack{r=r_1 \\ \omega=0}}$$

$$= \frac{ikr_2\sin\theta}{\pi R_{12}} e^{ikR_{12}} \int_{-\sqrt{k(R_{1A}-R_{12}+r_2-d)}}^{\infty} \frac{\exp\{i\mu^2\}}{(\mu^2 + 2kR_{12})^{\frac{1}{2}}} d\mu -$$

$$- \frac{kr_2\sin\theta}{\pi R_{12}} e^{ikR_{12}} \int_{-\sqrt{k(R_{1A}-R_{12}+r_2-d)}}^{\infty} \frac{\exp\{i\mu^2\}}{(\mu^2 + 2kR_{12})^{\frac{3}{2}}} d\mu +$$

$$+ \frac{\sin\theta}{2\pi} \frac{\exp\{ik(R_{1A}-R_{12}+r_2-d)\}}{[(R_{1A}+r_2-d)^2 - R_{12}^2]^{\frac{1}{2}}} \cdot \left[\frac{d}{R_{1A}+r_2-d} - \frac{r_2}{R_{12}}\right] \quad (108)$$

$$\frac{\partial}{\partial n_1} G_{(2)}(P_2,P_1) = \frac{\partial}{\partial n_1} G_{(2)}(P_2,P)\Big|_{P=P_1}$$

$$= \frac{1}{\pi r}\frac{\partial}{\partial \omega}\left[e^{ikR_2} \int_{+\sqrt{k(R_A+r_2-d-R_2)}}^{\infty} \frac{\exp\{i\mu^2\}}{(\mu^2 + 2kR_2)^{\frac{1}{2}}}\, d\mu \right]\Bigg|_{\substack{r=r_1 \\ \omega=0}}$$

$$= \frac{ikr_2\sin\theta}{\pi R_{12}} e^{ikR_{12}} \int_{+\sqrt{k(R_{1A}-R_{12}+r_2-d)}}^{\infty} \frac{\exp\{i\mu^2\}}{(\mu^2 + 2kR_{12})^{\frac{1}{2}}}\, d\mu -$$

$$- \frac{kr_2\sin\theta}{\pi R_{12}} e^{ikR_{12}} \int_{+\sqrt{k(R_{1A}-R_{12}+r_2-d)}}^{\infty} \frac{\exp\{i\mu^2\}}{(\mu^2 + 2kR_{12})^{\frac{3}{2}}}\, d\mu -$$

$$- \frac{\sin\theta}{2\pi} \frac{\exp\{ik(R_{1A}-R_{12}+r_2-d)\}}{\sqrt{(R_{1A}+r_2-d)^2 - R_{12}^2}} \left[\frac{d}{R_{1A}+r_2-d} - \frac{r_2}{R_{12}} \right] \qquad (109)$$

where we have put

$$R_{1A} = +(r_1^2 + d^2 - 2r_1 d\cos\theta)^{\frac{1}{2}} \qquad \text{and}$$

$$R_{12} = +(r_1^2 + r_2^2 - 2r_1 r_2\cos\theta)^{\frac{1}{2}}$$

Consequently

$$\frac{\partial}{\partial n_1}\left[G_{(2)}(\bar{P}_2, P_1) - G_{(2)}(P_2, P_1)\right]$$

$$= \frac{2ikr_2\sin\theta}{\pi R_{12}} e^{ikR_{12}} \int_{0}^{+\sqrt{k(R_{1A}-R_{12}+r_2-d)}} \frac{e^{i\mu^2}}{(\mu^2 + 2kR_{12})^{\frac{1}{2}}}\, d\mu -$$

$$- \frac{2kr_2\sin\theta}{\pi R_{12}} e^{ikR_{12}} \int_0^{+\sqrt{k(R_{1A}+r_2-d-R_{12})}} \frac{e^{i\mu^2}}{(\mu^2 + 2kR_{12})^{\frac{1}{2}}} d\mu +$$

$$+ \frac{\sin\theta \exp\{ik(R_{1A}+r_2-d-R_{12})\}}{\pi[(R_{1A}+r_2-d)^2 - R_{12}^2]^{\frac{1}{2}}} \left[\frac{d}{R_{1A}+r_2-d} - \frac{r_2}{R_{12}} \right] \qquad (110)$$

From eqs (104) and (105) we have

$$G_{(1)}(P_1,P) - G_{(1)}(\overline{P}_1,P) = \frac{2e^{ikR_1}}{\pi} \int_0^{+\sqrt{k(r_1+r-R_1)}} \frac{e^{i\mu^2}}{(\mu^2 + 2kR_1)^{\frac{1}{2}}} d\mu \qquad (111)$$

and so

$$\frac{\partial}{\partial n_2} [G_{(1)}(\overline{P}_1,P_2) - G_{(1)}(P_1,P_2)] = - \frac{1}{r_2} \frac{\partial}{\partial \omega} [G_{(1)}(P_1,P) - G_{(1)}(\overline{P}_1,P)] \Big|_{P=P_2}$$

$$= - \frac{1}{r_2} \frac{2}{\pi} \frac{\partial}{\partial \omega} \left[e^{ikR_1} \int_0^{+\sqrt{k(r_1+r-R_1)}} \frac{e^{i\mu^2}}{(\mu^2 + 2kR_1)^{\frac{1}{2}}} d \right] \Bigg|_{\substack{r=r_2 \\ \omega=\theta}}$$

$$= - \frac{2ikr_2\sin\theta}{\pi R_{12}} e^{ikR_{12}} \int_0^{+\sqrt{k(r_1+r_2-R_{12})}} \frac{e^{i\mu^2}}{(\mu^2 + 2kR_{12})^{\frac{1}{2}}} d\mu +$$

$$+ \frac{2kr_1\sin\theta}{\pi R_{12}} e^{ikR_{12}} \int_0^{+\sqrt{k(r_1+r_2-R_{12})}} \frac{e^{i\mu^2}}{(\mu^2 + 2kR_{12})^{\frac{1}{2}}} d\mu +$$

$$+ \frac{r_1 \sin\theta}{\pi R_{12}} \frac{\exp\{ik(R_1+r_2-R_{12})\}}{[(r_1+r_2)^2 - R_{12}^2]^{\frac{1}{2}}} \tag{112}$$

From eqs (106) and (107) we get

$$G_{(2)}(P_2,P) - G_{(2)}(\overline{P}_2,P) = -\frac{2e^{ikR_2}}{\pi} \int_0^{+\sqrt{k(R_A+r_2-d-R_2)}} \frac{e^{i\mu^2}}{(\mu^2 + 2kR_2)^{\frac{1}{2}}} d\mu \tag{113}$$

and thus we can refind eq. (110).

The four equations (100)-(103) which constitute the formal solution of the problem can be rewritten now in view of eqs (92), (94), (110), (111), (112) and (113).

$$X = \frac{\sin\theta}{\pi} \int_d^\infty [Y + ik\sin(\theta-\theta_o)\exp\{-ikr_2\cos(\theta-\theta_o)\}] \times$$

$$\times \left\{ \frac{2kr_2}{R_{12}} \exp(ikR_{12}) \left[\int_0^\xi \frac{e^{i\mu^2}}{(\mu^2 + 2kR_{12})^{\frac{1}{2}}} d\mu - i \int_0^\xi \frac{e^{i\mu^2}}{(\mu^2 + 2kR_{12})^{\frac{3}{2}}} d\mu \right] + \right.$$

$$\left. + \frac{\exp\{ik(R_{1A}+r_2-d-R_{12})\}}{[(R_{1A}+r_2-d)^2 - R_{12}^2]^{\frac{1}{2}}} \left[\frac{d}{R_{1A}+r_2-d} - \frac{r_2}{R_{12}} \right] \right\} dr_2 \tag{114}$$

with $R_{12} = +(r_1^2 + r_2^2 - 2r_1 r_2 \cos\theta)^{\frac{1}{2}}$

$R_{1A} = +(r_1^2 + d^2 - 2r_1 d\cos\theta)^{\frac{1}{2}}$

$\xi = +[k(R_{1A} + r_2 - d - R_{12})]^{\frac{1}{2}}$

$$Y = \frac{\sin\theta}{\pi} \int_0^\infty [X - ik\sin\theta_o \exp(-ikr_1\cos\theta_o)] \frac{r_1}{R_{12}} \times$$

$$\times \left[2k\exp(ikR_{12}) \left[- \int_0^{\xi'} \frac{e^{i\mu^2}}{(\mu^2 + 2kR_{12})^{\frac{1}{2}}} d\mu + i \int_0^{\xi'} \frac{e^{i\mu^2}}{(\mu^2 + 2kR_{12})^{\frac{1}{2}}} d\mu \right] - \right.$$

$$\left. - \frac{\exp\{ik(r_1+r_2-R_{12})\}}{[(r_1+r_2)^2 - R_{12}^2]^{\frac{1}{2}}} \right] dr_1 \qquad (115)$$

with $\xi' = +[k(r_1 + r_2 - R_{12})]^{\frac{1}{2}}$.

$$F_1(r,\omega) = -\frac{2}{\pi} \int_d^\infty [Y + ik\sin(\theta-\theta_o)\exp\{-ikr_2\cos(\theta-\theta_o)\}] \times$$

$$\times \exp(ikR_2) \left[\int_0^m \frac{e^{i\mu^2}}{(\mu^2 + 2kR_2)^{\frac{1}{2}}} d\mu \right] dr_2 \qquad (116)$$

with $R_2 = +[r^2 + r_2^2 - 2rr_2\cos(\theta-\omega)]^{\frac{1}{2}}$

$m = +[k(R_A + r_2 - d - R_2)]^{\frac{1}{2}}$

$R_A = +[r^2 + d^2 - 2rd\cos(\theta-\omega)]^{\frac{1}{2}}$.

$$F_2(r,\omega) = \frac{2}{\pi} \int_o^\infty [X - ik\sin\theta_o\exp(-ikr_1\cos\theta_o)]\exp(ikR_1) \times$$

$$\times \left[\int_o^{m'} \frac{e^{i\mu^2}}{(\mu^2 + 2kR_1)^{\frac{1}{2}}} d\mu \right] dr_1 \qquad (117)$$

with $R_1 = +(r^2 + r_1^2 - 2rr_1\cos\omega)^{\frac{1}{2}}$

$m' = +[k(r_1 + r - R_1)]^{\frac{1}{2}}$

We have now expressed the components F_1 and F_2 of the scattered field F_s in terms of the integral representation of the Green's functions

involved. Alternatively let us try to express the Green's functions in eqs (102) and (103) in terms of series of products of Bessel functions.

From eq. (70) we get for $\theta = 2\pi$

$$F(P,P_o) = \frac{i}{4} \sum_{m=o}^{\infty} \varepsilon_m J_{\frac{1}{2}m}(kr_<) H_{\frac{1}{2}m}(kr_>) \cos \frac{m\omega}{2} \cos \frac{m\omega_o}{2}$$

which means that

$$G_{(2)}(P_2,P) = \frac{i}{4} \sum_{m=o}^{\infty} (-1)^m \varepsilon_m J_{\frac{1}{2}m}(kr_<) H_{\frac{1}{2}m}(kr_>) \cos \tfrac{1}{2}m(\hat{\phi}+\theta-\omega) \tag{118}$$

$r_<$ and $r_>$ choosing the lesser and greater respectively among the values below, as described when deriving eq. (70)

$$r_<, r_> = \{r_2 - d, +[r^2 + d^2 - 2rd\cos(\theta-\omega)]^{\frac{1}{2}}\}$$

and $$\hat{\phi} = \arccos \frac{r-d\cos(\theta-\omega)}{[r^2+d^2-2rd\cos(\theta-\omega)]^{\frac{1}{2}}}$$

is the angle under which point P 'sees' the gap A0.

In the same manner we find

$$G_{(2)}(\overline{P}_2,P) = \frac{i}{4} \sum_{m=o}^{\infty} \varepsilon_m J_{\frac{1}{2}m}(kr_<) H_{\frac{1}{2}m}(kr_>) \cos \tfrac{1}{2}m(\hat{\phi}+\theta-\omega) \tag{119}$$

$$r_<, r_> = \{r_2 - d, +[r^2+d^2-2rd\cos(\theta-\omega)]^{\frac{1}{2}}\}$$

$$\hat{\phi} = \arccos \frac{r - d\cos(\theta-\omega)}{[r^2 + d^2 - 2rd\cos(\theta-\omega)]^{\frac{1}{2}}}$$

$$G_{(1)}(P_1,P) = \frac{i}{4} \sum_{m=o}^{\infty} \varepsilon_m J_{\frac{1}{2}m}(kr_<) H_{\frac{1}{2}m}(kr_>) \cos \tfrac{1}{2}m\omega \tag{120}$$

$$r_<, r_> = \{r_1, r\}$$

$$G_{(1)}(\bar{P}_1,P) = \frac{i}{4}\sum_{m=o}^{\infty}(-1)^m\varepsilon_m J_{\frac{1}{2}m}(kr_<)H_{\frac{1}{2}m}(kr_>)\cos\tfrac{1}{2}m\omega \qquad (121)$$

$$r_<,r_> = \{r_1,r\}$$

We find from eqs (118)-(121)

$$G_{(2)}(P_2,P) - G_{(2)}(\bar{P}_2,P) = -i\sum_{m=o}^{\infty}J_{m+\frac{1}{2}}(kr_<)H_{m+\frac{1}{2}}(kr_>)\cos(m+\tfrac{1}{2})(\hat{\phi}+\theta-\omega) \qquad (122)$$

$$r_<,r_> = \{r_2-d,\ R_A\}$$

Therefore

$$\frac{\partial}{\partial n_1}[G_{(2)}(P_2,P_1) - G_{(2)}(\bar{P}_2,P_1)] = \frac{1}{r}\frac{\partial}{\partial\omega}\left[G_{(2)}(P_2,P) - G_{(2)}(\bar{P}_2,P)\right]\Bigg|_{\substack{r=r_1\\ \omega=0}}$$

$$= -\frac{i}{r_1}\sum_{m=o}^{\infty}(m+\tfrac{1}{2})J_{m+\frac{1}{2}}(kR_{1A})H_{m+\frac{1}{2}}[k(r_2-d)]\sin(m+\tfrac{1}{2})(\hat{\phi}+\theta) +$$

$$+\frac{id\sin\theta}{R_{1A}^2}\sum_{m=o}^{\infty}(m+\tfrac{1}{2})J_{m+\frac{1}{2}}(kR_{1A})H_{m+\frac{1}{2}}[k(r_2-d)]\cos(m+\tfrac{1}{2})(\hat{\phi}+\theta) -$$

$$-\frac{ikd\sin\theta}{R_{1A}}\sum_{m=o}^{\infty}J_{m+\frac{3}{2}}(kR_{1A})H_{m+\frac{1}{2}}[k(r_2-d)]\cos(m+\tfrac{1}{2})(\hat{\phi}+\theta) \qquad (123)$$

for values $r_2-d > R_{1A} = +(r_1^2 + d^2 - 2r_1 d\cos\theta)^{\frac{1}{2}}$; when $r_2-d < R_{1A}$ the symbols J,H in eq. (123) must be interchanged.

We find too

$$G_{(1)}(P_1,P) - G_{(1)}(\bar{P}_1,P) = i\sum_{m=o}^{\infty}J_{m+\frac{1}{2}}(kr_<)H_{m+\frac{1}{2}}(kr_>)\cos(m+\tfrac{1}{2})\omega \qquad (124)$$

$$r_<,r_> = \{r_1,r\}$$

$$\frac{\partial}{\partial n_2}\left[G_{(1)}(P_1,P_2) - G_{(1)}(\overline{P}_1,P_2)\right] = \frac{1}{r}\frac{\partial}{\partial \omega}\left[G_{(1)}(P_1,P) - G_{(1)}(\overline{P}_1,P)\right]\Bigg|_{\substack{r=r_2\\ \omega=0}}$$

$$= -\frac{i}{r_2}\sum_{m=o}^{\infty}(m+\tfrac{1}{2})J_{m+\frac{1}{2}}(kr_<)H_{m+\frac{1}{2}}(kr_>)\sin(m+\tfrac{1}{2})\theta \qquad (125)$$

$$r_<, r_> = \{r_1, r\}$$

Substituting eqs (92),(94),(122),(123),(124) and (125) into eqs (100)-(103) we find

$$X(r_1,0) = -\frac{i}{r_1}\int_d^{\infty} Y \sum \sin\, dr_2 + \frac{id\sin\theta}{R_{1A}^2}\int_d^{\infty} Y \sum \cos\, dr_2 -$$

$$-\frac{ikd\sin\theta}{R_{1A}}\int_d^{\infty} Y \sum 3/2\, dr_2 + \frac{k\sin(\theta-\theta_o)}{r_1}\int_d^{\infty}\exp\{-ikr_2\cos(\theta-\theta_o)\}\sum\sin\, dr_2 -$$

$$-\frac{kd\sin\theta\sin(\theta-\theta_o)}{R_{1A}^2}\int_d^{\infty}\exp\{-ikr_2\cos(\theta-\theta_o)\}\sum\cos\, dr_2 +$$

$$+\frac{k^2d\sin\theta\sin(\theta-\theta_o)}{R_{1A}}\int_d^{\infty}\exp\{-ikr_2\cos(\theta-\theta_o)\}\sum 3/2\, dr_2 \qquad (126)$$

where $r_2-d > R_{1A}$ as before and

$$\sum_{\cos}^{\sin} = \sum_{m=o}^{\infty}(m+\tfrac{1}{2})J_{m+\frac{1}{2}}(kR_{1A})H_{m+\frac{1}{2}}[k(r_2-d)]_{\cos}^{\sin}(m+\tfrac{1}{2})(\hat{\phi}+\theta)$$

$$\sum 3/2 = \sum_{m=o}^{\infty} J_{m+\frac{1}{2}}(kR_{1A})H_{m+\frac{1}{2}}[k(r_2-d)]\cos(m+\tfrac{1}{2})(\hat{\phi}+\theta)$$

Similarly we obtain

$$Y(r_2,\theta) = -\frac{i}{r_2}\int_o^\infty X\ \Sigma\ dr_1 - \frac{k\sin\theta_o}{r_2}\int_o^\infty \exp(-ikr_1\cos\theta_o)\ \Sigma\ dr_1 \qquad (127)$$

where $\Sigma = \sum_{m=o}^{\infty} (m+\frac{1}{2})J_{m+\frac{1}{2}}(kr_<)H_{m+\frac{1}{2}}(kr_>)\sin(m+\frac{1}{2})\theta$

and $r_<, r_> = \{r_1, r_2\}$

For the functions F_1, F_2 we get

$$F_1(P) = -i\int_d^\infty Y\ S_1 dr_2 + k\sin(\theta-\theta_o)\int_d^\infty \exp\{-ikr_2\cos(\theta-\theta_o)\}S_1 dr_2 \qquad (128)$$

with $S_1 = \sum_{m=o}^{\infty} J_{m+\frac{1}{2}}(kr_<)H_{m+\frac{1}{2}}(kr_>)\cos(m+\frac{1}{2})(\hat{\phi}+\theta-\omega)$

$$r_<, r_> = \{r_2-d,\ R_A\}$$

and

$$F_2(P) = i\int_o^\infty X\ S_2 dr_1 + k\sin\theta_o\int_d^\infty \exp(-ikr_1\cos\theta_o)S_2 dr_1 \qquad (129)$$

with $S_2 = \sum_{m=o}^{\infty} J_{m+\frac{1}{2}}(kr_<)H_{m+\frac{1}{2}}(kr_>)\cos(m+\frac{1}{2})\omega$

$$r_<, r_> = \{r_1, r\}$$

We have again found functions F_1 and F_2 in another form - this time involving series of Bessel functions.

The first half of the terms in each of the eqs (126)-(129) are associated with the scattered wave and the second half with the incident plane waves. Each of the two sets of equations (114)-(117)

and (126)-(129) provide a formal solution to our problem. However the apparent complexity of the coupled integral equations poses difficulties in evaluating the unknowns X,Y numerically. This suggests a further investigation into the potential theory in order to substitute the kernels of the integral equations with simpler functions or even better to convert the integral equations to non-integral ones, i.e. not containing the unknown in the integrand, having in mind that some approximation may be inevitable at this stage. The following subsection deals in general with this problem of modification and with the presentation of the final result.

C3.3 The Solution to the Problem

C3.3.1 Some potential theory. The difficulties encountered in the previous subsection forced me to return to the fundamentals of the classical potential theory to search for any material useful for our task. An extension therefore of the remarks made in subsection C1.1 is exposed here briefly.

The most general two-dimensional velocity potential of period $2\pi/\sigma$ is of the form

$$f(r,\omega)\exp\{-i\sigma t\},$$

where f is a solution of the Helmholtz equation in two dimensions

$$(\Delta + k^2)f = 0$$

Now, if f is to represent the field due to line source in free space it has to be independent of the angle ω and it is evident that it is a solution of

$$\frac{d^2f}{dr^2} + \frac{1}{r}\frac{df}{dr} + k^2 f = 0$$

which is Bessel's equation of order zero and variable kr. The most convenient solutions of this equation are the Hankel functions which behave near the origin like $\pm\frac{2i}{\pi}\log r$ but have no other singularity at a finite distance. Let Γ be a closed contour bounding the region D in the (x,y) plane. If v and w are two functions whose first and second-order partial derivatives are continuous within and on Γ, Green's identity gives (Baker and Copson [14])

$$\int_\Gamma \{v\frac{\partial w}{\partial n} - w\frac{\partial v}{\partial n}\}ds = \iint_D (v\Delta w - w\Delta v)dx\,dy \qquad (130)$$

where $\partial/\partial n$ means differentiation along the outward normal to Γ, and ds the differential length on Γ. If v and w are both solutions of the Helmholtz equation formula (130) becomes

$$\int_\Gamma \{v\frac{\partial w}{\partial n} - w\frac{\partial v}{\partial n}\}ds = 0 \qquad (131)$$

or by taking $w = H_o(kr_1)$ where r_1 denotes the distance of the point P from a point on the contour, and letting v = f,

$$\int_\Gamma \{f\frac{\partial}{\partial n}H_o(kr_1) - H_o(kr_1)\frac{\partial f}{\partial n}\}ds = 0 \qquad (132)$$

provided that the point $P(r,\omega)$ and the singularities of f lie outside Γ. If, however, P lies inside Γ this means that $H_o(kr_1)$ has a singularity inside Γ and we have to apply Green's transformation to the region bounded externally by Γ and internally by a circle of centre P and radius ε. Formula (130) gives, after letting $\varepsilon \to 0$,

$$f(r,\omega) = \frac{i}{4}\int_{\Gamma}\{f\,\frac{\partial}{\partial n}H_o(kr_1) - H_o(kr_1)\,\frac{\partial f}{\partial n}\}ds \tag{133}$$

where $\partial/\partial n$ now means differentiation along the inward normal to Γ. The following two theorems summarize the results.

1. Interior problem Let f be a solution of the equation

$$(\Delta + k^2)f = 0$$

with continuous partial derivatives of the first and second orders within and on a closed curve Γ; then

$$\frac{i}{4}\int_{\Gamma}\{f\,\frac{\partial}{\partial n}H_o(kr_1) - H_o(kr_1)\,\frac{\partial f}{\partial n}\}ds = \begin{cases} f(r,\omega), & P \text{ inside } \Gamma \\ 0, & P \text{ outside } \Gamma \end{cases} \tag{134}$$

where r_1 is the distance from a fixed point $P(r,\omega)$ and $\partial/\partial n$ means differentiation along the inward normal to Γ.

2. Exterior problem Let f be a solution of the equation

$$(\Delta + k^2)f = 0$$

with continuous partial derivatives of the first and second orders outside and on a closed curve Γ; moreover f should behave like $H_o(kr)$ for large values of r; then

$$\frac{i}{4}\int_{\Gamma}\{f\,\frac{\partial}{\partial n}H_o(kr_1) - H_o(kr_1)\,\frac{\partial f}{\partial n}\}ds = \begin{cases} f(r,\omega), & P \text{ outside } \Gamma \\ 0, & P \text{ inside } \Gamma \end{cases} \tag{135}$$

where r_1 is the distance from a fixed point $P(r,\omega)$ and $\partial/\partial n$ means differentiation along the outward normal to Γ.

The requirement that f should behave like $H_o(kr)$ at infinity is the radiation condition, which in other words states that $f(r,\omega)\exp\{-i\sigma t\}$ must represent cylindrical waves diverging from the origin. We note here that for large r

$$H_o(kr) \sim \left(\frac{2}{\pi kr}\right)^{\frac{1}{2}} \exp\{i(kr - \tfrac{1}{4}\pi)\}$$

We turn now to the diffraction theory based upon the above considerations starting with Kirchhoff's approximation (see Bouwkamp [12]). Consider in a two-dimensional space a screen S of vanishing thickness covering a finite part of the plane x = 0, and a system of sources in the left half-space (x < 0) (fig. 17).

If the screen were absent the sources would produce a wave field $F_i(P)$ at P. The actual field F(P) is the sum of F_i and F_s, the scattered field due to the secondary sources on S. By Green's theorem

$$F_s(P) = \frac{i}{4} \int_S \{F \frac{\partial}{\partial n} H_o(kr_1) - H_o(kr_1) \frac{\partial F}{\partial n}\} ds \qquad (136)$$

with the usual notation. Kirchhoff made the following assumptions:

(a) On the 'illuminated' face of S (S_i) the values of F and $\partial F/\partial n$ may be replaced by the values of F_i and $\partial F_i/\partial n$ respectively.

(b) On the 'dark' face of S (S_d) both F and $\partial F/\partial n$ may be set equal to zero.

The total field then becomes, in Kirchhoff's approximation

$$F_i(P) + \frac{i}{4} \int_{S_i} \{F_i \frac{\partial}{\partial n} H_o(kr_1) - H_o(kr_1) \frac{\partial F_i}{\partial n}\} ds$$

and its limiting values when P tends to S are

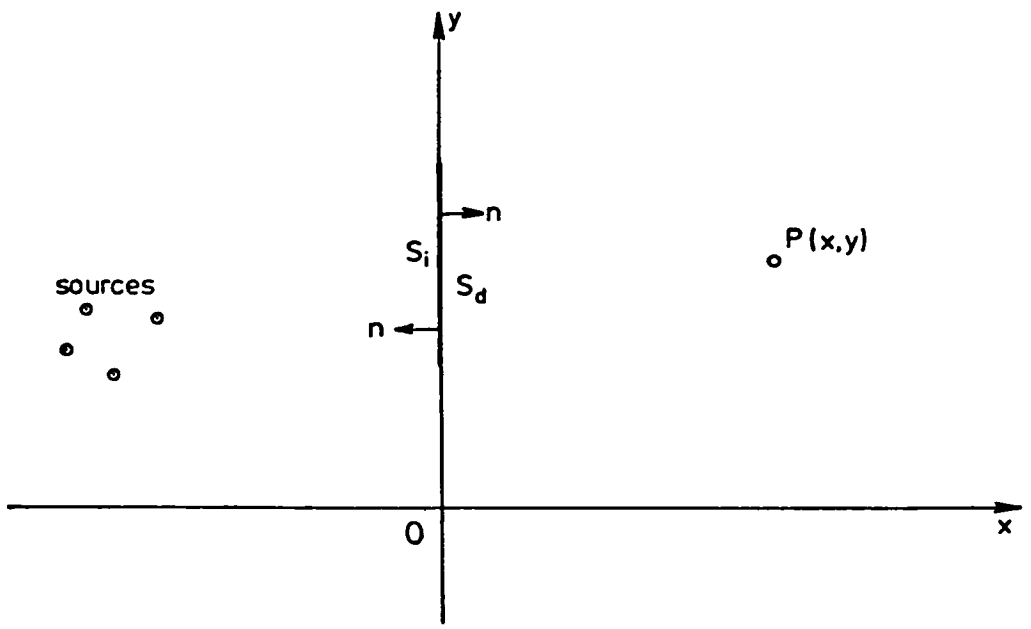

Fig. 17. Kirchhoff's approximation

$$\frac{1}{2} F_i(P) + \frac{i}{4} \int_{S_i} H_o(kr_1) \frac{\partial F_i}{\partial n} \, ds \quad , P \text{ on } S_d$$

$$\frac{3}{2} F_i(P) + \frac{i}{4} \int_{S_i} H_o(kr_1) \frac{\partial F_i}{\partial n} \, ds \quad , P \text{ on } S_i$$

We see that the assumed values $F_i(P)$ and 0 on S_i and S_d respectively are not reproduced unless

$$\frac{1}{2} F_i(P) + \frac{i}{4} \int_{S_i} H_o(kr_1) \frac{\partial F_i}{\partial n} \, ds = 0 \quad , P \text{ on } S$$

However, it is evident that this condition cannot be fulfilled for arbitrary S and F_i and therefore Kirchhoff's procedure is not self-

consistent. The reason for the inconsistency is that F and $\partial F/\partial n$ cannot simultaneously be described on S. Therefore the above solution is a rigorous one not of a boundary-value problem, but of a saltus problem in that it reproduces the jumps of the boundary values and not the actual values themselves.

The complementary problem where the finite aperture A is present in an infinite plane screen S is solved in the same manner. Assuming the same primary field F_i and noting that the integral over S is equal to that over S+A minus that over A, we find in Kirchhoff's sense

$$Ki(P) = \frac{i}{4} \int_A \{F_i \frac{\partial}{\partial n} H_o(kr_1) - H_o(kr_1) \frac{\partial F_i}{\partial n}\} dA \qquad (137)$$

P in $x > 0$, n drawn into $x > 0$

$$Ki(P) = F_i(P) - \frac{i}{4} \int_A \{F_i \frac{\partial}{\partial n} H_o(kr_1) - H_o(kr_1) \frac{\partial F_i}{\partial n}\} dA \qquad (138)$$

P in $x < 0$, n drawn into $x < 0$

The analytic continuation of the function (137) through the aperture is the function (138), and vice versa. There are no discontinuities in the apertures where we have the values

$$Ki(P) = \frac{1}{2} F_i(P) - \frac{i}{4} \int_A H_o(kr_1) \frac{\partial F_i}{\partial n} dA$$

n pointing $x > 0$

$$\frac{\partial Ki(P)}{\partial n} = \frac{1}{2} \frac{\partial F_i(P)}{\partial n} + (\Delta + k^2) \frac{i}{4} \int_A F_i H_o(kr_1) dA$$

In this case Kirchhoff's method avoids the difficulty of not reproducing any assumed values in the apertures, for the assumptions made concern only the screen S.

A modification of Kirchhoff's theory has been proposed for diffraction problems in two space dimensions. It is based on Rayleigh's formulas (41) and (42) where we shall assume as before that F, $\partial F/\partial n$ may be replaced by the corresponding unperturbed values. Working in two dimensions we give the first of the two solutions, corresponding to (41), often called the Rayleigh solutions, for the case of the finite aperture in which we now limit ourselves:

$$Ra(P) = -\frac{i}{2}\int_A H_o(kr_1)\,\frac{\partial F_i}{\partial n}\,dA, \quad P \text{ in } x > 0 \tag{139}$$

From eq. (42) we derive the second of the Rayleigh solutions:

$$\dot{Ra}(P) = \frac{i}{2}\int_A F_i\,\frac{\partial}{\partial n}\,H_o(kr_1)dA\ , \quad P \text{ in } x < 0 \tag{140}$$

Unlike Kirchhoff's theory, the modified theory is self-consistent. The reason is that it is sufficient to assume boundary values for either $\partial F/\partial n$ or F; the assumed values in the aperture are reproduced by the Rayleigh solutions when the point P tends to the plane x = 0 from the right (fig. 17). The continuation of these solutions into the 'illuminated' half-plane x < 0 is easy. We have

$$Ra(P) = F_i(P) - F_i(-P) - \frac{i}{2}\int_A H_o(kr)\,\frac{\partial F_i}{\partial n}\,dA\ , \quad P \text{ in } x < 0 \tag{141}$$

$$\dot{Ra}(P) = F_i(P) + F_i(-P) + \frac{i}{2}\int_A F_i\,\frac{\partial}{\partial n}\,H_o(kr_1)dA\ , \quad P \text{ in } x < 0 \tag{142}$$

where $F_i(-P)$ means the value of F_i at the reflection of point P in the plane x = 0.

Like Kirchhoff's solution, the Rayleigh solutions are exact

solutions of saltus problems. The normal derivative of Ra jumps across the screen from $2\partial F_i/\partial n$ to zero; similarly the function Ra' jumps from $2F_i$ to zero.

The modified theory provides a means of distinguishing between the two principal boundary value problems, the soft and the rigid screen, the latter being of interest to us. Since $\partial Ra/\partial n = 0$ on the 'dark' face of the screen, eq. (139) was proposed by Bouwkamp (see [14]) as an approximate expression for the diffracted field behind the aperture of a rigid screen for the incident field F_i. It is obvious that this approximation will be accurate immediately behind the screen but not so accurate in the vicinity of the gap. Rayleigh's solution provides the basis of our final formulation of the solution to our problem, a discussion of which is presented in subdivision C3.3.3.

If we try now to combine the Rayleigh solutions with the rigorous solution (eq. (44)) and its properties (2) and (4) we derive two sets of slightly different modifications of Kirchhoff's theory. Use of property (2) gives

$$\begin{aligned} F &= Ra \qquad , \text{ in } x > 0 \\ F &= 2F_i - Ra \quad , \text{ in } x < 0 \end{aligned} \tag{143}$$

Use of property (4) gives

$$F = Ra' \qquad \text{everywhere} \tag{144}$$

In eq. (143) the incorrect boundary conditions of Rayleigh's solution have been corrected but the function $\partial F/\partial n$ is no more continuous across the aperture. In eq. (144) the boundary conditions are still incorrect but the approximation is now continuous across the aperture

and produces the correct values of F ($=F_i$) there. It is obvious that when the field in the vicinity of the screen is important rather than the aperture, as our case is, then approximations (143) are to be preferred.

Our discussion so far in this subdivision concerns basically Green's (second) identity (eq. (130)) and the approximations based on it. Further study of this identity reveals its flexibility in the potential theory by the introduction of the Green's function which has already been mentioned in several instances.

A natural point of departure is formula (133) valid if f satisfies the Helmholtz equation. This formula expresses f at any interior point of Γ in terms of its boundary values and those of its normal derivative. But we know (Kellogg [31]) that the boundary values alone (or:their normal derivatives) determine f and it is natural to try to eliminate the normal derivatives (or: the boundary values). The problem of finding f after showing its existence is called the Dirichlet (Neumann) problem or the first (second) boundary problem of potential theory. In our application it is clear that we are interested in the Neumann problem because generally in hydrodynamics we know the values of the normal derivatives of the wave function along a boundary rather than the values of the function itself. We wish thus to eliminate f under the integral sign in

$$f(P) = \frac{i}{4} \int_{\Gamma} \{ f \frac{\partial}{\partial n} H_o(kr_1) - H_o(kr_1) \frac{\partial f}{\partial n} \} ds$$

by means of eq. (131):

$$0 = \frac{i}{4} \int_{\Gamma} \{ f \frac{\partial w}{\partial n} - w \frac{\partial f}{\partial n} \} ds$$

in order that f may be expressed in terms of the boundary values of its normal derivative alone. This could be achieved if we could find a function w, solution of the Helmholtz equation, with normal derivative such that by adding the last two equations to find

$$f(P) = -\frac{i}{4} \int_{\Gamma} \frac{\partial f(Q)}{\partial n} G(Q,P) ds \qquad (145)$$

The function G(Q,P) if it exists is known as the Green's function of the second kind for Γ, or in our case the Green's function since we no longer deal with the Dirichlet problem where by analogy we have the function of the first kind. It represents the total velocity potential at Q when the incident waves are due to a line source at P. If this diffraction problem were solved then eq. (145) would give the solution of all other diffraction problems with the same reflecting boundary Γ.

It is not difficult to formulate and prove uniqueness theorems for the functions found above. Care must be taken to apply the radiation condition to the appropriate part of the decomposed field as discussed in subsection C1.1. We suppose for the moment that there were two solutions f and f', we form their difference on their real and imaginary parts on which we apply Green's second identity. Finally we find that f = f' (see Stoker [13]).

C3.3.2 Integral equations. We have seen in subsection C1.1 that a powerful technique of tackling diffraction problems is by means of integral equations. The type of integral equation obtained for the simple problem of the slit in two dimensions is presented in eq. (46). Before trying to apply integral equations to the more difficult

problem of the two screens not being in the same plane, it is necessary to discuss briefly some of the theory of these equations to the extent it is useful for our work.

The general equations (134) and (135) give, when the point P is allowed to be on the contour of the integration where it is denoted by p, the following type of integral equation

$$s(p) = f(p) - \kappa\int f(q)K(p,q)dq \tag{146}$$

where the function f(p) can be evaluated by knowing $\partial F/\partial n$, κ a constant for any particular problem and the kernel K(p,q) of the equation depending on the derivative of the Hankel function $H_o(kr_1)$.

A classical method to solve eq. (146) is by successive approximations. We may take any appropriate function f_o as the zeroth order approximation, e.g. we take $f_o = s$ when the kernel is small. Then the first order approximation is

$$f_1(p) = s(p) + \kappa\int f_o(q)K(p,q)dq$$

the second

$$f_2(p) = s(p) + \kappa\int f_1(q)K(p,q)dq \quad \text{and so on.}$$

Or introducing the iterated kernels

$$K_n(p,q) = \int K_{n-1}(p,r)K(r,q)dr \quad , \; K_o(p,q) = K(p,q)$$

we find for the nth approximation

$$f_n(p) = s(p) + \kappa\int s(q)K(p,q)dq + \ldots + \kappa^{n-1}\int s(q)K_{n-2}(p,q)dq +$$

$$+ \kappa^n\int f_o(q)K_{n-1}(p,q)dq \tag{147}$$

The solution (147) with $f_o = s$ can be put into the form

$$f(p) = s(p) + \kappa\int s(q)R(p,q;\kappa)dq \qquad (148)$$

where the function

$$R(p,q;\kappa) = K(p,q) + \kappa K_1(p,q) + \kappa^2 K_2(p,q) + \ldots$$

is the resolvent of the kernel K(p,q) (Kellogg [31]).

The associated homogeneous integral equation obtained from eq. (146) is

$$f(p) = \kappa\int f(q)K(p,q)dq \qquad (149)$$

which generally has no non-trival solutions.

The kernel is said to be degenerate if it consists of a finite sum of products of functions of p only and of q only.

$$K(p,q) = \sum_{k=1}^{n} \tau_k(p)\sigma_k(q)$$

Equation (146) gives now

$$f(p) = s(p) + \kappa \sum_{k=1}^{n} x_k\tau(p)$$

where x_k are certain numbers given by

$$x_k = \int\sigma_k(q)f(q)dq$$

Thus the entire problem reduces to finding numbers instead of functions (see e.g. Smirnov [32]). Generally we can approximate the integral in eq. (146) by some simple form not involving the integral sign.

Indeed we can put

$$\int_a^b \psi(x)dx = \sum_{k=1}^{n} A_k \psi(s_k) + \varepsilon$$

where A_k and x_k are constant numbers for a given formula and ε is the error. Applying the above relation to eq. (146) we arrive at the equation

$$f(p) = s(p) + \kappa\tau(p) + \kappa \sum_{k=1}^{n} A_k K(p,q_k) f(q_k)$$

which in fact is a system of algebraic equations easy to be solved after neglecting the small quantity ε (see e.g. Kantorovich and Krylov [33]).

Much work has been done in the case where the kernel is singular; when the singularity occurs at $p = q$ we can remove the diagonal term of the matrix $K = K_{ij}$. In general we can use a composite formula for the evaluation of the integral avoiding the points of singularity (Delves and Walsh [34]).

So far we have seen only the second kind of the so-called Fredholm integral equations: eq. (146) is the general and eq. (149) is the homogeneous form. Equations of the first kind are of the type

$$\int K(p,q) f(q) dq = s(p) \qquad (150)$$

and the associated homogeneous is

$$\int K(p,q) f(q) dq = 0 \qquad (151)$$

We shall meet this kind of integral equation later, therefore let us see quickly the special difficulties it poses.

The main troublesome feature from a computational point of

view is that the problem is improperly posed, that is the solution f does not depend continuously on the data function s; thus a very small perturbation on s can give rise to an arbitrarily large perturbation in f. A method of solving the equation is of expanding the kernel and the given function into products of appropriate functions

$$K(p,q) = \sum_i k_i\, u_i(p) v_i(q)$$

$$s(p) = \sum_i s_i\, u_i(p)$$

hence the solution would be of the form

$$f(q) = \sum_i \frac{s_i}{k_i} v_i(q)$$

There are uniqueness theorems of course, together with conditions for convergence and compatibility. In general s(p) must not contain components which are not matched by a corresponding component in K(p,q). Use of other expansions can be made, as well as regularization or iterative method (Delves and Walsh [34], ch. 13).

Returning now to the diffraction problem, we rewrite eq. (134) for the interior problem under the same assumptions in a complete form taking into account the values of f at the boundary Γ

$$\int \{f(q) \frac{\partial}{\partial n} G(p,q) - G(p,q) \frac{\partial}{\partial n} f(q)\} dq = \begin{cases} f(p) , & p \in D \\ \frac{1}{2} f(p) , & p \in \Gamma \\ 0 , & p \in E \end{cases} \qquad (152)$$

where $G(p,q) = \frac{i}{4} H_o(kr)$ is the free space Green's function, r is the non-negative distance between the two points p and q, D the interior domain and E the exterior. Function f must satisfy the conditions of eq. (134) and it will be specified later in relation with the

familiar incident, scatterd and total fields. These equations are of the type considered above, namely Fredholm integral equations of the second kind. The integral

$$g(p) = -2 \int_{\Gamma} G(p,q) \frac{\partial}{\partial n} f(q)\, dq$$

is known for any given boundary Γ, so the second of eq. (152) gives

$$f(p) = g(p) + \int_{\Gamma} K(p,q) f(q)\, dq \tag{153}$$

where $K(p,q) = 2 \frac{\partial}{\partial n} G(p,q)$.

The last equation is identical with eq. (146) which permits the numerical treatment suggested previously. In fact we approximate the integral in eq. (153) by a quadrature formula

$$\int_a^b Q(t)dt \simeq \sum_j w_j Q(t_j)$$

say, and we get

$$f(p) \simeq g(p) + \sum_j w_j K(p,q_j) f(q_j) \tag{154}$$

To solve eq. (154), Fredholm put $p = q_i$, $i = 1,2, \ldots$ and arrived at the system of algebraic equations

$$f_i - \sum_j K_{ij} w_j f_j = g_i \tag{155}$$

By getting max i = max j = n we have n equations for the n unknown $f_i \equiv f(q_i)$, the q_i being quadrature points. Having found f_i by solving eqs. (155) we can calculate f(p) at non quadrature points via eq. (154). The normal procedure is to divide the contour into n equal arcs and take the value of f constant along each interval so that it comes out of the integral sign. When the points coincide

the kernel is non-singular for two-dimensional problems, in fact (Delves and Walsh [34], p. 286)

$$\lim_{q\to p} K(p,q) = \lim_{q\to p} \frac{\partial}{\partial n_q} 2G(p,q) = -\text{curvature at } p$$

In eqs (152) function f can clearly represent the scattered field F_s. Nevertheless in order to take advantage of the fact that for our case we have $\partial F/\partial n = 0$ along the solid boundary, where F is the total field, we give the following formulation of Burton and Miller [35]

$$F_i(p) + \int_\Gamma \{F(q) \frac{\partial}{\partial n} G(p,q) - G(p,q) \frac{\partial}{\partial n} F(q)\}dq = \begin{cases} F(p), & p \in D \\ \frac{1}{2}F(p), & p \in \Gamma \\ 0, & p \in E \end{cases} \quad (156)$$

which, when the boundary condition $\frac{\partial F}{\partial n} = 0$ is applied reduces to

$$F(p) = 2F_i(p) + 2 \int_\Gamma F(q) \frac{\partial}{\partial n} G(p,q)dq , \quad p \in \Gamma \quad (157)$$

a Fredholm equation of the second kind similar to (153).

In order to apply the above theory to our problem, a contour can be drawn as in fig. 18 in whose interior we try to evaluate the wave function F. Unfortunately I have encountered difficulties in finding a non-trivial solution; this is due to the fact that the second of eqs (156) - or (152) - does not hold for boundaries that have been shrunk to a double line segment and their interior domain has disappeared. A brief proof might be worthwhile, for I have not found anything similar presented explicitly in the literature.

Consider the contour S comprising the two identical arcs S_1, S_2 (fig. 19). We shall apply twice Green's identity taking the point p to be on S_1 or S_2 each time but with the same co-ordinates.

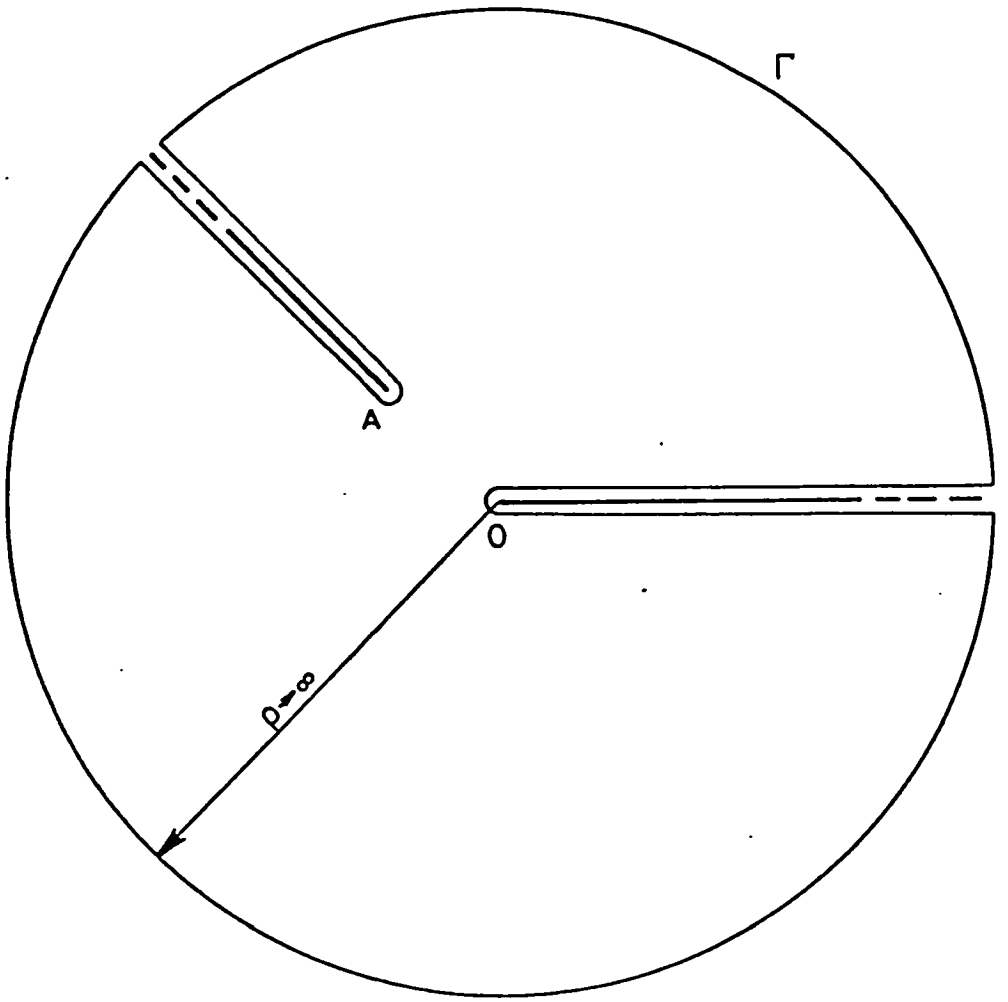

Fig. 18. A contour S for application of Green's identity

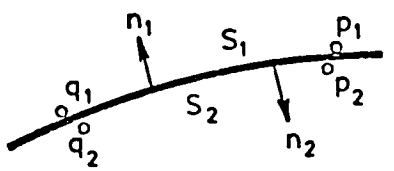

Fig. 19. A contour S with no interior

Applying Green's identity for the function f fulfilling all the necessary requirements of eq. (135) we have for the point p_1:

$$\frac{1}{2} f(p_1) = \int_{S_1} f(q_1) \frac{\partial}{\partial n_1} G(p_1,q_1)dq_1 + \int_{S_2} f(q_2) \frac{\partial}{\partial n_2} G(p_1,q_2)dq_2 -$$

$$- \int_{S_1} G(p_1,q_1) \frac{\partial}{\partial n_1} f(q_1)dq_1 - \int_{S_2} G(p_1,q_2) \frac{\partial}{\partial n_2} f(q_2)dq_2$$

For the point p_2:

$$\frac{1}{2} f(p_2) = \int_{S_1} f(q_1) \frac{\partial}{\partial n_1} G(p_2,q_1)dq_1 + \int_{S_2} f(q_2) \frac{\partial}{\partial n_2} G(p_2,q_2)dq_2 -$$

$$- \int_{S_1} G(p_2,q_1) \frac{\partial}{\partial n_1} f(q_1)dq_1 - \int_{S_2} G(p_2,q_2) \frac{\partial}{\partial n_2} f(q_2)dq_2$$

For our free space Green's function $G(p,q) = \frac{i}{4} H_o(k|p-q|)$ we can readily show that

$$G(p_1,q_1) = G(p_2,q_1),\ G(p_1,q_2) = G(p_2,q_2)$$

and

$$\frac{\partial}{\partial n_1} G(p_1,q_1) = \frac{\partial}{\partial n_1} G(p_2,q_1),\quad \frac{\partial}{\partial n_2} G(p_1,q_2) = \frac{\partial}{\partial n_2} G(p_2,q_2)$$

Hence we find $f(p_1) = f(p_2)$ which contradicts the assumption that we can ascribe whatever values of the function f at the boundary.

The contour of fig. 18 has now to be abandoned, in view of the above limitation. The only simple alternative is to draw two contours as in fig. 20. Our intention is to apply Green's identities to two separate contours and appropriate functions and to use

the continuity of the total potential F as well as of its normal derivative $\partial F/\partial n$ across the opening OA.

Employing the modified Green's identities (156) we get for region I, when the point p lies on the contour Γ_1

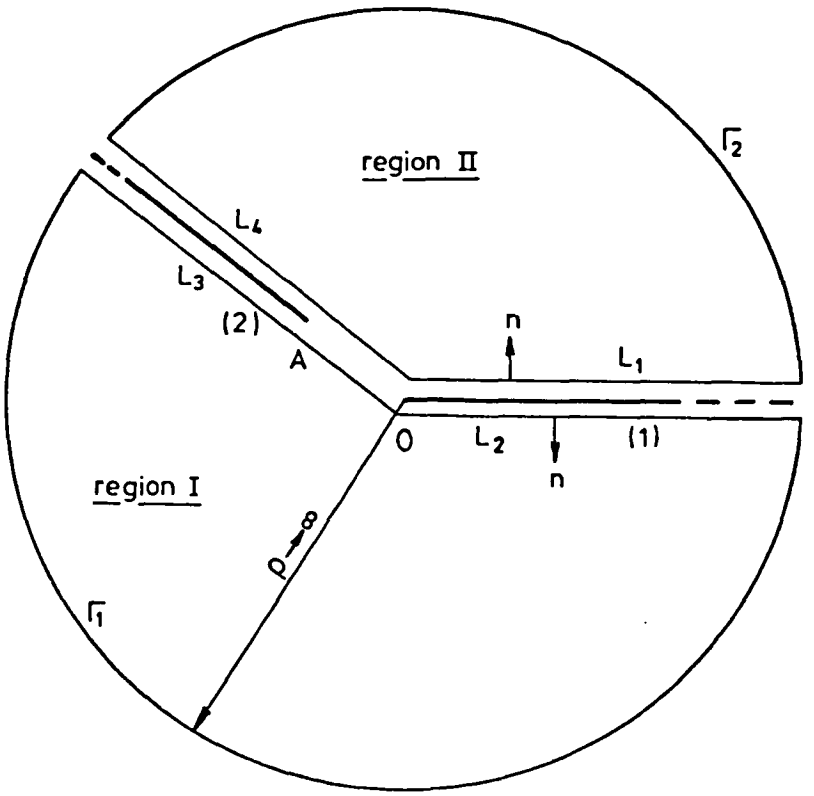

Fig. 20. Two regions I, II covering the whole plane

$$\frac{1}{2} F_s(p) = \int_{\Gamma_1} F(q) \frac{\partial}{\partial n_q} G(p,q)dq - \int_{\Gamma_1} G(p,q) \frac{\partial}{\partial n_q} F(q)dq$$

$$= \int_{L_2 \cup L_3} F(q) \frac{\partial}{\partial n_q} G(p,q)dq + \int_{OA_I} F(q) \frac{\partial}{\partial n_q} G(p,q)dq -$$

$$- \int_{OA_I} G(p,q) \frac{\partial}{\partial n_q} F(q)dq$$

taking into account boundary and radiation conditions. When p is on OA we get

$$\frac{1}{2} F_s(p) = \int_{L_2} F(q) \frac{\partial}{\partial n_q} G(p,q)dq - \int_{OA_I} G(p,q) \frac{\partial}{\partial n_q} F(q)dq \qquad (158)$$

Similarly working in region II we obtain

$$\frac{1}{2} F_s(p) = \int_{L_1} F(q) \frac{\partial}{\partial n_q} G(p,q)dq - \int_{OA_{II}} G(p,q) \frac{\partial}{\partial n_q} F(q)dq \qquad (159)$$

when p lies on segment OA_{II}.

It is clear that from eqs (158) and (159) we cannot formulate a system of algebraic equations as in eq. (155) because point p cannot occupy all the positions of point q; the need therefore to eliminate the first integrals in the above equations becomes apparent. Unfortunately, even if we differentiate these relations along the normal to OA, the fact that the two screens are not in the same plane leads in general to

$$\frac{\partial^2}{\partial n_q \partial n_p} G(p,q) \neq 0 ,$$

with p on OA and q on L_1 or L_2, and consequently the first integrals cannot be set equal to zero if the kernel remains the free space Green's function. This suggests, since we cannot have F = 0 along the arms, to try to achieve $\partial G/\partial n = 0$ there, in other words to employ the Green's function associated with our configuration rather than that of the free space; thus we could also limit our calculations to the finite segment OA instead of having infinite range of integration. Of course the pure numerical method, as we can label it, leading to the formulation of eqs (158) and (159), where the free

space Green's function is used, is of much use when we are dealing with finite and irregular configurations where analytical approach seems impossible. We shall mention again this method briefly in subsection E3.1 but for the rest of the present subsection let us try to arrive at the final formulation of our equations along the lines suggested above.

C3.3.3 Final formulation. As we have already seen the Green's function that satisfies the boundary conditions of the problem is no longer the free space Green's function; the former is a different function for each problem under consideration, while the latter remains the same. The form of a Green's function reveals its nature; generally a complicated function is associated with the actual problem as we have already seen in subsection C3.2 and presents simply the solution of the diffraction problem under consideration when a unit source is present.

Using the contours of fig. 20 we can write expressions for the two regions I and II employing suitable Green's functions. The wave function in each region will be the sum of the same potential if there were no aperture plus that due to the presence of the gap; thus by denoting the field in region I, for the same incident wave but with the aperture filled by extending plane (2) to the origin O so that a wedge is formed, by F_w we have for

$$\text{region I} : F_I = F_w + F_1 \tag{160}$$

$$\text{region II} : F_{II} = 0 + F_2 \tag{161}$$

where now,

$$F_1(p) = \int_o^d V(q)G_I(q,p)dq \tag{162}$$

$$F_2(p) = -\int_o^d V(q)G_{II}(q,p)dq \tag{163}$$

V(q) is the velocity derived from F as its normal derivative to OA pointing into the region II.

$G_I(q,p)$ is the total velocity potential at the point q in OA due to a line source at p for the wedge problem.

$G_{II}(q,p)$ is similarly the potential for the corner problem (see fig. 21).

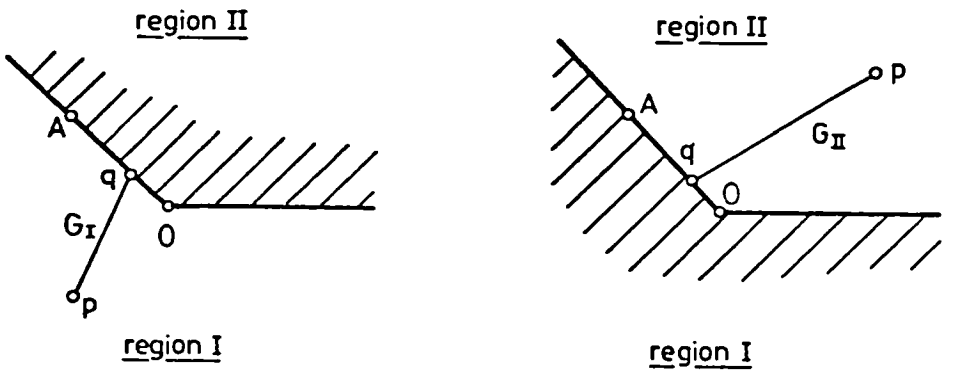

Fig. 21. G_I and G_{II} for the two regions

These functions are known and can be found in subsection C2.2. The solution consisting of eqs (160) to (163) is rigorous so far under our general assumptions;indeed we have implied continuity of the normal derivative V across the gap. We now imposed the other requirement that is continuity of F across the gap. Letting the points p of the two regions I and II coincide on the point q' on OA

we obtain from eqs (160) and (161)

$$F_w(q') + F_1(q') = F_2(q')$$

or using eqs (162) and (163)

$$\int_o^d V(q)\{G_I(q,q') + G_{II}(q,q')\}dq = - F_w(q') \qquad (164)$$

where $F_w(q')$ is the potential at q' due to our actual incident wave diffracted by the wedge of fig. 21, which again can be obtained from subsection C2.2. Equation (164) is a Fredholm integral equation of the first kind with unknown function V(q); solving this equation and substituting V(q) into eqs (162), (163) we obtain F_1, F_2 hence F_I, F_{II} by eqs (160), (161).

We deduce easily from eqs (70) and (72)

$$F_w(p) = \frac{2\pi}{2\pi-\theta} \sum_{m=o}^{\infty} \varepsilon_m J_\mu(kr)\cos\mu(2\pi-\omega)\cos\mu(2\pi-\theta_o)e^{-\frac{1}{2}i\mu\pi}$$

$$F_w(q') = \frac{2\pi}{2\pi-\theta} \sum_{m=o}^{\infty} (-)^m \varepsilon_m J_\mu(kr)\cos\mu(2\pi-\theta_o)e^{-\frac{1}{2}i\mu\pi}$$

$$G_I(q,p) = \frac{\pi i}{2(2\pi-\theta)} \sum_{m=o}^{\infty} (-)^m \varepsilon_m J_\mu(kr_<)H_\mu(kr_>)\cos\mu(2\pi-\omega)$$

$$G_I(q,q') = \frac{\pi i}{2(2\pi-\theta)} \sum_{m=o}^{\infty} \varepsilon_m J_\mu(kr_<)H_\mu(kr_>)$$

$$G_{II}(q,p) = \frac{\pi i}{2\theta} \sum_{m=o}^{\infty} (-)^m \varepsilon_m J_\nu(kr_<)H_\nu(kr_>)\cos\nu\omega$$

$$G_{II}(q,q') = \frac{\pi i}{2\theta} \sum_{m=o}^{\infty} \varepsilon_m J_\nu(kr_<) H_\nu(kr_>)$$

with $\nu = \frac{m\pi}{\theta} = \mu \left(\frac{2\pi}{\theta} - 1\right)$ and the rest of the notation as in eqs (70),(72).

Equation (164) becomes

$$\int_o^d V(q) \left\{ \sum_{m=o}^{\infty} \varepsilon_m J_\mu(kr_<) H_\mu(kr_>) + \left(\frac{2\pi}{\theta} - 1\right) \sum_{m=o}^{\infty} \varepsilon_m J_\nu(kr_<) H_\nu(kr_>) \right\} dq$$

$$= 4i \sum_{m=o}^{\infty} (-)^m \varepsilon_m J_\mu(kq') \cos\mu(2\pi - \theta_o) \exp\{-\tfrac{1}{2} i\mu\pi\} \qquad (165)$$

where $r_<, r_>$ take values from the set $\{q,q'\}$.

This is a Fredholm equation of the first kind of the type

$$\int_o^d K(x,y)\, f(y)dy = g(x) \quad , \quad (0 \leq x \leq d)$$

with f(y) representing the unknown function V(q),

$$K(x,y) = \sum_m k_m u_m(x) v_m(y) + \sum_m \ell_m u'_m(x) v'_m(y)$$

$$g(x) = \sum_m a_m u_m(x)$$

for the case of $y > x$;

u,v,u',v' represent the functions J_μ, H_μ, J_ν, H_ν respectively and a,k,ℓ are numbers. The fact that the kernel K is non-symmetrical and that $\mu \neq \nu$ in the products of Bessel functions introduces a big problem in finding an appropriate expansion, as discussed in the previous subdivision, for the right hand side of eq. (165). Therefore, a direct numerical solution seems to be very difficult. However, as

we have seen before, the fact that in this type of integral equations the problem is ill posed, which means that a small perturbation on g can give large perturbation in f, gives us a certain degree of freedom in choosing a priori the function f hoping that the 'error' in g would be limited; this seems to be a plausible assumption since K here has the character of a smoothing operator, its effect being to smooth any roughness in the f(y) on which it operates. And above all the simple fact that we are looking for an engineering application allowed me to take this step, namely to introduce an estimate of the function f(y) and then evaluate the quadrature of eqs (162) and (163). The function that has been chosen to substitute V(q) in these equations is the unperturbed value of the appropriate normal derivative of the incident field, a practice used elsewhere too (see e.g. Lacombe [4]).

We put therefore

$$V(q) = \frac{\partial F_o}{\partial n}(q) = -ik\sin(\theta-\theta_o)\ \exp\{-ikq\cos(\theta-\theta_o)\}$$

from eq. (95), and note that from now on we are interested only in the region II which represents the protected surface of the sea or in other words the harbour area; of course the potential in the outer region can be evaluated readily through eqs (160) and (162) but it does not present much interest in practice. Hence the other pair of equations give

$$F = F_{II} = -\frac{\pi^2}{\lambda\theta}\sin(\theta-\theta_o)\int_o^d \exp\{-ikq\cos(\theta-\theta_o)\}\sum_{m=o}^{\infty}(-)^m\varepsilon_m J_\nu(kr_<)\times$$

$$\times H_\nu(kr_>)\cos\nu\omega dq \qquad (166)$$

where $\nu = m\pi/\theta$, $0 \leq q \leq d$ and $r_<, r_>$ choose among the values $\{q,r\}$.

This is our final formulation of the solution to our problem and it forms the basis of the computations presented in the next chapter.

We shall confine ourselves mainly to the case of $r > q$ which means that the observation point has a distance from the origin larger than the maximum q i.e. the width d. There is no restriction in finding values of the potential near the gap, as eq. (166) shows, the only alteration being a mere change of symbols. This modification will be discussed in section E1.

Our remaining task now is to compute the above equation and find results for various combinations of the values of $r, \omega, \theta_o, d, \theta$; this is presented in the following section.

C4 COMPUTING PROCEDURE

C4.1 Calculation of Bessel Functions

As we have seen in the Introduction the characteristic that is of most importance to us is the diffraction coefficient, i.e. the ratio at any particular point of the actual maximum height of the waves to the corresponding height of the incident wave, which equals the unity as we have seen in section A1. The diffraction coefficient is expressed as in eq. (9)

$$K = |F|$$

or due to eq. (166)

$$K = -\frac{\pi^2 \sin\zeta}{\theta}\Bigg[\Bigg\{\int_o^\delta \Bigg\{\cos(2\pi x\cos\zeta)\sum_{m=o}^{N}(-1)^m \varepsilon_m \cos\frac{m\pi\omega}{\theta} J_{\frac{m\pi}{\theta}}(2\pi\rho)J_{\frac{m\pi}{\theta}}(2\pi x) +$$

$$+ \sin(2\pi x\cos\zeta)\sum_{m=o}^{N}(-1)^m \varepsilon_m \cos\frac{m\pi\omega}{\theta} J_{\frac{m\pi}{\theta}}(2\pi x)Y_{\frac{m\pi}{\theta}}(2\pi\rho)\Bigg\}dx\Bigg\}^2 +$$

$$+ \Bigg\{\int_o^\delta \Bigg\{\cos(2\pi x\cos\zeta)\sum_{m=o}^{N}(-1)^m \varepsilon_m \cos\frac{m\pi\omega}{\theta} J_{\frac{m\pi}{\theta}}(2\pi x)Y_{\frac{m\pi}{\theta}}(2\pi\rho) -$$

$$- \sin(2\pi x\cos\zeta)\sum_{m=o}^{N}(-1)^m \varepsilon_m \cos\frac{m\pi\omega}{\theta} J_{\frac{m\pi}{\theta}}(2\pi x)J_{\frac{m\pi}{\theta}}(2\pi\rho)\Bigg\}dx\Bigg\}^2\Bigg]^{\frac{1}{2}} \quad (167)$$

where we have now expressed all lengths in terms of the wavelength λ; thus $\delta = d/\lambda$, $x = q/\lambda$, $\rho = r/\lambda$ and $\zeta = 2\pi - (\theta_o - \theta)$, N a large integer.

Our first task is to achieve the computing of Bessel functions of non-integral order. To do this I have used a computer programme developed by P.W. Milne and J.J. Russell in FORTRAN language at the C.S.I.R.O. Installation, Melbourne, Australia. This routine is used in conjunction with a subroutine evaluating the corresponding gamma function and it is based on a recurrence technique explained in Goldstein and Thaler [36].

In general the relation

$$C_{\nu-1}(Z) + C_{\nu+1}(Z) = \frac{2\nu}{Z} C_{\nu}(Z) \tag{168}$$

is used where C may be either J or Y. If ν is a non-negative integer Y_o and Y_1 are found using the relations

$$Y_o(Z) = \frac{2}{\pi}\{(\log \frac{Z}{2} + \gamma)J_o(Z) + 2 \sum_{n=1}^{\infty}(-)^{n-1} \frac{J_{2n}(Z)}{n} \}$$

where γ is Euler's constant = 0.5772... , and

$$J_1Y_o - J_oY_1 = \frac{2}{\pi Z} \quad \text{(Watson [15], § 3.63),}$$

together with the recurrence relation (168).

If the positive ν is non integer Y_ν is obtained from the relation

$$Y_\nu = \frac{J_\nu \cos(\nu\pi) - J_{-\nu}}{\sin(\nu\pi)}$$

The above programme has been adapted to the requirements of the Imperial College Computer Centre.

At first a simple test has been carried out to check the computed values of J and Y for specific values of ν for which tables exist. The agreement was very good. The range of ν extended up

to 19 including fractional orders. For example we find for $J_1(2\pi)$ the number -0.1545 while by a linear interpolation from the tables we find -0.1542; or for a limited number of digits we have $Y_2(0.10) = -127.6$ where the tables give -127.64.

A second test followed to establish the summation procedure which has been performed on the values of J and Y as dictated by eq. (167). For this purpose a version of an addition theorem (Watson [15]) has been used. We have

$$H_o(Z) = J_o(w)H_o(W) + 2\sum_{n=1}^{\infty} J_n(w)H_n(W)\cos(n\chi)$$

where $Z = (w^2 + W^2 - 2wW\cos\chi)^{\frac{1}{2}}$

with the notation of fig. 22.

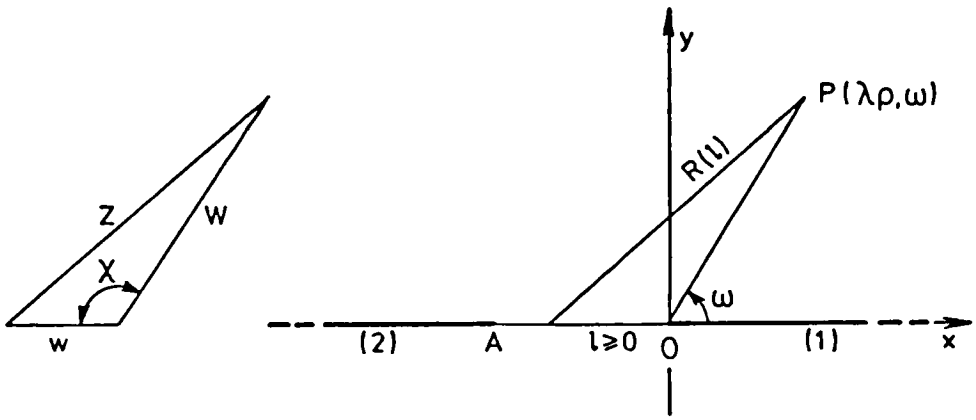

Fig. 22. The application of an addition theorem of Bessel functions

Or

$$H_o(Z) = \sum_{n=o}^{\infty} \varepsilon_n J_n(w)H_n(W)\cos(n\chi)$$

$$= \sum_{n=o}^{\infty} (-1)^n \varepsilon_n J_n(w)H_n(W)\cos n\omega \qquad (169)$$

with $Z = [(2\pi\ell)^2 + (2\pi\rho)^2 + 2(2\pi\ell)(2\pi\rho)\cos\omega]^{\frac{1}{2}} = 2\pi R(\ell)$

if $w = 2\pi\ell$, $W = 2\pi\rho$.

Putting $\rho = 3.0$, $\omega = 60^{\circ}$, $\ell = 1.0$ we have $R = \sqrt{13}$. Evaluating both sides of eq. (169) we find from left-hand side the number

$$-0.166249421789 + 0.021348251872i$$

and from the right-hand side

$$-0.166249421789 + 0.021348251862i$$

leading to a perfect agreement. The DO LOOP necessary for the summation had been repeated 20 times which proved to be enough for our order of accuracy that requires two decimal places for our final result K. However, it was found that with increasing δ we had to take more terms of the series to assure small error; for example for $\delta = 5.0$ more than 30 terms were needed, but for the results presented in the final chapter we have $\delta = 3.0$ at most so for these last cases 26 terms were taken instead.

C4.2 Evaluation of the Quadrature

The summation of the series having been preformed, it remains to evaluate the definite integrals that occur in eq. (167). The number of pivots, i.e. points that divide the range of integration into small segments, needed to obtain the answer to the required accuracy is not known beforehand, therefore we cannot use Gaussian approximation formulas (quadratures); the Patterson algorithm DOIACF of the Nottingham Algorithms Group has been used instead, which uses the optimum addition of points to a quadrature formula.

The routine evaluates a definite integral of the form

$$\int_a^b f(x)dx$$

using a method described in Patterson [37]. By a suitable change of variable

$$t = \frac{2}{b-a}x - \frac{b+a}{b-a}, \qquad x = \frac{b-a}{2}t + \frac{b+a}{2}$$

the integral is changed to the form

$$\int_{-1}^{1} Q(t)dt$$

which is then approximated by a quadrature formula $\sum_{k=1}^{n} A_k Q(X_k)$, where A_k are the weights and X_k are the pivots. The routine begins with the three-point Gauss rule and derives a new seven-point rule, three of which coincide with the original Gauss abscissae; the remaining pivots are chosen to give the greatest possible increase in accuracy. The procedure is repeated to produce 15,31,63,127 and 255 - point rules if required. The integration is based on the successive application of these rules until two results are obtained which differ by less than a prescribed value RELACC or absolutely by less than a value ABSACC. In order to prevent unnecessary amount of calculation for some special values of the integral, both these parameters have been specified. An error parameter gives a failure message if any error is detected. The integrand, which in our case is the already computed series of Bessel functions multiplied by a circular function, is called by an external function command.

A test programme operating on a simple Bessel function has been run at a first checking step. Use was made of the formula

$$\int_0^a J_1(bx)dx = \frac{1}{b}\{1 - J_o(ab)\}, \qquad a > 0$$

which for a = 1, b = 2π gives the result

$$\frac{1}{2\pi}\{1 - J_o(2\pi)\} \simeq 0.124$$

The routine gave the same result using 15 points in the range of integration. The difference between the last two successive estimates of the integral was 0.5606×10^{-8}.

A second test was then carried out by computing the integral

$$\int_0^\delta \cos(2\pi x\cos\zeta) J_{\frac{m\pi}{\theta}}(2\pi x)dx$$

for various values of the parameters δ, ζ, θ, m.
The output reproduced the answer 0.124 for $\delta = 1.0$, $\theta = \pi$, $\zeta = 3\pi/2$, $m = 1$ using again 15 points and obtaining relative error 0.561×10^{-8}.

A final checking has been performed on eq. (167) for $\theta = \pi$, $\delta = 2$, $\zeta = 3\pi/2$, $\rho = 3.0$, $\omega = \pi/3$. Under the same assumptions we have for this case

$$F(P) = 2\int_0^2 \frac{\partial F}{\partial n}\frac{i}{4} H_o(kR)dx = \frac{k}{2}\int_0^2 H_o[k\sqrt{\rho^2 + x^2 + 2\rho x\cos\omega}]dx$$

and

$$K = |F| = \pi\left[\{\int_0^2 J_o(2\pi\sqrt{x^2 + \rho^2 + 2x\rho\cos\omega})dx\}^2 + \right.$$

$$\left. + \{\int_0^2 Y_o(2\pi\sqrt{x^2 + \rho^2 + 2x\rho\cos\omega})dx\}^2\right]^{\frac{1}{2}}$$

which equals $\frac{1}{4}$ for $\rho = 3$, $\omega = 60^o$.

Our equation (167) gives for that case the answer 0.2503... , while a parallel computing of the above relation gives the same result to the seventh decimal place.

We now procede to obtaining results for our applications. Two sets of such results were sought; the first set was intended to be compared with our experimental results and the second to produce plots presenting the diffraction coefficient for different cases. All these have been included in the final chapter.

C5 ANOTHER APPROACH

C5.1 Some Theory of Matched Asymptotic Expansions

As has been mentioned in section A2, an independent approach to those presented in subsection C1.1 occupies the rest of this chapter. The approach is based on a method known as matched asymptotic expansions and provides some checking of our main theoretical results of section C3. An elementary account of this method is given here.

We can find the first hints of the method in the works of Rayleigh and Lamb; in fact eq. (37) is a direct result of Lamb's argument ([5], p. 532) that in the two-dimensional problem of waves passing through an aperture and in the immediate neighbourhood of the aperture the motion 'must resemble the flow of a liquid through the same aperture' and an approximation is obtained by comparison with the results of the theory of the steady two-dimensional fluid motion as developed by the use of conformal transformations. The same procedure is used here as the basis of our method.

The modern theory of matched expansions can be said to have been established by M. Van Dyke in his book 'Perturbation methods in fluid mechanics' [38]. In general the space where the solution of our problem applies is divided into two overlapping regions, the inner and outer region, and by a suitable choice of the variables we have to solve two independent problems, the inner and the outer. It is evident that for each one of these problems we lose some boundary condition which is replaced by the asymptotic matching principle which

states that the m-term inner expansion of the n-term outer expansion = the n-term outer expansion of the m-term inner expansion. This principle proposed by Van Dyke has been slightly modified in the more general work due to Fraenkel [39] where the necessity of grouping together logarithmic with algebraic terms is implied (see also [26], appendix).

More formally if we denote by $f(r;\varepsilon)$ and $\psi(R;\varepsilon)$ the wave functions expressed in outer and inner variables r and R respectively, with $r = \varepsilon R$, it is assumed that the function $f(r;\varepsilon)$ has an expansion, uniformly valid for $r >> \varepsilon = ka$, a being a characteristic length of the problem

$$f(r;\varepsilon) \sim \sum_{n,m} \varepsilon^n (\log\varepsilon)^m f_{n,m}(r) \qquad \text{as } \varepsilon \to 0 \tag{170}$$

The angular parameter is suppressed in the above expressions of the wave functions because it should be common to each expansion; otherwise the matching could not be performed.

It is further assumed that the constituent functions $f_{n,m}$ also have expansions as $r \to 0$ of the form

$$f_{n,m}(r) \sim \sum_{i,j} r^i (\log r)^j a_{nijm} \qquad \text{as } r \to 0 \tag{171}$$

where the a's are numbers independent of r.
Usually the numbers m,j are finite integers, while n,i are rational numbers.

Similarly the inner potential $\psi(R;\varepsilon)$ is assumed to have an expansion of the same type valid for $r << 1$

$$\psi(R;\varepsilon) \sim \sum_{p,q} \varepsilon^p (\log\varepsilon)^q \psi_{pq}(R) \qquad \text{as } \varepsilon \to 0, \quad r << 1 \tag{172}$$

with

$$\psi_{p,q}(R) \sim \sum_{k,l} R^{-k}(\log R)^{l} b_{pklq} \qquad \text{as } R \to \infty \tag{173}$$

Under the above assumptions there is a common region of validity

$$\varepsilon << r << 1$$

where the matching principle is to be applied. To describe this principle we use the notation $f^{(N)}$ to denote the expansion (170) up to terms of order ε^N, and $f^{(N,M)}$ to denote the function $f^{(N)}$ written in terms of $R = r/\varepsilon$ and expanded as $\varepsilon \to 0$, R fixed, up to terms of order ε^M; similarly for the function ψ. Now, the matching principle asserts that

$$f^{(N,M)} = \psi^{(M,N)} \tag{174}$$

and enables us to find the coefficient of all terms of the series.

C5.2 The Outer Problem

C5.2.1 Ocean. We choose for our purpose the low frequency range of the problem, a practice that in most cases shows that the result holds good for the intermediate frequency range as well. The problem involves two independent length scales d and λ, therefore we see it as a singular perturbation problem which means that a single solution cannot be found valid throughout the flow field. We introduce the parameter $\varepsilon = kd$ and express the expansions of the wave function in terms of this parameter; as $\varepsilon \to 0$ it is clear that the field in the outer region of the ocean part ($\theta < \omega < 2\pi$) will tend to the known

solution of the diffraction by a wedge f_w, so we can assume an expansion for the outer approximation

$$f(w,y) \sim f_w(w,y) + \sum_n g_n(\varepsilon) f_n(x,y) \qquad (175)$$

where in f_w the incident plane wave has been incorporated, and $g_n(\varepsilon) \to 0$ as $\varepsilon \to 0$.

Some of the functions f_n will contain the behaviour of a line source at the origin, because at long distance from it the flow resembles that caused by a negative line source located at the opening of the two breakwaters. Such a behaviour is expressed simply by

$$-\frac{i}{4} H_o(kr) \qquad (176)$$

The difficulty that arises now is that when ε is small enough but not zero the order of magnitude of the 'source field' becomes greater than that of the 'wedge field' which is the reverse to what happens when $\varepsilon = 0$. This difficulty forced me to perform the matching of the two basic solutions to a low order, as we will see in subsection C5.4

The asymptotic expansions of f_w and of (176) are respectively

$$A + B(kr)^{\pi/\theta} + C(kr)^{2\pi/\theta} + \ldots \quad , kr \to 0 \qquad (177)$$

$$-\frac{i}{4} - \frac{1}{2\pi}(\log 2 - \gamma) + \frac{1}{2\pi}\log(kr) \quad , kr \to 0 \qquad (178)$$

where A,B,C are constants that can be derived from eq. (73).
We write here for reference the expansion of the Hankel function up to the sixth order of the argument

$$H_o(x) = J_o(x) + iY_o(x) \sim \left(1 - \frac{x^2}{4} + \frac{x^4}{64} - \frac{x^6}{9216} + \ldots\right) +$$

$$+ i\left[\frac{2\gamma}{\pi} + \frac{2}{\pi}\log\frac{x}{2} - \frac{x^2}{2\pi}\left(\log\frac{x}{2} + \gamma - 1\right) + \frac{x^4}{32\pi}\left(\log\frac{x}{2} + \gamma - \frac{3}{2}\right) -\right.$$

$$\left. - \frac{x^6}{2340\pi}\left(\frac{1}{2}\log\frac{x}{2} + \frac{\gamma}{2} - \frac{11}{3}\right) + \ldots\right]$$

The last two expansions are true in free space; here, where we have an occupied sector of the entire two-dimensional space of angle θ, we must write instead of eqs (176) and (178)

$$- \frac{\pi i}{2(2\pi-\theta)} H_o(kr) \qquad (179)$$

$$- \frac{\pi i}{2(2\pi-\theta)} - \frac{1}{2\pi-\theta}(\log 2 - \gamma) + \frac{1}{2\pi-\theta}\log(kr) \;,\; kr \to 0 \qquad (180)$$

C5.2.2 Harbour. An observer far away in the lee of the breakwaters sees the flow as caused by a line source at the origin; consequently we will have corresponding expressions to eqs (170) and (180) of opposite sign

$$+ \frac{\pi i}{2\theta} H_o(kr) \qquad (181)$$

$$+ \frac{\pi i}{2\theta} + \frac{1}{\theta}(\log 2 - \gamma) - \frac{1}{\theta}\log(kr) \;, \quad kr \to 0 \qquad (182)$$

C5.3 The Inner Problem

This is worked out in two levels of accuracy, the difference between them lying on the geometrical representation of the opening. First we deal with the less accurate reproduction of our original problem as approximated in fig. 23.

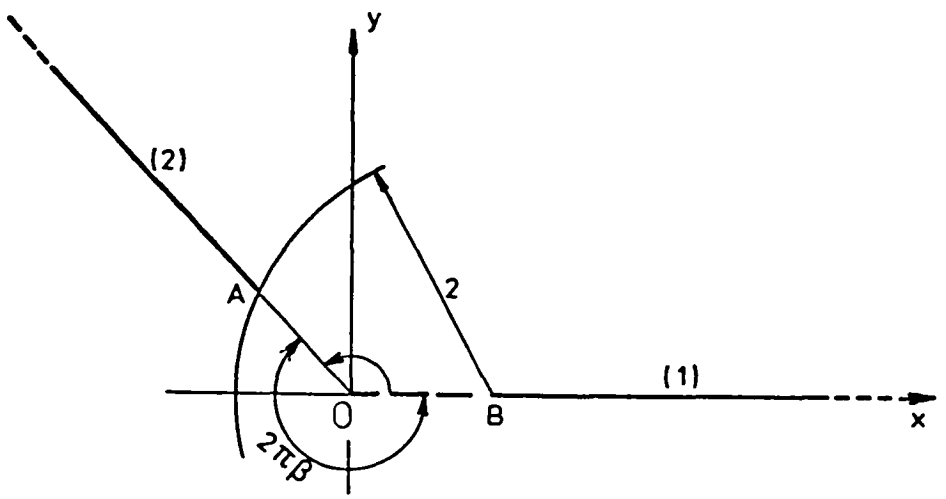

Fig. 23. The inner problem with the segment OB(=OA) not taken into account

We have seen in subsection C5.1 that the basic inner solution comes from the corresponding two-dimensional fluid motion problem; in fact we give here results obtained by Harris [40] (see also Lamb [5], p. 75). By a suitable rotation of the co-ordinate system through an angle $\pi - \frac{\theta}{2} = \pi\beta$ we get x,y in terms of the potential f¶ and the stream function p:

$$x = \frac{\beta^{\beta}(1-\beta)^{1-\beta}}{\sin(1-\beta)\pi}\left[e^{\beta f}\cos\beta(p-\pi) + e^{(\beta-1)f}\cos(1-\beta)(p-\pi)\right] \qquad (183)$$

$$y = \frac{\beta^{\beta}(1-\beta)^{1-\beta}}{\sin(1-\beta)\pi}\left[e^{\beta f}\sin\beta(p-\pi) - e^{(\beta-1)f}\sin(1-\beta)(p-\pi)\right] \qquad (184)$$

¶ It should not be confused with the velocity potential ϕ of the unsteady state.

When our angle θ lies between 90^{o} and 180^{o}, β lies between $\frac{3}{4}$ and $\frac{1}{2}$. An important point in this analysis is that the length of the segment OB is no longer independent (equal to d), but has the value

$$(AB) = (OA) = \csc(1-\beta)\pi$$

so that we always have (AB) = 2 independently of the angle θ. Writing eqs (183) and (184) in compact form with $z = x + iy$, $w = f+ip$ we derive

$$z = \frac{\beta^{\beta}(1-\beta)^{1-\beta}}{\sin(1-\beta)\pi} e^{\beta(w-i\pi)}(1 - e^{-w}) \qquad (185)$$

Moving now to a higher level of accuracy, we take into account the segment OB of the breakwater (1) and we try to find the corresponding relation to eq. (185). From the Dictionary of Conformal Representations by Kober [41] we find through a Schwarz-Christoffel transformation that for this geometry

$$z = x + iy = \left[\frac{1}{2\beta} w^{2\beta} + \frac{a-c}{2\beta-1} w^{2\beta-1} + \frac{ac}{2(1-\beta)} w^{2\beta-2} \right] e^{-2\pi i\beta} \qquad (186)$$

where $a > 0$ depends on the position of point B (fig. 23), and $c > 0$ on the gap width. We no longer require OA to be equal to OB. Relation (186) maps the whole z plane with two semi-infinite slits to the half-plane $p > 0$. This equation gives for the point B the coordinates

$$x_B = (-a)^{2\beta-2}\left[\frac{1}{2\beta} a^2 - \frac{a-c}{2\beta-1} a + \frac{ac}{2(1-\beta)} \right], \quad y_B = 0$$

We require the point B to coincide with 0; therefore putting $x = 0$ we find the value of a in terms of β,c

$$a = \frac{\beta}{1-\beta} c$$

and our original eq. (186) becomes

$$z = \left[\frac{1}{2\beta} w^{2\beta} + \frac{c}{1-\beta} w^{2\beta-1} + \frac{\beta c^2}{2(1-\beta)} w^{2\beta-2} \right] e^{-2\pi i\beta} \qquad (187)$$

describing the mapping of fig. 24.

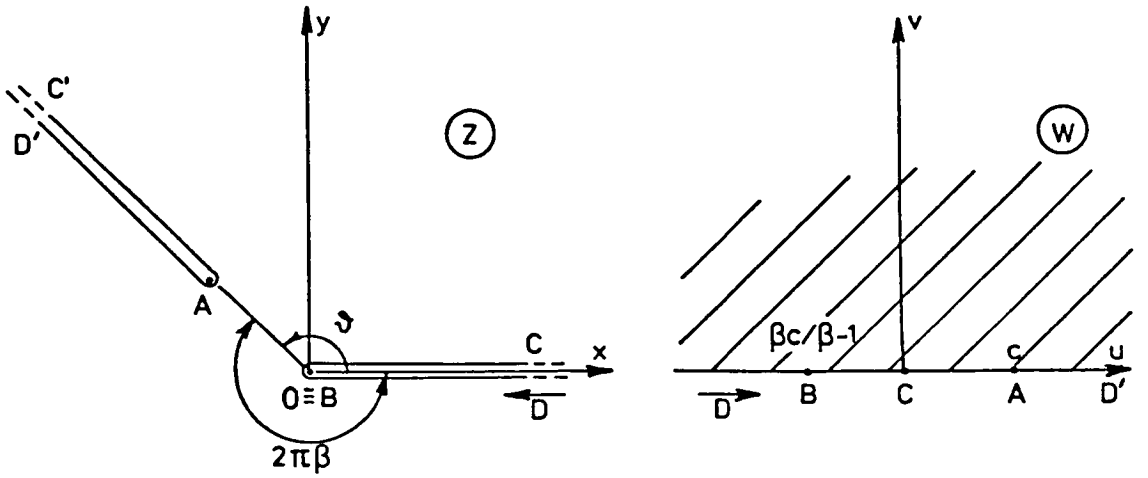

Fig. 24. The mapping of equation (187)

For the point A we find easily the co-ordinates

$$z_A = c^{2\beta}\, 2\beta(1-\beta)^2\, e^{-2\pi i\beta}$$

so that in order to have $|z_A| = d$, we put $c = [2d\beta(1-\beta)^2]^{\frac{1}{2\beta}}$ (188)

Obviously we need to express the function w in terms of z, so that we can easily obtain f = Re(w) which is of importance for our matching procedure. We return therefore to eq. (185) and try to inverse it; for this purpose we construct graphically the mapping it represents in fig. 25.

Putting $p = \pi$, we find the line

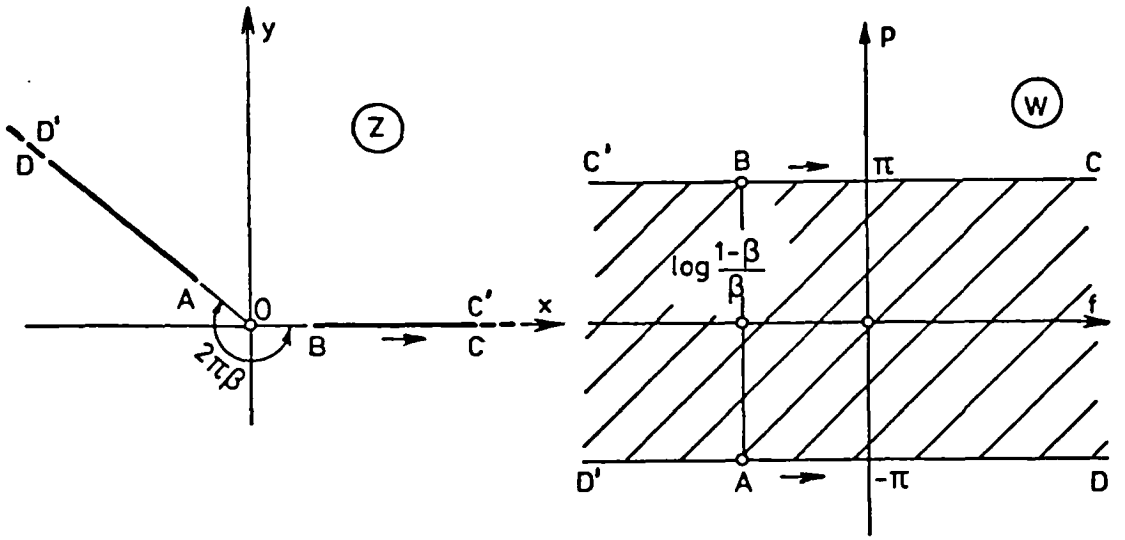

Fig. 25. The mapping of equation (185)

$$z = \frac{\beta^{\beta}(1-\beta)^{1-\beta}}{\sin(1-\beta)\pi} e^{\beta f}(1 + e^{-f})$$

which has a minimum at the point B where

$$\frac{d}{df}\{e^{\beta f} + e^{(\beta-1)f}\} = 0$$

whence

$$f_{\beta} = \log \frac{1-\beta}{\beta}$$

We see from fig. 25 that for the ocean side we have $\mathrm{Re}(w) \to \infty$; therefore as a first approximation we can ignore the second term in eq. (185) and find

$$w \sim -\frac{1}{\beta} \log F(\beta) + i\pi + \frac{1}{\beta} \log z$$

where $F(\beta) = \dfrac{\beta^{\beta}(1-\beta)^{1-\beta}}{\sin(1-\beta)}$

or taking the real parts

$$f \sim -\frac{1}{\beta}\log F(\beta) + \frac{1}{\beta}\log r \quad , r \to \infty \quad \text{(ocean)} \tag{189}$$

To the second order we have

$$w \sim \frac{1}{\beta}\log\frac{z}{A} + \frac{1}{\beta}\log\{1 + (\frac{z}{A})^{\frac{1-2\beta}{\beta}}\}$$

with $A = F(\beta)\exp\{-\beta\pi i\}$

For the harbour side we have $\mathrm{Re}(w) \to -\infty$, therefore ignoring the first term in eq. (185) we find to the first order

$$w \sim \frac{1}{1-\beta}\log A - \frac{\pi i}{\beta-1} + \frac{1}{\beta-1}\log z = \frac{1}{1-\beta}\log F(\beta) + \pi i + \frac{1}{\beta-1}\log z$$

and taking the real part

$$f \sim \frac{1}{1-\beta}\log F(\beta) + \frac{1}{\beta-1}\log r \quad , r \to \infty \quad \text{(harbour)} \tag{190}$$

The task of inversing eq. (187) is more difficult. From fig. 24 we see that for the ocean side we have $|w| >> 1$ for $|z| \to \infty$, therefore we find accordingly, to the first order

$$w \sim -(2\beta z)^{\frac{1}{2\beta}}$$

Substituting this value of w into eq. (187) we obtain easily for the second order

$$w \sim -(2\beta z)^{\frac{1}{2\beta}} - \frac{c}{1-\beta}$$

We repeat the same procedure and find to the third order

$$w \sim -(2\beta z)^{\frac{1}{2\beta}} - \frac{c}{1-\beta} - \frac{c^2}{(1-\beta)^2}\{\tfrac{3}{2}\beta - 1\}(2\beta z)^{-\frac{1}{2\beta}}$$

and to the fourth

$$w \sim -(2\beta z)^{\frac{1}{2\beta}} - J - L(2\beta z)^{-\frac{1}{2\beta}} - M(2\beta z)^{-\frac{1}{\beta}} + O[(2\beta z)^{-\frac{3}{2\beta}}], |z| \to \infty \tag{191}$$

where we have put

$$J = \frac{c}{1-\beta} \quad ,$$

$$L = J^2\{\tfrac{1}{2}\beta - 1\} \quad ,$$

$$M = J^3 \frac{1}{3}(13\beta^2 - 15\beta + 5)$$

For the harbour side of the plane (x,y) we remark from fig. 24 that for $|z| \to \infty$ we have $|w| << 1$; therefore we treat the terms of eq. (187) in the reverse order of magnitude than previously. After successive approximations and some algebra I found

$$w \sim (\alpha z)^{\frac{1}{2(\beta-1)}} t + N(\alpha z)^{\frac{1}{\beta-1}} t^2 + P(\alpha z)^{\frac{3}{2(\beta-1)}} t^3 + \ldots \quad , \quad |z| \to \infty \qquad (192)$$

where $\alpha = \frac{2}{\beta} J^{-2}$

$$t = \exp\{\frac{\pi i \beta}{\beta-1}\}$$

$$N = \frac{\beta}{4(1-\beta)} J^3$$

$$P = \frac{J^2}{8(1-\beta)}\{\beta^2 J^4 \frac{2\beta+1}{4(1-\beta)} + 1\}$$

Taking the real parts of eqs (191) and (192) we have respectively

$$f \sim -(2\beta r)^{\frac{1}{2\beta}} \cos\frac{\omega}{2\beta} - J - L(2\beta r)^{-\frac{1}{2\beta}} \cos\frac{\omega}{2\beta} - M(2\beta r)^{-\frac{1}{\beta}} \cos\frac{\omega}{\beta} + \ldots$$

$$r \to \infty, \quad \text{(ocean)} \qquad (193)$$

$$f \sim (\alpha r)^{\frac{1}{2(\beta-1)}} \cos\omega^* + N(\alpha r)^{\frac{1}{\beta-1}} \cos 2\omega^* + P(\alpha r)^{\frac{3}{2(\beta-1)}} \cos 3\omega^* + \ldots$$

$$r \to \infty, \quad \text{(harbour)} \qquad (194)$$

where $\omega^* = \frac{\omega+2\pi\beta}{2(\beta-1)}$

C5.4 The Matching

Having the solutions of the inner and outer basic approximations at our disposal we can proceed to the matching of their expansions. Since our purpose is not a rigorous mathematical approach, but a rather rough answer to our original problem we shall perform a matching only of the first terms of the expansions; in fact a more detailed work would be in contrast with the restrictions of the method when applied to problems of intermediate range of the perturbation parameter ε, where our case finds itself.

A crucial point arises when trying to put the terms of eq. (175) in order of magnitude; indeed we have to find out if the first after the constant term in the f_w expansion of the wedge solution is more 'influential' than the source-like effect in the construction of the total field. Inspection of the equations of both inner expansions related to figs 23 and 24, together with work done in similar problems (Liu [42]) suggest that the source-like effect is more pronounced in the early stages of the approximation technique. So we have, in the usual notation, for the outer solution

Ocean part

$$f \sim f_w - Q \frac{1}{\beta} \frac{i}{4} H_o(kr) \qquad (195)$$

where Q is a constant representing the strength of the line source to be determined by matching.

Harbour part

$$f \sim Q \frac{1}{1-\beta} \frac{i}{4} H_o(kr) \tag{196}$$

The expansions of the above equations are respectively

$$f \sim -\frac{iQ}{4\beta}\{1 + \frac{2i}{\pi}(\gamma + \log\frac{k}{2})\} + \frac{1}{\beta} + \frac{Q}{2\pi\beta}\log r + B(kr)^{\frac{1}{2\beta}} + \ldots$$

$$kr \to 0 \tag{197}$$

$$\text{with} \quad B = \frac{4(\frac{1}{2})^{\frac{1}{2\beta}}}{\Gamma(\frac{1}{2\beta})} e^{-i\pi/4\beta} \cos\frac{\omega}{2\beta} \cos\frac{\theta_o}{2\beta}$$

$$f \sim \frac{iQ}{4(1-\beta)}\{1 + \frac{2i}{\pi}(\gamma + \log\frac{k}{2})\} - \frac{Q}{2\pi}\frac{1}{1-\beta}\log r, \quad kr \to 0 \tag{198}$$

The inner problem has been solved for two degrees of accuracy; we shall use here both results for the sake of comparison. For the lower degree we have the expansions

Ocean part

$$x+jy = \frac{d'F(\beta)}{2} \exp\{\beta[m(f+jp) + n]\} + \ldots, \quad mf+n << 1 \tag{199}$$

with m,n constants to be determined according to a method used by Newman [43] and $j(\neq i)$ the unit in the complex planes of fig. 25.

Harbour part

$$x+jy = -\frac{d'F(\beta)}{2} \exp\{(\beta-1)[m(f+jp) + n]\} + \ldots, \quad mf+n << 1 \tag{200}$$

In the above expressions d' represents the distance (AB). A factor $\exp\{-j\pi\beta\}$ is omitted because the orientation of the two breakwaters plays no role any more since we decided to carry out the matching only to the terms of the expansions of order greater than

$(kr)^{1/2\beta}$ which do not bring in the angle dependence. The above eqs (199) and (200) give respectively

$$f \sim -\frac{1}{\beta m}\log\frac{d'F(\beta)}{2} - \frac{n}{m} - \frac{1}{\beta m}\log r + \ldots\ldots \quad , \quad r \to \infty \tag{201}$$

$$f \sim \frac{1}{m}\frac{1}{1-\beta}\log\frac{d'F(\beta)}{2} - \frac{n}{m} - \frac{1}{(1-\beta)m}\log r + \ldots \, , \quad r \to \infty \tag{202}$$

Carrying out a simple matching we equate the constant terms and the multipliers of the logr terms of eq. (197), with their counterparts in eq. (201), and obtain

$$-\frac{n}{n} - \frac{1}{\beta m}\log\frac{d'F(\beta)}{2} = \frac{1}{\beta} - \frac{iQ}{4\beta}\left\{1 + \frac{2i}{\pi}\left(\gamma + \log\frac{k}{2}\right)\right\}$$

$$\frac{1}{\beta m} = \frac{Q}{2\pi\beta}$$

from this system we find

$$Q = \frac{-2\pi}{\log\frac{d'F(\beta)}{2} + \beta n + \gamma + \log\frac{k}{2} - \frac{i\pi}{2}}$$

$$m = \frac{2\pi}{Q}$$

From eqs (198) and (202) we get similarly

$$\frac{1}{(1-\beta)m}\log\frac{d'F(\beta)}{2} - \frac{n}{m} = \frac{iQ}{4(1-\beta)}\left\{1 + \frac{2i}{\pi}\left(\gamma + \log\frac{k}{2}\right)\right\}$$

from which by substituting the values of Q and m we obtain

$$n = \frac{\log\frac{d'F(\beta)}{2} + I}{1 - \beta} \, ,$$

where

$$I = \gamma + \log\frac{k}{2} - \frac{i\pi}{2}$$

Now, Q and m become

$$Q = \frac{-2\pi(1-\beta)}{\log \frac{d'F(\beta)}{2} + I} \tag{203}$$

$$m = n$$

We are primarily interested in the harbour region, therefore we find for it

$$f \sim \frac{iQ}{4(1-\beta)} H_o(kr) = -\frac{\pi i}{2} H_o(kr) \frac{1}{\log \frac{d'F(\beta)}{2} + I} \tag{204}$$

and $$|f| = \pi \left[\frac{J_o^2 + Y_o^2}{4U^2 + \pi^2}\right]^{\frac{1}{2}}$$

where $U = \gamma + \log \frac{k}{2} + \log \frac{d'F(\beta)}{2}$

and J_o, Y_o the usual Bessel functions of argument kr.

In order to facilitate computation of a numerical result we form the ratio $\left|\frac{f_1}{f_2}\right|$ that represents the ratio of wave height at a particular point for two values of angle θ; we find easily

$$\left|\frac{f_1}{f_2}\right| = \left[\frac{4U_2^2 + \pi^2}{4U_1^2 + \pi^2}\right]^{\frac{1}{2}} \tag{205}$$

We shall come again to this result during the discussion in subsection E2.2.

If we wish to feed in more information about the details of the gap we should use eq. (187) which yields eqs (191) and (192) for the expansions in the ocean and the harbour side of the field respectively; these substitute eqs (199) and (200) of the inner expansions.

The potential is as if caused by a line-source located at the

point C in the w-plane of fig. 24; therefore we shall have generally

$$F \sim -\frac{1}{2\pi} \log w + C$$

where C is an arbitrary constant.

From eq. (191) we have, after suppressing the factor $\exp\{+2\pi i\beta\}$,

$$w \sim (2\beta z)^{\frac{1}{2\beta}}$$

whence

$$\log w \sim \frac{1}{2\beta} \log 2\beta + \frac{1}{2\beta} \log z$$

which gives

$$F \sim -\frac{1}{4\pi\beta} \log r + C - \frac{1}{4\pi\beta} \log 2\beta \qquad (206)$$

For the harbour side we have from eq. (192) for the same as above co-ordinate system

$$w \sim (\alpha z)^{\frac{1}{2(\beta-1)}}$$

and

$$\log w \sim \frac{1}{2(\beta-1)} \log \alpha + \frac{1}{2(\beta-1)} \log z$$

which gives for the potential

$$F \sim \frac{1}{4\pi(1-\beta)} \log r + C + \frac{1}{4\pi(1-\beta)} \log \alpha \qquad (207)$$

If we put for convenience

$$C + \frac{1}{4(1-\beta)\pi} \log \alpha = 0$$

which is legitimate provided we keep C constant (see Tuck [44]), we find for eqs (106) and (207)

$$F \sim \frac{1}{4\pi(1-\beta)} \log r \tag{208}$$

$$F \sim -\frac{1}{4\pi\beta} \log r + \frac{1}{4\pi} V \tag{209}$$

where

$$\beta(1-\beta)V = \log d + 2\beta\log\beta + 2(1-\beta)\log(1-\beta) \tag{210}$$

We put as before $F = mf+n$ and by equating the constant terms as well as the coefficients of logr-terms of the eqs (198), (197) and (208), (209), we find the relations

$$-\frac{1}{m}\frac{1}{4\pi\beta} = \frac{Q}{\beta}\frac{1}{2\pi}$$

$$\frac{1}{4\pi(1-\beta)}\frac{1}{m} = -\frac{1}{2\pi}\frac{Q}{1-\beta}$$

$$\frac{1}{4\pi m} V - \frac{n}{m} = \frac{QI}{2\beta\pi} + \frac{1}{\beta}$$

$$-\frac{n}{m} = -\frac{Q}{1-\beta}\frac{I}{2\pi}$$

The excessive equation confirms our correct choice of the coefficient of Q in the outer ocean and harbour expansions. Solving the system we find easily

$$m = -1/2Q$$

$$Q = -\frac{2\pi(1-\beta)}{\beta(1-\beta)V + I}$$

$$n = -I/4\pi(1-\beta)$$

Substituting this value of Q into eq. (196) we obtain for the potential in the harbour side which is of interest to us

$$f \sim -\frac{i\pi H_o(kr)}{2} \frac{1}{\beta(1-\beta)V + I} \tag{211}$$

on the assumption that the incident wave is of unit amplitude as already noted. The absolute value of f which represents the ratio of maximum wave height at a point to the corresponding height of the incident wave is found to be

$$f \sim \pi\left[\frac{J_o^2 + Y_o^2}{4W^2 + \pi^2}\right]^{\frac{1}{2}}$$

where J_o, Y_o the usual Bessel functions of argument kr and

$$W = \gamma + \log\frac{k}{2} + \beta(1-\beta)V, \quad \gamma \text{ Euler's constant } (=0.5772...).$$

As before we form the ratio of two absolute values of f at the same point and get

$$\left|\frac{f_1}{f_2}\right| = \left[\frac{4W_2^2 + \pi^2}{4W_1^2 + \pi^2}\right]^{\frac{1}{2}} \tag{212}$$

A solution is thus found for the field in the harbour the orientation of which has not come into the equations because we have performed the matching procedure to the first order; repeating the technique to the next terms of the expansions will inevitably involve the factor B of eq. (197) which includes the cosines of both the angle of incidence and that of the observation point $P(r,\omega)$. However, the results obtained above although qualitative rather to

this order can give an idea about the relations of the parameters involved and support in a way the solution of the theoretical investigation of section C3. Some comparisons and discussion on this subject is included in the final chapter (E2.2).

To make easier the drawing of any conclusions there, we investigate here a little closer the function W that appears in eq. (212). It can be written as

$$W = 1.722 + \log\delta + 2\beta\log\beta + 2(1-\beta)\log(1-\beta) \qquad (213)$$

where $\delta = d/\lambda$ as usual.

The range of values of β that is of interest to us is $1/2 < \beta < 3/4$ and we can see from eq. (211) that for any two of these values $\beta_1 > \beta_2$ we must have $|f_1| > |f_2|$ which means $|W_2| > |W_1|$ through eq. (212). Equation (213) can readily lead to the conclusion that if $W_1 > 0$, $W_2 > 0$, we must satisfy the inequality

$$\beta_1\log\beta_1 + (1-\beta_1)\log(1-\beta_1) < \beta_2\log\beta_2 + (1-\beta_2)\log\beta_2 \qquad (214)$$

A rough plot of the function

$$Y(\beta) = \beta\log\beta + (1-\beta)\log(1-\beta)$$

is necessary at this stage. We note first that its minimum value occurs for

$$\frac{dY}{d\beta} = 0 = \log\beta - \log(1-\beta)$$

whence $\beta_o = \frac{1}{2}$ and the corresponding value of Y is

$$Y_{min} = -\log 2 = -0.693$$

We see also that $\beta\log\beta$ tends to zero when β tends to zero from

positive values (see Hardy [45]). Finally we easily find that the function $(1-\beta)\log(1-\beta)$ is the mirror image of the $\beta\log\beta$ relative to the $\beta = \frac{1}{2}$ line. We can now readily draw a rough plot of the function $Y = Y(\beta)$ as in fig. 26.

Evaluating $\frac{d^2Y}{d\beta^2}$ we deduce that there are no points of deflection in the interval $1/2 < \beta < 3/4$ and consequently for $\beta_1 > \beta_2$ we have $Y_1(\beta) > Y_2(\beta)$ for the same interval. Therefore inequality (214) cannot hold for these values of β which in turn means that we are not allowed to put $W > 0$, or in terms of the gap width we must always

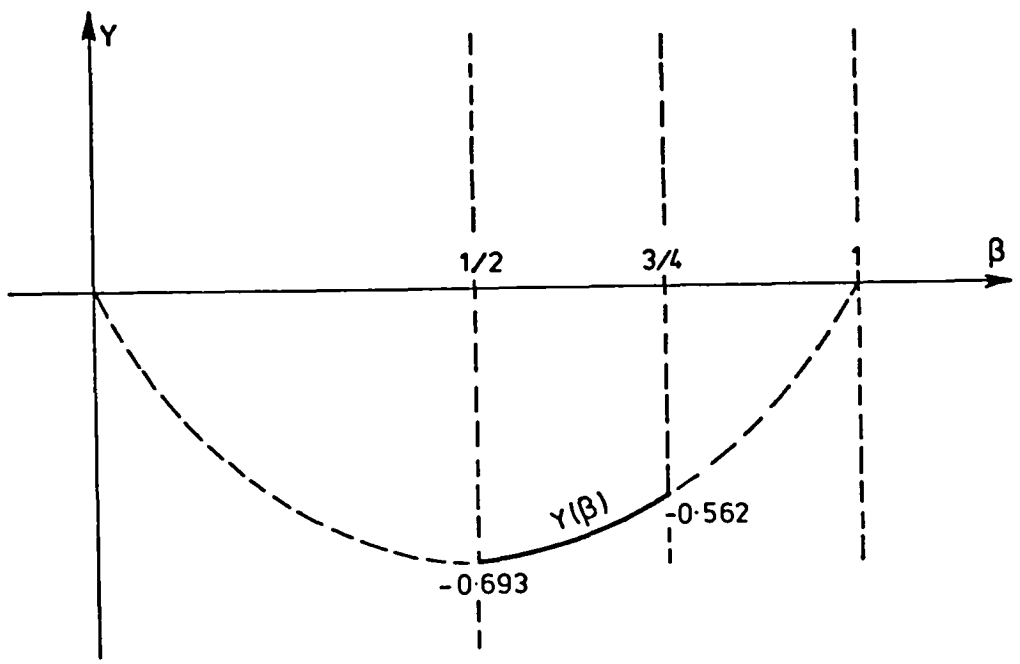

Fig. 26. Graphical representation of $Y(\beta) = \beta\log\beta + (1-\beta)\log(1-\beta)$

have $\delta < 0.4$; this corresponds to the minimum values of Y, $Y_{min} = -0.693$ while the safer value is $\delta < 0.31$ which corresponds to the maximum value of Y for the interval under consideration, $Y_{max} = -0.562$. More will be said in subsection E2.2 where we shall see in addition that

the calculated source strength Q can form a type of transmission coefficient of energy through the gap for various values of the angle θ between the two breakwaters.

Concluding the present chapter we note that the solution of the wave function in the harbour (eq. (211)) is consistent with the inner solution, because its limit for $kr \to 0$ is exactly equation (208) which after substituting $F(\beta)$ by

$$mf + n = -\frac{1}{2Q} f - \frac{I}{4\pi(1-\beta)}$$

gives

$$f \sim \frac{\log r + I}{\beta(1-\beta)V + I}$$

C H A P T E R D

EXPERIMENTS

D1 OUTLINE OF THE CHAPTER

In this chapter we are dealing with the experiments conducted to verify the theory exposed in the previous chapter. Some theoretical considerations of aspects frequently met in wave experiments in basins and in particular those of interest to us occupy the next section while the remainder is devoted to describing the experiments actually carried out. So in section D2 brief notes are included about the theory of the wave maker, the filters that are usually put in front of it, the wave 'anomalies' by which we mean secondary waves that are present in the basin caused by any source such as harmonics of the wave generator, instability of the wave form etc. and finally something is said about the absorbing beaches and reflection from them. We refer only to those conclusions from the general discussion outlined above, that could be applied if possible in section D3. There we describe the problem due to various factors that emerged during the experiments as well as the remedies that were thought suitable, the equipment used and the experimental procedure followed.

D2 GENERAL CONSIDERATIONS

D2.1 The Wave Generator

There are two main classes of mechanical wave generators that are used in laboratory studies: the first is the moveable wall type machine generally moving harmonically in the direction of the wave propagation and the second is the plunger-type wave maker, which generates waves by oscillating vertically in the water surface. In the first category are included the piston and paddle type wave generators; in view of the fact that the work has been carried out with a plunger-type wave maker we shall limit our discussion to this type of machine which has been studied by Wang [46]. Nevertheless until this recent publication many papers had appeared dealing with the former type of wave generators, some of which are an important contribution to a full investigation of the problem. Having in mind that our plunger can be approximated by a paddle-type wave maker and that the conclusions drawn for the latter are quite general we also quote here briefly some results of studies by Biesel and Suquet [47] and Ursell et al. [48].

The problem consists, in simple terms, of finding the wave characteristics when the shape and motion of the wave maker are known and vice-versa i.e. determining the shape and motion of the machine when waves of given characteristics are to be generated. The substance of this theory is presented in an article by Havelock [49].

The orbits of the water particles in a sinusoidal wave motion are well known from the hydrodynamic theory of first order for

infinite or finite depth (see e.g. Lamb [5]). To obtain such a motion we should presumably have harmonic motion of the generator, a justifiable assumption. However the system water waves-generator allows for interactions between its components and it is here that the difficulty arises. Assuming as usual an inviscid and incompressible fluid and irrotational flow over infinite depth we seek a solution of the equation

$$\Delta\phi = 0$$

satisfying the following boundary conditions:

(a) the linearized free-surface condition;

(b) normal velocity of the fluid at the plunger surface is equal to the velocity component of the forced oscillation in that direction; and

(c) at large distance from the plunger the disturbed surface behaves like outgoing progressive waves (radiation condition).

Early works dealing with the partial solution of this problem have been summarized by Schuler [50]. Following here a procedure by Wang [46] we assume that the physical plane of the two-dimensional model can be conformally mapped in a unit-circle, thus permitting the representation of the solution as a superposition of source and multipole potentials at the origin. The solution is general including any shape of the plunger provided it can be conformally transformed in a quarter of the unit-circle presented in fig. 27.

The final result is somewhat complicated but it takes into account the fact that the motion of the plunger is prescribed as $s_o \sin\sigma t$ vertically, thus permitting boundary condition (b) to be

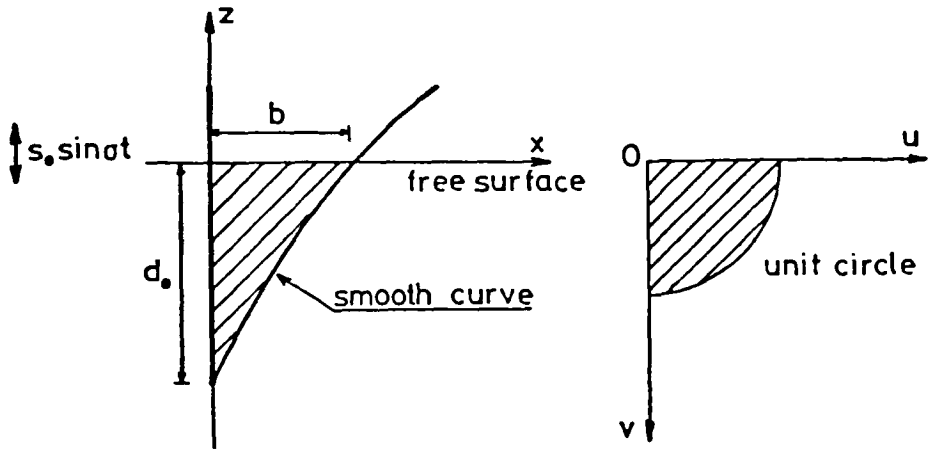

Fig. 27. Conformal transformation of a plunger

written as

$$-\frac{\partial \psi}{\partial s} = s_o \sigma \cos\sigma t \frac{\partial x}{\partial s}$$

where s is the vertical displacement and ψ the stream function conjugate to the required velocity potential ϕ. This condition can lead to evaluation of coefficients of the solution ϕ, from which the amplitude ratio equation can be deduced, i.e. the ratio of the maximum wave amplitude to the corresponding plunger amplitude; this equation shows that for a given plunger geometry the ratio depends only upon the frequency parameter $\frac{\sigma^2}{g} b$.

Experiments made by the same investigator give a satisfactory deviation of only 6.5% from the theory although it has been assumed that the depth is infinite. The theory suggests that we ought to keep h/d_o above a limiting value, in order to apply its results; this value decreases with increasing d_o/b and

increases with increasing sectional area coefficient p of the plunger at mean position (p = plunger section area under mean water surface/bd_o). At the above-mentioned experiments the ratio h/d_o was below the minimum value; nevertheless the agreement was good as already noted.

An assumption that was found to be reasonable is that the height of the generated waves at large distance depends only upon the depth, width and sectional area of the plunger, which means that the wave elevation is not sensitive to the geometrical details of the body other than its principal characteristics. This conclusion has been noted many years ago by Biesel and Suquet [47] while analysing the paddle-type wave maker, a good approximate of the plunger; they suggest that at distances greater than three times the depth of the channel the irregularities due to any defective form of the generator are negligible.

Their analysis shows further that a moving wave maker is capable of reflecting an incident wave as a stationary wall, a fact that requires the use of filters as will be seen in the next subsection. In addition to these reflections, other deformations that persist far from the wave generator are due to higher harmonics and higher order phenomena which will be studied later in this section.

Finally we make a note related to the diffraction of the generated wave around the edges of the wave maker. This fact has two effects; firstly it is likely that interfering waves be introduced and secondly the amplitude is maintained only in a certain region whose breadth decreases with increasing distance from the wave generator. A sketch is presented in fig. 28 of section D3 where we apply the information gained in the present section to our actual

experiment.

D2.2 Wave Filters

It will be seen in the following subsection that apart from the first-order sinusoidal wave, on which the preceding theory is based, there are other sorts of waves present; of course it would be fortunate if we could eliminate all these parasitic (relative to our viewpoint) waves, or at least some of them.

A common technique to achieve this is the use of some kind of wave filter running along the straight wave front that is to be filtered. It is to be remembered that we are dealing with the generation of two-dimensional waves. In general two types of filters can be distinguished:

(a) filters that reflect small amount of the energy of the impinging wave while they absorb a substantial amount of it, and

(b) those that are mainly reflective and do not dissipate a great proportion of the whole energy.

The energy balance can be stated as

$$E_i = E_t + E_r + E_a$$

where E_i the energy of the incident wave,

E_t the energy of the transmitted wave,

E_r the energy of the reflected wave,

E_a the energy absorbed by the filter.

Clearly for the same incident and transmitted waves the balance will

be determined by E_r and E_a, where for the type (a) of filters ('dissipative') we have E_r small, E_a large and for the type (b) ('reflective') E_r large, E_a small.

The dissipation of energy that occurs in the 'dissipative' filters comes mainly from generation of turbulence when the wave passes through the filter; this turbulence can be convected downstream and be another source of inconvenience when taking measurements.

The idea underlying the other type of filter is that it tends to allow through it more of the energy associated with the long wavelengths than of the energy associated with the short wavelengths. The disadvantage of this filter is that in order to be of any practical use in diminishing the harmonics, it has to present a small percentage of openings to the wave front. This leads to non-uniformity in the wave pattern immediately downstream of the filter due to the pronounced diffraction; these patterns may need to travel over a distance of several wavelengths to die out completely usually by interactions along the lines of symmetry of the components of the filter. Some compromise between these two opposing factors has to be made for each individual case, the task being not always an easy one.

A kind of 'dissipative' filter that was used in the Neyrpic Laboratory, Grenoble, France, is described by Biesel [51], where we see that in order to have both,i.e. transmitted wave of measurable height even after diffraction around a breakwater say, and some good effect on the harmonics sent out by the wave maker,we need a very powerful wave machine indeed. It is also said in the same article that for example for 50% reduction of the height of the fundamental wave the first harmonic will be reduced to 1/7.1 of its original

height. It may be of some interest to note there the corresponding value that we get from an imaginary filter of the 'reflective' type consisting of a thin screen which is interrupted by a series of vertical, equal and equidistant slits. Applying for the moment the result obtained by Lamb ([5], § 306) for the acoustical case we find the value 1/7 compared with 1/7.1 of Biesel's; for this value we have for the wavelength $\lambda = 2.14 \times$ (distance between two consecutive slits) if the width of a slit is one tenth of this distance.

This simple example should serve if anything to illustrate how difficult it is to construct a 'reflective' filter for the wavelengths usually employed in the laboratories. The relatively small free cross-section offered to the wave front demands distance of many wavelengths downstream for the disturbed uniformity of the wave to be re-established.

Of course the above example from the theory of sound is far from rigorous in this case. The main reasons, apart from the lack of finite thickness of the wall which could be allowed for, are

(a) in water waves there is a free surface which carries the waves that we try to filter whereas in acoustics there is not; and

(b) we have a variation of the wave characteristics with water depth especially in small and intermediate values of wavelength whereas in sound we suppose uniformity along each and every plane.

Unfortunately therefore, the theoretical results and information gained from the study of the general theory of diffraction through apertures in acoustics, electromagnetism etc., cannot in general be applied to the study of the filters of water waves (see e.g. Tuck [52]).

The gap is partly filled with experimental studies of configurations resembling wave filtering devices. The simplest cases seem to be a straight row of vertical (a) circular and (b) rectangular cylinders. The first of these cases has been examined from a different point of view by Costello [53], whence we quote the result of the nearly linear dependence of the transmission factor on the steepness of the wave that passes through the structure, a conclusion not far away from both the results of Lamb as noted above and of a recent work by Grüne and Kohlhase [54] on the second of the above cases, where they find linear dependence. In this last paper several shapes of wall-element have been studied and the variation of the transmission coefficient with the wall thickness is found to be small especially for small ratios of the solid face to the whole area presented to the wave front.

We see in general that the sound theory results are more sensitive to wavelength changes than the experiments on reflective obstructions of water waves would suggest. Nevertheless it was felt that a region more liable to an application of the sound theory would be the comparison of the shape and distribution of holes on the would-be filter which for simplicity is supposed to be a vertical wall. A limited study was therefore carried out, a brief account of which runs as follows.

The notion of conductivity is borrowed from Rayleigh [11] where he defines it as a constant c for each shape of the hole, such that the ratio of the wave energy that gets through to the energy of the incident wave measured on the area of the hole is $2c^2/\pi$. For the circle we have c = 2R, R radius of the circle, for the ellipse

$$c = 2\sqrt{\frac{a}{\pi}}\left[1 + \frac{e^4}{64} + \frac{e^6}{64} + \ldots\right]$$

a is the area of the ellipse and e its eccentricity. We deduce immediately that if the eccentricity is small, the conductivity of an elliptical hole is nearly the same as that of a circular aperture of equal area. Among various forms of aperture of constant area the circle has the minimum conductivity which gives, transmitted energy = 0.81 × (incident energy).

The same applies if we compare one circle with n equal circles of the same total area acting independently; we find that the conductivity of the n circles is greater than that of the one; nevertheless the energy transmission coefficient remains the same. In practice one would expect slightly greater coefficient because the holes do not act independently especially when their distance is small.

In general therefore the more the opening is elongated the greater will be the transmission coefficient, while when the opening is broken up there is no or very small change to this coefficient. The above hold under the theoretical assumption of zero thickness of the wall. When it has a finite thickness t we have from Rayleigh again

$$c = \frac{\pi R^2}{t + \alpha(t)} \qquad (215)$$

where $1.370R < \alpha(t) < 1.698R$ and $\alpha \simeq 1.64R$ for most cases, for a circular hole with both ends open.

The results obtained above for zero thickness are no longer valid because after simple calculation we get from eq. (215)

$$\frac{\text{transmitted energy}}{\text{incident energy on the void area}} = \frac{2R^2}{(t+\alpha)^2} \quad \text{for one hole,}$$

while for n holes of the same total area we find the same ratio equal to

$$\frac{2R^2}{(t\sqrt{n}+\alpha)^2} < \frac{2R^2}{(t+\alpha)^2} \quad , \quad n > 1$$

Our conclusion therefore for the case of finite thickness, which is of interest in application, is that the energy transmission coefficient increases when the opening is elongated and decreases when the opening is broken up to more than one aperture of the same shape with the original and of total area equal to it. Unfortunately we have not at our disposal the relevant formula for the conductivity of any shape other than the circular when $t > 0$; so it is difficult to compare e.g. two ellipses with one circle of the same wall thickness.

From simple considerations and the above theory I have developed two semi-empirical formulas relating the ratio

$$\frac{\text{force on a perforated plane wall}}{\text{force on the rigid wall}} = \frac{R'}{R}$$ to the ratio of perforated area to the whole area α, in two cases:

(1) n circular holes, thickness of wall t

$$\frac{R'}{R} = 1 - \left[0.5 + \frac{0.707}{t\sqrt{n} + \beta} \right] \alpha, \quad \beta = 1.6 \div 1.7$$

(2) holes of any shape of conductivity c and area a

$$\frac{R'}{R} = 1 - \left[0.5 + 0.4 \frac{c}{\sqrt{a}} \right] \alpha$$

The above expressions are related to our filtering problem which is finally answered in subdivision D3.1.3. Incidentally these semi-empirical formulas compare well with other more sophisticated theory and with experiments (see e.g. Kenny et al. [55], fig. 3, p.334).

D2.3 The Waves in the Basin

D2.3.1 Instability. The Stokes wave[¶] which has been assumed for this report suffers from instability. The comparatively recent discovery of this is attributed mainly to Benjamin [56]. Non-linear dispersive systems, as the case of the water, can carry periodic, progressive wavetrains of finite amplitude and steady waveform. In water waves when there are present 'parasitic' waves of small amplitude and of frequencies and wave numbers close to those of the fundamental, gradual disintegration of the original wavetrain can occur. The problem is a practical one as well because such sidebands can be picked-up by the wavetrain from the background noise spectrum that is transferred to the water through the wave maker; this has been verified experimentally as reported in the above-mentioned paper.

¶ $ak \ll \varepsilon$, $\varepsilon = 1$ or $(kh)^3$ which ever is the smallest.

Using the second-order theory of the Stokes wave we allow for non-linear interaction between each of the two parastic waves with the first harmonic of the primary wave, thus producing two new waves. The pair of interactions becomes resonant when the argument of each one of the new waves coincides with the argument of the side band of the other pair of interaction; then we have instability. This requirement is found to be for water waves of depth h

$$kh > 1.363 \tag{216}$$

The distance required for such an instability to develop in a frictionless fluid is much greater than $1/2k^3a^2$ from the wave maker, a being the amplitude of the fundamental wave.

The above analysis applies to one-dimensional propagation of straight-crested water waves. Investigation for the two-dimensional problem of the same waves shows that instability can occur for values $kh < 1.363$ in directions forming an angle $\psi \neq 0$ with the direction of propagation (Hayes [57]). Practically we can have instability for $kh > 0.5$ for various values of ψ; for example for $kh = 0.5$ instability occurs only along the direction $\psi \simeq 24^o$, the maximum range of ψ for which instability occurs is about $0 < \psi < 42^o$ for $kh \simeq 2$, while the limit of this range is about $0 < \psi < 35.2^o$ for very large values of the number kh.

D2.3.2 Secondary waves. Apart from frequencies that can be transferred incidentally in the wave system and lead to instability as shown in the previous subdivision, it is likely that first and higher harmonics emanate from the wave maker itself, being a by-product of its motion which is supposed to be very close to sinusoidal.

In laboratory experiments with waves over a horizontal bed the fundamental wave is accompanied by one or more extra wave crests of a smaller height and with a lower propagation speed. We shall not go into details of the theoretical interpretation of the phenomenon that had caused several disagreements; instead we will adopt one view point and follow the account of Hulsbergen [58], where he supposes generation of water waves by a piston-type wave maker moving sinusoidally, but the results are assumed to be applicable to our case as well.

The existence of a free wave of half the period of the fundamental emanating from the wave machine is accepted, as predicted by Fontanet [59] in his second-order theory of the wave maker. This free wave of period T/2 and celerity C_F interacts with the fundamental Stokes wave (T,C), which is supposed to consist of its three components (T,C), (T/2,C), (T/3,C). The products of the interaction are shown to be two waves (T,C_1), $(T/3,C_2)$ with $C_1 = \frac{\alpha\lambda}{1-\alpha} / T$, $C_2 = \frac{\alpha\lambda}{1+\alpha} / \frac{T}{3}$, λ being the fundamental wavelength and $\lambda_F = \alpha\lambda < \lambda$.

We now have three different pairs of waves each of which forms by vectorialaddition the corresponding harmonic of the wave record we get from the experiment. In each pair both waves have equal period as follows

Stokes Wave	Record
fundamental (T,C) + (T,C_1)	A_1
1st harmonic (T/2,C) + $(T/2,C_F)$ 1st harmonic free wave	A_2
2nd harmonic (T/3,C) + $(T/3,C_2)$	A_3

With respect to the amplitudes we see that if we denote by a that of the fundamental we can evaluate it through the experi-

mental results of the spatial variation of A_i using the relation

$$a = \tfrac{1}{2}(A_{1\,max} + A_{1\,min})$$

where reflection does not interfere.

For the amplitude of the Stokes first harmonic we have

$$a_2 = \tfrac{1}{2}(A_{2\,max} + A_{2\,min})$$

and for the first harmonic free wave

$$a_F = \tfrac{1}{2}(A_{2\,max} - A_{2\,min}) \quad .$$

Similarly for the second harmonics

$$a_3 = \tfrac{1}{2}(A_{3\,max} + A_{3\,min})$$

and for the amplitude a_3' of the wave $(T/3, C_2)$

$$a_3' = \tfrac{1}{2}(A_{3\,max} - A_{3\,min})$$

From the same source [58] and for the first harmonic we get for a typical value of the ratio depth/λ = 0.20, $a_F \simeq 0.5a_2$ and $a_F \simeq 0.5\,\frac{a^2}{h}$ whence $a_2 \simeq a^2/h$, h depth of still water. For greater values of h/λ the components of the first harmonic A_2 decrease further. The small component a_1' of the fundamental A_1 is difficult to be measured especially for Ursell's parameter (= $2a\lambda^2/h^3$) less than 28, because then the reflection from the beach appears to be the dominating feature.

D2.3.3 Attenuation. Hunt [60] calculated the dissipation of energy caused by the boundary layers of the rigid faces of a channel where the larger part of the dissipation occurs. Thus viscosity

causes through dissipation of energy a slight attenuation of the wave height. If we describe this attenuation by a damping factor exp{-Dx}, it is found that for a progressive wavetrain, with the usual notation

$$D = \frac{k}{B}\left(\frac{2\nu}{\sigma}\right)^{\frac{1}{2}} \frac{kB + \sinh 2kh}{2kh + \sinh 2kh} \tag{217}$$

where B is the width of the channel and ν the kinematic viscosity.

A far less important dissipation of energy occurs due to the existence of a boundary layer at the free surface. It can be shown (Lamb [5]) that the amplitude decreases as

$$a\exp\{-D'\sigma t\}\ , \quad \text{where } D' = 2\nu k^2/\sigma \tag{218}$$

so that the damping of the waves reduces their amplitude to a fraction $\exp\{-4\pi\nu(k^3/g)^{\frac{1}{2}}\}$ of the initial value after one period. The analysis is valid only if the thickness of the boundary layer is small compared with the wavelength, that is if (Batchelor [61])

$$\left[\frac{\nu k^{\frac{3}{2}}}{4\pi^2 g^{\frac{1}{2}}}\right]^{\frac{1}{2}} \ll 1 \tag{219}$$

D2.4 Reflection from the Beach

To simulate the conditions of the open sea we have to have a kind of wave energy absorber at the end of any wave basin, so that we do not have any reflection of the waves from the end wall. Perfect absorption being impossible in practice we seek for the structure that gives minimum reflection for the characteristics of the individual case with which we are concerned. In general sloping

beaches give quite good results.

The finite dimensions of any laboratory wave basin are bound to produce surges of the water body as a second-order effect. In particular starting and stopping of the wave maker cause a sort of impulse, the effects of which persist for some time. When the steady state has been reached we are left with the incident wavetrain, and that reflected from the beach. The incident is the sum of the primary wave generated by the wave maker and the reflection from it of the primary wave partially reflected by the beach. The reflected wavetrain consists only of the primary wave reflected by the beach. It is clear that we have ignored any subsequent reflections from both the beach and the wave machine; this is plausible because even if we assume perfect reflection from the wave maker we come to very small amplitudes of the primary wave after its second reflection from the beach, of the order of ε_r^2 which is negligible provided that the reflection coefficient of the beach ε_r is small which is usually the case.

The regions close to the wave maker and the beach suffer from effects of this proximity and therefore care must be taken so that measurements be taken in the middle of the wave basin.

The amplitude of the recorded oscillation being A, we have at a distance x from the wave maker and under the above assumptions the following (Ursell et al. [48]),

$$A = a[1 + \varepsilon\cos(2kx + \delta) + \varepsilon\cos\delta] \qquad (220)$$

where a is as usual the amplitude of the primary or fundamental wave, and

ε, δ parameters depending on beach characteristics and length

of basin.

It is found that the reflection coefficient of the beach can be expressed as

$$\varepsilon_r = \frac{A_{max} - A_{min}}{A_{max} + A_{min}} = \frac{\varepsilon}{1 + \varepsilon\cos\delta} \simeq \varepsilon \qquad (221)$$

We need to take measurements at least along a distance of half the wavelength of the incident wave which equals the wavelength of the variation of A as predicted by eq. (220); thus ε_r can be obtained. The amplitude a is given by

$$a = \frac{\overline{A}}{1 + \varepsilon\cos\delta} \simeq \overline{A} \qquad (222)$$

where $\overline{A}$ denotes the average of the recorded amplitude over half a wavelength of the primary wave.

D3 EXPERIMENTAL EQUIPMENT AND PROCEDURE

D3.1 Equipment Used and Factors Affecting the Measurements

D3.1.1 Wave Basin. A general layout of the basin where the experimental work took place is shown in fig. 28; the model is not yet shown. The floor is nearly horizontal and the walls are formed by precast concrete kerbstones that allow for a maximum usable depth of water of about 38 cm. The energy absorbers can be seen along the three sides of the basin, the floor and the walls of which are covered by a heavy polythene sheet. In the constant depth region a reference grid of 1 m x 1 m square was marked on the floor and labelled as in fig. 28. Line AA coincides with the back face of the plunger; line 33 is the perpendicular to it at the mid-point.

Part of the preliminary experimental work included in this subsection, such as calibrations, measurements of reflection coefficient etc., was carried out together with Mr R.W.P. May whom I thank for his co-operation. He has found [62] that the floor of the basin was not quite horizontal; therefore we took measurements of the vertical distance of several points of the bottom from an arbitrary reference level. The results are given in Table 1. Point G corresponds to the pointer gauge located at one end of the basin to measure still water level at any time when the wave generator was not operating. The other points refer to the grid crossings of the corresponding row and line.

The average of the values in the table, excluding point G as being far from the 'working' area, is 72.19 cm which means that we

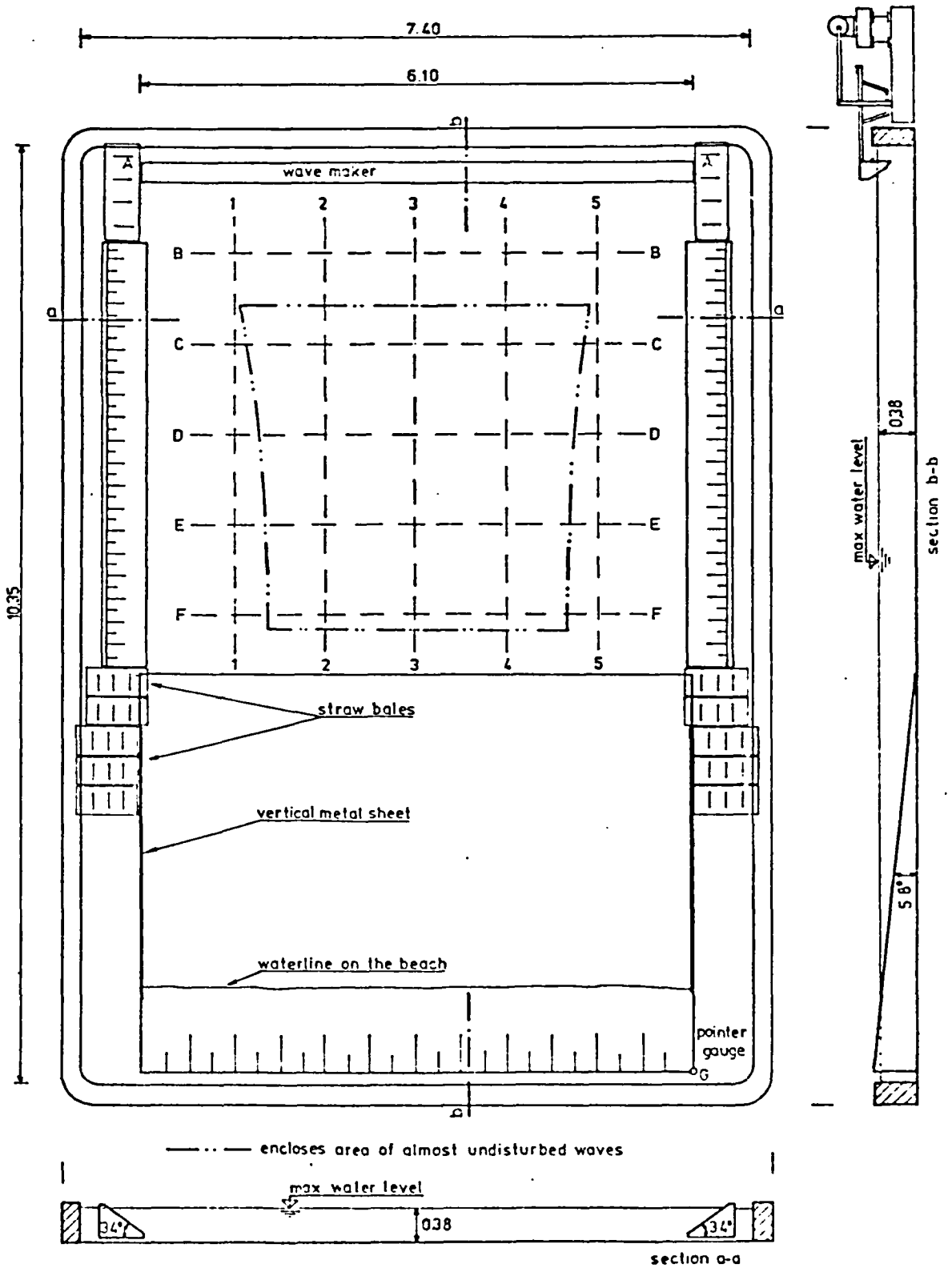

Fig. 28. Plan and sections of the experimental basin

point	altitude (cm)	point	altitude (cm)
G (pointer-gauge)	72.03	C3	72.20
A1	72.15	C4	72.25
A2	72.00	C5	72.40
A3	72.00	D1	72.18
A4	72.12	D2	72.37
A5	72.34	D3	72.38
C1	72.18	D4	72.28
C2	71.92	D5	72.22

Table 1. Levelling of basin floor

have to add 0.16 cm to the actual reading of the pointer-gauge at G to get an average value of the water depth in the basin.

The various parts of the basin, e.g. the beach, the wave maker etc. are discussed separately, in the rest of this subsection.

D.3.1.2 Wave height measurement. This was done with the aid of a frequency modulation unit, a wave gauge and a recorder. The gauge was a simple capacitance-wire device consisting of a double length of coated wire suitably isolated from a metal rod that kept it into position, which has to be the vertical when taking measurements. The wire is partially immersed and so, together with the surrounding water, form a kind of capacitor, the coating acting as dielectric. As waves pass the gauge, the change of water depth alters the capacitance, producing an effect on the carrier signal fed into the gauge through an oscillator. This signal after leaving the gauge is converted from alternating to a direct voltage output through a

transducer. The frequency modulated signal arrived finally at the recording unit which translated the frequency changes into a proportional change in the output voltage, which in turn activated a thin beam of ultra-violet light. The actual recording was made on a moving light-sensitive paper where the position of the beam, which moved always on a straight line, was registered in time, thus producing the function $\eta(t)$ of the water elevation at one point of the basin. The recorder has virtually no inertia, the maximum trace speed of the light beam being 25,000 cm/sec [62], thus capable of recording easily much steeper waves than those used in the experiment.

The wave gauge has to respond linearly to the height of the wave profile so that the record we get represents the waves undistorted. A calibration was therefore carried out to find the curve of the wave gauge, i.e. the change that produced in the final recording a known change of water level for the full range of water depths that the length of the gauge allowed. A measuring cylinder with a pointer gauge was used and three wave gauges were tested. The curve for the best of these appears in fig. 29; the maximum deviation from the linear law is 0.1 cm. The settings of the frequency modulation unitkept constant throughout the calibration; it was found later that for a different set of settings one gets different conversion factor, i.e. slope of the straight line in fig. 29. However it was required only that the settings be kept constant throughout the experiment as long as we were interested in relative wave heights.

D3.1.3 Wave maker and waves produced. As shown in fig. 28 the wave generator is of the plunger type and is driven by an asynchronous electric motor of power 1 HP, through a variator of gear ratio 22.1

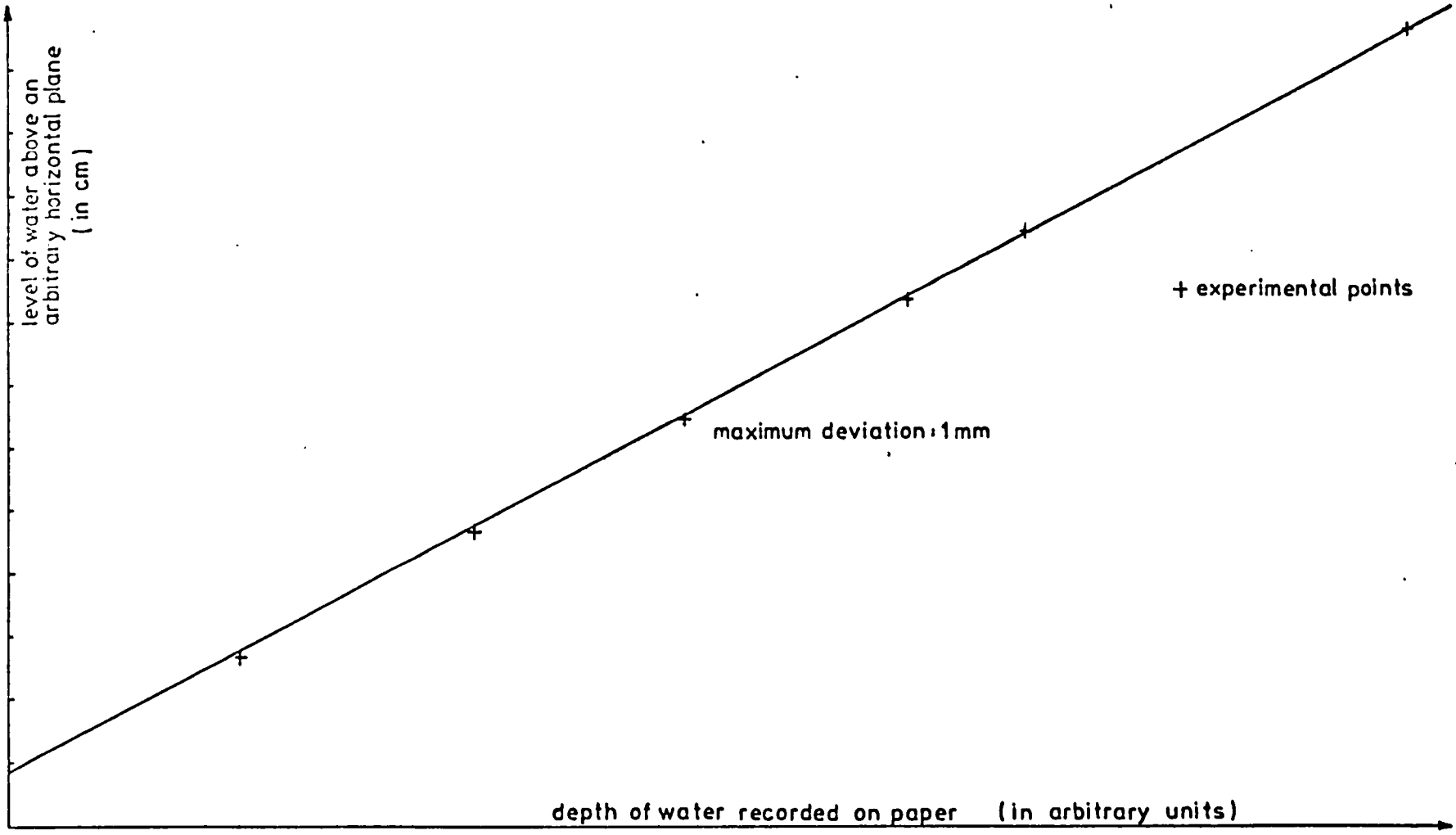

Fig. 29. Calibration of the wave gauge

which can set the period of the wave maker anywhere between its two limits. A three-phase starter is included in the system. The stroke of the plunger could be adjusted to produce the desired wave amplitude.

The section of the front face of the plunger has a point of mild discontinuity and care was taken to keep this point well below the water surface when generating waves, otherwise non-uniform waves would appear.

Another point of some concern was that either end of the wave maker left a gap of about 65 cm between it and the nearest wall perpendicular to its axis. This could result in leakage around the ends of the plunger which together with diffraction effects discussed in subsection D2.1 reduced somewhat the 'working area' of the basin. The precaution taken was two-fold: firstly we put some straw bales at both ends of the wave maker so as to reduce leakage and diffraction effects and secondly the model was built and the measurements were taken in a central area of the basin when the wave crests appeared to be straight.

When exposing some elements of the theory of the plunger-type wave maker (subsection D2.1), we have found that the amplitude of the generated wave is a function of the stroke of the wave maker and its speed; indeed in our case the stroke could be altered by changing the eccentricity of the drive. The speed, or frequency, was measured from the chart recording where the paper speed is known and checked from time to time against the frequency found by counting the number of immersions of the plunger over a known period of time.

Another result of the theoretical notes included in the preceding section was that the wave form is not sensitive to the

geometry of the plunger after a distance of say 3h, h water depth, from it. This has been taken into account whenever measurements were taken, thus establishing another boundary to our 'working area' (see fig. 28).

We have seen also that the moving wave maker acts as a stationary reflecting surface to waves travelling towards it (subsection D2.1). This remark together with the fact that the wave generator is bound to produce higher than the fundamental harmonics (subdivision D2.3.2), calls for closer investigation of the form and behaviour of the generated waves.

In our experiments the amplitude a of the fundamental wave was about 1.4 cm, the wavelength about 68 cm and the water depth 38 cm; therefore the parameter $2a\lambda^2/h^3$ gives a value not greater than 0.3 which is much less than 28, a kind of criterion for the importance of the free first harmonic (D2.3.2). The conclusion that the amplitude a_F of this harmonic is not so important for our measurements is supported by Ursell et al.([48]) where it is shown that the maximum difference of amplitude recordings is

$$A_{max} - A_{min} = 2a\{1 + O(\varepsilon^2)\}$$

where now $\varepsilon = a_F/a \ll 1$, and naturally ε^2 is of negligible order.

In order to assess how the waves in the basin behaved as regards the first and higher harmonics we took at a given point recordings of waves of various frequencies by altering the setting of the variator and the stroke of the wave machine. The records were examined visually and some analyzed through a Fourier analysis computer programme compiled by Mr May.

It was desirable while being in the region of the sinusoidal

wave theory ($2a\lambda^2/h^3<15$) to use waves with high steepness so that the diffracted waves would be of measurable amplitude; on the other hand the harmonics should be kept to a minimum, thus justifying the use of first order linear theory. The amplitude of the first harmonic varies like a^2; by diminishing the amplitude a of the fundamental wave the reflection coefficient of the main beach increased because, as we shall see in the next subdivision, the greater the steepness of the wave the greater absorption its energy suffers from a reflecting slope. We had therefore to compromise taking into account also other factors, mainly the capacity of the wave generator and the actual form of the produced wave, which should be as close as possible to a Stokes wave. The stroke of the generator was thus adjusted to produce waves of double amplitude $2\bar{A}$ = 2.75 cm for the constant depth of 38 cm as noted before. The next step was to decide about the frequency of these waves.

Above a certain limit the machine started to vibrate ;

on the other hand the wave crests became 'spilling', so it was decided to use frequencies lower than the above limit corresponding to a period of about 0.6 sec/cycle. The range of periods 0.6-0.8 sec/cycle was investigated for the same point of the basin located near D3, i.e. the crossing of the lines DD and 3-3 (fig. 28). Two speeds of the recorder paper were used, the high speed giving a more or less undistorted form of an individual wave and the low speed enabling us to follow the variation of the wave height over many wave crests passing by the semi-immersed wave gauge. This was mounted by a clamp on a vertical rod supported by a horizontal plate on the bottom of the basin; this arrangement was found to have negligible effect on our recordings provided it was suitable positioned.

The water depth was kept always at about 38 cm. Comparison of the recordings led to the decision that a period of 0.66 sec/cycle (variator setting 150) be used. The wavelength is $\lambda = 1.561 \times 0.66^2 = 0.68$ m $< 2h = 2 \times 0.38 = 0.76$ m, so we are in the deep water waves region. Parts of the recordings are reproduced in fig. 30.

A Fourier analysis done by Mr May showed that for a wavetrain of the above frequency and of amplitude about 3.3 cm we get for the fundamental and the two first harmonics the ratio of their amplitudes like the numbers 1:0.026:0.020, where from the first and second harmonic the Stokian components have been subtracted. We see clearly that the contribution of the first and higher non-Stokian harmonics to the total amplitude is negligible, especially for our case where the amplitude of the waves is less than half of the above. It appeared therefore that use of filters in front of the wave maker to eliminate the free harmonics produced by it, would not be advisable because it would be very difficult to maintain the amplitude of the fundamental wave as high as 1.4 cm. We did not want further reduction of the amplitude in order to keep low the percentage of the absolute experimental errors, e.g. the deviation of the wave gauge. These errors are dominant over the relative errors, e.g. first harmonic, which are low in our case.

Having in mind the difficulties that the construction of an effective filter presents as well as the above considerations I decided not to use filters in front of the wave maker. The problems associated with filters have been discussed in subsection D2.2 where we noted the disturbed pattern of the waves downstream of the filter and the need for very powerful wave generator, a conclusion reached above by another way.

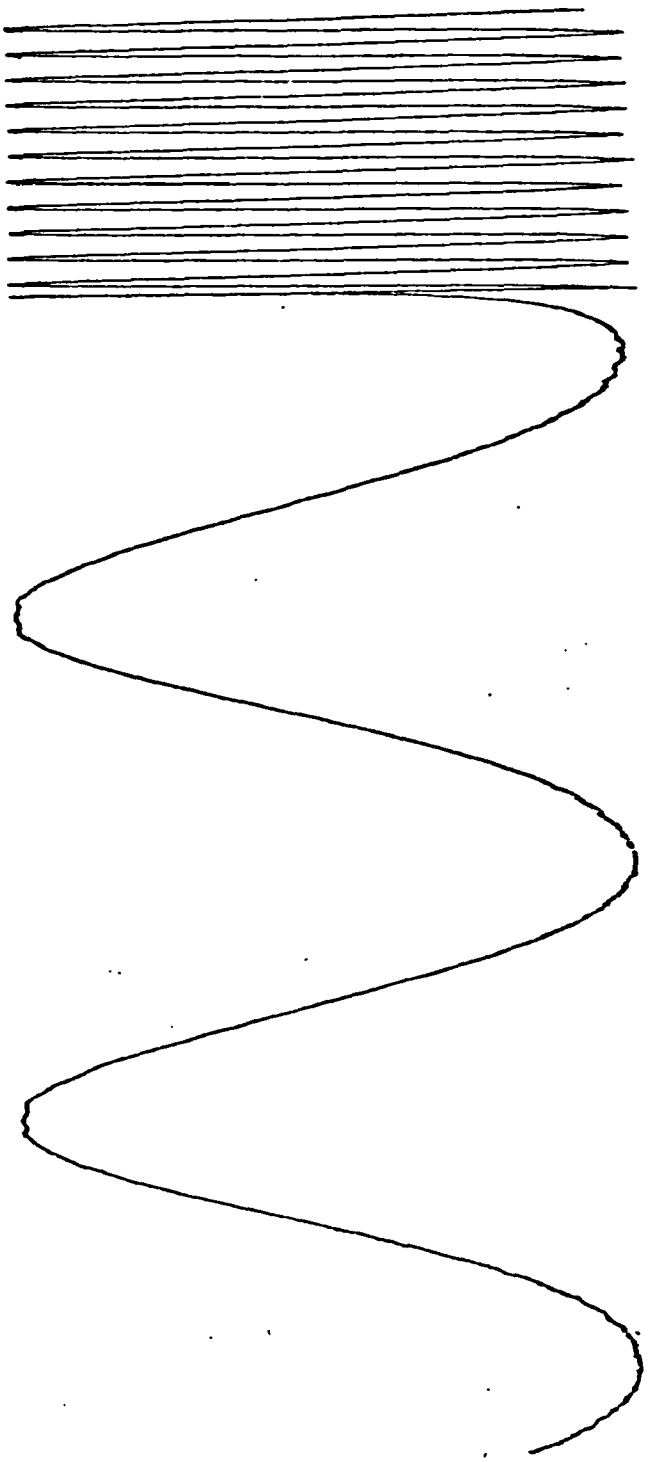

Fig. 30. Recording of the wave used in the experiments

In subdivision D2.3.1 we pointed out some comparatively recent results on the instability of wavetrains. It was noted that the distance required for an instability of the kind examined to start developing is greater than $1/2k^3a^2$ which in our case gives about 34 m. Given that the effective length of the basin is under 10 m it is evident that there is no sufficient length from the wave maker for such an instability to develop, therefore it is not taken into account.

D3.1.4 Beach and wave reflection. The sloping beach at the far end of the basin was constructed of impermeable metal sheet mounted on a heavy frame resting on the bottom of the basin. The slope was 5.8 degrees. As may be seen in fig. 28, along the two long sides of the basin there were put wooden slopes, steeper than the main beach, at an angle of 34 degrees; the aim was to absorb the reflected waves from the front faces of the two breakwaters. More about these slopes will be said in the next subsection where the actual model and problems associated with it will be described.

Straw bales were placed where pronounced discontinuities of the boundary occurred (fig. 28), namely at both ends of the wave maker and where the side slopes met the main beach. The purpose of putting bales was to smooth the discontinuities thus eliminating any diffraction effects due to these and at the same time absorbing any waves travelling towards them. We have already pointed out the problem caused by a wave generator not spanning the full width of the channel in reducing the area of uniform wave crests; the bales

at both ends of the wave maker helped to minimize this effect. They were constructed of chicken-wire in the form of hollow circular cylinders lightly filled with straw. The diameter of the base circle was 0.32 m and their height 0.87 m.

Whatever the precautions, thereis always bound to be some sort of reflection mainly along the direction of the wave propagation and this reflection we have tried to evaluate by applying eq. (221). Measurements were taken at 5 cm intervals and finally a figure of 10% for the reflection coefficient was found for the period of 0.66 sec that was used throughout the experiment. This coefficient is the ratio of amplitudes of the reflected to the incident wave.

The variation of wave amplitude with distance from the wave maker is due to the partial reflection of the incident wave from the beach which causes a partial standing wave system in the basin. The measurement of the wave height against distance is given in fig. 31. We see that the wavelength of the height variation is very close to the theoretically predicted $\lambda/4 = 68/4 = 17$ cm. Miche's formula [63]based on the ratio of the wave steepness to the number $\left(\frac{2\beta}{\pi^3}\right)^{\frac{1}{2}} \sin^2\beta$, where β is the slope of the beach, underestimates in our case the reflection coefficient giving an answer of about 6%. Greater deviations from Miche's results have been recorded in the past; in Ursell et al. [48] for example we see that for wave steepness over 0.01 the formula underestimates the reflection coefficient found experimentally and for steepness below 0.01 overestimates it. The steepness of our wave was 2.75/68 = 0.04 therefore an underestimation using Miche's method was probable.

A recording at low speed for a given point over a period of fifteen minutes from the starting of the wave maker revealed that

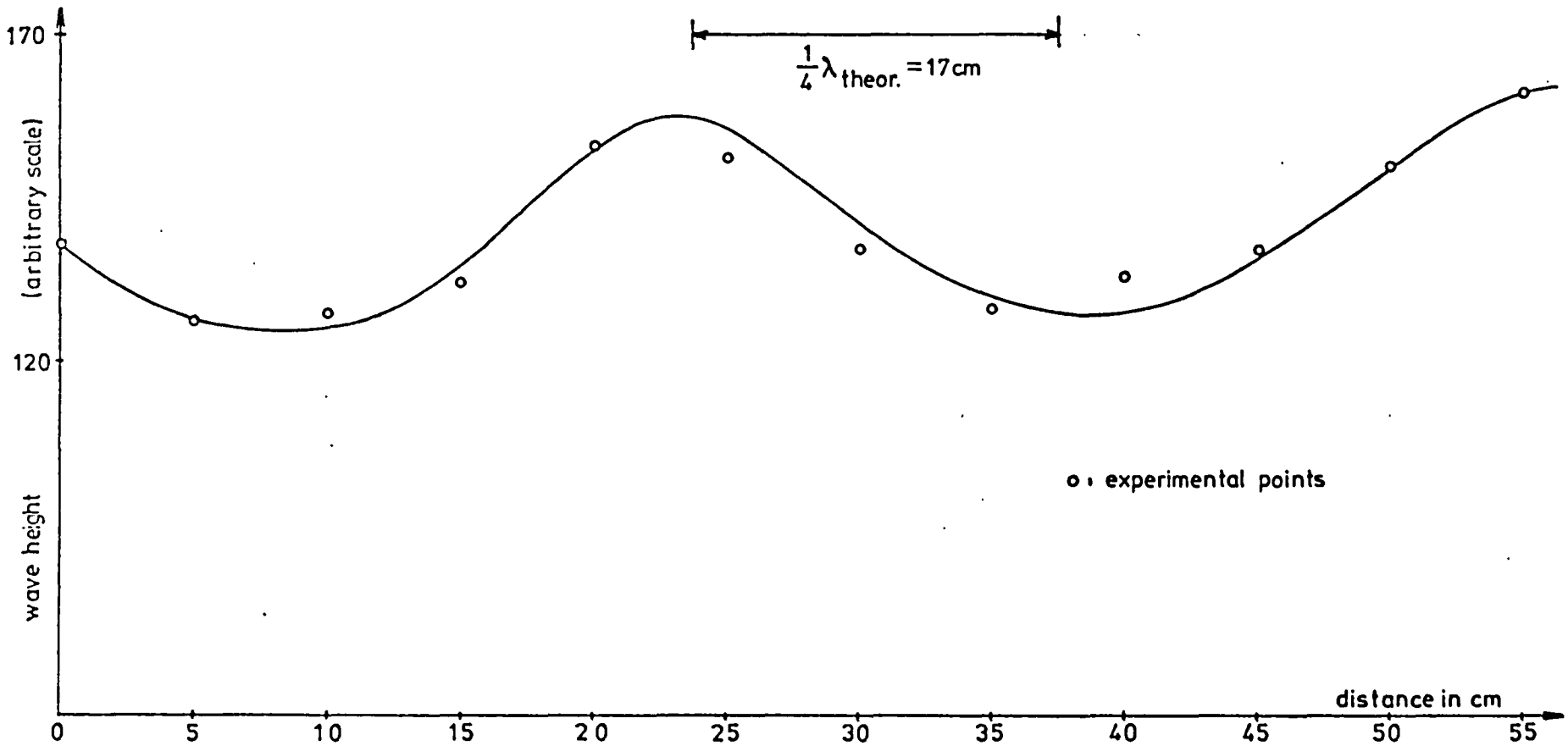

Fig. 31 . Wave height at various stations

the recorded amplitude varied considerably with time until it reached a rather stable condition. The first part of these deviations was attributed to the initial disturbance of the wave maker which started moving from rest thus creating a Cauchy-Poisson type of situation; this part lasted for about one minute. The smaller deviations, that persisted for more than ten minutes, were thought to be due to the excitation of surges along the basin and so a considerable time to reach a steady,more or less,state was needed. A third cause of deviations from the average amplitude that did not die out during the whole of the recording time was probably the transverse waves travelling across the direction of propagation of the fundamental wave. A little more about this effect will be said in subdivision D3.1.6.

To avoid the above cause of inaccuracies in the measurement of the wave amplitude, it was decided to leave the generator working at constant frequency for 13 minutes before any measurements were taken.

D3.1.5 Attenuation of the wave height. It has been explained in subdivision D2.3.3 that the attenuation of the waves due to viscous effects can be described by two parameters D, D' depending on the boundary layers at the fixed and free boundary respectively. If we denote the wave amplitude by a_1, a_2 at two positions x_1, x_2 we have accordingly

$$a_2 = a_1 e^{-(D+D')(x_2-x_1)} \qquad (223)$$

From eqs (217) and (218) we obtain for our case ($\nu = 0.011$ cm^2/sec): $D = 5.88 \times 10^{-4} m^{-1}$, $D' = 0.507 \times 10^{-4} m^{-1}$ while the condition (219) gives the requirement

$$2.51 \times 10^{-7} << 1$$

which is valid in our case.

The absolute error involved in our measuring procedure was estimated at about 0.1 cm. Therefore if we wish the attenuation to be just detectable, we get from eq. (223) $x_2 - x_1 = 3.13$ m. The point closest to the wave maker that we took measurements was $x_1 = 3h = 3 \times 0.38 = 1.04$ m, so that $x_2 = 1.04 + 3.13 = 4.17$ m. This is the maximum distance from the wave generator where the damping of the waves cannot be measured. Since almost all the points we took measurements were within the above distance, the damping effect was neglected altogether.

D3.1.6 Other effects. It may be seen in the general layout of the basin (fig. 28) that along the two edges of the main beach parallel to the axis of the basin pieces of metal sheet have been secured vertically to prevent leakage of the breaking waves at these edges of the beach which would result in undesirable scattering.

The comparatively large width of the basin gives room for any waves across the main propagation to develop. Such transverse waves have been mentioned already in subdivision D3.1.4; they may be due to three-dimensional causes such as (a) seepage past the edges of the wave maker (see subdivision D3.1.3), (b) dissipation along the side absorbers, (c) three-dimensional instabilities as examined in subdivision D2.3.1. These three dimensional effects are difficult to be predicted and are too small to be measured.

Finally it may be worth noting that before each measurement a small amount of wetting agent was applied around the wave probe to

reduce the effect of the surface tension of the water on the readings as well as the effect of any capillary waves present.

D3.2 The Model

In any experimental study dealing with diffraction around some configuration of vertical plates the problem of the wave reflected by these is present. The waves generated by the wave maker are reflected by the model breakwaters towards the wave machine where they are again reflected, thus building a resonant wave system that does not simulate either the reality or the theory that is going to be checked.

Experiments on diffraction around a semi-infinite breakwater or through a gap in a screen encounter the above problem. Investigators on these topics have used a practical method that separates geometrically the incident wave from its reflection by the barrier(s) (see e.g. Putnam and Arthur [8], Blue and Johnson [10]). According to this plates are put vertically parallel to the direction of propagation covering the distance from the tip(s) of the breakwater(s) to the wave generator. These plates are often called splitters for obvious reasons. The waves reflected by the model are thus isolated in a region separated from the area where measurements are to be taken; it is assumed that this region is of no interest. The effect of separating the incident from the reflected wave has been proved to be of minor significance for the cases of one or two co-planar semi-infinite breakwaters especially for great distances behind the opening. This has been verified experimentally and so the arrangement is justified.

It was thought originally to apply the same method to our experiment. The corresponding theoretical problem, sketched in fig. 32, has not been solved so far, although results exist for simpler similar cases as when two faces of the wedges are in line (see e.g. Nussenzueig [64] or Teague and Zitron [65]). An extension of these theories to include our case seemed possible at least in principle. However, a closer investigation revealed many difficulties in obtaining the solution. This fact combined with the apparent complexity of our original solution found in subdivision C3.3.3 that does not allow for a separate treatment of the reflected and incident wave components, called for an alternative arrangment. This is shown schematically in fig. 33.

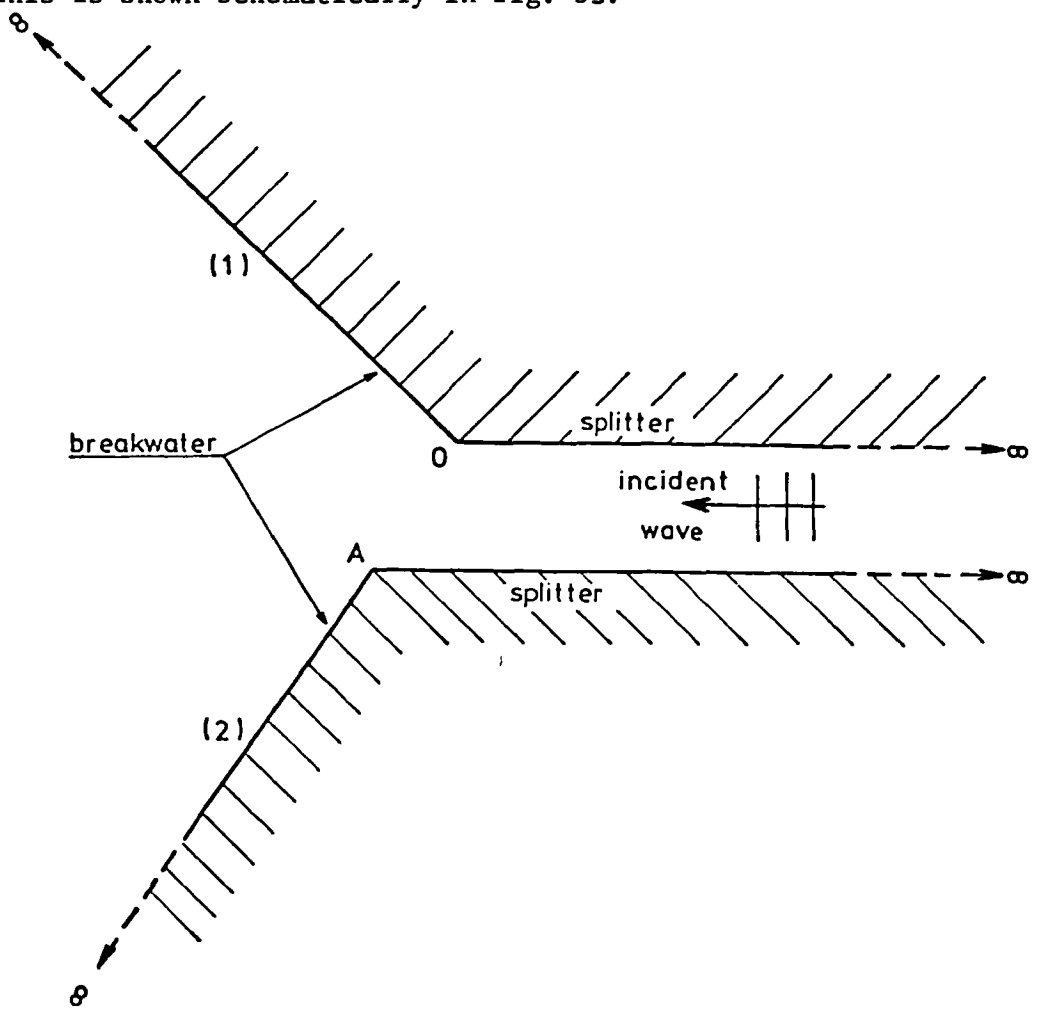

Fig. 32. An arrangement with splitters

Six absorbers had been placed along the sides of the basin to receive the reflected waves. The inclined position of the breakwaters relatively to the incident waves gave the opportunity to direct the reflected waves towards the long sides of the basin where the energy absorbers were. These were mainly impermeable wooden slopes as said in subdivision D3.1.1. At the two corners of the basin between the side slopes and the plunger straw bales serve as absorbers. A limiting case is shown in fig. 33, where the reflected

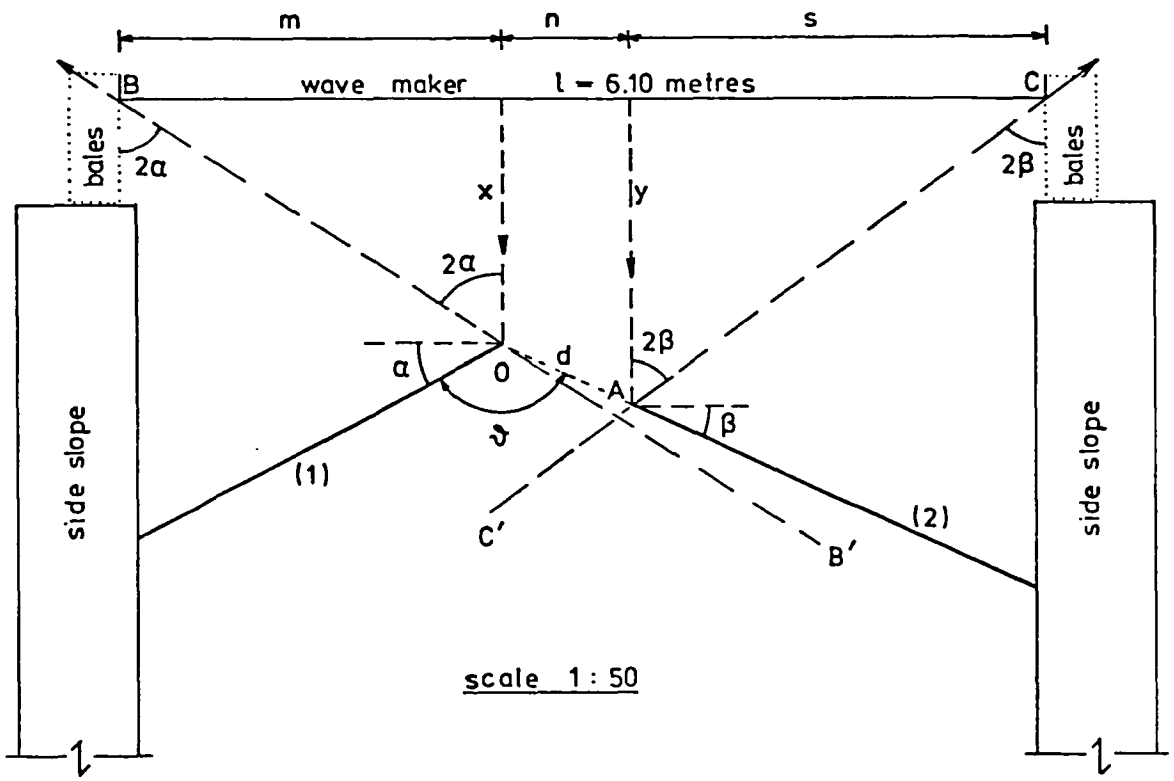

Fig. 33. Reflections by the two breakwaters

'rays' from the two tips 0 and A of the plates can just pass by the edges of the wave maker not reflected by it.

To reduce the many possible positions of the two screens we define a priori the values of $x > 3h$ and α as well as the variables

θ and d (see fig. 33); then simple geometrical relations give the position of the breakwaters through the following equations

$$m = x \tan 2\alpha$$

$$s = \ell - m + d \cos(\alpha + \theta)$$

$$n = \ell - m - s = 6.10 - m - s$$

$$y = - s/\tan 2(\alpha + \theta)$$

This set of equations defines the limiting case we have already discussed. Of course we may have many positions of the breakwaters fulfilling the requirement of only one reflection of the generated wave, by a suitable increase of angles α and β with simultaneous adjustement of the distances m, n, d.

A practical rule of finding the position of the two screens may run as follows:

(a) Give a value to θ

(b) Find $(180^{\circ} - \theta)/2 = \tau$

(c) Fix angle α in the range $\tau < \alpha < 2\tau$

(d) Draw two lines BB' and CC' from the ends of the wave maker at angles 2α and $2(180^{\circ} - \theta - \alpha) = 2\beta$.

(e) Put a line segment of value d', less than d to be on the safe side, between the lines BB' and CC' so that if forms an angle α+θ with the wave maker.

(f) Extend d' to the full length d and finally draw the screens (1) and (2) at angles α and β respectively as in fig. 33.

The actual position of the model in our experiment is shown in fig. 34. The material used was 3 mm thick steel plates of an inverse T-shape section 48 cm high. Four lengths of 2 feet and four

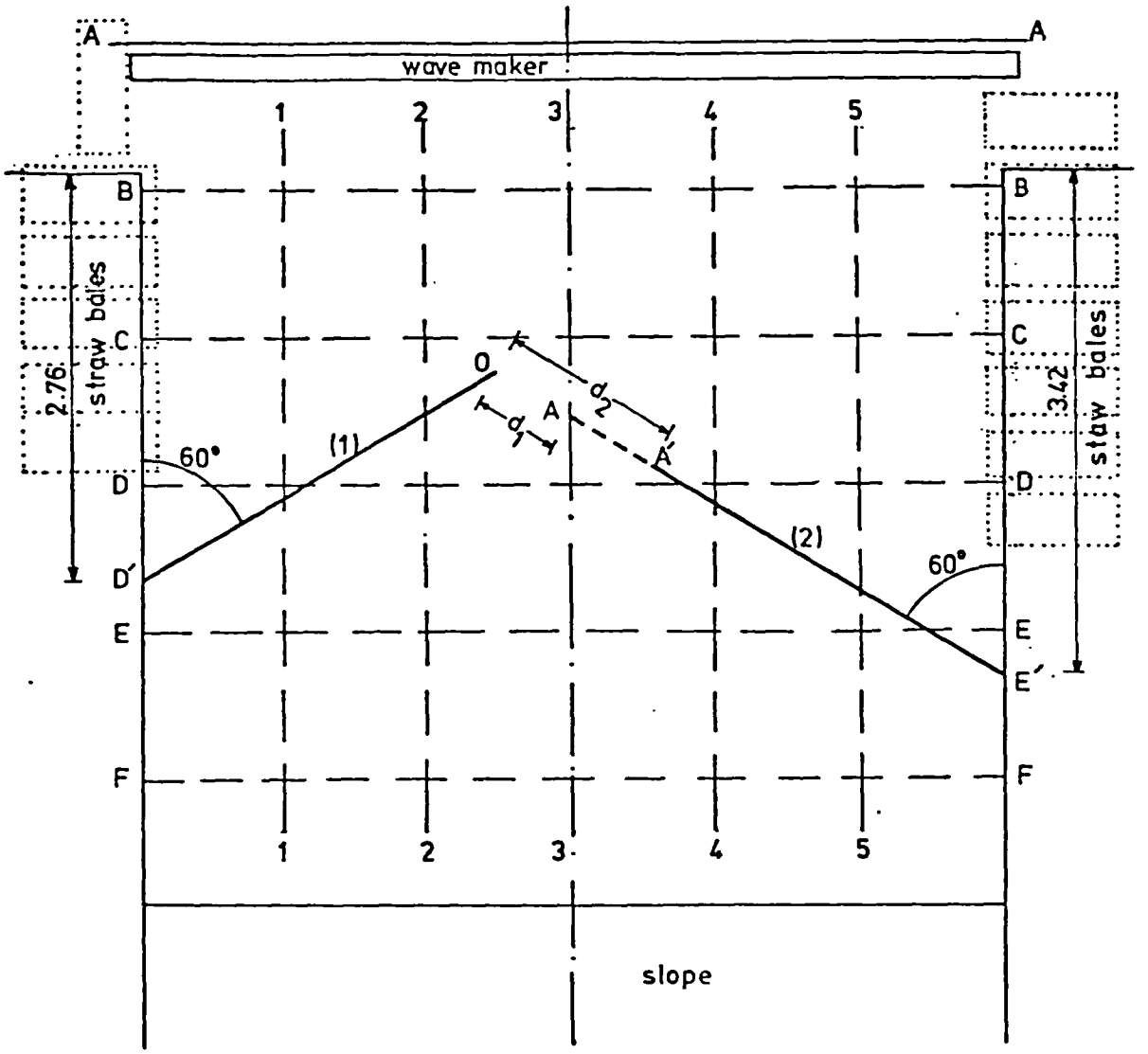

scale 1 : 50

co-ordinates
of breakwater tips (m)

O : CC + 0.215 , 2·2 + 0.44

gap widths

case I A : CC + 0.55 , 3·3

$$\delta_1 = \frac{d_1}{\text{wavelength}} = \frac{0.642}{0.68} = 0.944$$

case II A' : CC + 0.58 , 3·3 + 0.555

$$\delta_2 = \frac{d_2}{\text{wavelength}} = \frac{1.25}{0.68} = 1.845$$

Fig. 34. The model in place

of 3 feet were provided. Solving a multivalue simple geometrical problem as explained above I placed the two model breakwaters as in fig. 34. One angle θ was used throughout the experiment because among other reasons explained in the following subsection the elements of the two breakwaters that were resting on the side absorbers of the basin could not fit to more than one slope.

The angle between the two screens was $\theta = 120^{o}$ and the angle of incidence $\zeta = 240^{o}$. Two gap widths could be obtained by lifting and putting away one 2 feet long element of the screen (2). Thus we had

$$d_1 = 0.642 \text{ m} \quad \text{or} \quad \delta_1 = 0.944$$

$$d_2 = 1.255 \text{ m} \quad \text{or} \quad \delta_2 = 1.845$$

The leakage of water through the lines of contact between the metal elements was prevented by using waterproof tape and plasticene.

D3.3 Description of Experimental Procedure

The experiment was conducted to provide a direct comparison with the results of the theory; the experimental results are presented and discussed in subsection E2.3.

The measurements of the wave height were taken by using the equipment described in subdivision D3.1.2. The wave gauge was mounted on a metal beam spanning the whole width of the basin and resting on the side walls. As noted already, before taking any measurement a time of about 13 minutes was allowed to elapse from the moment the generator was started. A simple calibration of the gauge was performed after each measurement. The wave parameters

throughout the experiments were

water depth	38 cm
wave period	0.66 sec/cycle
wavelength	68 cm
incident wave height	2.75 cm

In the region between the wave maker and the model strong reflections by the side slopes were experienced initially that were upsetting the incident wave pattern. To reduce this effect straw bales were put along the slopes as indicated in fig. 34. This arrangement worked quite well as may be seen from the wave recordings at points along the opening where waves of virtually constant height were present (see fig. 35). This suggested that little if any disturbance caused by the subsequent wave reflections taking place in the 'weather side' passed through the opening and interfered with the wave pattern in the leeside which was to be measured.

It was planned originally that three cases of different θ and δ should be studied experimentally. However, practical reasons dictated reducing the cases to two of the same θ but different δ. One of the reasons has been explained in the previous subsection. A second one was that a variation of the experimental set-up should have to be of considerable magnitude at least of the order of the experimental error (10-20%), so that we could measure any effect due to such a change. The problem of finding a new position of the two barriers with its additional limitations mentioned earlier produced solutions where both the gap width and the distance of the plates from the wave maker were large and so reducing very much the area where acceptable measurements could be taken.

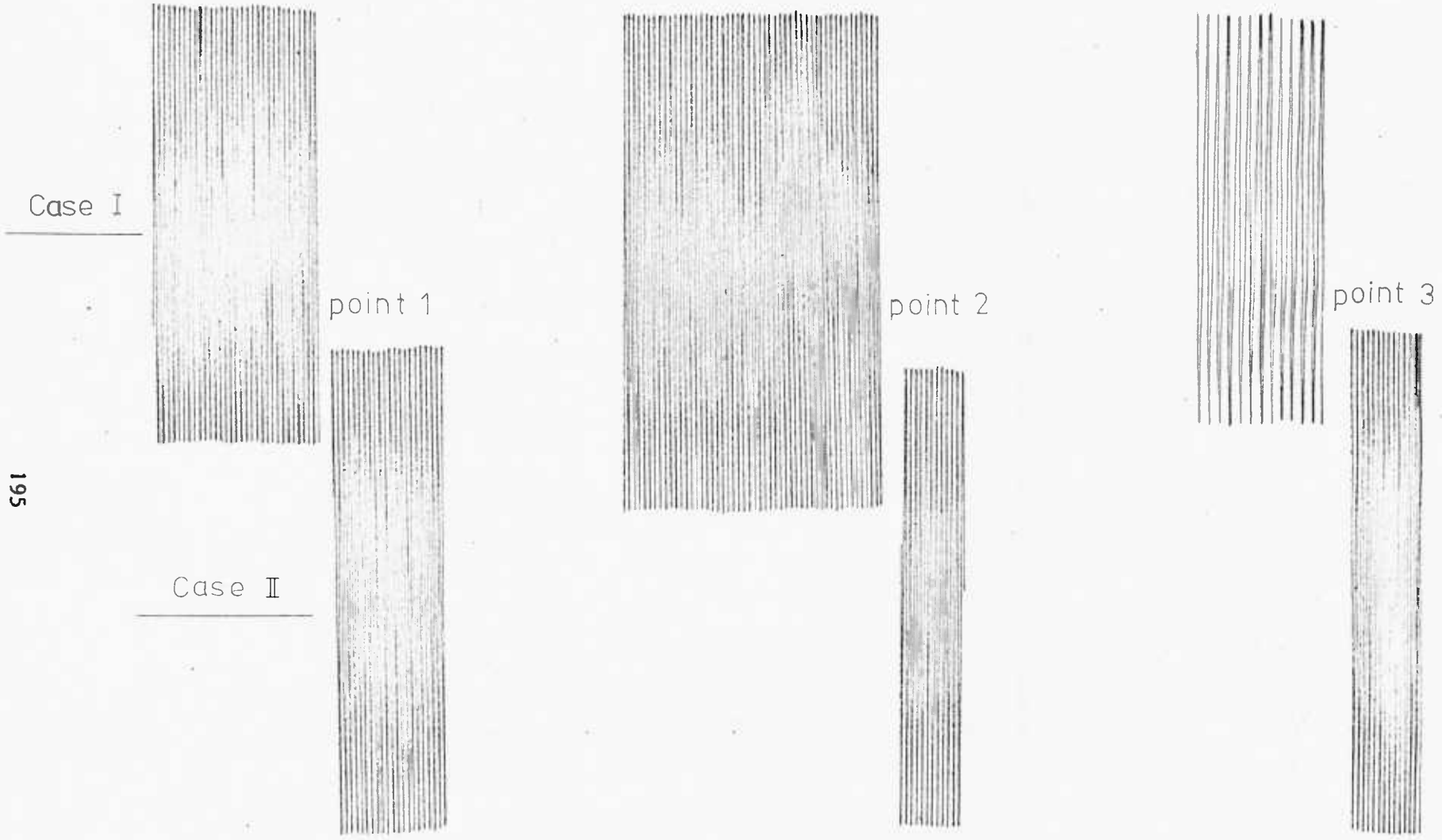

Fig. 35. Wave recordings at points along the opening; cases I and II (see figs 36,37)

On the other hand comparisons at angles θ different from the above were carried out with other theories (section E2); it was decided therefore to restrict experimental investigations to the following two separate cases.

Case I $\theta = 120^{o}$, $\delta = 0.944$, $\zeta = 240^{o}$

Case II $\theta = 120^{o}$, $\delta = 1.845$, $\zeta = 240^{o}$

The measurements were taken at the following points (ρ,ω) the positions of which are presented in figs 36 and 37.

Case I

point	1	2	3	4	5	6	7
$\omega(^{o})$	120	120	120	86	101	113	60
ρ	0.448	0.596	0.626	1.324	1.575	1.000	1.412
point	8	9	10	11	12	13	14
$\omega(^{o})$	21	14	35	23	42	73	96
ρ	1.690	2.618	2.735	3.071	2.440	2.381	2.880
point	15	16	17	18	19	20	21
$\omega(^{o})$	109	97	107	80	58	45	28
ρ	3.540	4.290	4.920	3.617	3.408	3.510	3.981
point	22	23	24	25	26	27	
$\omega(^{o})$	10	6	98	85	66	47	
ρ	3.142	3.000	5.765	4.920	4.520	4.594	

Case II

point	1	2	3	4	5	6	7
$\omega(^{o})$	120	120	120	110	19	26	50
ρ	0.382	1.295	1.603	2.365	2.352	2.720	2.280

point	8	9	10	11	12	13	14	15
$\omega(^{o})$	89	107	94	110	83	51	35	72
ρ	2.487	3.019	3.840	4.830	3.473	3.222	3.660	3.473
point	16	17	18	19	20	21	22	23
$\omega(^{o})$	65	49	45	87	95	101	81	31
ρ	4.515	4.560	4.650	5.050	5.570	5.980	4.810	5.140
point	24	25	26	27	28	29	30	
$\omega(^{o})$	60	18	10	47	94	68	85	
ρ	2.678	3.660	3.142	0.941	1.103	1.369	0.529	

The diffraction coefficient measured is presented in figs 68 and 69.

The wave gauge was calibrated at frequent intervals and the deviations noted were not great, of the order of 5% where some part of the maximum absolute uncertainty of 0.1 cm (see D3.1.2) might have been present.

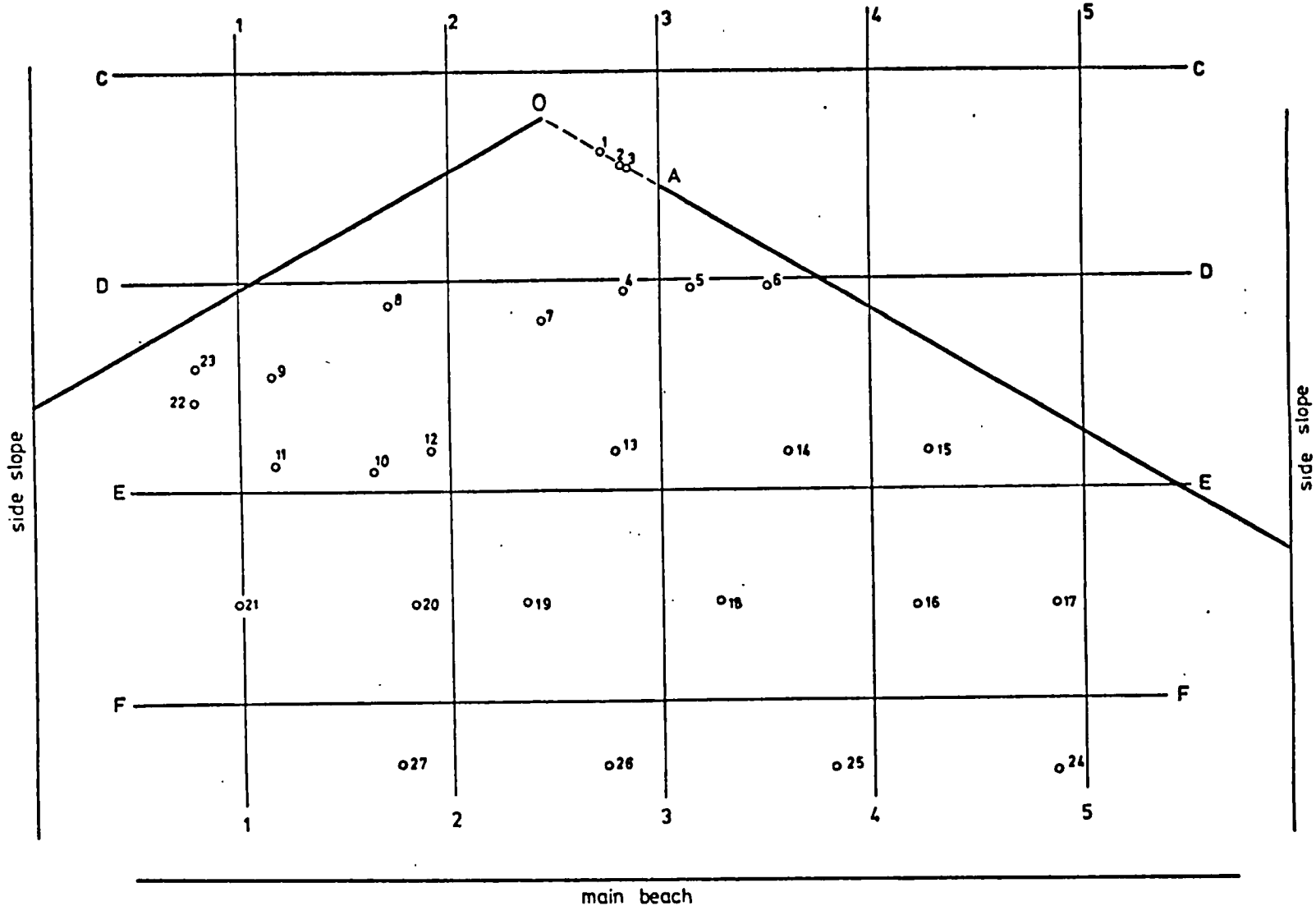

Fig. 36. Positions of the points where measurements were taken. Case I

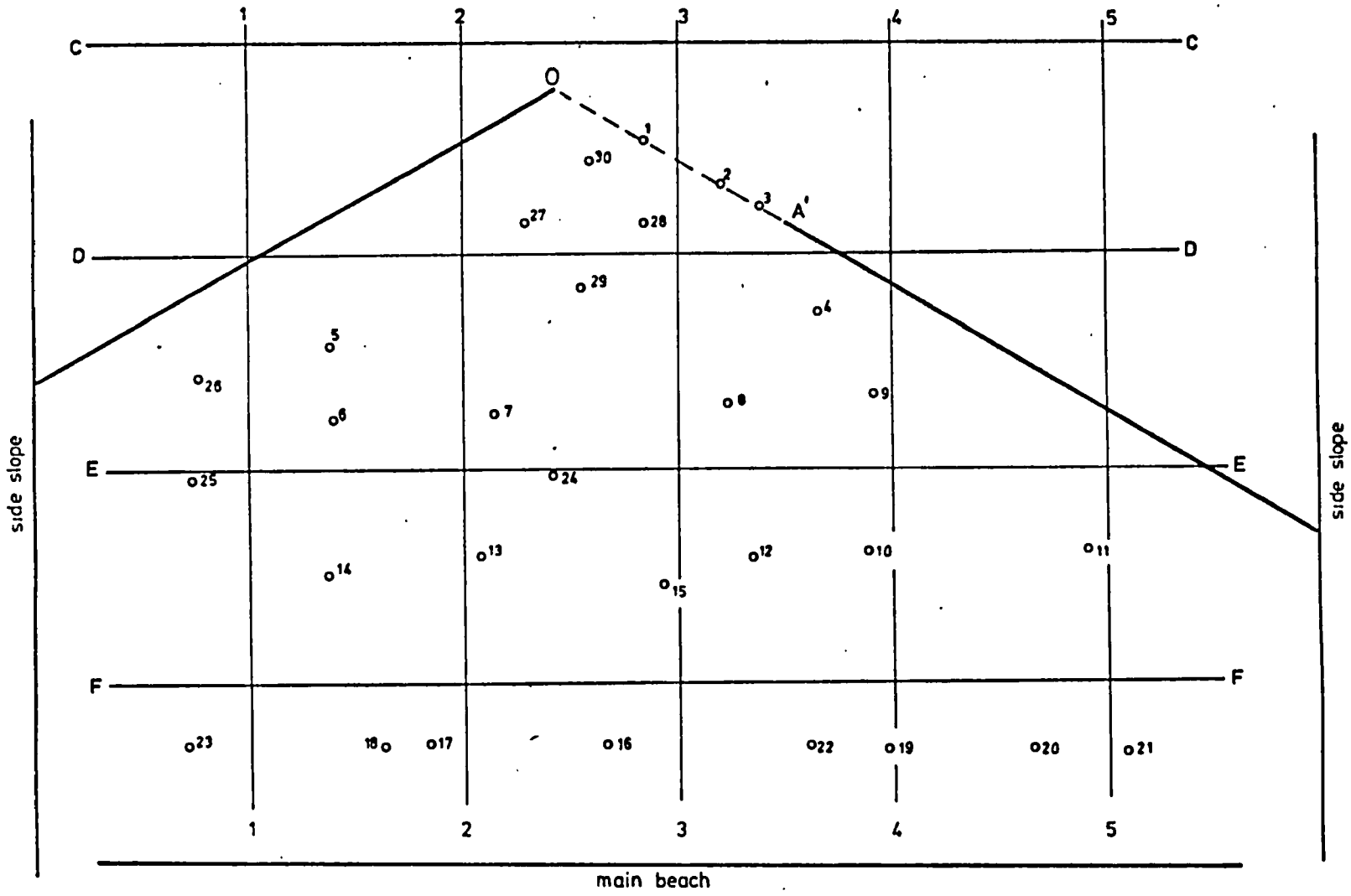

Fig. 37. Positions of points where measurements were taken. Case II

C H A P T E R E

RESULTS AND DISCUSSION

E1 RESULTS

Application of the computing procedure explained in section C4 gives the wave heights at any point $P(r,\omega)$ for various combinations of the parameters of the problem: angle between the two breakwaters θ, width of opening between the two breakwaters d, angles of incident plane wave $\zeta = 2\pi + \theta - \theta_o$. Although the theory puts no restriction on the above values the results obtained cover the cases most likely to be encountered in practice. Accordingly I limited θ in the range $\frac{\pi}{2} < \theta < \pi$ and ω in the range $0 \leq \omega \leq \theta$ which means that we are interested in the region leeside of the breakwaters. r was kept $\geq$ d so that information over the unlimited area $d \leq r < \infty$, $0 \leq \omega \leq \theta$ was obtained; as already mentioned the basic equations (166) can be used after a slight modification to produce results applicable in the region $0 < r < d$, $0 \leq \omega \leq \theta$.

The relevant equation for this region is

$$F(r,\omega) = -\frac{\pi^2}{\lambda\theta}\sin\zeta\left[\int_r^d \exp\{-ikq\cos\zeta\}\sum_{m=o}^{\infty}(-)^m\varepsilon_m J_{\frac{m\pi}{\theta}}(kr)H_{\frac{m\pi}{\theta}}(kq)\cos\frac{m\pi}{\theta}\omega\,dq + \right.$$

$$\left. + \int_o^r \exp\{-ikq\cos\zeta\}\sum_{m=o}^{\infty}(-)^m\varepsilon_m J_{\frac{m\pi}{\theta}}(kq)^r H_{\frac{m\pi}{\theta}}(kr)\cos\frac{m\pi}{\theta}\omega\,dq\right]$$

whence the diffraction coefficient $K = |F|$ is derived

$$|F| = -\frac{\pi^2}{\theta}\sin\zeta\,(Re^2+Im^2)^{\frac{1}{2}}$$

with $$Re = \int_o^{\delta}\cos\hat{q}\,JJ_q + \int_o^{\rho}\sin\hat{q}\,J_qY + \int_{\rho}^{\delta}\sin\hat{q}\,JY_q$$

$$Im = -\int_o^{\delta}\sin\hat{q}\,JJ_q + \int_o^{\rho}\cos\hat{q}\,J_qY + \int_{\rho}^{\delta}\cos\hat{q}\,JY_q$$

where the integrands are written in reduced notation; for example

$$\cos \hat{q}\, JY_q \text{ stands for } \cos(2\pi q\cos\zeta) \sum_{m=o}^{\infty} (-)^m \varepsilon_m J_{\frac{m\pi}{\theta}}(2\pi\rho) Y_{\frac{m\pi}{\theta}}(2\pi q)\cos\frac{m\pi}{\theta}\omega\, dq,$$

etc.

However the field close to the opening was not thoroughly investigated for the following reasons:

(a) In this region higher-order effects due to the proximity of the two edges bounding the gap are of considerable importance and the linear theory tends to be inadequate.

(b) Our approximation of the velocity as being uniform along the gap, when 'viewed' from small distance may give results deviating from the true value more than could be accepted (Bouwkamp remarks on this also [12], p. 52).

(c) In general the limited area close to the entrance of a harbour as defined above, is less important to the engineer than the rest of the sheltered area where the various harbour installations are built.

However, given the above limitations, some values of the diffraction coefficient were calculated for the field close to the gap for the cases of relatively large opening and are presented together with the rest of the results. This was done to check the continuity and consistency of the theory and to get an idea about the values of K in the above-mentioned region for the cases that should give more reliable information, i.e. big gaps. These results suggest a smooth and consistent transition across the r = d arc as can be seen in the relevant tables and figures. They also provide a source of information for the engineer since the discrepancies with the experimental results are not great as will be seen in the next section, despite

the reservations expressed above.

Twenty seven cases of different combinations of the variables θ, d, ζ have been treated. Contours of equal wave height have been drawn at intervals of one tenth of the height of the incident wave represented by unity. The following values of the three parameters of the structure and of the position of the observation point $P(r,\omega)$ were used:

θ = 90, 120, 145 degrees

d = 1, 2, 3 wavelengths

ζ = 200, 250, 270 degrees

ω = 0, 20, 40, ... , θ degrees

r = d, $d+\lambda$, ... , $d+9\lambda$

In the nine cases with $\delta = d/\lambda = 3.0$ for which the field near the gap has been calculated different ω and ρ were used as shown in the following tables.

The numerical results are presented in tables 2-28 and graphs with plotted contours in figs 38-64.

$\theta = 90^{\circ}, \quad \delta = 1.0, \quad \zeta = 200^{\circ}$

ω (°) \ ρ	1.0	2.0	3.0	4.0	5.0	6.0	7.0	8.0	9.0
0	0.154	0.076	0.041	0.024	0.015	0.010	0.007	0.005	0.004
20	0.116	0.095	0.094	0.089	0.083	0.079	0.074	0.070	0.067
40	0.150	0.194	0.176	0.158	0.144	0.133	0.124	0.117	0.110
60	0.307	0.252	0.200	0.169	0.150	0.135	0.125	0.116	0.109
80	0.501	0.274	0.210	0.177	0.156	0.140	0.129	0.120	0.113
90	0.582	0.275	0.210	0.177	0.156	0.141	0.130	0.121	0.113

Table 2. Diffraction coefficient at points (ρ, ω)

$\theta = 90^{\circ}, \quad \delta = 1.0, \quad \zeta = 250^{\circ}$

ω (°) \ ρ	1.0	2.0	3.0	4.0	5.0	6.0	7.0	8.0	9.0
0	0.538	0.695	0.678	0.635	0.594	0.557	0.526	0.499	0.475
20	0.692	0.615	0.506	0.434	0.383	0.347	0.319	0.294	0.278
40	1.037	0.718	0.547	0.455	0.397	0.356	0.326	0.302	0.282
60	1.010	0.468	0.334	0.273	0.237	0.212	0.194	0.180	0.168
80	0.681	0.235	0.167	0.136	0.117	0.104	0.095	0.088	0.082
90	0.561	0.208	0.149	0.122	0.105	0.094	0.085	0.079	0.074

Table 3. Diffraction coefficient at points (ρ,ω)

$\theta = 90^{o}, \quad \delta = 1.0, \quad \zeta = 270^{o}$

ω (^{o}) \ ρ	1.0	2.0	3.0	4.0	5.0	6.0	7.0	8.0	9.0
0	0.1358	1.255	1.092	0.969	0.876	0.805	0.748	0.701	0.662
20	1.014	0.667	0.503	0.418	0.365	0.329	0.302	0.281	0.264
40	0.825	0.393	0.270	0.217	0.187	0.167	0.152	0.141	0.132
60	0.751	0.267	0.183	0.149	0.129	0.116	0.106	0.099	0.093
80	0.418	0.074	0.039	0.027	0.021	0.017	0.015	0.013	0.012
90	0.418	0.065	0.033	0.021	0.015	0.011	0.009	0.007	0.006

Table 4. Diffraction coefficient at points (ρ,ω)

$\theta = 90^{\circ}, \quad \delta = 2.0, \quad \zeta = 200^{\circ}$

ω ($^{\circ}$) \ ρ	2.0	3.0	4.0	5.0	6.0	7.0	8.0	9.0
0	0.097	0.105	0.086	0.066	0.050	0.038	0.029	0.023
20	0.084	0.046	0.068	0.074	0.074	0.071	0.067	0.064
40	0.176	0.125	0.075	0.069	0.074	0.078	0.081	0.082
60	0.213	0.319	0.319	0.296	0.273	0.254	0.238	0.225
80	0.676	0.482	0.386	0.331	0.295	0.268	0.248	0.232
90	0.831	0.478	0.382	0.328	0.292	0.266	0.246	0.230

Table 5. Diffraction coefficient at points (ρ,ω)

$\theta = 90^{\circ}, \quad \delta = 2.0, \quad \zeta = 250^{\circ}$

ω (°) \ ρ	2.0	3.0	4.0	5.0	6.0	7.0	8.0	9.0
0	0.651	0.534	0.358	0.230	0.160	0.138	0.143	0.157
20	0.453	0.546	0.679	0.715	0.710	0.690	0.666	0.641
40	1.099	1.113	0.895	0.730	0.618	0.539	0.481	0.436
60	1.111	0.495	0.280	0.196	0.155	0.131	0.115	0.104
80	0.646	0.206	0.139	0.111	0.095	0.084	0.076	0.070
90	0.649	0.211	0.148	0.120	0.103	0.092	0.083	0.077

Table 6. Diffraction coefficient at points (ρ,ω)

$\theta = 90^{o}, \quad \delta = 2.0, \quad \zeta = 270^{o}$

ω (^{o}) \ ρ	2.0	3.0	4.0	5.0	6.0	7.0	8.0	9.0
0	0.762	1.105	1.295	1.347	1.338	1.305	1.263	1.219
20	1.278	1.126	0.879	0.698	0.576	0.491	0.429	0.384
40	1.019	0.601	0.400	0.305	0.253	0.220	0.197	0.181
60	0.639	0.288	0.215	0.181	0.160	0.146	0.134	0.126
80	0.529	0.115	0.065	0.047	0.037	0.032	0.028	0.025
90	0.445	0.086	0.047	0.032	0.023	0.018	0.015	0.012

Table 7. Diffraction coefficients at points (ρ,ω)

$\theta = 90^{o}, \quad \delta = 3.0, \quad \zeta = 200^{o}$

ω (^{o}) \ ρ	1.0	2.0	3.0	4.0	5.0	6.0	7.0	8.0	9.0
0	0.08	0.11	0.041	0.052	0.074	0.077	0.072	0.064	0.055
20			0.080	0.062	0.081	0.084	0.077	0.067	0.056
30	0.17	0.12							
40			0.140	0.074	0.104	0.111	0.101	0.087	0.073
60	0.25	0.29	0.289	0.205	0.271	0.304	0.310	0.307	0.299
80			0.761	0.655	0.539	0.469	0.421	0.385	0.357
90	0.64	0.89	1.003	0.633	0.520	0.453	0.408	0.374	0.347

Table 8. Diffraction coefficient at points (ρ,ω)

$\theta = 90^{o}, \quad \delta = 3.0, \quad \zeta = 250^{o}$

ω (^{o}) \ ρ	1.0	2.0	3.0	4.0	5.0	6.0	7.0	8.0	9.0
0	0.60	0.56	0.498	0.263	0.270	0.359	0.410	0.428	0.426
20			0.612	0.516	0.448	0.535	0.632	0.697	0.732
30	0.71	0.77							
40			0.928	1.231	1.128	0.926	0.752	0.619	0.520
60	1.14	1.14	1.115	0.544	0.323	0.251	0.217	0.194	0.178
80			0.844	0.230	0.130	0.093	0.075	0.063	0.056
90	1.00	1.23	0.543	0.121	0.069	0.047	0.035	0.028	0.023

Table 9. Diffraction coefficient at points (ρ,ω)

$\theta = 90^{o}, \quad \delta = 3.0, \quad \zeta = 270^{o}$

ω (^{o}) \ ρ	1.0	2.0	3.0	4.0	5.0	6.0	7.0	8.0	9.0
0	1.05	1.05	1.148	0.837	0.770	0.923	1.085	1.201	1.275
20			0.999	1.115	0.971	0.781	0.621	0.499	0.407
30	0.87	0.88							
40			1.132	0.770	0.494	0.340	0.252	0.198	0.162
60	1.05	0.97	0.842	0.317	0.133	0.080	0.066	0.062	0.060
80			0.601	0.158	0.091	0.066	0.053	0.046	0.040
90	0.86	0.83	0.469	0.097	0.056	0.039	0.029	0.023	0.019

Table 10. Diffraction coefficient at points (ρ,ω)

$\theta = 120^{\circ}, \quad \delta = 1.0, \quad \zeta = 200^{\circ}$

ω ($^{\circ}$) \ ρ	1.0	2.0	3.0	4.0	5.0	6.0	7.0	8.0	9.0
0	0.098	0.085	0.075	0.067	0.061	0.056	0.052	0.049	0.046
20	0.089	0.060	0.044	0.035	0.030	0.026	0.023	0.021	0.019
40	0.073	0.023	0.026	0.030	0.031	0.031	0.031	0.030	0.029
60	0.071	0.108	0.110	0.103	0.096	0.090	0.085	0.080	0.076
80	0.206	0.224	0.189	0.165	0.147	0.135	0.125	0.116	0.110
100	0.414	0.278	0.216	0.183	0.161	0.146	0.134	0.125	0.117
120	0.587	0.281	0.216	0.182	0.161	0.145	0.134	0.124	0.117

Table 11. Diffraction coefficient at points (ρ,ω)

$\theta = 120^{o}, \quad \delta = 1.0, \quad \zeta = 250^{o}$

ω (°) \ ρ	1.0	2.0	3.0	4.0	5.0	6.0	7.0	8.0	9.0
0	0.149	0.032	0.052	0.067	0.074	0.077	0.077	0.077	0.076
20	0.213	0.218	0.217	0.208	0.197	0.187	0.177	0.169	0.162
40	0.514	0.558	0.508	0.460	0.421	0.390	0.365	0.343	0.325
60	0.853	0.714	0.577	0.491	0.434	0.392	0.361	0.335	0.315
80	1.035	0.606	0.443	0.362	0.313	0.280	0.255	0.236	0.220
100	0.943	0.391	0.283	0.232	0.202	0.181	0.165	0.153	0.143
120	0.634	0.289	0.219	0.184	0.161	0.146	0.134	0.124	0.117

Table 12. Diffraction coefficient at points (ρ,ω)

$\theta = 120^{o}, \quad \delta = 1.0, \quad \zeta = 270^{o}$

ω (°) \ ρ	1.0	2.0	3.0	4.0	5.0	6.0	7.0	8.0	9.0
0	0.542	0.564	0.532	0.496	0.464	0.437	0.413	0.393	0.375
20	0.582	0.540	0.473	0.421	0.382	0.351	0.327	0.307	0.290
40	0.811	0.665	0.547	0.471	0.418	0.380	0.350	0.326	0.306
60	1.003	9.642	0.475	0.388	0.334	0.297	0.270	0.249	0.232
80	0.909	0.361	0.231	0.178	0.148	0.129	0.116	0.105	0.098
100	0.548	0.108	0.060	0.043	0.034	0.029	0.025	0.023	0.021
120	0.414	0.069	0.040	0.029	0.024	0.020	0.018	0.016	0.015

Table 13. Diffraction coefficient at points (ρ,ω)

$\theta = 120^{o}, \quad \delta = 2.0, \quad \zeta = 200^{o}$

ω^{o} \ ρ	2.0	3.0	4.0	5.0	6.0	7.0	8.0	9.0
0	0.073	0.048	0.033	0.022	0.015	0.011	0.007	0.004
20	0.046	0.057	0.061	0.059	0.056	0.053	0.050	0.047
40	0.079	0.042	0.023	0.026	0.033	0.036	0.038	0.039
60	0.067	0.101	0.084	0.062	0.045	0.033	0.024	0.018
80	0.179	0.123	0.168	0.182	0.182	0.178	0.172	0.166
100	0.415	0.454	0.386	0.338	0.303	0.277	0.257	0.241
120	0.839	0.486	0.389	0.335	0.299	0.272	0.252	0.236

Table 14. Diffraction coefficient at points (ρ,ω)

$\theta = 120^{o}, \quad \delta = 2{,}0, \quad \zeta = 250^{o}$

ω (°) \ ρ	2.0	3.0	4.0	5.0	6.0	7.0	8.0	9.0
0	0.197	0.079	0.040	0.053	0.071	0.082	0.090	0.095
20	0.304	0.325	0.303	0.271	0.241	0.215	0.193	0.175
40	0.451	0.282	0.296	0.348	0.382	0.399	0.405	0.405
60	0.630	0.903	0.904	0.832	0.757	0.693	0.640	0.595
80	1.282	0.902	0.591	0.428	0.335	0.277	0.237	0.208
100	0.806	0.217	0.134	0.111	0.099	0.091	0.085	0.081
120	0.737	0.280	0.211	0.177	0.156	0.141	0.130	0.121

Table 15. Diffraction coefficient at points (ρ,ω)

$\theta = 120^{\circ}, \quad \delta = 2.0, \quad \zeta = 270^{\circ}$

ω (°) \ ρ	2.0	3.0	4.0	5.0	6.0	7.0	8.0	9.0
0	0.579	0.476	0.386	0.315	0.262	0.221	0.189	0.164
20	0.340	0.333	0.402	0.447	0.469	0.477	0.477	0.472
40	0.704	0.904	0.899	0.838	0.773	0.713	0.662	0.618
60	1.283	0.921	0.603	0.416	0.305	0.233	0.186	0.152
80	0.769	0.315	0.242	0.210	0.187	0.170	0.157	0.146
100	0.695	0.227	0.129	0.093	0.074	0.062	0.055	0.049
120	0.451	0.089	0.053	0.039	0.031	0.027	0.023	0.021

Table 16. Diffraction coefficient at points (ρ,ω)

$\theta = 120^{\circ}, \quad \delta = 3.0, \quad \zeta = 200^{\circ}$

ω ($^{\circ}$) \ ρ	1.0	2.0	3.0	4.0	5.0	6.0	7.0	8.0	9.0
0	0.10	0.05	0.015	0.019	0.029	0.034	0.037	0.38	0.039
20			0.066	0.048	0.032	0.023	0.021	0.022	0.023
30	0.06	0.08							
40			0.066	0.061	0.038	0.024	0.026	0.032	0.036
60	0.13	0.11	0.067	0.086	0.052	0.028	0.033	0.044	0.051
80			0.123	0.172	0.113	0.073	0.074	0.087	0.098
90	0.24	0.27							
100			0.371	0.512	0.501	0.461	0.425	0.394	0.369
120	0.65	0.90	1.018	0.643	0.529	0.462	0.416	0.382	0.355

Table 17. Diffraction coefficient at points (ρ,ω)

$\theta = 120^{o}, \quad \delta = 3.0, \quad \zeta = 250^{o}$

ω (°) \ ρ	1.0	2.0	3.0	4.0	5.0	6.0	7.0	8.0	9.0
0	0.37	0.32	0.200	0.103	0.047	0.043	0.064	0.082	0.096
20			0.288	0.280	0.229	0.179	0.141	0.118	0.107
30	0.32	0.31							
40			0.244	0.353	0.360	0.300	0.229	0.174	0.143
60	0.60	0.65	0.746	0.742	0.968	1.054	1.048	1.004	0.949
80			1.315	1.036	0.607	0.359	0.229	0.162	0.129
90	1.19	1.14							
100			0.959	0.511	0.321	0.238	0.193	0.164	0.144
120	1.03	1.23	0.569	0.124	0.073	0.053	0.041	0.034	0.029

Table 18. Diffraction coefficient at points (ρ,ω)

$\theta = 120^{\circ}, \quad \delta = 3.0, \quad \zeta = 270^{\circ}$

ω (°) \ ρ	1.0	2.0	3.0	4.0	5.0	6.0	7.0	8.0	9.0
0	0.60	0.52	0.327	0.179	0.105	0.110	0.140	0.166	0.186
20			0.519	0.525	0.453	0.373	0.310	0.269	0.248
30	0.54	0.55							
40			0.604	0.757	0.946	1.017	1.016	0.982	0.935
60	0.88	1.01	1.329	1.053	0.656	0.400	0.264	0.200	0.175
80			0.962	0.554	0.287	0.152	0.089	0.062	0.055
90	1.08	0.96							
100			0.594	0.293	0.188	0.139	0.112	0.095	0.083
120	0.84	0.83	0.493	0.100	0.061	0.045	0.036	0.031	0.027

Table 19. Diffraction coefficient at points (ρ,ω)

$\theta = 145^{\circ}$, $\delta = 1.0$, $\zeta = 200^{\circ}$

ω (°) \ ρ	1.0	2.0	3.0	4.0	5.0	6.0	7.0	8.0	9.0
0	0.044	0.040	0.036	0.033	0.031	0.029	0.027	0.026	0.025
20	0.051	0.044	0.038	0.034	0.031	0.029	0.027	0.025	0.024
40	0.070	0.051	0.040	0.033	0.028	0.025	0.023	0.021	0.019
60	0.078	0.029	0.012	0.009	0.010	0.011	0.011	0.012	0.012
80	0.061	0.077	0.084	0.082	0.078	0.074	0.071	0.067	0.064
100	0.159	0.198	0.174	0.153	0.139	0.127	0.118	0.111	0.104
120	0.361	0.271	0.213	0.181	0.160	0.145	0.134	0.124	0.117
140	0.557	0.281	0.216	0.182	0.161	0.145	0.134	0.124	0.117
145	0.585	0.281	0.216	0.182	0.161	0.145	0.133	0.124	0.117

Table 20. Diffraction coefficient at points (ρ,ω)

$\theta = 145^{\circ}, \quad \delta = 1.0, \quad \zeta = 250^{\circ}$

ω (°) \ ρ	1.0	2.0	3.0	4.0	5.0	6.0	7.0	8.0	9.0
0	0.214	0.148	0.118	0.101	0.090	0.082	0.075	0.070	0.066
20	0.180	0.095	0.063	0.047	0.038	0.032	0.028	0.026	0.023
40	0.163	0.178	0.185	0.182	0.178	0.167	0.160	0.154	0.148
60	0.382	0.450	0.422	0.388	0.358	0.334	0.313	0.296	0.281
80	0.726	0.666	0.557	0.483	0.430	0.391	0.361	0.337	0.317
100	1.005	0.664	0.499	0.413	0.360	0.322	0.295	0.273	0.255
120	1.033	0.472	0.341	0.281	0.244	0.218	0.200	0.185	0.173
140	0.704	0.321	0.244	0.205	0.181	0.163	0.150	0.139	0.131
145	0.656	0.314	0.240	0.202	0.178	0.161	0.148	0.137	0.124

Table 21. Diffraction coefficient at points (ρ,ω)

$\theta = 145^{\circ}, \quad \delta = 1.0, \quad \zeta = 270^{\circ}$

ω (°) \ ρ	1.0	2.0	3.0	4.0	5.0	6.0	7.0	8.0	9.0
0	0.177	0.177	0.169	0.159	0.150	0.142	0.135	0.129	0.124
20	0.249	0.248	0.232	0.215	0.201	0.188	0.178	0.169	0.161
40	0.469	0.464	0.423	0.386	0.356	0.331	0.311	0.294	0.279
60	0.764	0.675	0.574	0.502	0.451	0.412	0.381	0.357	0.336
80	0.990	0.685	0.520	0.430	0.373	0.333	0.303	0.280	0.261
100	0.973	0.447	0.297	0.232	0.195	0.171	0.153	0.140	0.130
120	0.660	0.159	0.093	0.069	0.057	0.049	0.043	0.039	0.036
140	0.359	0.057	0.030	0.020	0.015	0.013	0.011	0.009	0.008
145	0.396	0.056	0.030	0.020	0.016	0.013	0.011	0.010	0.009

Table 22. Diffraction coefficient at points (ρ,ω)

$\theta = 145^{o}, \quad \delta = 2.0, \quad \zeta = 200^{o}$

ω (°) \ ρ	2.0	3.0	4.0	5.0	6.0	7.0	8.0	9.0
0	0.054	0.050	0.046	0.043	0.040	0.038	0.036	0.034
20	0.044	0.033	0.025	0.019	0.016	0.013	0.011	0.009
40	0.017	0.019	0.026	0.029	0.030	0.029	0.028	0.028
60	0.066	0.052	0.032	0.018	0.010	0.007	0.008	0.010
80	0.048	0.073	0.081	0.073	0.064	0.055	0.048	0.042
100	0.168	0.080	0.090	0.112	0.121	0.124	0.124	0.123
120	0.290	0.394	0.359	0.322	0.293	0.270	0.251	0.236
140	0.783	0.490	0.392	0.337	0.301	0.274	0.254	0.237
145	0.839	0.487	0.390	0.336	0.300	0.273	0.253	0.236

Table 23. Diffraction coefficient at points (ρ,ω)

$\theta = 145^{\circ}, \quad \delta = 2.0, \quad \zeta = 250^{\circ}$

ω (°) \ ρ	2.0	3.0	4.0	5.0	6.0	7.0	8.0	9.0
0	0.254	0.219	0.196	0.178	0.164	0.152	0.143	0.135
20	0.174	0.116	0.084	0.068	0.060	0.056	0.054	0.053
40	0.157	0.200	0.206	0.197	0.184	0.171	0.159	0.148
60	0.387	0.246	0.154	0.147	0.171	0.192	0.207	0.217
80	0.467	0.708	0.798	0.788	0.750	0.707	0.667	0.631
100	1.211	1.060	0.778	0.601	0.490	0.416	0.363	0.325
120	0.993	0.284	0.123	0.079	0.064	0.058	0.055	0.053
140	0.662	0.291	0.220	0.186	0.164	0.149	0.137	0.128
145	0.764	0.295	0.223	0.188	0.166	0.151	0.139	0.130

Table 24. Diffraction coefficient at points (ρ,ω)

$\theta = 145^{\circ}, \quad \delta = 2.0, \quad \zeta = 270^{\circ}$

ω (°) \ ρ	2.0	3.0	4.0	5.0	6.0	7.0	8.0	9.0
0	0.233	0.229	0.223	0.215	0.207	0.199	0.191	0.184
20	0.273	0.237	0.202	0.173	0.151	0.134	0.120	0.108
40	0.313	0.174	0.147	0.171	0.195	0.213	0.224	0.230
60	0.542	0.765	0.826	0.813	0.778	0.738	0.700	0.664
80	1.246	1.063	0.795	0.608	0.484	0.399	0.339	0.295
100	0.956	0.330	0.190	0.166	0.157	0.149	0.142	0.136
120	0.693	0.314	0.196	0.146	0.119	0.102	0.090	0.082
140	0.360	0.078	0.043	0.029	0.022	0.018	0.015	0.013
145	0.443	0.076	0.042	0.029	0.022	0.018	0.015	0.013

Table 25. Diffraction coefficient at points (ρ,ω)

$\theta = 145^{\circ}$, $\delta = 3.0$, $\zeta = 200^{\circ}$

ω ($^{\circ}$) \ ρ	1.0	2.0	3.0	4.0	5.0	6.0	7.0	8.0	9.0
0	0.06	0.06	0.053	0.048	0.043	0.040	0.037	0.035	0.033
20			0.020	0.014	0.015	0.017	0.019	0.020	0.021
30	0.06	0.02							
40			0.042	0.037	0.027	0.018	0.011	0.007	0.005
60	0.05	0.05	0.030	0.048	0.045	0.035	0.024	0.016	0.009
80			0.040	0.065	0.070	0.053	0.035	0.022	0.014
90	0.14	0.11							
100			0.107	0.126	0.132	0.102	0.071	0.049	0.036
120	0.28	0.33	0.319	0.336	0.397	0.396	0.379	0.360	0.342
140			0.928	0.656	0.538	0.469	0.422	0.387	0.359
145	0.65	0.89	1.027	0.645	0.531	0.463	0.417	0.383	0.356

Table 26. Diffraction coefficient at points (ρ,ω)

$\theta = 145^{\circ}, \quad \delta = 3.0, \quad \zeta = 250^{\circ}$

ω ($^{\circ}$) \ ρ	1.0	2.0	3.0	4.0	5.0	6.0	7.0	8.0	9.0
0	0.13	0.15	0.172	0.160	0.155	0.150	0.145	0.140	0.135
20			0.118	0.083	0.053	0.032	0.017	0.010	0.012
30	0.24	0.16							
40			0.128	0.169	0.169	0.152	0.131	0.111	0.093
60	0.32	0.36	0.231	0.208	0.277	0.295	0.280	0.252	0.220
80			0.699	0.533	0.626	0.771	0.848	0.874	0.873
90	0.70	0.85							
100			1.183	1.285	0.963	0.683	0.492	0.365	0.279
120	1.25	1.03	0.945	0.550	0.393	0.311	0.262	0.228	0.204
140			0.483	0.133	0.077	0.054	0.042	0.035	0.030
145	1.04	1.25	0.599	0.116	0.065	0.046	0.036	0.030	0.025

Table 27. Diffraction coefficients at points (ρ, ω)

$\theta = 145^{\circ}, \quad \delta = 3.0, \quad \zeta = 270^{\circ}$

ω ($^{\circ}$) \ ρ	1.0	2.0	3.0	4.0	5.0	6.0	7.0	8.0	9.0
0	0.23	0.25	0.267	0.251	0.242	0.232	0.224	0.216	0.208
20			0.191	0.132	0.085	0.054	0.036	0.031	0.035
30	0.38	0.26							
40			0.257	0.325	0.329	0.303	0.266	0.229	0.194
60	0.57	0.69	0.599	0.528	0.670	0.795	0.863	0.889	0.891
80			1.273	1.272	0.986	0.712	0.511	0.371	0.275
90	0.96	1.03							
100			0.926	0.621	0.430	0.299	0.212	0.155	0.116
120	1.03	1.06	0.670	0.280	0.223	0.184	0.157	0.138	0.124
140			0.336	0.092	0.052	0.036	0.027	0.022	0.019
145	0.82	0.82	0.513	0.088	0.049	0.034	0.027	0.022	0.019

Table 28. Diffraction coefficient at points (ρ,ω)

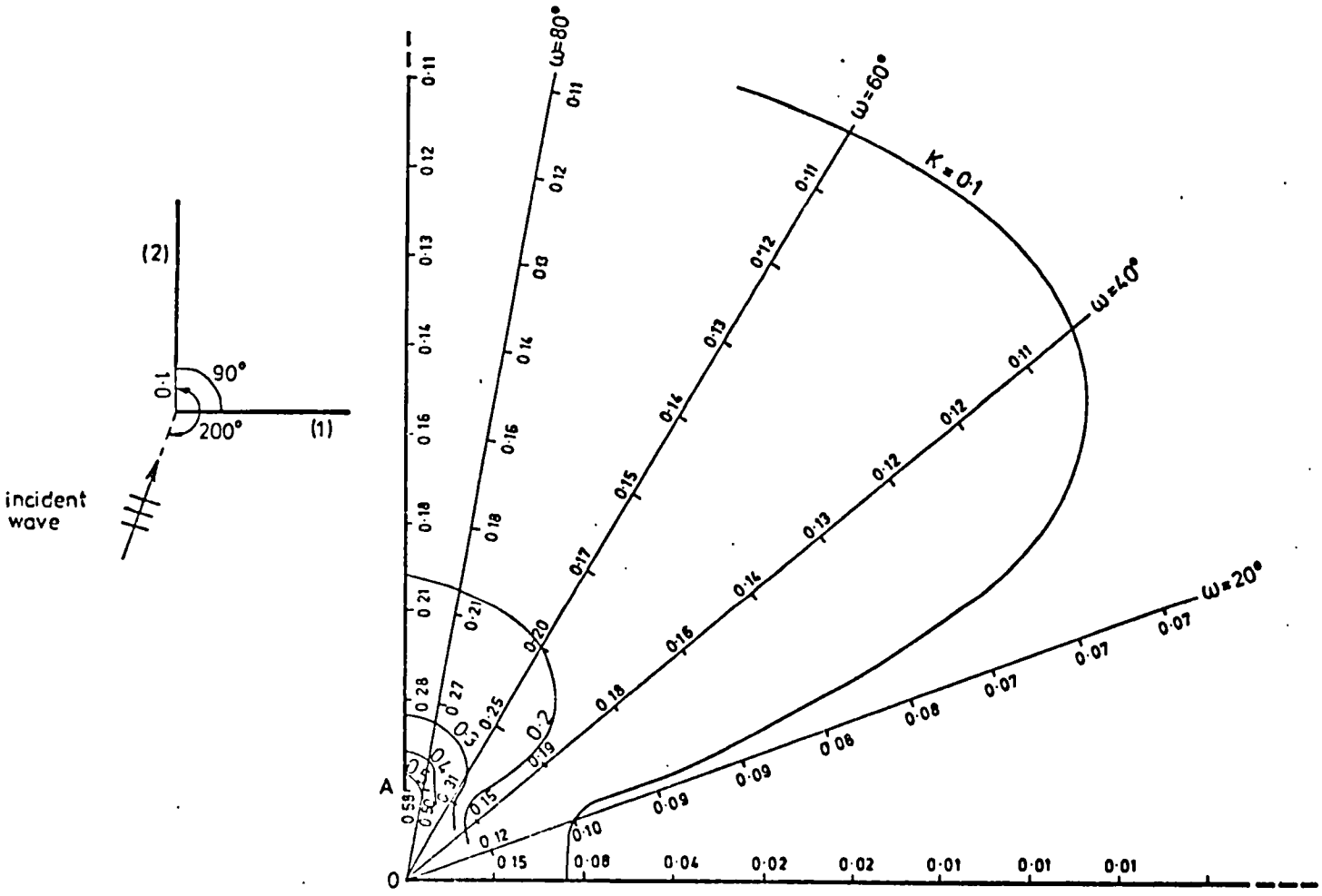

Fig. 38. Curves of equal diffraction coefficient K

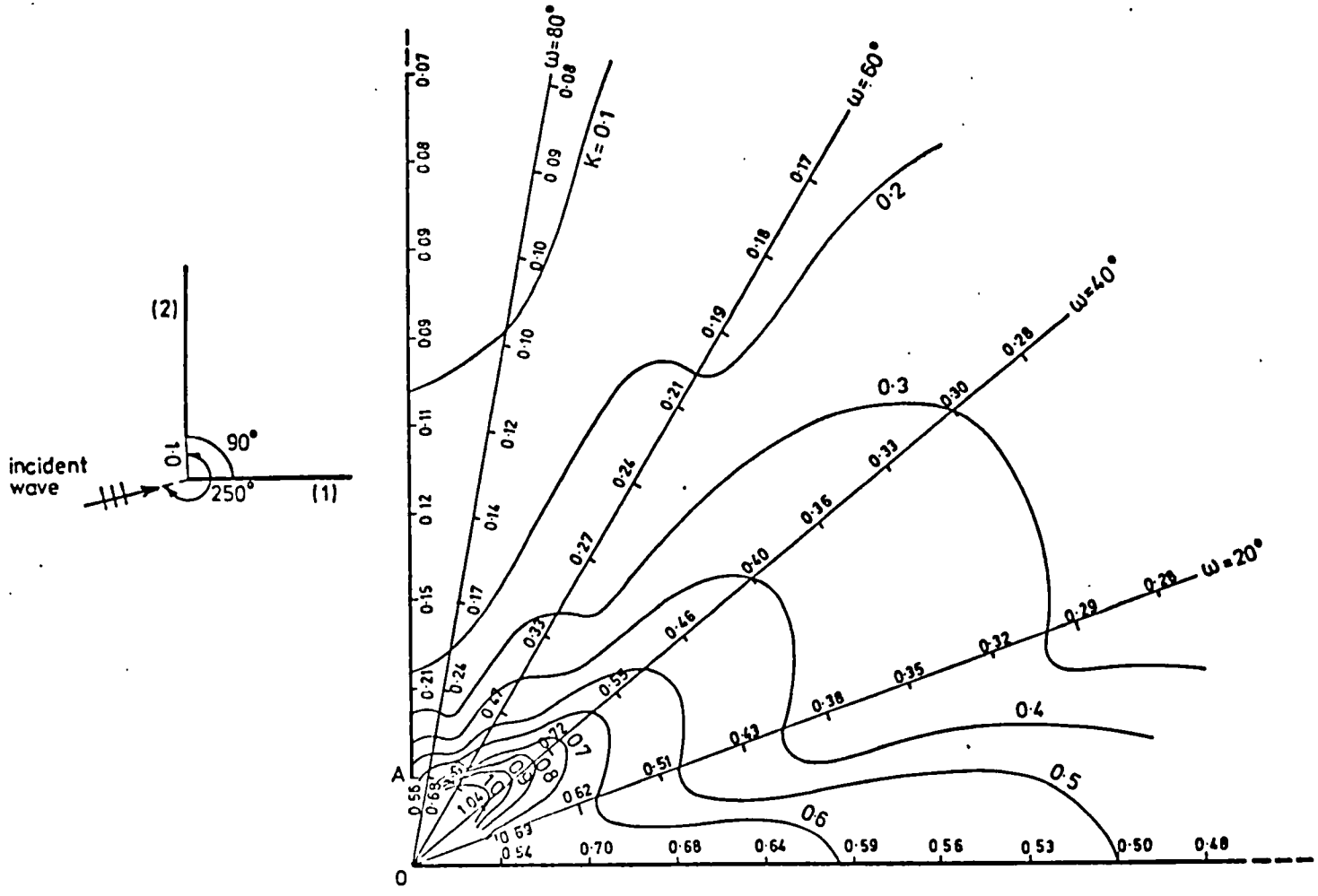

Fig.39. Curves of equal diffraction coefficient K

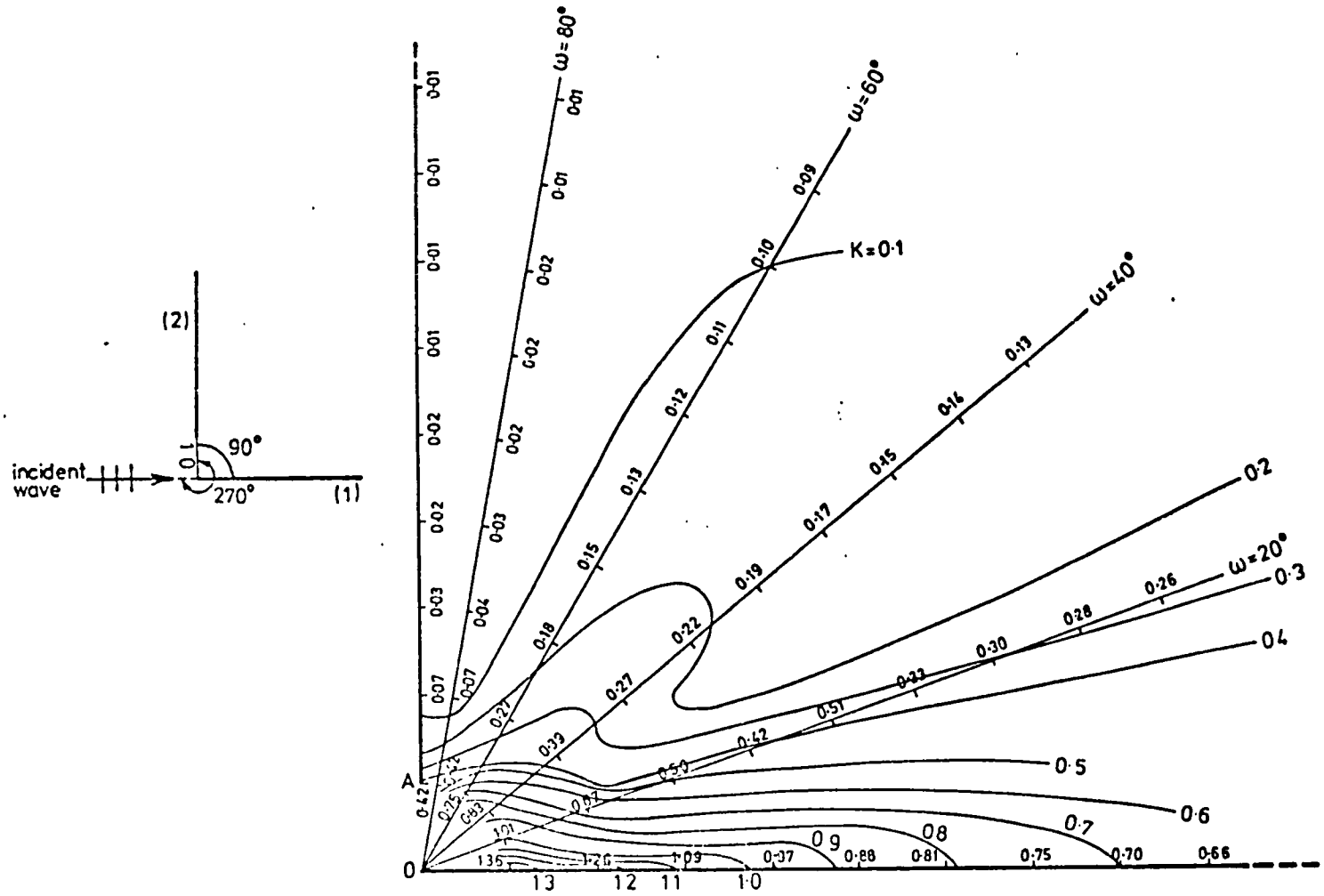

Fig. 40. Curves of equal diffraction coefficient K

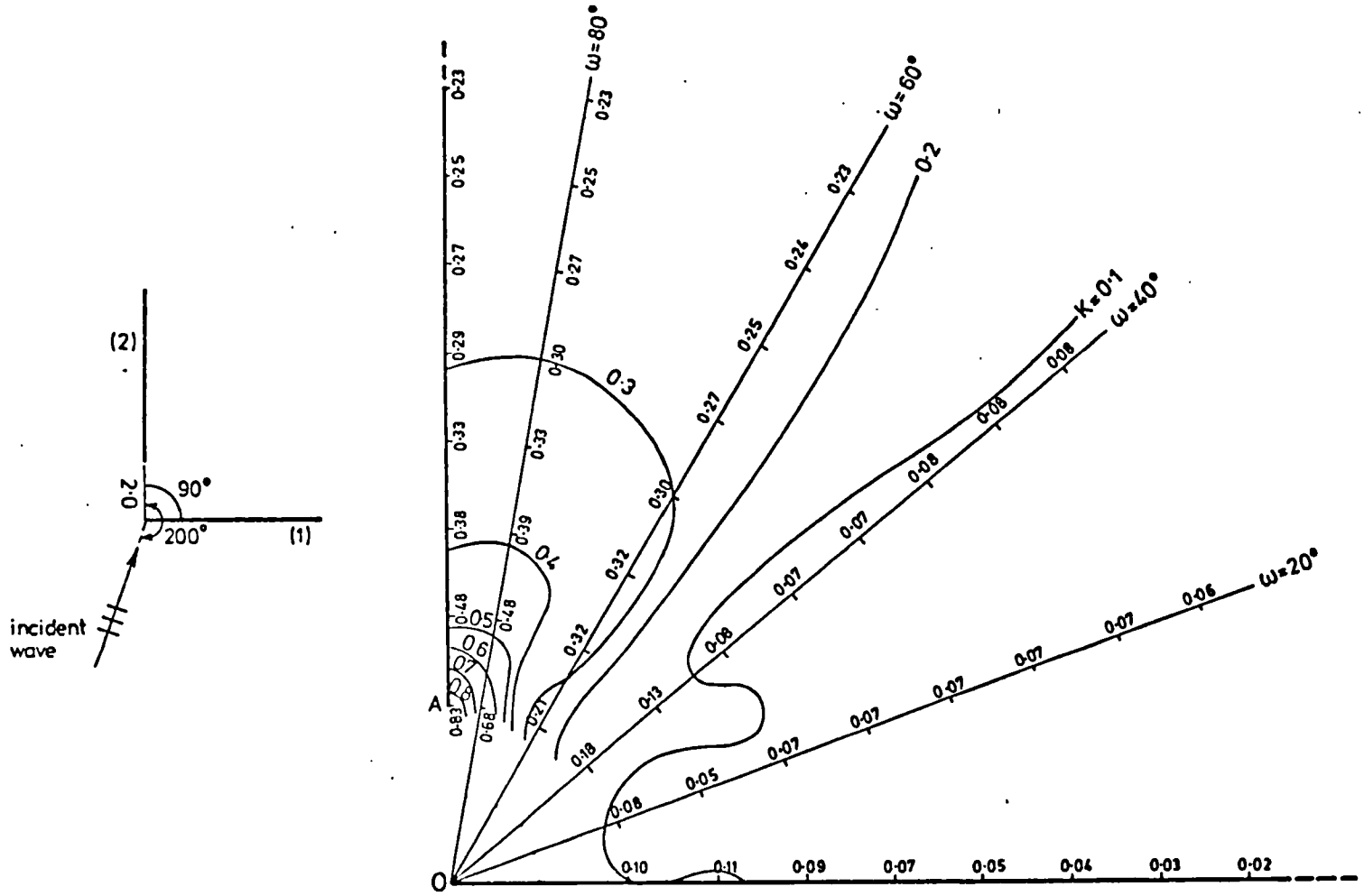

Fig. 41. Curves of equal diffraction coefficient K

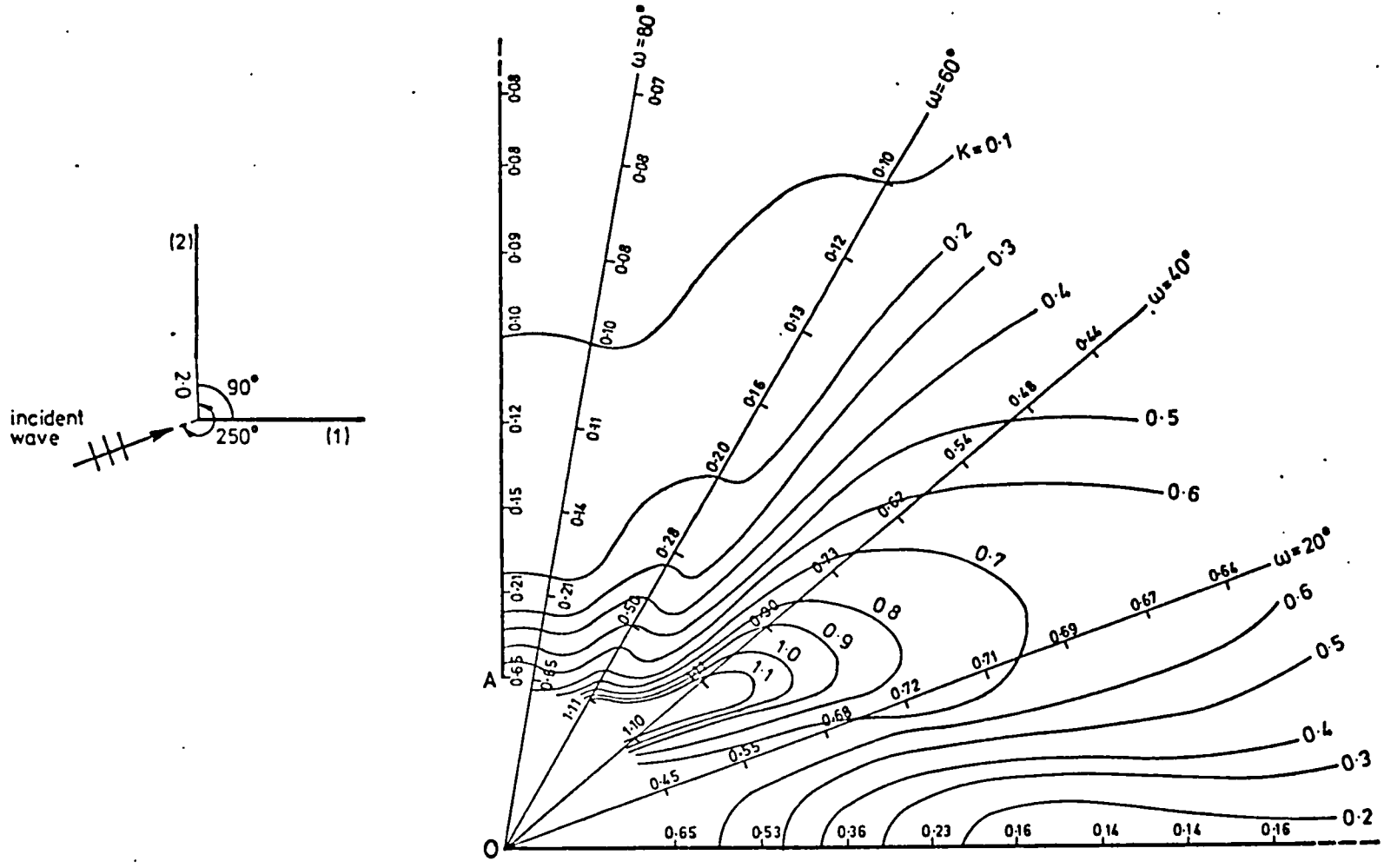

Fig. 42. Curves of equal diffraction coefficient K

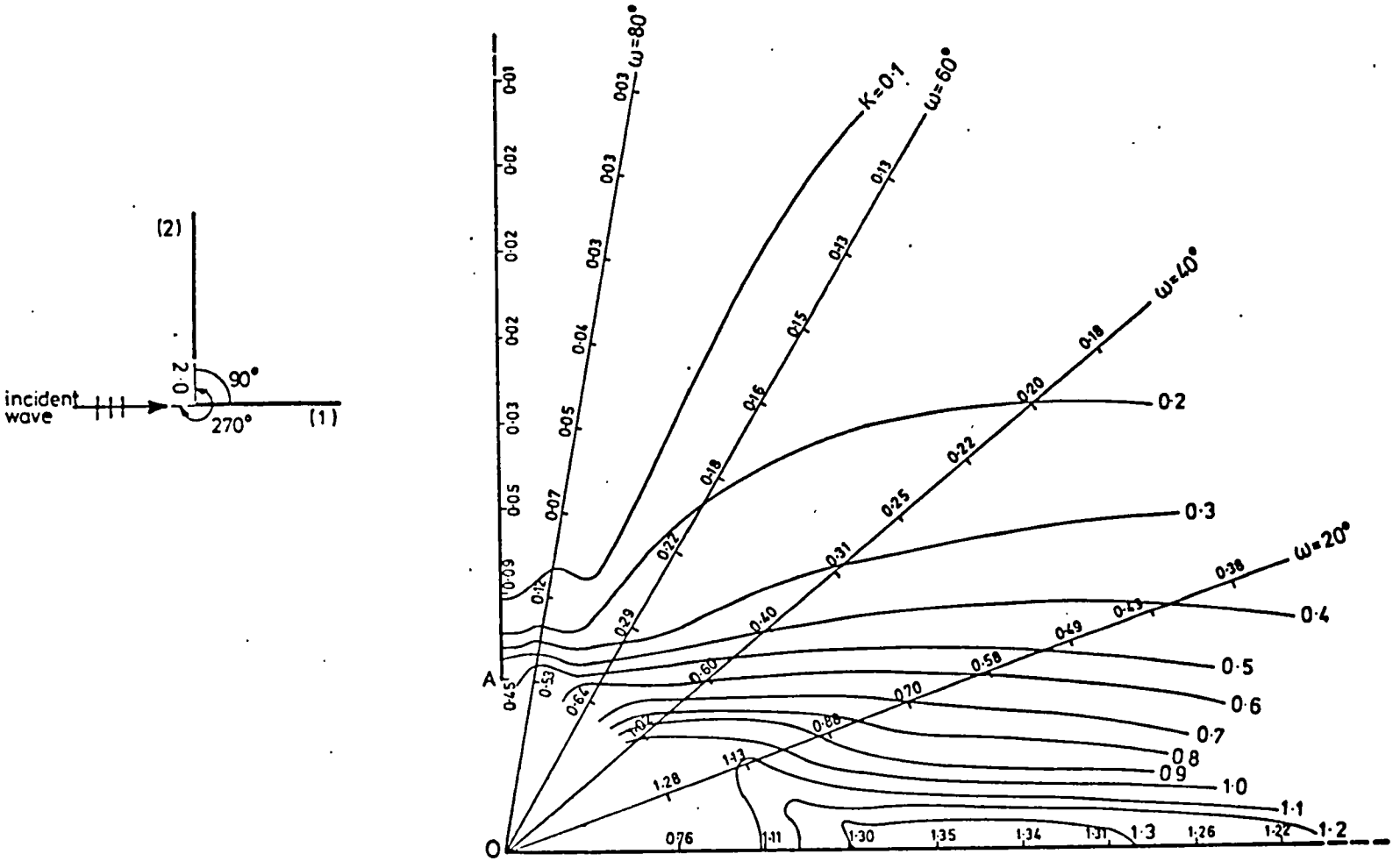

Fig.43. Curves of equal diffraction coefficient K

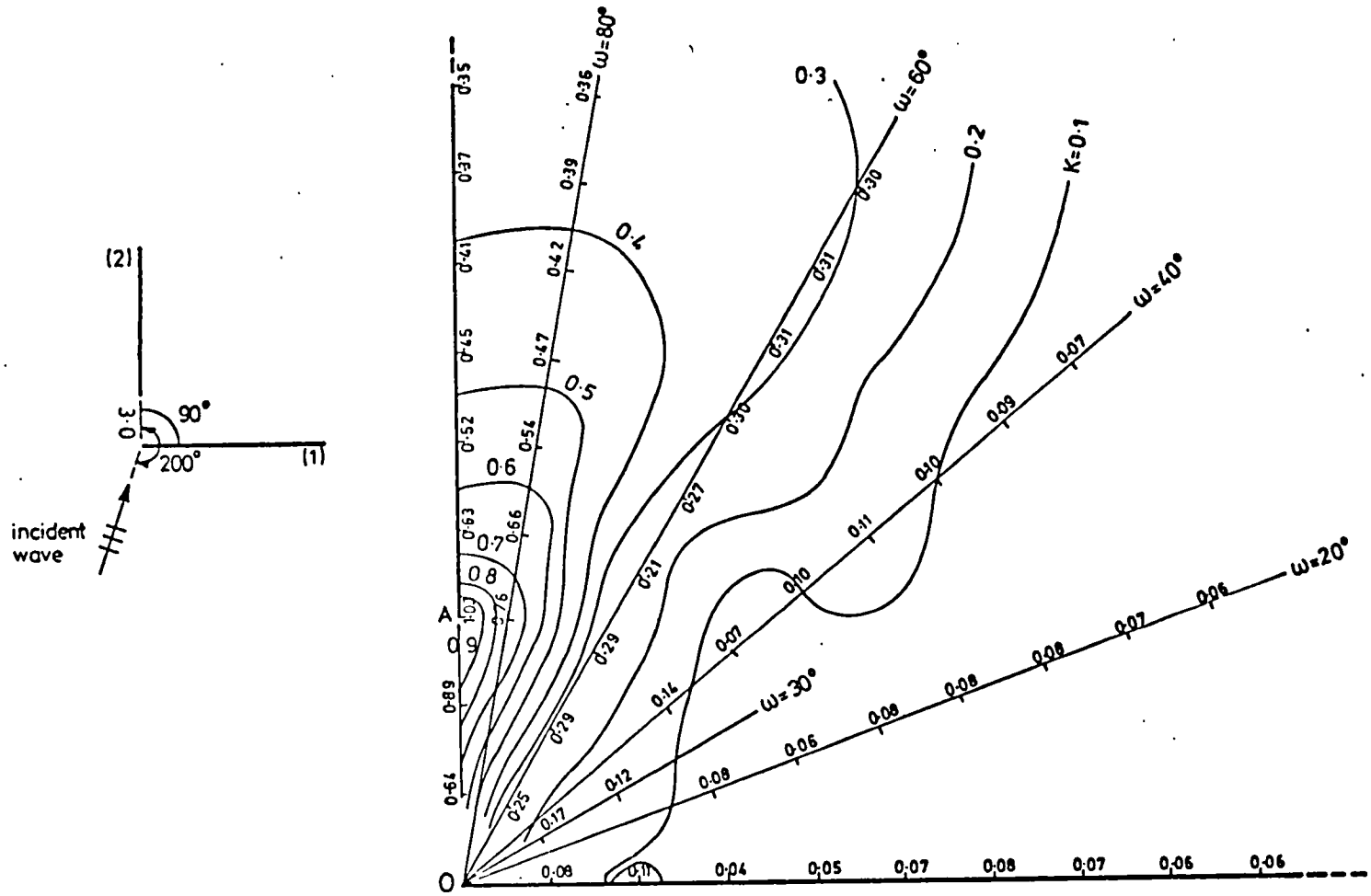

Fig. 44. Curves of equal diffraction coefficient K

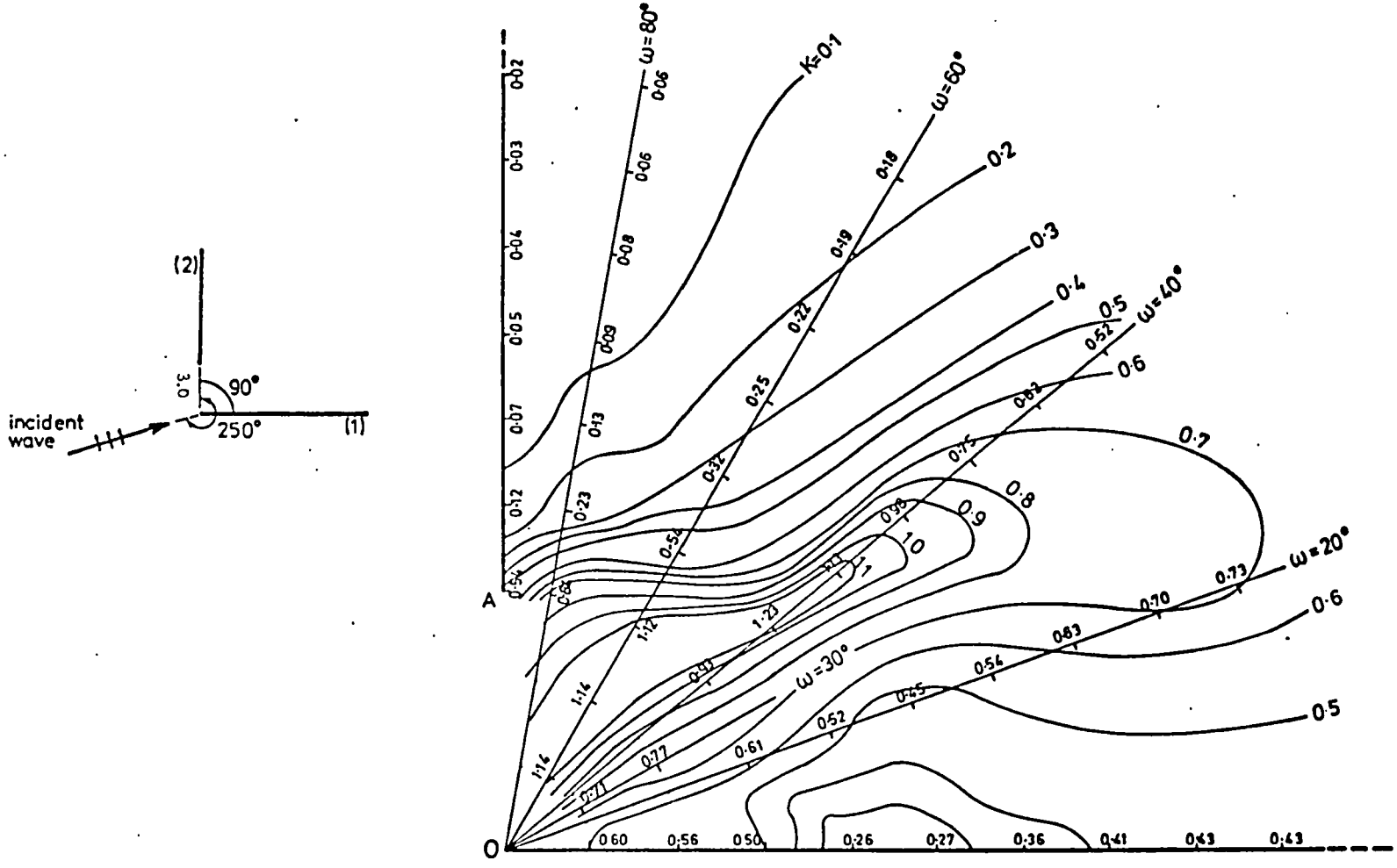

Fig. 45. Curves of equal diffraction coefficient K

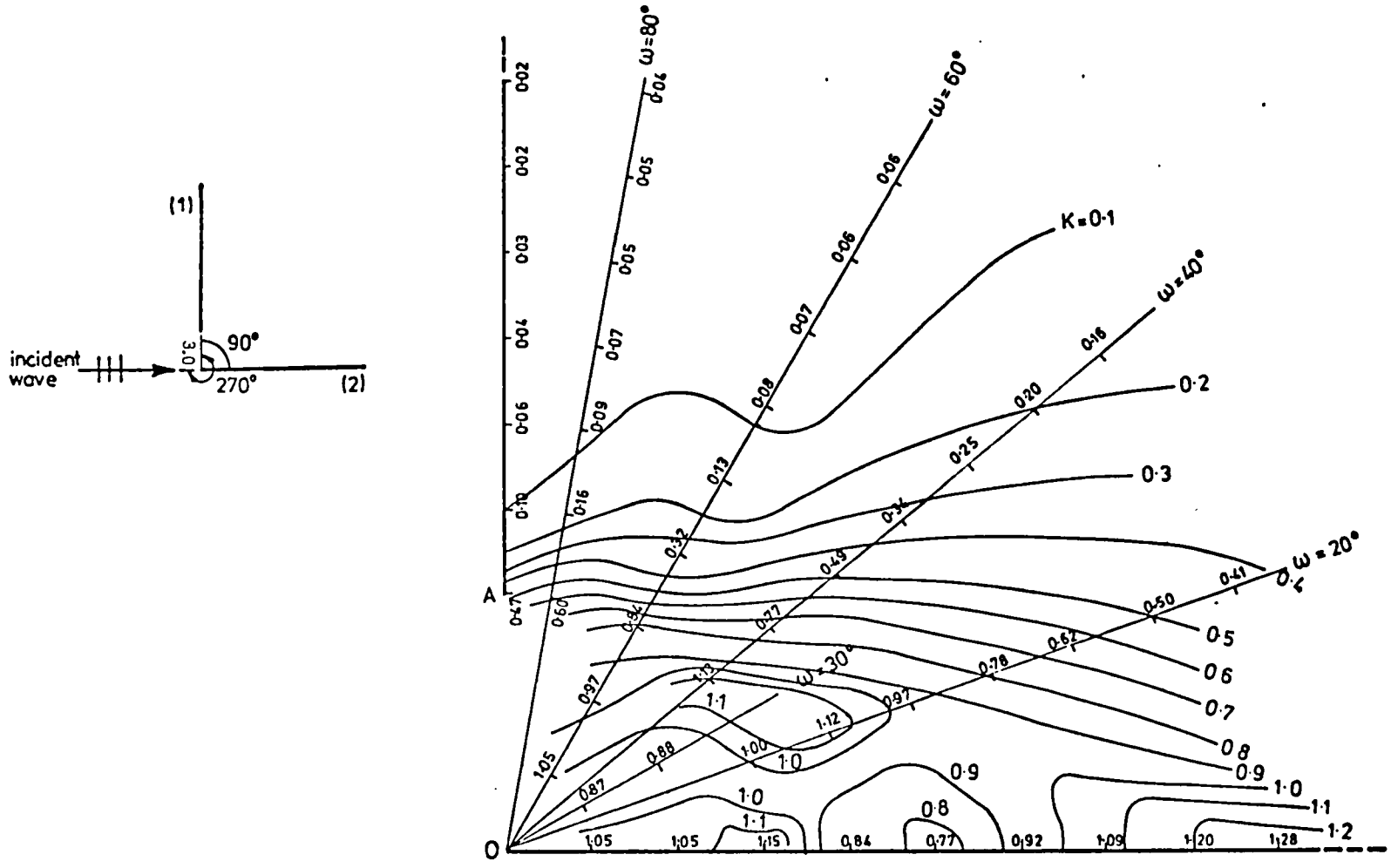

Fig. 46. Curves of equal diffraction coefficient K

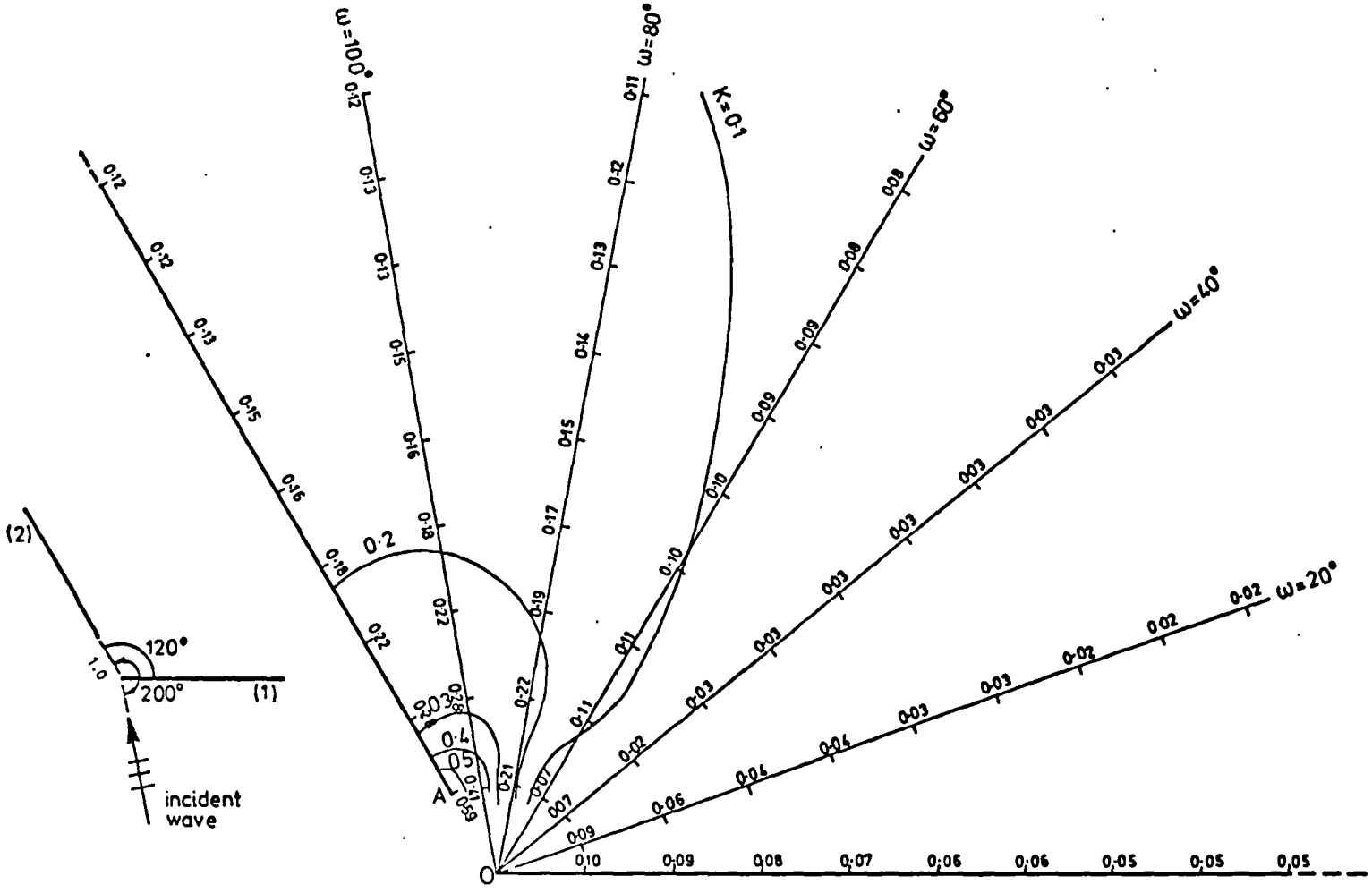

Fig. 47. Curves of equal diffraction coefficient K

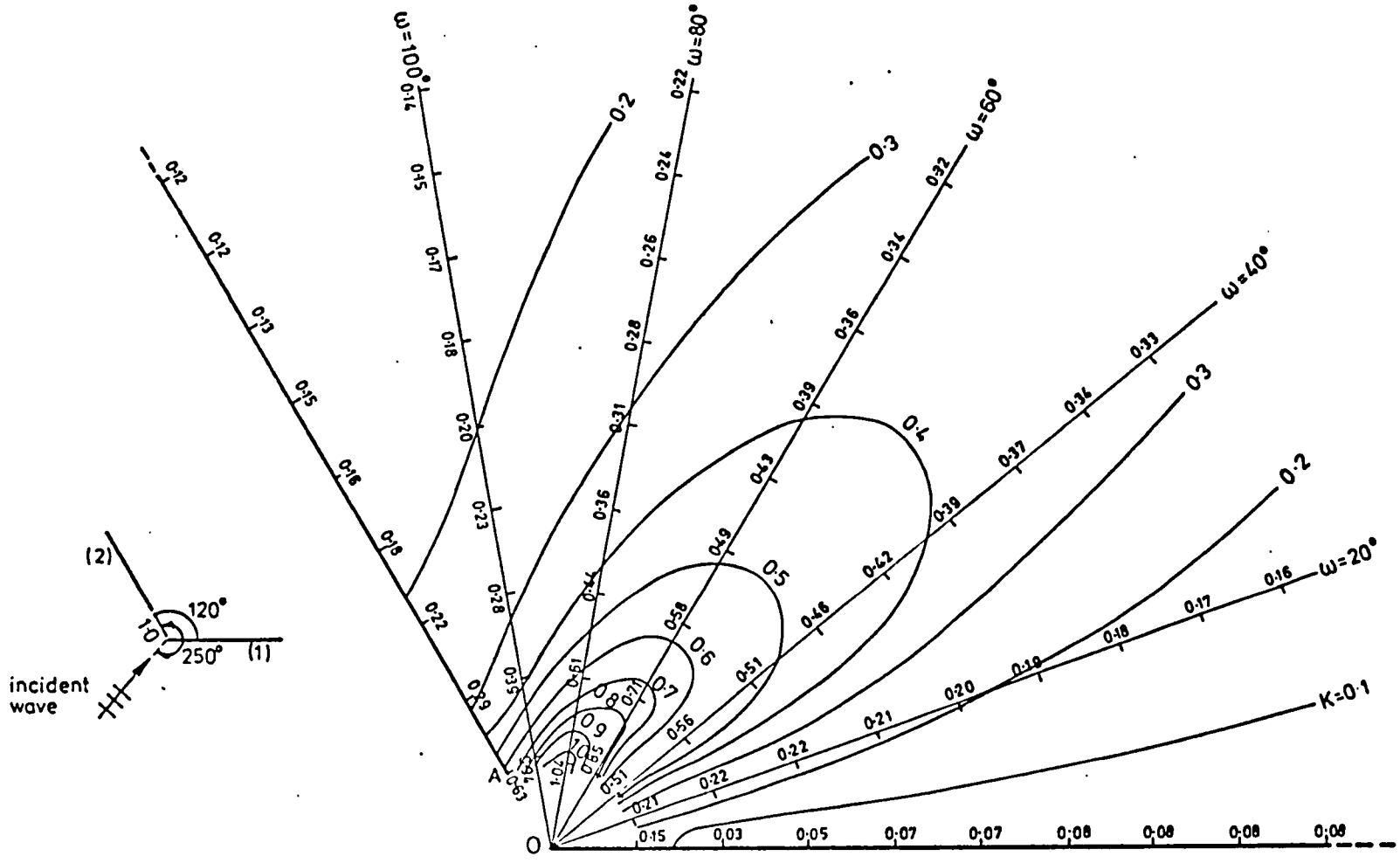

Fig. 48. Curves of equal diffraction coefficient K

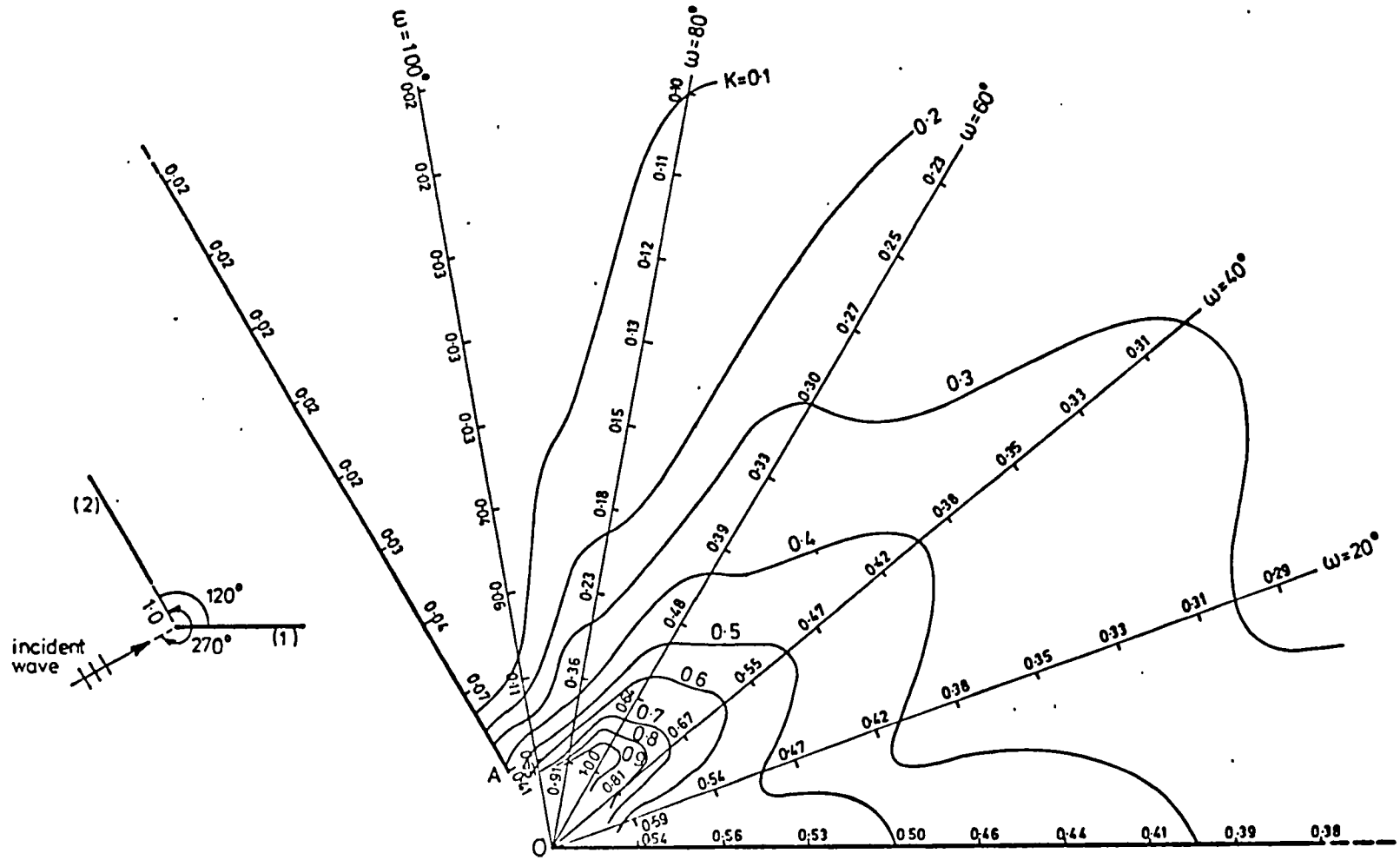

Fig. 49. Curves of equal diffraction coefficient K

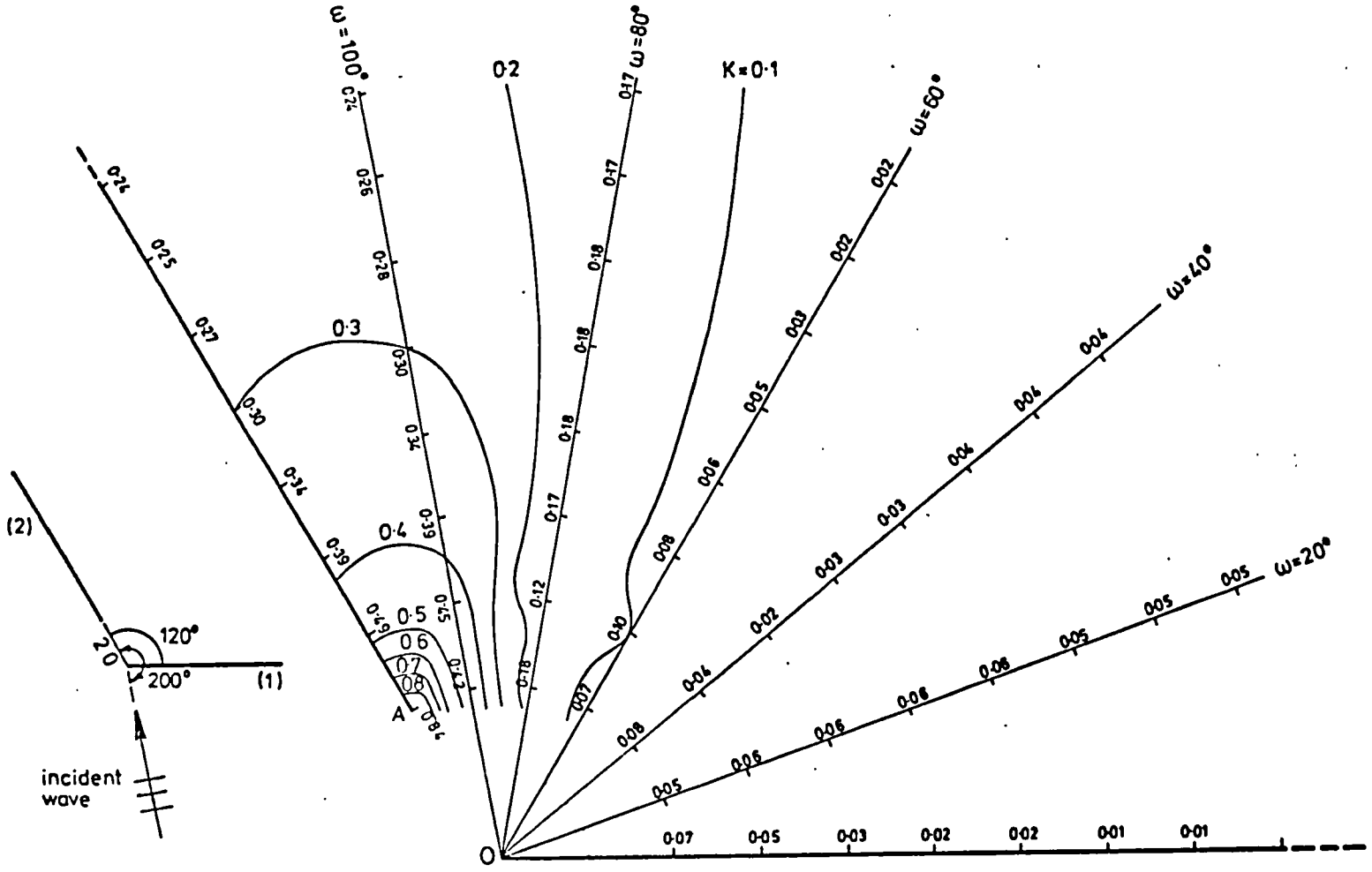

Fig. 50. Curves of equal diffraction coefficient K

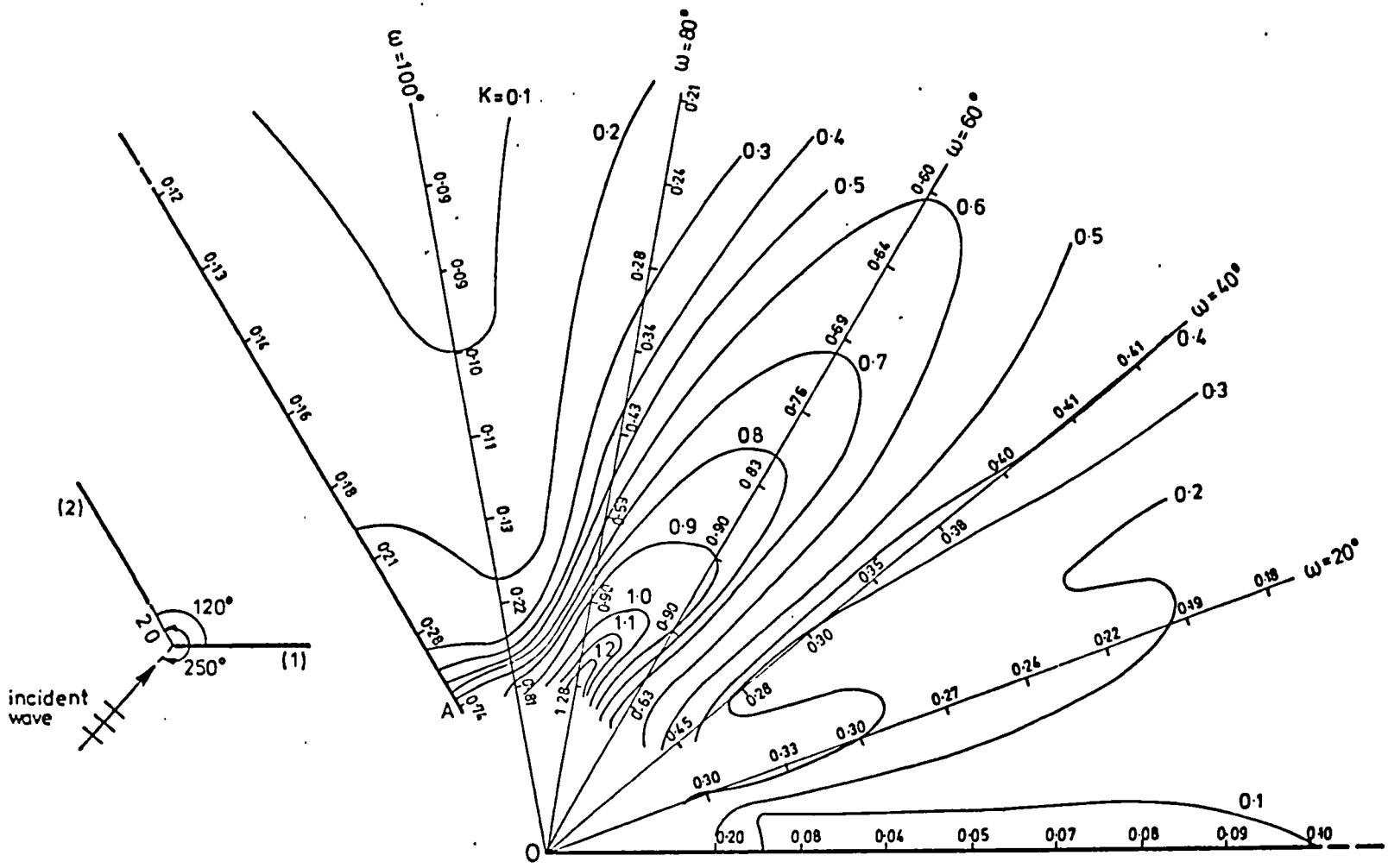

Fig. 51. Curves of equal diffraction coefficient K

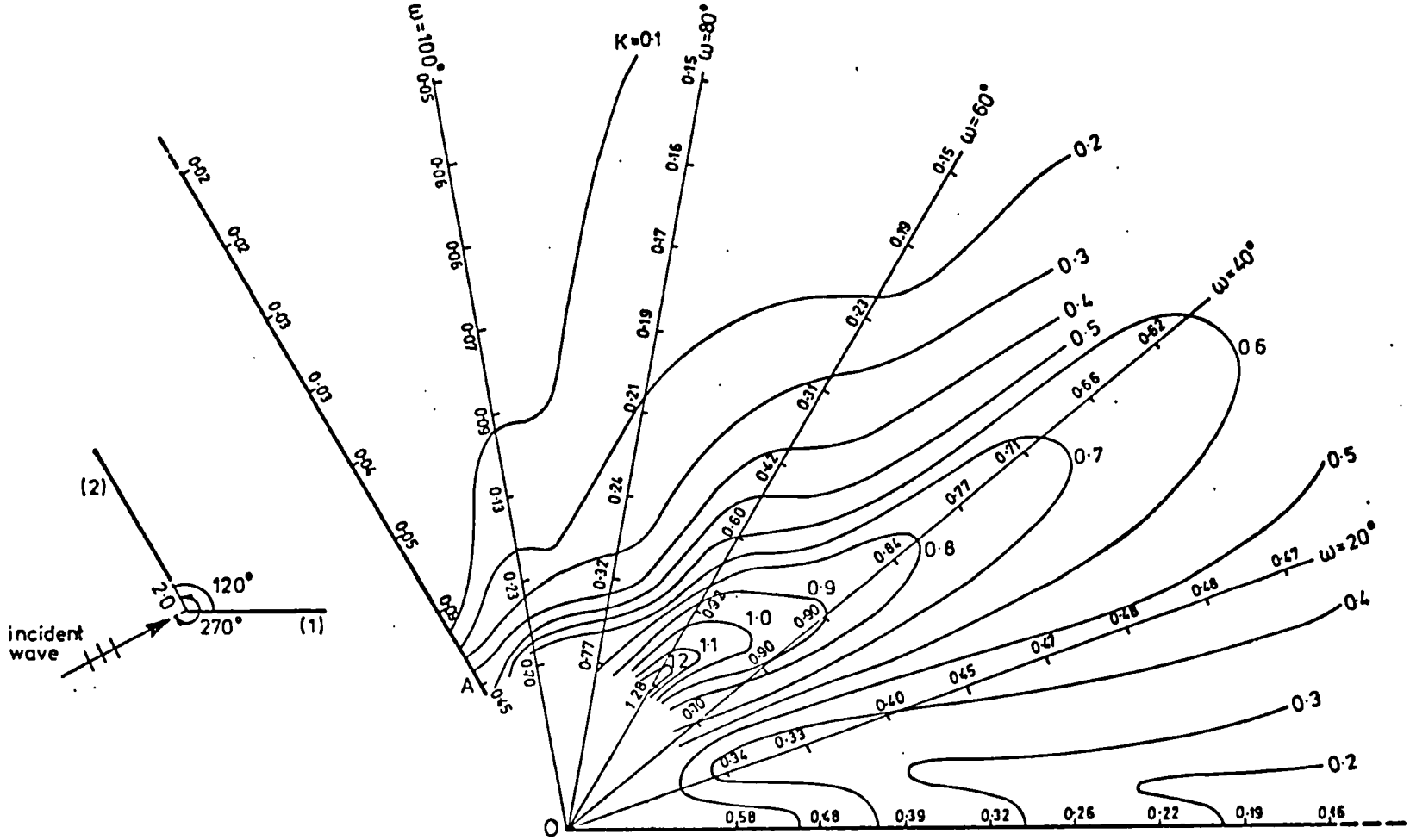

Fig. 52. Curves of equal diffraction coefficient K

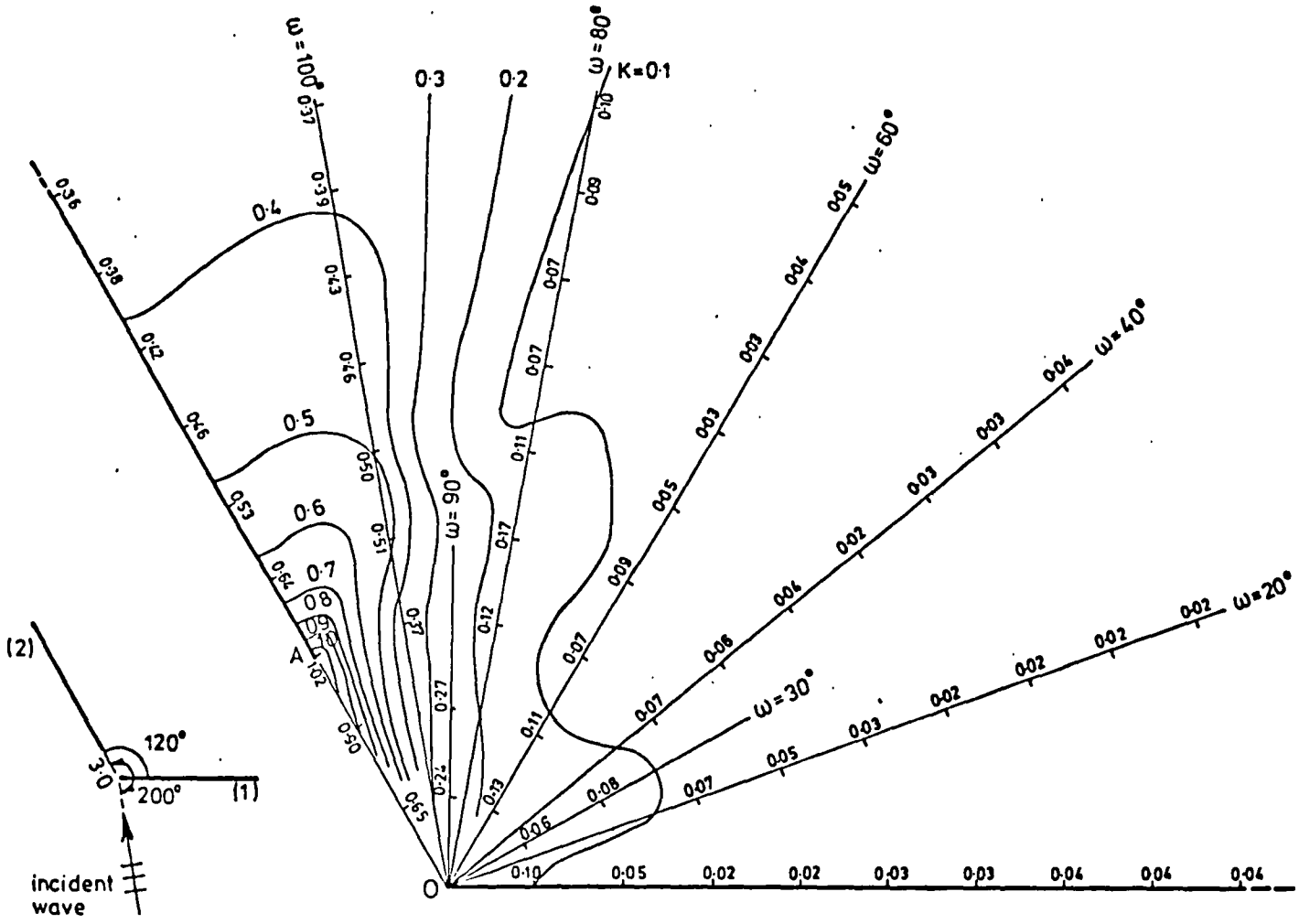

Fig. 53. Curves of equal diffraction coefficient K

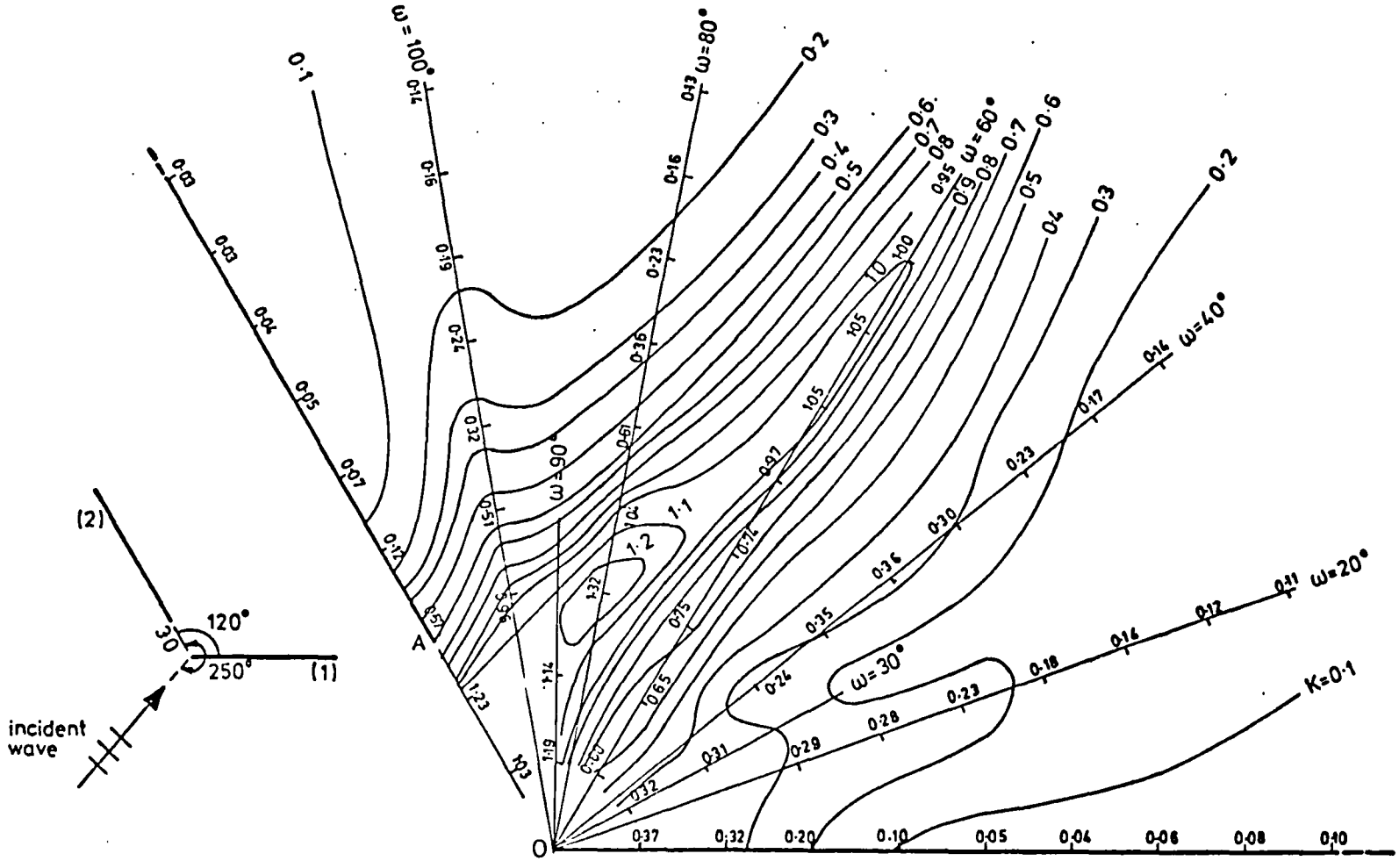

Fig. 54. Curves of equal diffraction coefficient K

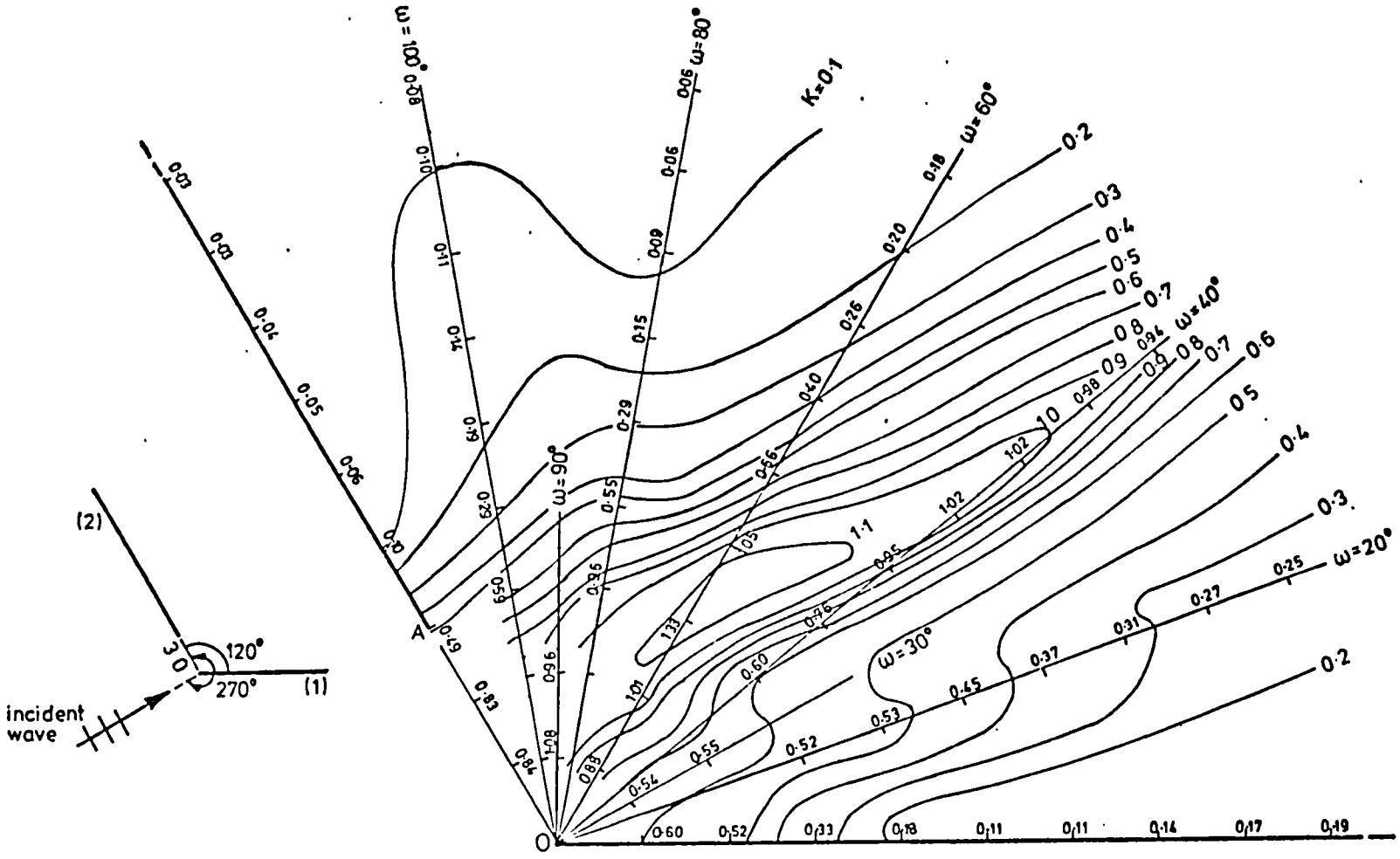

Fig.55. Curves of equal diffraction coefficient K

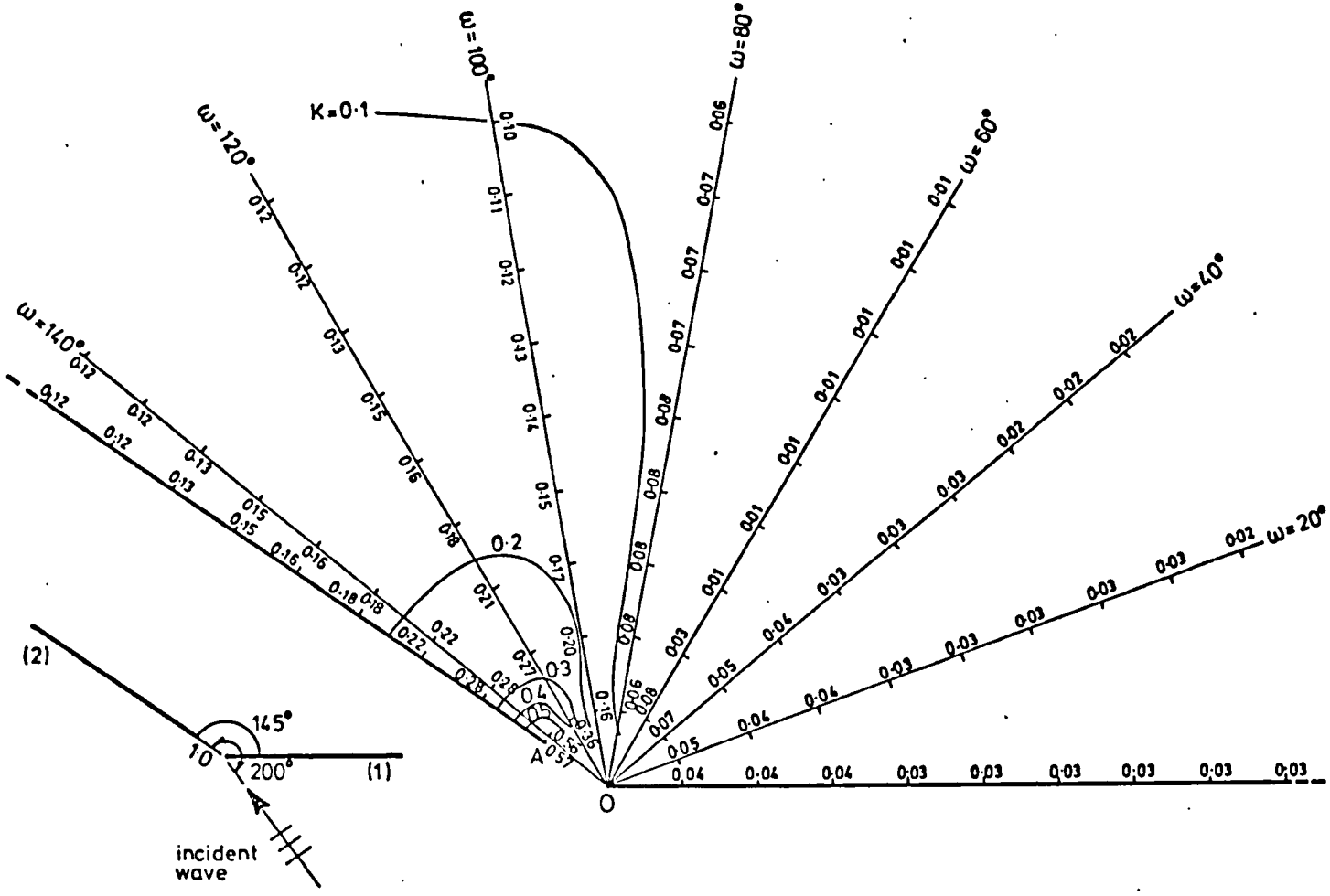

Fig. 56. Curves of equal diffraction coefficient K

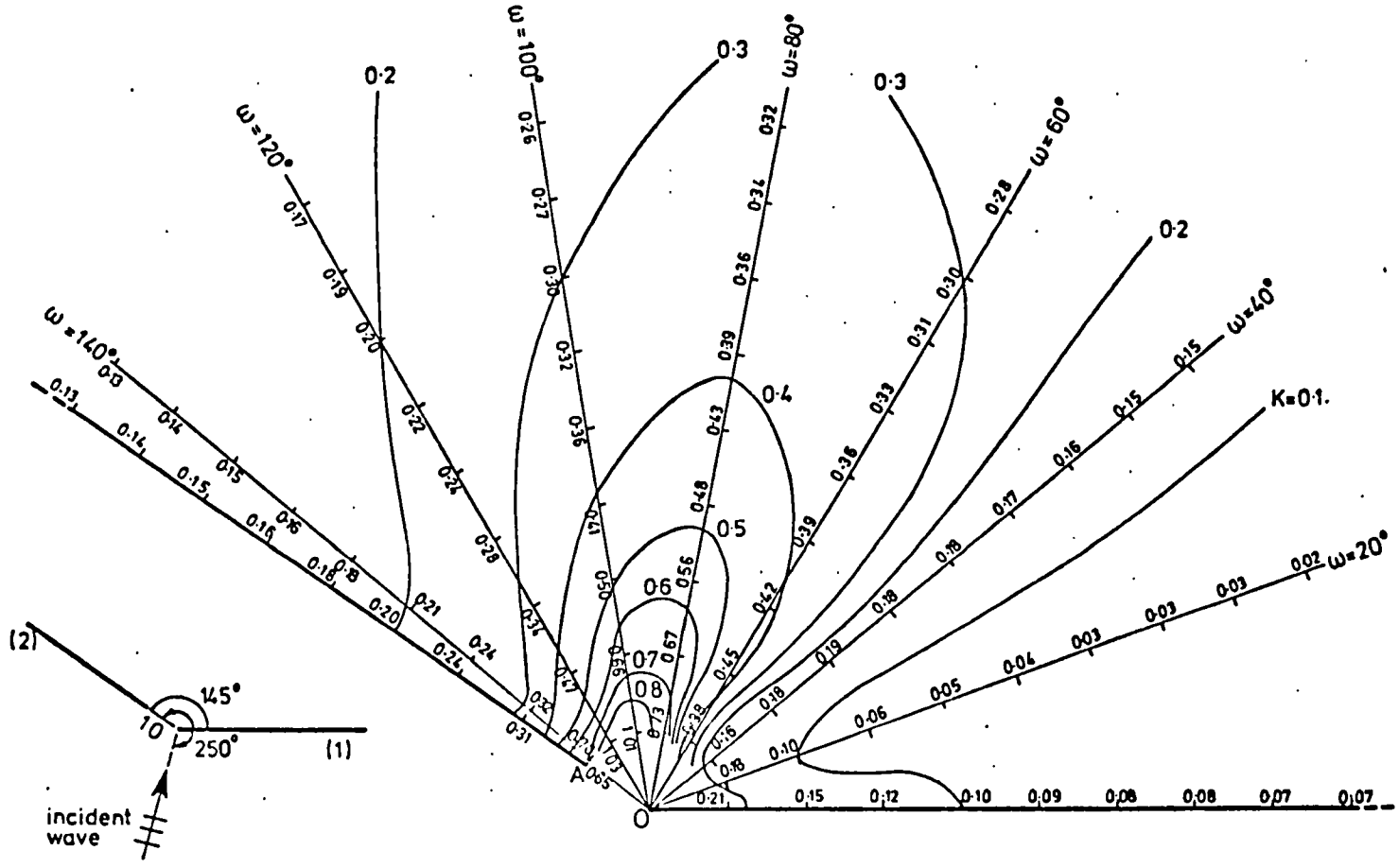

Fig. 57. Curves of equal diffraction coefficient K

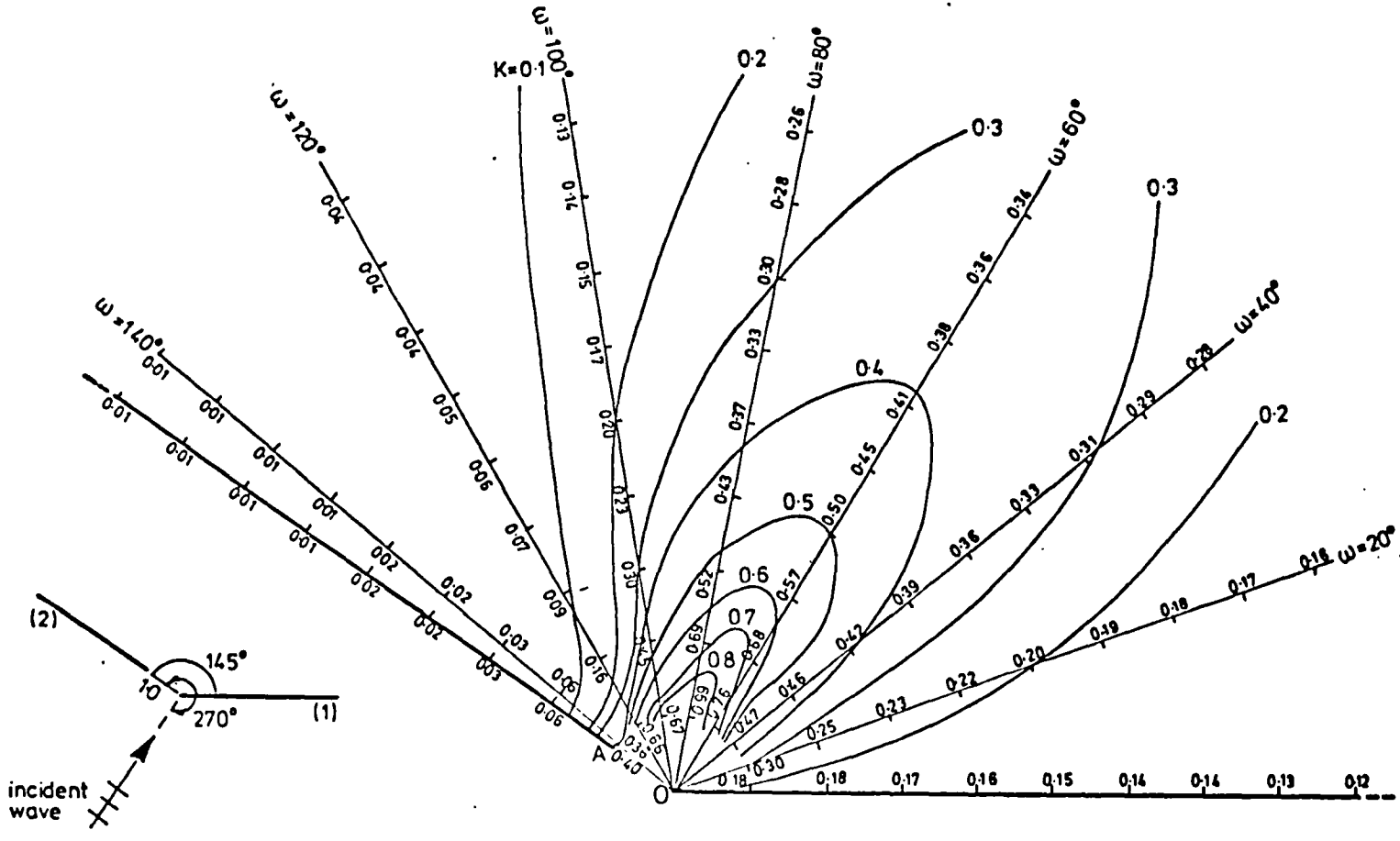

Fig. 58. Curves of equal diffraction coefficient K

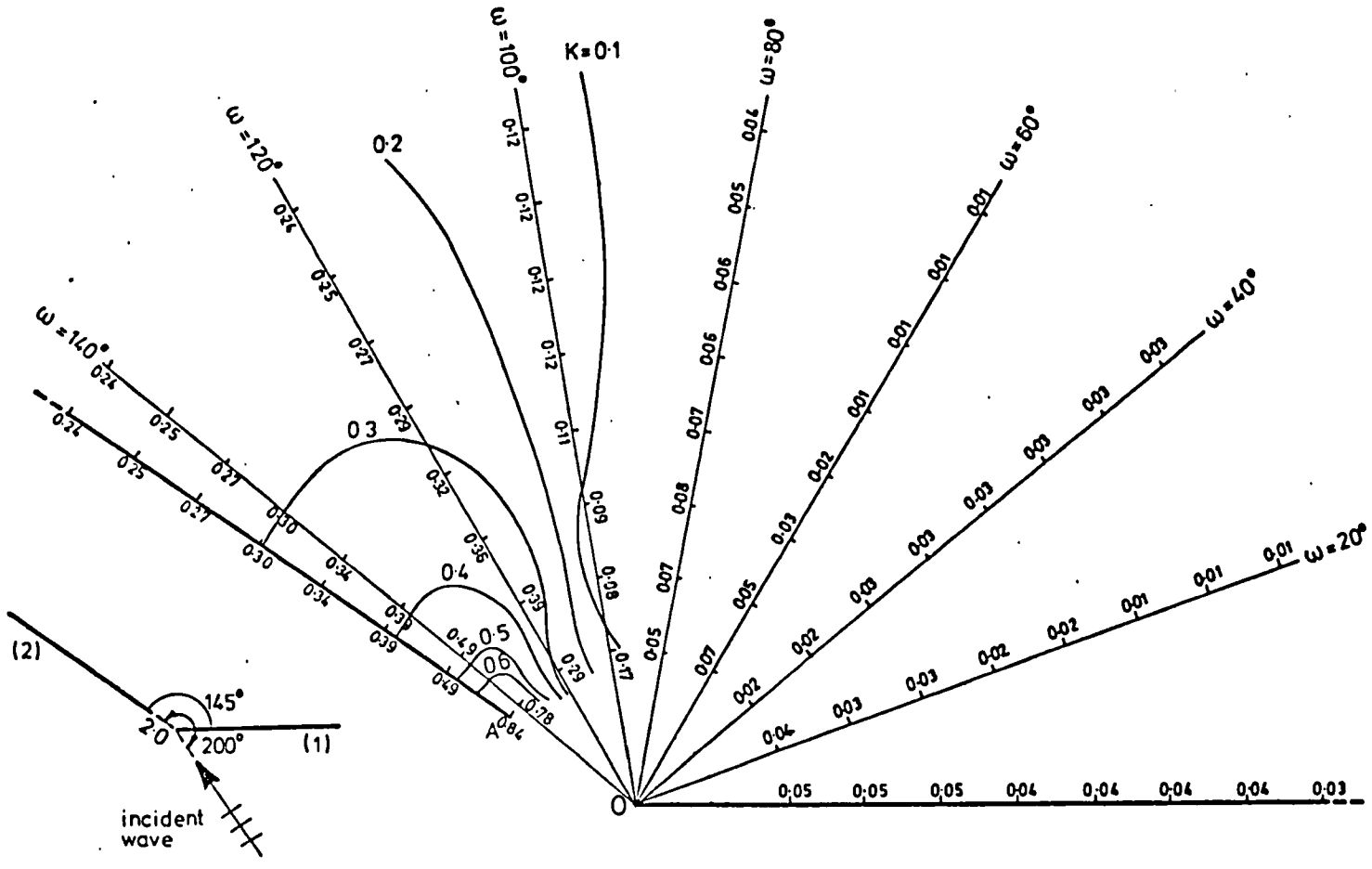

Fig. 59. Curves of equal diffraction coefficient K

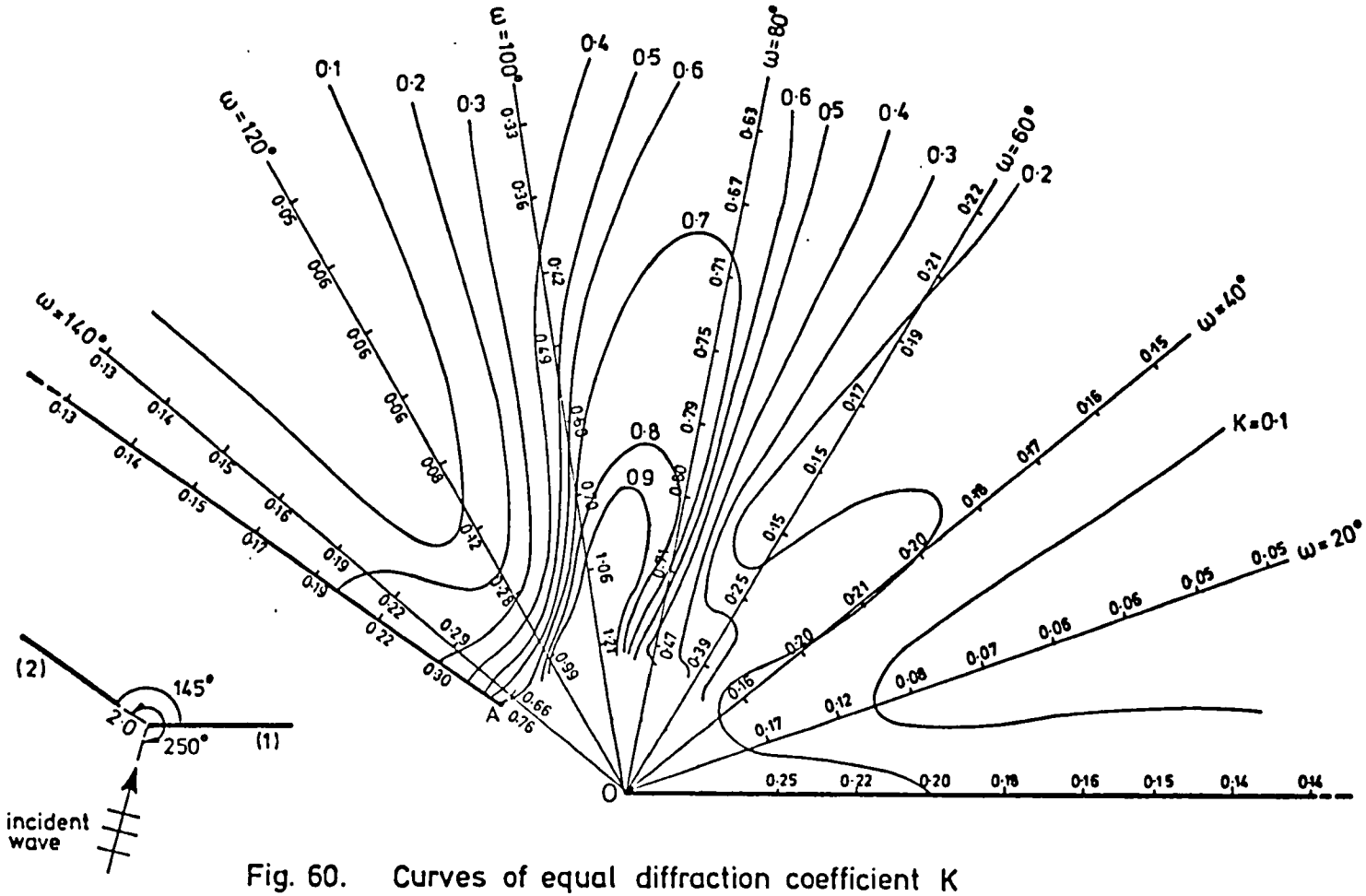

Fig. 60. Curves of equal diffraction coefficient K

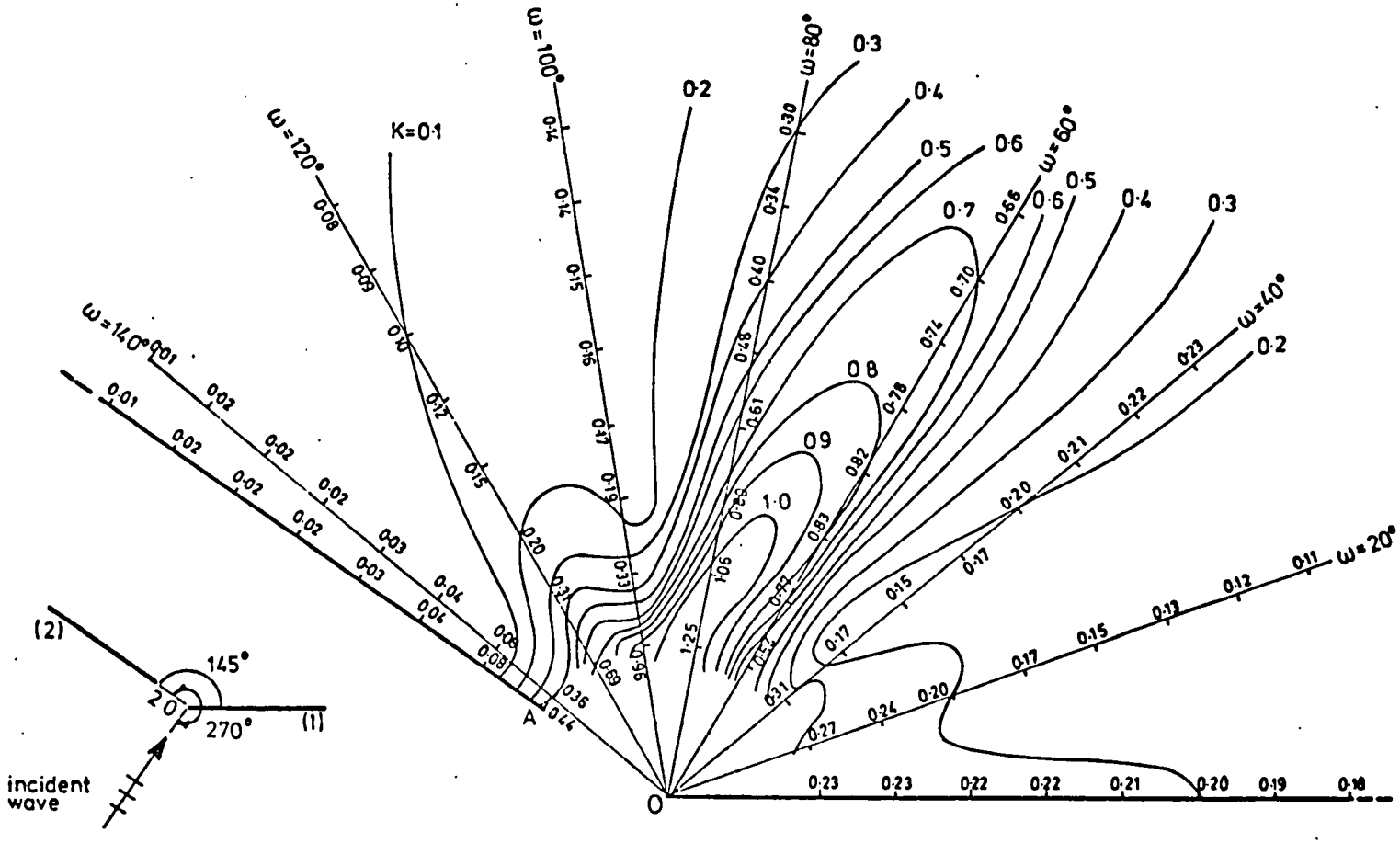

Fig. 61. Curves of equal diffraction coefficient K

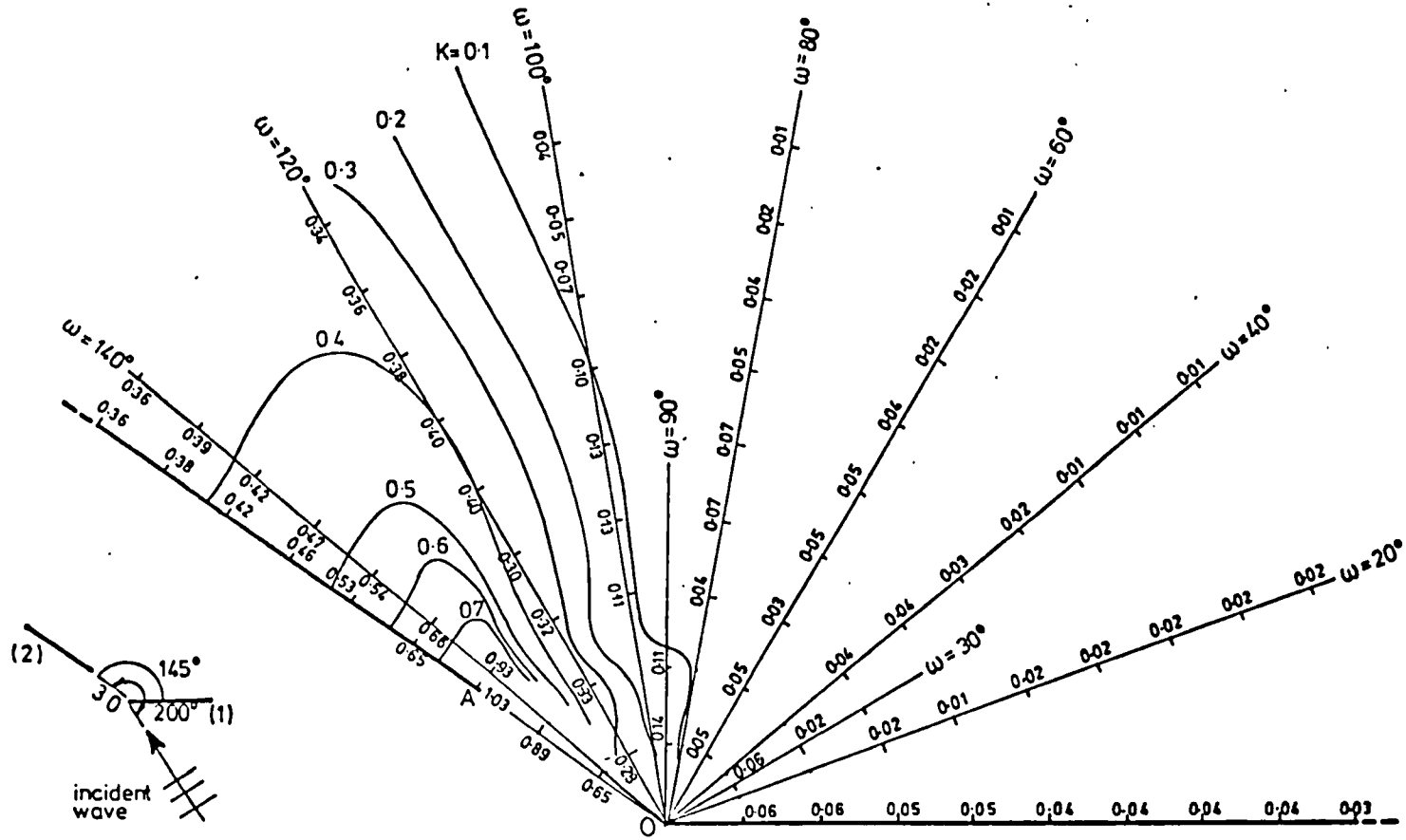

Fig. 62. Curves of equal diffraction coefficient K

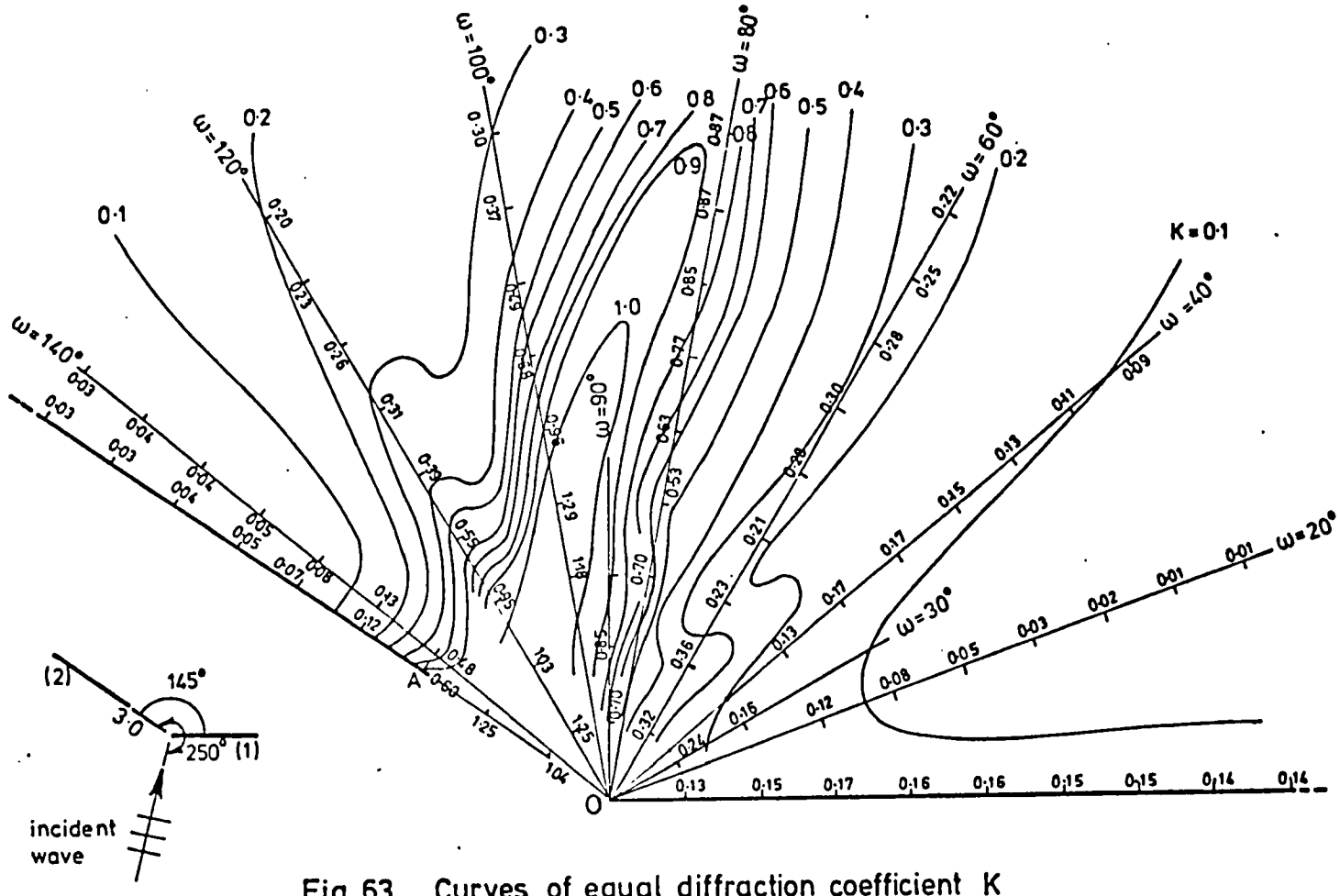

Fig. 63. Curves of equal diffraction coefficient K

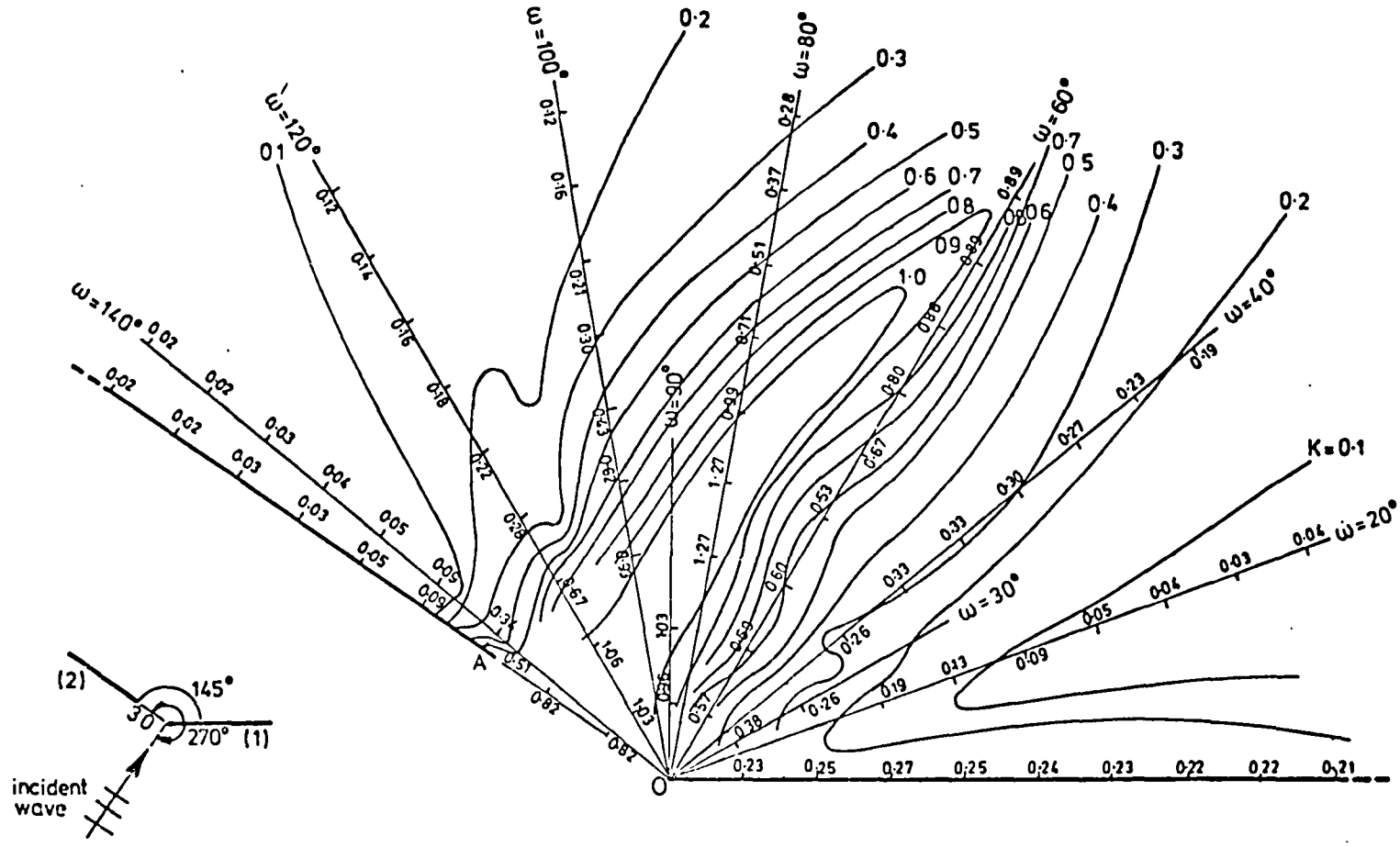

Fig. 64. Curves of equal diffraction coefficient K

E2 COMPARISONS

E2.1 With Previous Work

Results that could be compared with ours are known only for the special case $\theta = 180^{\circ}$ where the two breakwaters lie on the same plane. At the short wavelength limit a comparison can be done with Penney and Price's method (subdivision B3.1.1) that assumes independent functioning of the two branches (1) and (2). At the large wavelength limit qualitative checks and observations can be made with the help of the asymptotic expansions theory (section C5) or Lamb's method (subdivision B3.1.1).

The general outlook of the graphs especially those of wide angle θ reveals shapes similar to Lacombe's 'diffraction leaves' [4]; for smaller angles θ however the picture becomes confused although traces of the 'leaves' can be detected in the closed elongated contours.

In fig. 65 our theory is compared with results based on Penney and Price's method as presented in Figure 2-42 of the Shore Protection Manual [66]. The major deviations between the two theories are only presented because unavoidable tracing errors put limitations on the presentation of very small deviations; we can note for example that the curve $K = 0.4$ of the graph against which our theory is compared is plotted obviously non-symmetric although the theory it is based on predicts symmetry. The case covered is of $\theta = 180^{\circ}$, $\delta = 2.0$, $\zeta = 270^{\circ}$ and very good agreement is found. The deviations noted are in accordance with the corresponding deviations of the exact solution

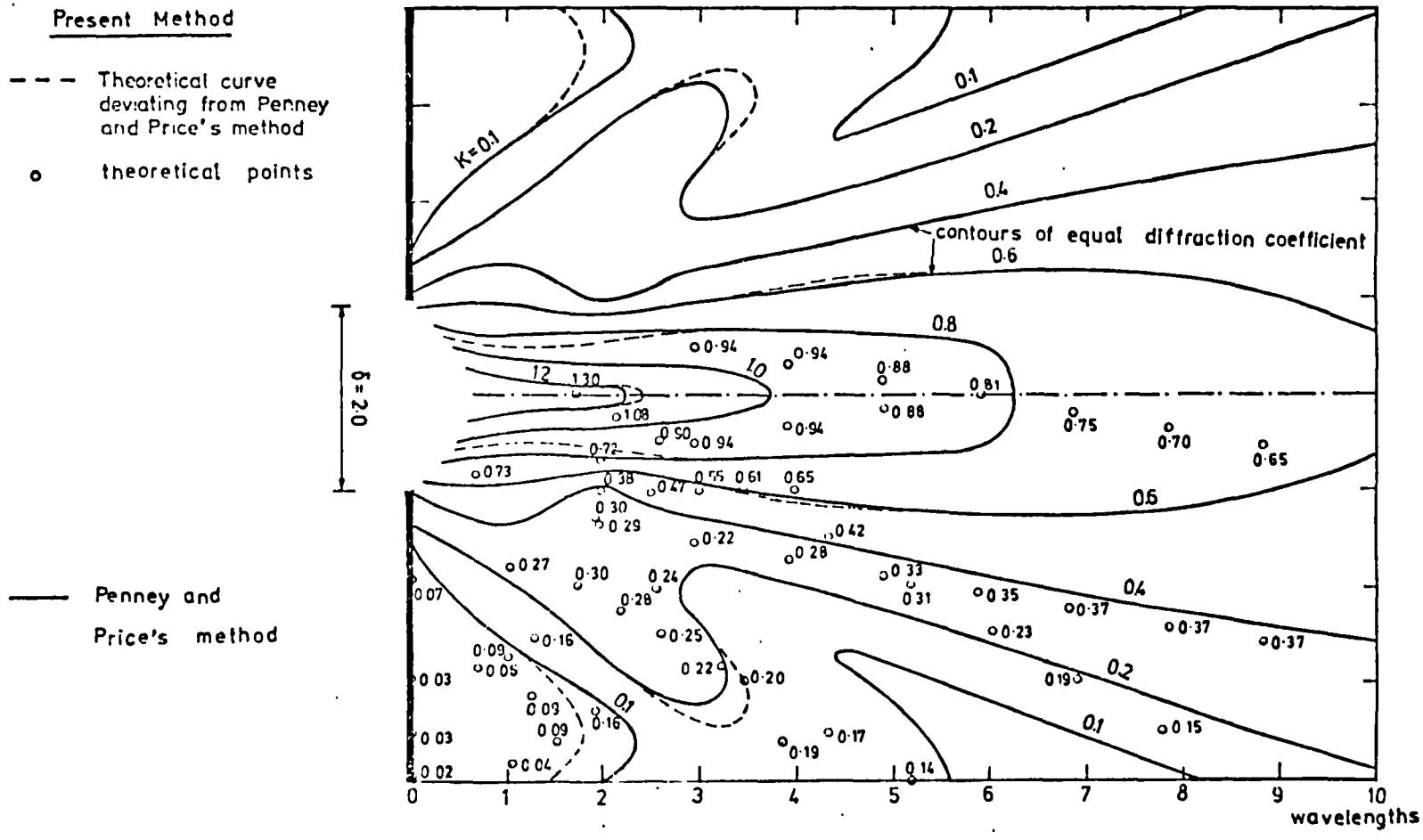

Fig. 65 . Comparison with results of Penney and Price's method
(Shore Protection Manual [66])

of Morse and Rubinstein [2] from the same Penney and Price's theory which is approximate but is acceptable for gap widths larger than about two wavelengths. A qualitative comparison of two diagrams obtained by the above theories, exact and approximate, can be found in the discussion by M.E. Stelzriede in Johnson's paper ([67], fig. 19).

A means of cross-checking for the same case of co-planar breakwaters and normal incidence is provided by our fig. 40 where the case $\theta = 90^{\circ}$, $\delta = 1.0$, $\zeta = 270^{\circ}$ is presented. This can be interpreted as being half the picture of the case $\theta = 180^{\circ}$, $\delta = 2.0$, $\zeta = 270^{\circ}$, because screen (1) of the former case occupies the axis of symmetry of the latter thus not changing the wave pattern. We find firstly that our theory is reproduced and secondly that a direct comparison of the values of the diffraction coefficient at corresponding points along breakwaters (1) and (2) of fig. 40 with the values given in the diagram of the Shore Protection Manual (our fig. 65) based on Penney and Price's method gives very good agreement. In fact we get at points along breakwater (1) the values

ρ =	1.0	2.0	3.0	4.0	5.0	6.0	7.0	8.0	9.0
Penney and Price's method:	1.32	1.23	1.11	0.97	0.88	0.81	0.76	0.71	0.66
Present method:	1.36	1.26	1.09	0.97	0.88	0.81	0.75	0.70	0.66

and for breakwater (2) the values

ρ =	1.0	2.0	3.0	4.0
Penney and Price's method:	0.44	0.06	0.01	0.01
Present method:	0.42	0.07	0.03	0.02

This agreement suggests that our assumption for the velocity along

the gap is close to reality and it tends to include the effect of the reflected wave as well. This effect has been taken into account in the above derivation of the values by Penney and Price's method.

The exact theory, again in the case of $\theta = 180^{o}$, is used for comparisons covering in fig. 66 a relatively small opening of $\frac{\lambda}{2}$ while in fig. 67 we have an oblique approach of the incident wave. Graphs after Carr and Stelzriede [1] presented by Johnson [68] have been reproduced in the above figures together with the results of the present theory for the corresponding cases defined in the figures. Again the major deviations between the two theories are shown.

In fig. 67 an approximation proposed by Johnson has been included. This is simply the application of Penney and Price's method, as modified by Blue and Johnson, for an imaginary gap formed by the projection of the actual opening on the line perpendicular to the wave propagation. The theory for the normal incidence is applied then for the gap of breadth - $d\sin\theta_{o}$ with the usual notation.

The comparisons presented in figs 66 and 67 show overall good agreement between our results and the existing theory, which it must be added is represented by its asymptotic form i.e. not strictly the exact solution but a good approximation at points where the radius of curvature of the wave crest is as little as about three wavelengths (Carr and Stelzriede [1]).

E2.2 With the Theory of Section C5

We have seen that the results obtained in section C5 by using principles of the theory of matched expansions are not suitable for a point-to-point direct comparison with the main solution presented

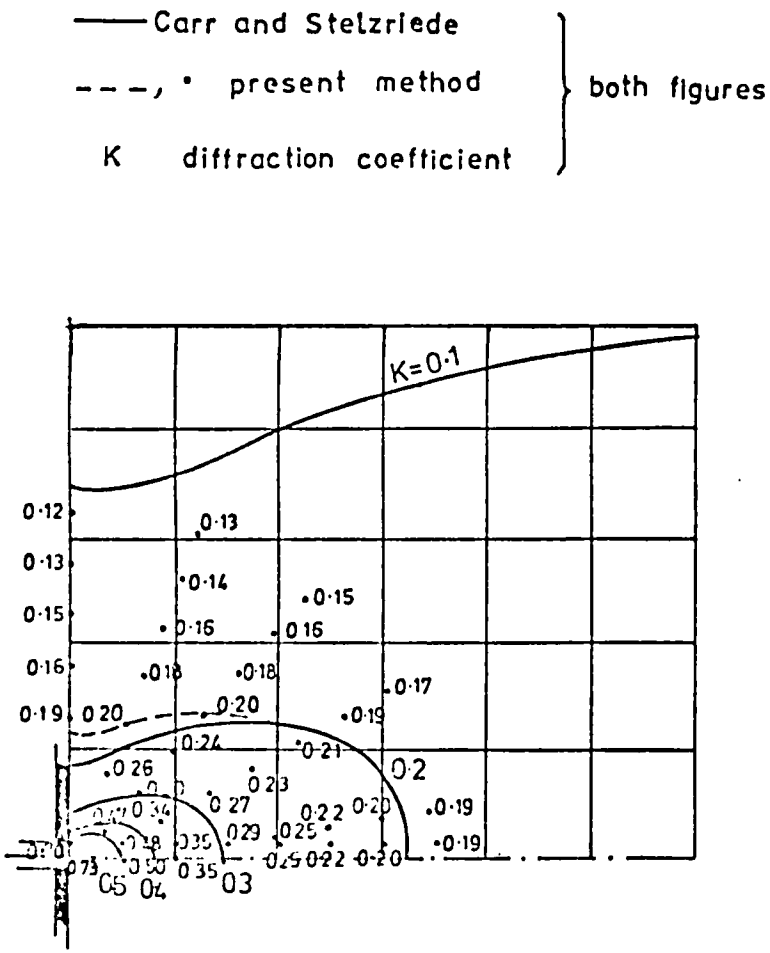

Fig. 66. Comparison with Carr and Stelzriede's method (Johnson [68])

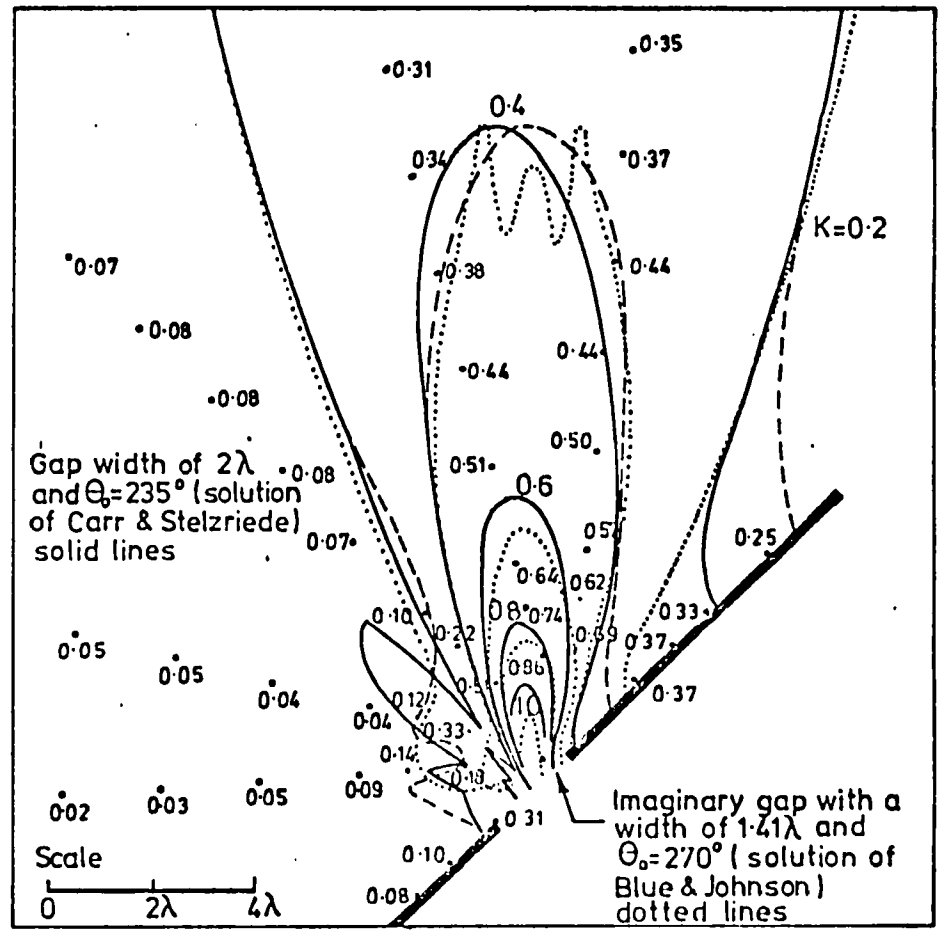

Fig. 67. Comparison with Carr and Stelzriede's method and with Johnson's application of Blue and Johnson's method (Johnson [68])

in section C3. This is more so due to the low order of terms taken into account during the matching procedure. So the final equation giving the velocity potential does not include the parameter of angle of incidence which means that we are in the large wavelength region where the corresponding theory of sound waves applies.

However, we can attempt an indirect checking by establishing a quantity T relative to the transmission factor of energy often used at such studies of propagation of waves through passages. Following the notation of section C5 we put

$$T = |Q|$$

where Q denotes the strength of the source we had put at the wedge apex when doing the matching. Using the definition by Carr and Stelzriede ([1], p. 121) we write

$$T = \frac{\int_0^{\theta} H^2(r,\omega)\, r\, d\omega}{H_{in}^2 d}$$

where H_{in} is the height of the incident wave and $H(r,\omega)$ the wave height at the point (r,ω). This relation can be written

$$T = \frac{\rho}{\delta} \sum_i K_i^2\, \theta_i \qquad (224)$$

where K_i is the diffraction coefficient at the point P_i of the arc $(0, \rho;\ 0 < \omega < \theta)$. If K_i is assumed uniform over the arc, eq. (224) gives

$$T = \frac{\theta\rho}{\delta} K^2 = \frac{\theta\rho}{\delta} |f|^2 \qquad (225)$$

From eq. (211) —or the corresponding eq. (204) of the theory with the approximation to the gap geometry— we deduce after introdu-

cing the expansion

$$J_o^2(kr) + Y_o^2(kr) \sim \frac{1}{\pi^2\rho} - \ldots \qquad \text{for large } kr,$$

$$|f|^2 = \frac{1}{\rho}\frac{1}{4W^2 + \pi^2} \qquad \left(\text{or } \frac{1}{\rho}\frac{1}{4U^2 + \pi^2}\right)$$

Thus eq. (225) becomes

$$T = \frac{\theta}{\delta}\frac{1}{4W^2 + \pi^2} \qquad \left(\text{or } \frac{\theta}{\delta}\frac{1}{4U^2 + \pi^2}\right) \tag{226}$$

where $W = \gamma + \log(\pi\delta) + 2\beta\log\beta + 2(1-\beta)\log(1-\beta)$, $2\pi\beta = 2\pi-\theta$

$$U = \gamma + \log\frac{k}{2} + \log\frac{d'F(\beta)}{2}, \quad F(\beta) = \frac{\beta^{\beta}(1-\beta)^{1-\beta}}{\sin(1-\beta)\pi}$$

which combined with eq. (224) gives

$$\frac{\theta}{4W^2 + \pi^2} = \rho \sum_i K_i^2\,\theta_i \tag{227}$$

$$\left(\text{or } \frac{\theta}{4U^2 + \pi^2} = \rho \sum_i K_i^2\,\theta_i\right)$$

In these equations θ_i represents the measure of the ith portion of the angle θ which has been divided in many small angles in order to facilitate the original integration. If we take $\theta_1 = \theta_2 = \ldots = \theta_i = \ldots = \hat{\theta}$, then eq. (227) becomes

$$\frac{\theta}{4W^2 + \pi^2} = \hat{\theta}\rho \sum_i K_i^2 \tag{228}$$

It is reminded that the equations displaying the symbol U originate from the symmetric breakwaters case, while those with W come from the treatment of the asymmetrical case (see section C5). When $\theta = \pi$ both

groups of equations coincide and give for the transmission factor

$$T = \frac{\pi}{\delta} \frac{1}{4(\gamma+\log\frac{\pi\delta}{4})^2+\pi^2} = \frac{1}{\delta} \frac{1}{3.272 + 0.844\log\delta + 1.272\log^2\delta}$$

which coincides with Lamb's result ([5] p. 533, eq. (22)).

For $\delta = 0.1$ the last equation gives a transmission factor of 1.24. The ratio of this factor associated with an angle θ to the corresponding one of the angle $\theta = \pi$ is

$$\frac{T_\theta}{T_\pi} = \frac{\theta}{\pi} \frac{4(\gamma + \log\frac{\pi\delta}{4})^2 + \pi^2}{4W^2 + \pi^2}$$

with the obvious alternative of the symmetrical case, where W is replaced by U.

The quantity W (or U) contains the information of the geometry of the opening combined with the position of the two screens that form it; in other words it represents something similar to the effective size of a hole (see Tuck [52]) or the conductivity of an orifice (Rayleigh [11], see also the historical introduction to the same work by R.B. Lindsay).

It is possible to use the above knowledge for a comparison with our main theoretical results, by applying eq. (228) taking the following precautions.

We have found elsewhere that the asymptotic theory can be applied up to about $\delta = 0.3$. Therefore it was thought advisable to check at this least unfavourable value of the breadth of the opening. Further since the incidence of the original field played no role, an approach of the incident wave symmetrical to both breakwaters

seemed promising because this was the case when $\theta = \pi$ (normal incidence) where our equations of the matched expansions theory coincided with well founded results as shown above. Finally we chose a rather long radius $\rho = 10.0$ to allow the diffracted wave to regain its uniformity along the crest, so that not many points P_i should be required.

We chose therefore for the checking through eq. (228),

$\theta = 120^{\circ}$ or $\beta = 2/3$

$\delta = 0.3$

$\zeta = 240^{\circ}$

$\rho = 10.0$

and $\hat{\theta} = 10^{\circ}$

We found for these values

$W(\beta = 2/3, \delta = 0.3) = -0.755$, and the left hand side of eq. (228) gave the number

$$\frac{120}{12.15} = 9.87$$

The computer programme of the main theory for the same values gives the diffraction coefficient K_i at the points $P_i(\rho,\omega_i)$ as follows

$\omega_i(^{\circ})$	10	20	30	40	50	60	70	80	90
K_i	0.122	0.118	0.112	0.106	0.098	0.092	0.086	0.081	0.077

$\omega_i(^{\circ})$	100	110	120
K_i	0.074	0.073	0.072

Now the right hand side of eq. (228) gives

$$10 \times 10.0(K_1^2 + K_2^2 + \ldots + K_{12}^2) = 10.67$$

which corresponds to an average diffraction coefficient K = 0.094 while the left hand side gives for the same coefficient the value K = 0.091 the two values differing by less than 3%, which suggests a good agreement of the two totally different theoretical approaches.

E2.3 With Experimental Results

Figures 68 and 69 present the diffraction coefficient measured at the points defined in subsection D3.3; they also contain curves of equal wave height drawn from the theoretical results for the cases I and II considered. The comparison between experiment and theory is easy. We see that for the majority of the points the agreement is good. In fact we find that for both cases about 85% of the measurements agree very well with the predicted values. The points with great discrepancy were concentrated in the lee and close to breakwater (1); it was believed that for these points, apart from other sources of error present all over the area of measurements, the proximity of the side slope responsible for the absorption of the waves travelling from the point O along the lee of the adjacent arm was affecting the measurements. Furthermore in this area we had small wave heights which relatively increased the inevitable absolute experimental error.

The rest of the measured diffraction coefficients were close to the predicted values. In case I a maximum deviation of 13% is found. In case II a maximum of 16% occurs. These errors cannot be considered as great when compared with other experimental studies done in

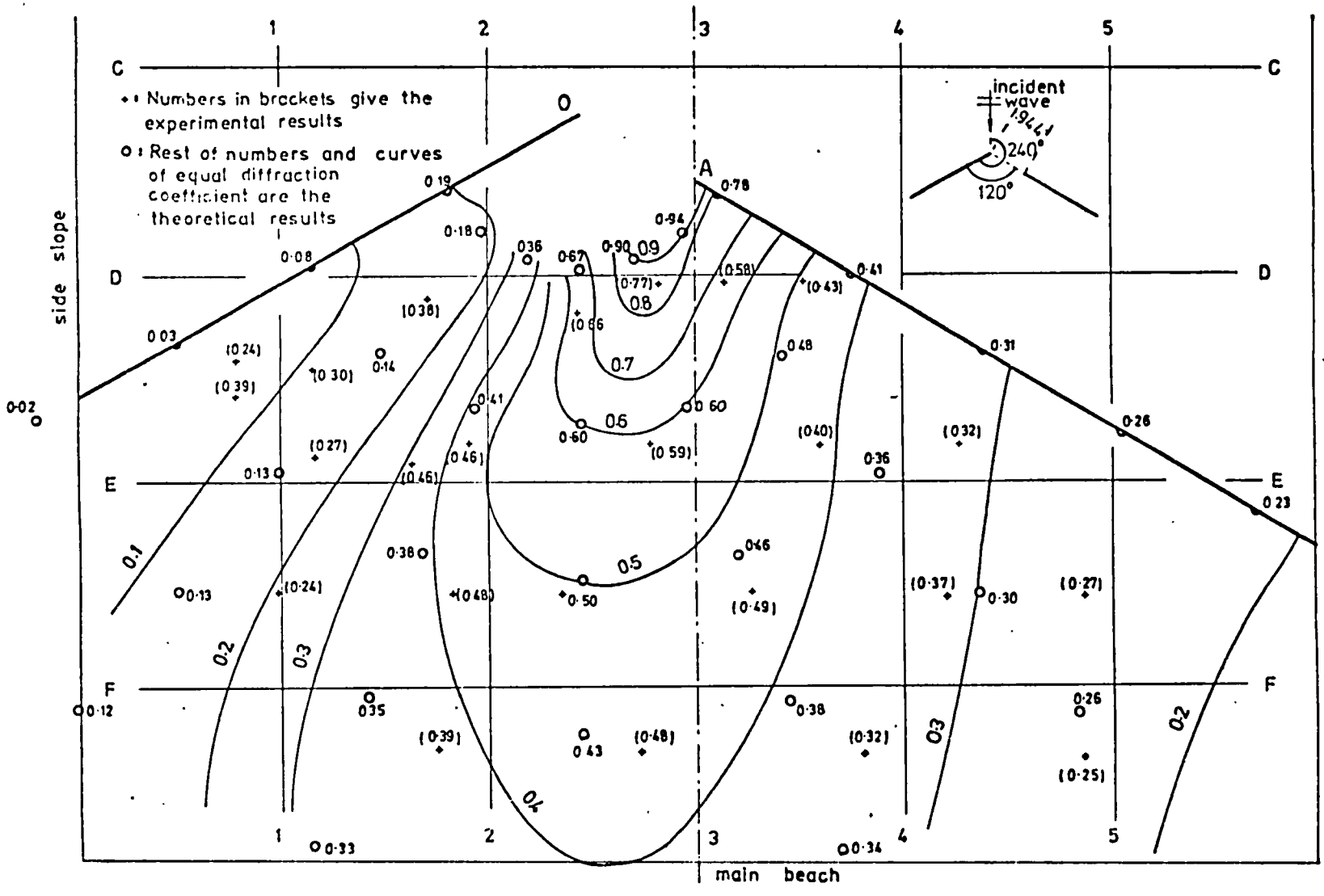

Fig. 68. Comparison of theory and experiment. Case I

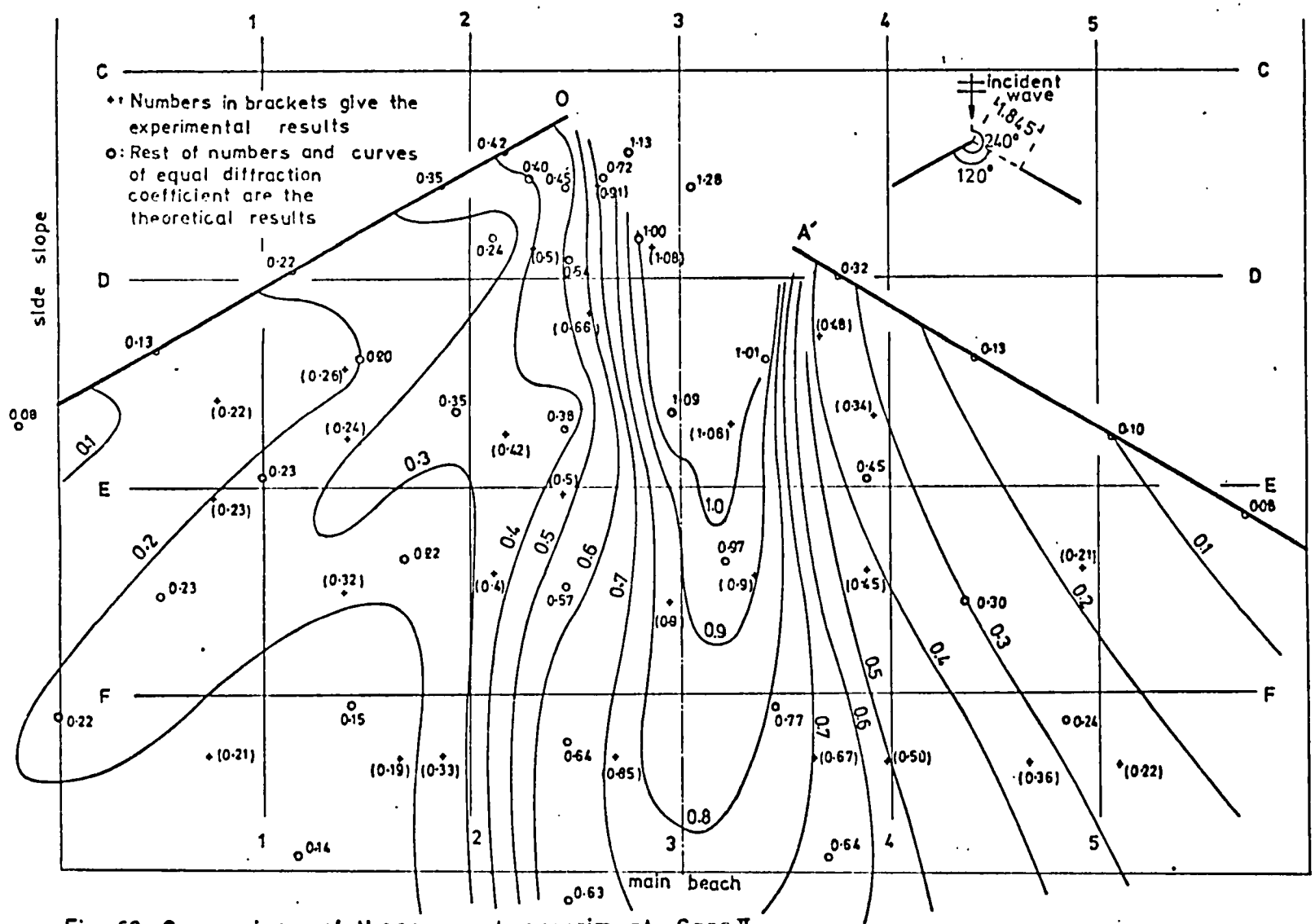

Fig. 59. Comparison of theory and experiment. Case II

the same field of diffraction of water waves. Putnam and Arthur [8] report an error of 12%, Blue and Johnson [10] more than 20% while Blue in his PhD thesis records a considerable scattering of experimental results of up to 90% for diffraction through a gap ([9], fig. 23).

The main sources of wave height error in our experiments were

(a) reflection from the main beach reaching a maximum of 10% (subdivision D2.13);

(b) 1st harmonic component of the wave about 3% at maximum (subdivision D3.1.3).

The main sources of absolute error were

(a) the non-linearity of the wave gauge 0.1 cm at maximum;

(b) other errors associated withe the measuring procedure 0.05 cm.

Considering the above sources of possible error we conclude that a figure of about 15% is a quite acceptable value.

A minor source of discrepancy was the vibration of the plates under the wave action. The maximum amplitude of the vibrating plate at the water surface was of the order of 0.1 cm. The reduced stiffness of the structure presented to the waves, resulted in a slight increase in the wave heights in the lee of it. Some leakage also occurred at the bottom underneath the side absorbers transferring a small proportion of the undulations in front of the plates to the lee of them. Other possibilities of uncertainties were examined but their overall effect was found to be insignificant; these were

(a) Abnormal conditions along the gap due to the consecutive reflection in the seaward area. As noted already the measurements taken along the gap showed no significant change of amplitude with time at the same point (fig. 35). Therefore

it was assumed that no parasitic waves entered the area of measurements through the gap.

It is reminded that the Rayleigh approximation that forms the basis of our theory is self-consistent and the values of the velocity assumed in the aperture are reproduced by the solution (subdivision C3.3.1). Furthermore the continuity of the velocity potential and its normal derivative holds across the aperture as is easily shown (eqs (141) and (142) with a slight modification to the geometrical optics terms).

(b) Viscous separation at the tips of the plates forming the aperture. Small spirals were observed at the edges of the opening due to the detachment of the shear layer. These spirals were alternat--ely occupying both sides of the plates following the frequency of the fundamental wave. They were comprising vorticity shed from the boundary layers on the two surfaces of the plates, which vorticity carried away from the edge by the fluid. Due to the limited strength of the spiral vortex sheet, the phenomenon had no significant effect on the measurements.

E3 RELATED STUDY

E3.1 Numerical Solution

As has been noted in subsection C1.4, we speak of numerical methods whenever the numerical treatment is applied on the basic integral equations that can describe any diffraction problem (see C1.1, C3.3.2). One of the first attempts to adapt to electronic computing the solution of diffraction problems through integral equations involving Hankel functions can be found in Biesel and Ranson [69] (see also Gallagher et al. [24]). Any such method applied to our problem leads to severe difficulties exposed elsewhere. The main cause of these is the unbounded nature of the two breakwaters. This means that if we limit the length of the two barriers and close the leeside opening along a ficticious shore, we can successfully apply a numerical method. In this way we arrive at a more or less specific harbour configuration that displays no variables whatsoever; a small change in the geometry of it or a change of the incidence of the wave will call for a new solution starting again from the basic equations.

We can easily see therefore that the numerical methods are suitable for application on a specific harbour alignment either having already been constructed or undergoing the final study stage of its design. In contrast, an analytical method such as the one used in this work is advantageous during the preliminary stages of a study as well as for drawing theoretical and practical conclusions by varying one or more parameters of the problem and observing the changes of the

wave pattern caused by it. A little more about the method used and the results gained is to said when pointing out some engineering aspects in the next section.

E3.2 Wave Spectra

In reality ocean waves are wind generated and so they are not of simple sinusoidal form of constant height and direction of propagation. Wind generated waves in the ocean propagate in two dimensions and display a wide range of frequencies and amplitudes. Thus the term wave of classical theory is replaced by the wave record(s) out of which the wave spectra are drawn by statistical methods and give us an idea of the parameters of the wavetrains under consideration, e.g. the average wave height.

It would be desirable to know whether the classical diffraction theory and particularly the theory developed in this work, based on the assumption of only one sinusoidal wave present at a time, can be applied with sufficient accuracy for a realistic wave spectrum.

It is evident that the discipline of stochastic processes will be invaluable at this new formulation under which the assumption is made that the motion must still obey the classical equations. A furhter assumption is generally accepted, namely that the wave records are ergodic, that is that averages over a single representative record may replace the averages over an ensemble of records. Under these assumptions it has been shown by W.J. Pierson, Jr. that a linear forecast is generally possible (see e.g. the account by Kinsman [70]). This means that having sufficient information of the waves at a point A we can specify statistical parameters enough to estimate the

behaviour of the waves at a point B, provided that the mechanism of determining the wave at B from that at A is known in the classical theory. A difficulty in determining resonant frequencies of a harbour by using regular rather than irregular waves (see e.g. Ouellet and Morin [71]) is not present in our case because of the infinite nature of the two breakwaters that do not form a semi-closed boundary with one opening which would lead to resonance.

It seems now possible, at least in principle, that our theory can be applied in more complicated wave regimes closer to reality by making use of the laws of statistics. Indeed a simpler diffraction problem has been treated in such a way by Mobarek and Wiegel [72]. They investigated the simple semi-infinite breakwater under a two-dimensional wave spectrum by applying the well-known classical theory to the components of the spectrum and adding the results for a given point. They give evidence supporting the linearity of the diffraction process and conclude that the knowledge of the wave spectra can be used together with the classical theory to predict the energy spectra of waves in the lee of a breakwater within an accuracy acceptable for many engineering problems.

Application of statistical methods has been made also to the refraction problem of predicting the wave spectrum at a point of the sea surface of different water depth from that of another point for which the spectrum is known (Pierson et al. [73]).

E3.3 Diffraction Forces

The diffraction of waves by fixed bodies immersed in the fluid occurs generally with the simultaneous imposition on the body of a

hydrodynamic pressure force. From Bernoulli's equation

$$\frac{p}{\rho_o} = -gz - \frac{\partial\phi}{\partial t} - \tfrac{1}{2}(\text{grad}\phi)^2 + C \quad , \quad \rho_o \text{ the water density}$$

the pressure p can be obtained from the velocity potential ϕ and includes a linear and a quadratic term ϕ. Thus, if ϕ is harmonic in time, there will generally be a linear harmonic pressure force and a second-order force. The first-order oscillatory force should dominate second-order components in the case of most fixed bodies.

The linear wave force can be decomposed into a component associated with the incident wave potential and a component associated with the diffraction potential. The diffraction force is the more difficult component to evaluate because it requires that the diffraction potential first be obtained.

Calculation of forces on structure can therefore be carried out from the knowledge of the total velocity potential that our theory gives. Such structures can be either the elements of the breakwaters themselves, where a decomposition of the field into incident and diffraction is appropriate, or any other structure in the lee of the breakwaters. A numerical integration of the pressure p will yield the linear term of the force as mentioned above by making use of the relations generally employed for this purpose

$$F_x = \oint \int_{-h}^{o} p \, dz \, 1(s) ds = \frac{\rho_o g}{k} \tanh kh \oint a(s) 1(s) \, ds$$

$$F_y = \oint \int_{-h}^{o} p \, dz \, m(s) ds = \frac{\rho_o g}{k} \tanh kh \oint a(s) m(s) \, ds$$

where a(s) is the surface elevation along the circumference s of the

structure and (l,m) is the directional cosine of the inward normal to s.

The phase difference ϵ between the various points of computation can be evaluated from the relationship

$$\epsilon = \arg\{F\}$$

where F the wave function.

The knowledge of ϵ is essential when calculating instantaneous forces.

E3.4 Littoral Processes

The presence of a breakwater can upset the previously existing regime of the littoral transport in three ways:

(a) It poses a physical impermeable barrier to any transfer of material across it.

(b) Through the diffraction mechanism it changes the energy distribution on the sea surface which in turn modifies the driving force of any littoral movement.

(c) The diffraction due to the breakwater changes the direction of propagation of the waves which as a result may attack the shoreline at an angle, thus generating longshore currents resulting in littoral movements again.

The knowledge of the diffraction pattern of the waves for any serious study of littoral processes is therefore of great importance.

In general a breakwater initially causes littoral drift to deposit on the shore in its lee by reducing the wave forces that cause littoral transport. As material is deposited a seaward

projection of the shore is formed in the still water behind the breakwater. If the barrier is offshore, then the projection of the shore advances and acts in turn as a groin which causes the updrift shoreline to advance. If the offshore breakwater is long enough, relatively to its distance from the shore, to act as a complete littoral barrier the depositing action may continue until the shoreline reaches the breakwater (Shore Protection Manual [66]).

The places of erosion and accretion, the shape of the deposit and changes with time can be studied when we know more or less precisely the wave energy distribution or in other words the solution of the diffraction problem.

E3.5 Further Study

A possible extension of the present work could be tried along the lines discussed in subsection C3.2. A random sea could be simulated by an appropriate spectrum to which the diffraction procedure could be applied with the aim of predicting the energy spectrum at any point in the lee of our breakwaters (1) and (2).

Another possibility is the more sophisticated approximation of the velocity along the opening. The amplitude of this velocity has been taken unity all over the gap in this study; for instance a parabolic distribution of this amplitude may prove closer to reality. Denoting by q(r) this amplitude normal to the opening and using a normalisation relation e.g.

$$\int_0^d q(r)dr = d$$

with d the gap width as usual,

we find for the parabolic distribution

$$q(p^*) = 6p^*(1 - p^*)$$

where $p^* = r/d$ is the distance of a point in the opening from the origin expressed in gap widths. Various other distributions might be tried.

E4 CONCLUSION

By examining the figures where some results are presented it is not easy to form clearcut rules and principles covering the diffraction phenomenon due to two converging breakwaters. However, I would make the following general remarks regarding the features of the process.

(a) The decisive factor affecting the degree of protection that the breakwater arms offer to their lee is the angle of incidence. The smaller the angle that the propagation of the incident wave forms with the lee of one breakwater, the greater the disturbance in the region close to the relative barrier.

(b) In general the larger the opening the greater the disturbance in the harbour area.

(c) The resulting diffraction pattern is more sensitive to the angle of wave approach than to the angle θ between the two barriers.

(d) With decreasing θ the wave heights increase along the leeward side of the arm more exposed to the incident wave.

(e) The greater the 'distance' between the two breakwaters - which depends on the distance of their tips as well as on their angle - the less effect the two'independent' diffraction patterns have on each other. Comparing for instance fig. 40 with fig. 46 we see that for the larger breadth of opening the wave pattern is closer to that of a semi-infinite breakwater with incident wave normal to it than is the pattern for the small gap width.

It was shown in subsection C3.1 that the application of the

results of the diffraction problem for a semi-infinite screen to the case where two barriers forming an angle are present is not satisfactory for many combinations of angle of incidence and gap width. Therefore this study supported by good comparisons evidence (section E2) can be regarded as a first step toward the full investigation of the diffraction of water waves due to two converging semi-infinite breakwaters. Such an investigation could provide the engineer with new understanding of the principle features of the diffraction process due to a configuration that is frequently encountered in harbour or other coastal works. Furthermore, aided by the use of tables and charts of diffraction coefficient the harbour engineer would be able to predict more accurately the regions of least energy intensity suitable for moorings, docks and other facilities.

The applicability of the present method was pointed out in subsection E3.1 in regard particularly with preliminary studies; the five parameters of the equations are at the disposal of the design engineer who can try more than one solution to determine the optimum gap width, angle between the arms, angle between the breakwaters and the prevailing sea, and areas of least agitation in combination of course with other non-hydraulic factors.

REFERENCES

CHAPTER B

1. CARR, J.H. and STELZRIEDE, M.E. (1952) Diffraction of Water Waves by Breakwaters. U.S. Natl. Bur. Stds, Circ. No. 521, pp. 109-125.
2. MORSE, P.M. and RUBENSTEIN, P.J. (1938) The Diffraction of Waves by Ribbons and by Slits. Phys. Rev., 54, pp. 895-898.
3. PENNEY, W.G. and PRICE, A.T. (1952) The Diffraction theory of Sea Waves and the Shelter Afforded by Breakwaters. Phil. Trans. Roy. Soc. A, 244, pp. 236-253.
4. LACOMBE, H. (1965) Cours d'océanographie physique, pp. 342-361. Paris, Gauthier-Villars.
5. LAMB, H. (1932) Hydrodynamics. Cambridge University Press (6th edition).
6. SOMMERFELD, A. (1896) Mathematische Theorie der Diffraktion. Math. Ann., 47, pp. 317-374.
7. BOWMAN, J.J., SENIOR, T.B.A., USLENGHI, P.L.E. (Ed.) (1969) Electromagnetic and acoustic scattering by simple shapes. Amsterdam, North-Holland Publishing Company.
8. PUTNAM, J.A. and ARTHUR, R.S. (1948) Diffraction of water waves by breakwaters. Trans., Am. Geoph. Un., 29,pp. 581-190.
9. SILVESTER, R. and LIM, Teck-Kong (1968) Application of wave diffraction data. Proc. 11th Conf. Coast. Eng., pp. 248-270.
10. BLUE, F.L. Jr. and JOHNSON, J.W. (1949) Diffraction of water waves passing through a breakwater gap. Trans., Am. Geoph. Un., 30, pp. 705- 718.

11. RAYLEIGH, J.W.S. (1945) The Theory of Sound. New York, Dover Publications (re-publication of the 2nd edition).

CHAPTER C

12. BOUWKAMP, C.J. (1954) Diffraction Theory. Rep. Progr. Phys., XVII, pp. 35-100.

13. STOKER, J.J. (1957) Water Waves. New York, Interscience Publishers, Inc.

14. BAKER, B.B. and COPSON, E.T. (1950) The Mathematical Theory of Huygens' Principle. Oxford, University Press (2nd edition).

15. WATSON, G.N. (1966) A treatise on the Theory of Bessel Functions. Cambridge, University Press (2nd edition).

16. LEVINE, H. and SCHWINGER, J. On the Theory of Diffraction by an Aperture in an Infinite Plane Screen.
(1948) I. Phys. Rev., 74, pp. 958-974.
(1948) II. Phys. Rev., 75, pp. 1423-1432.

17. DOLPH, C.L. (1961) Recent developments in some non-self-adjoint problems of mathematical physics. Bull. Am. Math. Soc., 67, pp. 1-69.

18. WIENER, N. and HOPF, E. (1931) Über eine Klasse singulärer Integralgleichungen. Sitz. Preuss. Akad. Wiss., Phys.-Math. Klasse, pp. 696-706.

19. SNEDDON, I.N. (1972) The Use of Integral Transforms. New York, McGraw-Hill, Inc.

20. TITCHMARSH, E.C. (1968) The Theory of Functions. Oxford, University Press (2nd ed.).

21. MUSKHELISHVILI, N.I. (1953) Singular Integral Equations. Groningen-Holland, P. Noordhoff N.V.

22. COPSON, E.T. (1946) On an Integral Equation arising in the Theory of Diffraction. Quart. J. Math. (Oxford Series), 17, pp. 19-34.

23. KARP, S.N. (1950) Wiener-Hopf Techniques and Mixed Boundary Value Problems. Comm. Pure Appl. Math., 3, pp. 411-426.

24. GALLAGHER, R.H., ODEN, J.T., TAYLOR, C. and ZIENKIEWICZ, O.C. (1975) Finite Elements in Fluids. John Wiley.

25. JONES, D.S. (1953) The eigenvalues of $\nabla^2 u+\lambda u = 0$ when the boundary conditions are given on semi-infinite domains. Proc. Camb. Phil. Soc., 49, pp. 668-684.

26. LEPPINGTON, F.G. (1972) On the radiation and scattering of short surface waves, part 1. J. Fluid Mech., 57, pp. 101-119.

27. JONES, D.S. (1964) The theory of electromagnatism. Pergamon Press.

28. OBERHETTINGER, F. (1958) On the Diffraction and Reflection of Waves and Pulses by Wedges and Corners. J. Research NBS, 61, pp. 343-365.

29. FELSEN, L.B. and MARCUVITZ, N. (1973) Radiation and Scattering of Waves. Englewood Cliffs, Prentice-Hall, Inc.

30. SCHWARZSCHILD, K. (1902) Die Beugung und Polarisation des Lichts durch einen Spalt. I. Math. Ann., 55, pp. 177-247.

31. KELLOGG, O.D. (1929) Foundations of potential theory. (Band XXXI von 'Die Grundlehren der mathematischen Wissenschaften' herausgegeben von R. Courant) Berlin, Julius Springer.

32. SMIRNOV, V.I. (1964) A course of Higher Mathematics, Vol.IV. Pergamon Press.

33. KANTOROVICH, L.V. and KRYLOV, V.I. (1958) Approximate methods of higher analysis. Groningen, P. Noordhoff.

34. DELVES, L.M. and WALSH, J. (editors) (1974) Numerical solution of integral equations. Oxford, Clarendon Press.

35. BURTON, A.J. and MILLER, G.F. (1971) The application of integral equation methods to the numerical solution of some exterior boundary-value problems. Proc. Roy. Soc. Lond. A.,323 pp. 201-210.

36. GOLDSTEIN, M. and THALER, R.M. (1959) Recurrence Techniques for the Calculation of Bessel Functions. MTAC, 13, pp. 102-108.

37. PATTERSON, T.N.L. (1968) The Optimum Addition of Points to Quadrature Formulae. Math. Comp., 22, pp. 847-856.

38. VAN DYKE, N. (1964) Applied mathematics and mechanics, vol. 8: Perturbation methods in fluid mechanics. Academic Press.

39. FRAENKEL, L.E. (1969) On the method of matched asymptotic expansions. Proc. Camb. Phil. Soc., 65, pp. 209-284.

40. HARRIS, R.A. (1901) On two-dimensional fluid motion through spouts composed of two plane walls. Ann. of Math., (2),ii, pp. 73-76.

41. KOBER, H. (1957) Dictionary of Conformal Representations. New York, Dover Publications, Inc.

42. LIU, P.L.-F. (1975) Scattering of Water Waves by a Pair of Semi-Infinite Barriers. ASME, J. Appl. Mech., 42, pp. 777-779.

43. NEWMAN, J.N. (1974) Interaction of Water Waves with Two Closely Spaced Vertical Obstacles. J. Fluid Mech., 66, pp. 97-106.

44. TUCK, E.O. (1971) Transmission of water waves through small apertures. J. Fluid Mech., 49, pp. 65-74.

45. HARDY, G.H. (1952) A Course of Pure Mathematics (10th ed.). Cambridge, University Press.

46. WANG, SHEN (1974) Plunger-type wavemakers: theory and experiment. J. Hydr. Res., 12, pp. 357-388.

47. BIESEL, F. and SUQUET, F. (1954) Laboratory wave generating apparatus. English transl. of a series of articles from La Houille Blanche by St. Anthony Falls Hydraulic Laboratory, Report 39, Minnesota U., Minnesota.

48. URSELL, F., DEAN, R.G. and YU, U.W. (1960) Forced small-amplitude water waves: a comparison of theory and experiments. J. Fluid Mech., 7, pp. 33-52.

49. HAVELOCK, T.H. (1929) Forced Surface-Waves on Water. Phil Mag. Series 7, 8, pp. 569-576.

50. SCHULER, M. (1936) Erzeugung von Oberflächenwellen durch schwingende Körper. Zeit. Angew. Math. Mech., 16, Heft 2, pp. 65-72.

51. BIESEL, F. (1948) Le Coin du Laboratoire: Filtre à houle (Système Neyrpic). La Houille Blanche, 3, pp. 276-284.

52. TUCK, E.O. (1975) Matching Problems Involving Flow through Small Holes. Advances in Appl. Mech., 15, pp. 89-158.

53. COSTELLO, R.D. (1952) Damping of water waves by vertical circular cylinders. Trans., Am. Geoph. Un., 33, pp. 513-519.

54. GRUENE, J. and KOHLHASE, S. (1974) Wave transmission through vertical slotted walls. Proc. 14th Coast. Eng. Conf., v.III, pp. 1906-1923.

55. KENNY, F.M., JAMES, J.D., MELLING, T.H. (1976) Waveforce analysis of perforated marine structures. Interocean '76, 3rd International Conference and Exhibition for Ocean Engineering and Maring Sciences, Düsseldorf, Germany.

56. BENJAMIN, T.B. (1967) Instability of periodic wavetrains in non-linear dispersive systems. Proc. Roy. Soc. A., pp. 59-75.

57. HAYES, W.D. (1973) Group velocity and nonlinear dispersive wave propagation. Proc. R. Soc. Lond. A., 332, pp. 199-221.

58. HULSBERGEN,C.H. (1974) Origin, effect and supression of secondary waves. Proc. 14th Coast. Eng. Conf., VI, pp.392-411.

59. FONTANET, P. (1961) Théorie de la génération de la houle cylindrique par un batteur plan. La Houille Blanche, 16, pp. 3-31, 174-197.

60. HUNT, J.N. (1952) Amortissement par viscosité de la houle sur un fond incliné dans un canal. La Houille Blanche, 7, pp. 836-842.

61. BATCHELOR, G.K. (1970) An Introduction to Fluid Dynamics. Cambridge, U. Press.

62. MAY, R.W.P. (1974) The diffraction and scattering of finite amplitude water waves. M.Sc. report, U. of London.

63. MICHE, M. (1951) Le pouvoir réfléchissant des ouvrages maritimes exposés a l'action de la houle. Ann. Pont. Ch., 121, pp. 285-319.

64. NUSSENZUEIG, H. (1959) Solution of a diffraction problem. I. The wide double wedge. II. The narrow double wedge. Phil. Trans. Roy. Soc. A, 252, pp. 1-51.

65. TEAGUE, B.R. and ZITRON, N.R. (1972) Diffraction by an aperture between two wedges. Appl. Sci. Res., 26, pp. 127-137.

CHAPTER E

66. U.S. ARMY COASTAL ENGINEERING RESEARCH CENTRER (1975) Shore protection manual (2nd ed.). Department of the Army, Corps of Engineers, Washington.

67. JOHNSON, J.W. (1953) Engineering aspects of diffraction and refraction. Trans., ASCE, 118, pp. 617-651.

68. JOHNSON, J.W. (1952) Generalized wave diffraction diagrams. Proc. 2nd Conf. Coast. Eng., pp. 6-23.

69. BIESEL, F. and RANSON, B. (1961) Calculs de diffraction de la houle. 9th Conv. I.A.H.R., pp. 688-699.

70. KINSMAN, B. (1965) Wind Waves. Their generation and propagation on the ocean surface. Englewood Cliffs, N.J., Prentice-Hall, Inc.

71. OUELLET, Y. and MORIN, Y. (1975) Effect of Structures on Irregular Waves Compared to Regular Waves. Journal of the Waterways, Harbors and Coastal Engineering Division, ASCE, 101, pp. 231-146.

72. MOBAREK, I.E. and WIEGEL, R.L. (1966) Diffraction of wind generated water waves. Proc. 10th Conf. Coast. Eng., v.I, pp. 185-206.

73. PIERSON, W.J., Jr., TUTTELL, J.J. and WOOLLEY, J.A. (1953) The theory of the refraction of a short crested Gaussian sea surface with application to the northern New Jersey coast. Proc. 3rd Conf. Coast. Eng., pp. 86-108.